UNIVERSITY OF BIRMINGHAM

Novel biomarkers in recurrent differentiated thyroid cancer

Hannah Nieto

A thesis presented to The University of Birmingham
for the degree of Doctor of Philosophy

Institute of Metabolism and Systems Research
College of Medical and Dental Sciences
December 2019

Abstract

Thyroid cancer is increasing in incidence worldwide and while outcomes are generally good, up to 25% of patients have tumours which recur after treatment, with a significant impact on their quality of life and life expectancy. The hypothesis of this PhD was that thyroid tumours which subsequently recur display a distinct pattern of driver mutations, or RNA and microRNA expression patterns to those that do not, and that the molecular characterisation of these alterations will reveal novel mechanisms involved in thyroid tumour recurrence. Controlled access TCGA data on thyroid cancer were downloaded and a bioinformatic whole exome sequencing analysis was performed on 43 recurrent patients. This identified mutations in genes including IMPDH2, PFKFB4 and DICER1. A differential expression analysis of RNA and microRNA compared recurrent (n=43) to non-recurrent (n=457) TCGA patients. In the RNA analysis genes involved in matrix adhesion and thyroid cancer pathogenesis were most differentially expressed in recurrent patients, including fibronectin 1 (FN1), α3 integrin (ITGA3) and the proto-oncogene MET. MicroRNA analysis highlighted miR 221, 486 and 1179 as significantly differentially expressed miRs in cancer recurrence. Functional in vitro analysis of demonstrated potential functional roles for the candidate genes highlighted by the RNA and microRNA analysis. This suggests that altered RNA and miRNA expression levels may be key to predicting thyroid cancer recurrence.

Dedication

For Tom and Tilly,

And for my parents, my sisters and my parents-in-law

Acknowledgments

I would like to thank Professor Chris McCabe for his supervision, you have inspired and supported me at the right moments. I would also like to thank the rest of the McCabe group, especially Cait Thornton and Dr Martin Read, for their help and support, with CRISPR and miR RT respectively. Never another CRISPRmas please. Thank you, Dr Alice Fletcher, for the advice in and out of the lab. I would also like to thank my supervisors: Professor Jean-Baptiste Cazier - thank you for agreeing to be my supervisor and trying to teach a medic how to code, I had fun and will always appreciate it. Professor Hisham Mehanna thank you for always making time for my updates and for being my clinical link. Thank you also to Dr Albert Nobre de Menezes for your unending patience and teaching, and thank you to Dr Vicki Smith for your consistently excellent lab advice. Thanks to Dr Kristien Boelaert for the support and careers advice, and to Bhav, Kate, Mohammed, Duncan and Pip for the trouble shooting, counsel and tea. Thank you to Mr Neil Sharma for paving the way and to Mr John Watkinson for supporting me on this path. Thank you to Charlie for equipping me with the skills to get this thesis written. Finally thank you to Tom, for everything; I aspire to be as good as you.

The project was funded by several generous fellowships and grants, and I am grateful to the Get Ahead Charitable Trust for their support, The Royal College of Surgeons England, The Institute of Translational Medicine (ITM) at the University of Birmingham and the Midlands Institute of Otolaryngology (MIO). The results shown in this thesis are largely based upon data generated by the TCGA Research Network, found

at: https://www.cancer.gov/tcga, who kindly granted me access to their controlled access research data to complete the project.

Contents

List of figures

List of tables

Abbreviations

% w/v	percentage weight volume
5% milk	5% w/v skimmed milk powder
ATA	American Thyroid Association
ATP	adenosine triphosphate
BCA	bicinchoninic acid
bp	base pairs
BRAF-like	BRAF V600E-like
BrdU	Bromodeoxyuridine / 5-bromo-2'-deoxyuridine
BSA	bovine serum albumin
BTA	British Thyroid Association
BWA	Burrows Wheeler Algorithms
cDNA	complementary DNA
CF	cystic fibrosis
CFTR	cystic fibrosis transmembrane conductance regulator
cm^2	square centimetre
CML	chronic myeloid leukaemia
CRISPR	clustered regularly interspaced short palindromic repeats
CSC	cancer stem cells
CT	computed tomography
dbSNP	The Single Nucleotide Polymorphism Database
ddG	stability change (in protein)
ddH_20	double distilled water
DMEM	Dulbecco Modified Eagle's Media

DNA	deoxyribonucleic acid
dNTP	deoxyribonucleotide triphosphate
dsDNA	double stranded deoxyribonucleic acid
DTC	differentiated thyroid cancer
E	glutamic acid
EBRT	high-dose external beam radiotherapy
EDTA	ethylenediaminetetraacetic acid
EGF	epidermal growth factor
EMT	epithelial to mesenchymal transition
ECM	extracellular matrix
esiRNA	endoribonuclease-prepared siRNA
FATHMM	Functional Analysis through Hidden Markov Models
FBS	fetal bovine serum
FDR	false discovery rate
FDG	^{18}fluoro-deoxy-glucose
FFPE	formalin-fixed paraffin-embedded
FGF10	fibroblast growth factor
FNAc	fine-needle aspiration cytology
FTC	Follicular thyroid carcinoma
FOX	Forkhead box
FRAX	Fracture Risk Assessment Tool
FT-UMP	follicular tumour of uncertain malignant potential
g	gram
GC content	guanine-cytosine content

gRNA	guide RNA
H_2O_2	hydrogen peroxide
HIF-1α	hypoxia inducible factor-1α
I-TASSER	Iterative Threading ASSEmbly Refinement
IFNγ	interferon gamma
IKK	IκB kinase
indel	insertion-deletion mutations
L	litre
LB	lysogeny broth
LOH	loss of heterozygosity
MACIS	Metastasis, patient Age, Completeness of resection, local Invasion, and tumour Size
MAPK	MAP kinase
MDT	multidisciplinary team
MEN	multiple endocrine neoplasia
$MgSO_4$	magnesium sulphate
miR-Amp	miR-amplification
miRNA	micro ribonucleic acid
mM	milimolar
MNG	multinodular goitre
MRI	magnetic resonance imaging
mRNA	messenger ribonucleic acid
MTC	medullary thyroid cancer

MTS	aqueous soluble tetrazolium 3-(4,5-dimethylthiazol-2-yl)- 5-(3-carboxymethonyphenol)-2-(4-sulfophenyl)-2H-tetrazolium
$NaHCO_3$	sodium bicarbonate
NFQ-MGB	non- fluorescent quencher minor groove binder
ng	nanograms
NGS	next generation sequencing
NIFTP	non-invasive follicular thyroid neoplasm with papillary nuclear features
NIS	Sodium iodide symporter
^oC	degrees centigrade
PAM	protospacer adjacent motif
PBS	phosphate-buffered saline
PCR	polymerase chain reaction
PDTC	poorly differentiated thyroid cancer
PET-CT	positron emission tomography-computed tomography
PTC	papillary thyroid carcinoma
PVDF	polyvinylidene difluoride
RCF	Relative Centrifugal Force
RISC	RNA-induced silencing complex
RNA	ribonucleic acid
RNA-seq	RNA sequencing
rpm	revolutions per minute
RRA	radioiodine remnant ablation
RSEM	RNA-Seq by Expectation Maximization

RTqPCR	Real Time quantitative PCR
S.O.C.	Super Optimal broth with Catabolite repression media
SDS	sodium dodecyl sulfate
SIFT	Sorting Intolerant from Tolerant
siRNA	small interfering ribonucleic acid
SLC5A8	apical iodide transporter
SNVs	single nucleotide variants
T-reg	T regulatory
T3	triiodothyronine
T4	thyroxine
T7E	T7 Endonuclease 1
TBG	thyroxine-binding globulin
TBS-T	Tris-buffered saline with Tween®20
TCGA	The Cancer Genome Atlas
TDS	Thyroid Differentiation Score
TG	thyroglobulin
TIMP3	Tissue Inhibitor of Metalloproteinase 3
TNF	tumour necrosis factor
TNM	Tumour Node Metastasis
TPO	thyroid peroxidase
TRH	thyrotropin-releasing hormone
TSH	thyroid stimulating hormone
TSHR	thyroid stimulating hormone receptor
USA	United States of America

V	valine
v/v	volume/volume
vcf	variant call format
WBS	^{131}I whole body scintigraphy
WDT-UMP	well differentiated tumour of uncertain malignant potential
WES	whole exome sequencing
WGS	whole genome sequencing
x g	g force
µg	microgram
µg/ml	microgram per millilitre
µl	microlitres

Chapter 1 General Introduction

1 Introduction

1.1 The Thyroid Gland

1.1.1 Anatomy of the thyroid

The thyroid gland is located in the midline of the neck, sitting anteriorly over the trachea, directly inferior to the larynx. It is a bilobed butterfly-shaped gland, with the lateral lobes connected via the isthmus. Occasionally, a third lobe called the pyramidal lobe occurs as a normal anatomical variant. The pyramidal gland projects cranially from the isthmus with a variable incidence rate reported (15 - 75 %) (Braun et al. 2007). The four parathyroid glands sit on the posterior aspect of the thyroid gland.

1.1.2 Physiology of the thyroid

Thyroid hormone biosynthesis is under the control of the hypothalamo-pituitary axis and is demonstrated below in Figure 1.1. The hypothalamus releases thyrotropin-releasing hormone (TRH) and this travels through the long portal vein to stimulate the anterior pituitary (Mariotti 2016). The anterior pituitary synthesises and releases thyroid-stimulating hormone (TSH) which acts upon the thyroid (Dohan et al. 2003).

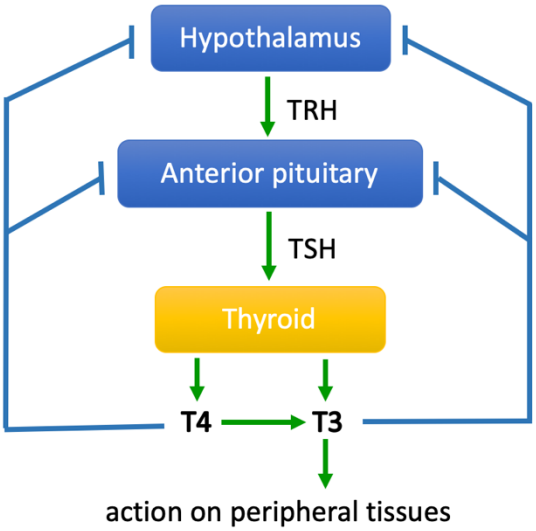

Figure 1.1: The hypothalamo-pituitary axis, demonstrating the negative feedback loop that contributes to homeostasis in normal thyroid physiology. T3 is the active form of thyroid hormone and T4 is peripherally converted to T3. TRH, Thyrotropin-releasing hormone; TSH, thyroid-stimulating hormone; T4, thyroxine; T3, triiodothyronine (Mariotti 2016).

TSH binds to the TSH receptor located on follicular thyroid cells. TSH functions as a growth factor and activates the adenylate cyclase pathway, facilitating thyroid hormone synthesis via expression of genes such as thyroglobulin (TG), thyroid peroxidase (TPO) and the sodium iodide symporter (NIS) and thyroid gland growth (Nieto and Boelaert 2016). Thus, the consequent release of triiodothyronine (T3) and thyroxine (T4) is dependent on TSH.

1.1.3 Thyroid hormone biosynthesis

Triiodothyronine (T3) and thyroxine (T4) release into the circulation is dependent on the factors required to synthesise the hormones. Iodide is required and is taken up

from the circulation by the sodium iodide symporter NIS, located on the basolateral thyroid cell membrane (Figure 1.2). Iodide diffuses out of the cell into the follicular lumen via the transporter pendrin, which is located on the apical membrane. Here, thyroid peroxidase (TPO) with hydrogen peroxide (H_2O_2) oxidises the iodide, which binds to tyrosyl residues creating monoiodotyrosine (MIT) and diiodotyrosine (DIT) within the macromolecule thyroglobulin (TG). Coupling by TPO then generates T3 and T4, and these TG complexes are endocytosed into the cell. Proteolysis then releases T3 and T4 from TG, and the liberated thyroid hormones are released into the circulation via monocarboxylate transporter 8 and 10 (MCT8 and MCT10) (Kogai and Brent 2012, Di Cosmo et al. 2010, Dohan et al. 2003). Peripherally, the thyroid hormones impact their targets via thyroid hormone receptors. Most of the circulating hormones are protein bound to thyroxine-binding globulin (TBG), transthyretin or albumin. Triiodothyronine is the active form of thyroxine, and T4 is converted into T3 peripherally by deiodination (Sapin and Schlienger 2003).

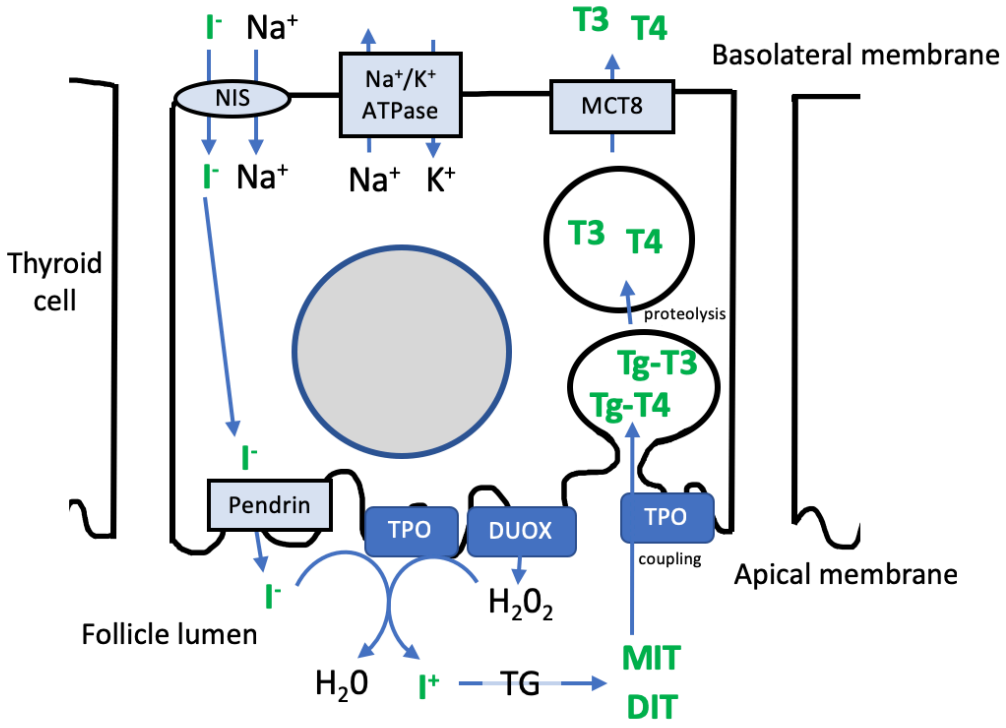

Figure 1.2: Thyroid hormone synthesis. Circulating iodide from the blood stream is transported into the thyrocyte by NIS. Transport through the cell and back into the circulation as T3 and T4 is demonstrated. Hydrogen peroxide (H_2O_2) is produced by dual oxidase 2 (DUOX2). Adapted from (Kogai and Brent 2012, Di Cosmo et al. 2010). I^-, iodide; Na^+, sodium; Na^+/K^+ ATPase, sodium-potassium ATPase enzyme; MIT, monoiodotyrosine; DIT, diiodotyrosine; TPO, thyroid peroxidase; DUOX, Dual oxidase 2; MCT8, Monocarboxylate transporter 8.

1.2 Thyroid Cancer

1.2.1 Classification of thyroid cancer

Thyroid cancer is the most common endocrine malignancy and is increasing in incidence over the last few decades (Kitahara and Sosa 2016, Sipos and Mazzaferri 2010). Classically thyroid tumours were described as papillary, follicular, medullary or anaplastic, with papillary and follicular known as well differentiated thyroid carcinoma. The 2017 'World Health Organisation (WHO) Classification of Thyroid Tumours'

updated the classification system. These changes included outlining Hürthle cell carcinoma (previously categorised under follicular carcinomas) as their own entity, favouring the term anaplastic over undifferentiated carcinoma, and adding the terms 'follicular tumour of uncertain malignant potential' (FT-UMP), 'well differentiated tumour of uncertain malignant potential' (WDT-UMP) and 'non-invasive follicular thyroid neoplasm with papillary-like nuclear features' (NIFTP). These borderline tumours are comparable to carcinoma in situ in other tissues (Cameselle-Teijeiro and Sobrinho-Simoes 2018).

1.2.1.1 Papillary thyroid cancer

Papillary thyroid carcinoma (PTC) is the most common thyroid malignancy, accounting for 75 – 80 % of thyroid carcinomas. PTC predominantly occurs in females of reproductive age and presents as a painless neck lump. Risk factors include exposure to ionising radiation (Nikiforov 2006), iodine deficiency, raised TSH and environmental factors (Pellegriti et al. 2013). PTC is a differentiated malignant epithelial tumour and certain nuclear changes are required for diagnosis. Papillary microcarcinomas are a PTC of less than one centimetre, and although they can progress, they are often representative of indolent disease which is identified incidentally. Recent guidelines suggest hemithyroidectomy or active surveillance to manage these cases (Cho et al. 2019). The addition of NIFTP to the recent classification of thyroid cancer recognises the non-aggressive nature of the papillary thyroid tumours previously categorised as well encapsulated. It is not possible to differentiate NIFTP from PTC on cytology, and therefore hemithyroidectomy (the full extent of the treatment required for NIFTP) is

recommended as first line treatment above total thyroidectomy (Zhang et al. 2019, Tallini et al. 2019).

PTC is increasing in incidence and although some of this is explained by an increase in incidental findings, the rise in overall mortality with PTC indicates that there is also a true rise in incidence too (Roman et al. 2017). The majority of PTC is treatable, by total thyroidectomy and adjuvant radioactive iodine treatment (Mazzaferri and Jhiang 1994). However, up to 20% of these tumours recur and recurrent disease brings an increased morbidity and mortality for the affected patients (Kruijff et al. 2014, Young et al. 2013).

1.2.1.2 Follicular thyroid cancer

Follicular thyroid cancer (FTC) is the next most common thyroid cancer and is also well differentiated. The histopathological definition of FTC is a malignant thyroid follicular cell neoplasm without the nuclear features observed in PTC. These are further categorised into: minimally invasive follicular carcinoma, encapsulated angioinvasive follicular carcinoma and widely invasive follicular carcinoma. The lack of nuclear features on histology means that it is not possible to differentiate follicular adenoma from adenocarcinoma on cytology – capsular invasion has to be assessed to determine malignant from benign (Paschke et al. 2017). This means that for follicular neoplasms diagnosed on fine needle aspirate cytology (FNAc) a diagnostic hemithyroidectomy is performed. Overall, the prognosis of follicular carcinoma is similar to that of papillary carcinoma once age and tumour extent at diagnosis are corrected for (Perros et al. 2014).

1.2.1.3 Hürthle cell carcinoma

Hürthle cell carcinoma has been reclassified into its own category due to the differences in molecular, oncological and histopathological characteristics (Cameselle-Teijeiro and Sobrinho-Simoes 2018) from FTC. The subtypes match those of the follicular tumours that they were previously categorised with. Separating Hürthle cell carcinoma from FTC should facilitate research into clinicopathological outcomes of this disease, helping to assess the long-term outcomes from this distinct pathology (Corver and Morreau 2019).

1.2.1.4 Poorly differentiated thyroid cancer

Poorly differentiated thyroid cancer (PDTC) is a category between differentiated thyroid cancer (DTC; papillary and follicular carcinoma) and anaplastic (undifferentiated) thyroid cancer. PDTC is diagnosed by use of the Turin classification, which is a consensus system to diagnose the dedifferentiation which is defined in part by tumour necrosis and high mitotic activity (Volante et al. 2007). These patients have a variable, but generally poor prognosis, characterised by late stage diagnosis, low radioactive iodine avidity and metastatic disease (de la Fouchardière et al. 2018).

1.2.1.5 Anaplastic thyroid cancer

Anaplastic thyroid cancer was formerly known as undifferentiated thyroid cancer. It has recently been defined as a progressive dedifferentiation from differentiated thyroid cancer via the accumulation of an increased mutational burden (Landa et al. 2016, Giordano 2018) (Figure 1.3). Anaplastic thyroid cancer has a devastatingly poor prognosis with median survival of four months (Smallridge et al. 2009). Even though

anaplastic thyroid cancers contribute to 1-2 % of all thyroid cancers, due to the associated morbidity results in a significant clinical burden (Smallridge et al. 2009).

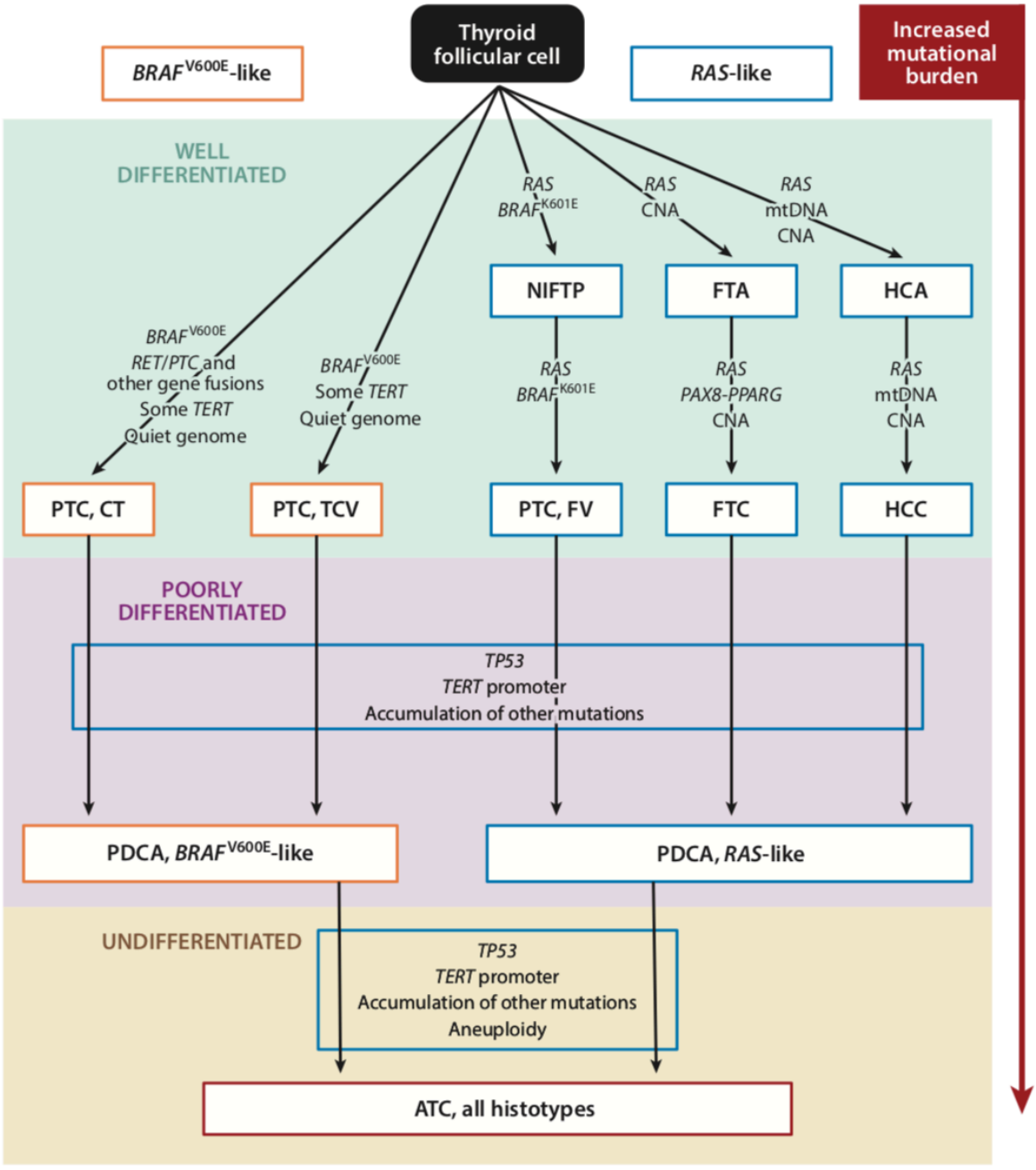

Figure 1.3: Progression from well differentiated (papillary and follicular) thyroid carcinoma to anaplastic thyroid cancer. Abbreviations: ATC, anaplastic thyroid (undifferentiated) carcinoma; CNA, copy number alterations; CT, classical type; FTA, follicular thyroid adenoma; FTC, follicular thyroid carcinoma; FV, follicular variant; HCA, Hürthle cell/oncocytic adenoma; HCC,

Hürthle cell/oncocytic carcinoma; mtDNA, mitochondrial deoxyribonucleic acid; NIFTP, noninvasive follicular neoplasm with papillary-like nuclear features; PDCA, poorly differentiated carcinoma; PTC, papillary thyroid cancer; TC, thyroid cancer; TCV, tall cell variant. From Giordano 2018.

1.2.1.6 Medullary thyroid cancer

Medullary thyroid cancer (MTC) arises from the parafollicular cells (C cell), which canonically secrete calcitonin. Calcitonin slows osteoclast activity and therefore regulates the amount of calcium and phosphate in the circulation, keeping a homeostatic balance countered by parathyroid hormone. Medullary thyroid cancer accounts for 1-2 % of thyroid cancer and is treated predominantly with surgery, as the parafollicular cells are not susceptible to radioiodide treatment. MTC is associated with multiple endocrine neoplasia (MEN) 2A and MEN2B syndromes. Nearly all MEN patients and up to 50 % of sporadic medullary thyroid cancers have mutations in the proto-oncogene RET (Wells et al. 2015). Due to the familial nature of medullary thyroid cancer, and its inherent lack of susceptibility to radioiodine it is categorised separately to the other differentiated thyroid cancers.

1.2.1.7 Other cancers of the thyroid

Other tumours of the thyroid arise from non-thyroid cells, such as lymphoma. There are also metastatic tumours from other tissues, and these are treated as determined by their original tissue type.

This thesis focusses predominantly on differentiated papillary thyroid cancer and associated recurrent disease.

1.2.2 Molecular profile of differentiated thyroid cancer

1.2.2.1 BRAF

BRAF is a serine/threonine-protein kinase that is the most powerful MAP kinase (MAPK) pathway driver (Caronia et al. 2011). This signal transduction pathway activates cellular proliferation, growth and survival (Cheng et al. 2018). The most common pathogenic mutation in BRAF is the missense mutation T1799A, which causes the valine (V) amino acid to be substituted for glutamic acid (E). This BRAF V600E mutation causes constitutive activation of the monomeric BRAF protein, which in its wildtype form is only activated as a homodimer, increasing MAPK signalling. Somatic BRAF V600E is associated with multiple tumours, including PTC, anaplastic thyroid cancer and melanoma (Cheng et al. 2018).

The increased activation of the MAPK pathway associated with BRAF V600E mutation results in a more aggressive thyroid cancer phenotype. This is in part due to the association of BRAF V600E with a reduction in radioiodide avidity, probably driven by the suppression of iodide metabolising genes. The presence of BRAF V600E not only reduced expression of TG, thyroid stimulating hormone receptor (TSHR), NIS and TPO but also reduced localisation of NIS to the plasma membrane (Xing 2007) where NIS is functional (Figure 1.2). While the BRAF V600E mutation can be used as a positive correlator with aggressive disease it is limited in its ability for negative predictive value, as other MAPK pathway-associated mutations can be alternative primary drivers of aggressive disease (Romei and Elisei 2012).

The overactivation of the BRAF-driven MAPK pathway has been therapeutically exploited with some clinical success in radioiodide resistant thyroid cancers. Initially, the multikinase inhibitor sorafenib demonstrated a partial response rate and increased progression-free survival in phase II clinical trials (Caronia et al. 2011). However, the considerable side effect profile of such drugs needs due consideration in such treatment. The BRAF inhibitor vemurafenib has been used in BRAF V600E mutant thyroid cancers which are radioiodine refractory and has successfully restored radioiodine uptake efficacy in some patients (Dunn et al. 2018). Similar findings have been observed with the BRAF kinase inhibitor dabrafenib (Rothenberg et al. 2015) which is FDA approved in melanoma. However, these do not appear to have an effect in all patients. Furthermore, for dedifferentiated tumours which acquire a heavy mutational burden it may be that multiple pathways require targeting (for example MAPK and PI3K/Akt) for effective therapy (Xing 2007, Ljubas et al. 2019).

1.2.2.2 RAS

Mutations of the Rat sarcoma (RAS) gene are the second most common mutation found in thyroid cancer (Howell et al. 2013). The RAS gene has three isoforms NRAS, HRAS and KRAS all of which are membrane-associated proteins that activate the MAPK pathway and the PI3K-Akt pathway. RAS is activated by GTP, and missense mutations cause abnormal activation by increased binding to GTP or reduction of GTP-ase activity. The most common mutation is NRAS Q61R (Cerami et al. 2012). A complicated feature of RAS mutations is the presence of RAS mutations in benign follicular adenomas (occurring in 48% of cases) as well as follicular thyroid carcinoma (57%) and papillary thyroid carcinoma (21%) (Howell et al. 2013), rendering it

ineffective as a diagnostic biomarker when used alone (Xing 2016). This suggests that RAS mutations are likely to be early events in thyroid carcinogenesis. Despite the association of RAS mutations with benign follicular disease, the presence of a RAS mutation in PTC has sometimes been associated with a poorer prognosis (Hara et al. 1994). The presence of RAS mutations in poorly differentiated and anaplastic thyroid cancers alongside p53, PTEN and PI3KCA gene mutations has been suggested to support the theory that RAS mutations occur early in oncogenesis and also strengthen the argument for de-differentiation of DTC to PDTC and ATC (Howell et al. 2013, Landa et al. 2016). Overall, the presence of a RAS mutation is associated with follicular thyroid adenoma, carcinoma and follicular-variant papillary thyroid cancer, and present a generally indolent, but variable tumour composition (Medici et al. 2015, Gupta et al. 2013).

1.2.2.3 RET/PTC

The rearranged during transfection (RET) proto-oncogene has a pathogenic role in thyroid carcinoma – it is a protein tyrosine kinase receptor influencing cell proliferation and differentiation (Romei and Elisei 2012). The RET/PTC rearrangement causes activation of the RET tyrosine kinase in thyroid cells, which causes upregulation of the MAPK pathway. PTC/RET rearrangements are associated with ionising radiation exposure (Romei and Elisei 2012), with the most common rearrangements being RET/PTC1 (fusion with CCDC6) and RET/PTC3 (fusion with NCOA4). Despite the clearly strong links to DTC, the RET/PTC rearrangement does not appear to influence the aggressiveness off DTC (Puxeddu et al. 2003) and does not have a role in diagnosis of PTC (Pizzolanti et al. 2007).

1.2.2.4 The PI3K/Akt pathway and its interactions with PTEN and PAX8/PPARG

The PI3K/Akt pathway modulates cell survival, cell cycle progression, differentiation and migration, and functions normally by PI3K phosphorylation of Akt, which is antagonised by PTEN (Robbins and Hague 2016). Further downstream to this are the tumour suppressor FOXO proteins and the mTOR pathway, which control protein synthesis and cell cycle progression (Massague 2004, Nozhat and Hedayati 2016). The pathway can be aberrantly activated by RAS mutations, which activate the pathway by binding PI3K, activating mutations in the PIK3CA gene, or inactivating mutations in the PTEN tumour suppressor gene (Robbins and Hague 2016).

PIK3CA mutations are found in aggressive PTC and anaplastic carcinomas and have been postulated to be predictive events for dedifferentiation. However, one study showed that while PI3K-Akt-MOR pathway mutations were present at a rate of 39%, the mutations were often not seen in the precedent papillary carcinoma pathology, suggesting this is a transformative event for such tumours (Oishi et al. 2017), which limits its prognostic applicability.

The PPARγ/Pax8 rearrangement is found in follicular thyroid neoplasia, as is RAS, although in follicular carcinomas RAS mutations and PPARγ/Pax8 rearrangements are distinct from each other and represent separate mutational drivers (Howell et al. 2013). The PPARγ/Pax8 rearrangement reduces PAX8 expression, which normally upregulates PTEN (Xing 2010) to affect PTEN control of the PI3K/Akt pathway.

The PI3K/Akt pathway is an alternative pathway (to the MAPK pathway) that is often over activated in thyroid cancer. This pathway appears to be of particular importance in FTC (Xing 2010) and has been postulated as an area of potential target in tumours needing chemotherapy (Nozhat and Hedayati 2016, Beadnell et al. 2018). Further to this, there is a putative role of Src inhibition (gatekeeping the PI3K/Akt pathway) in mediating resistance to inhibition of the MAPK pathway (Beadnell et al. 2018).

1.2.2.5 PBF

Pituitary tumour-transforming gene (PTTG)-binding factor (PBF; PTTG1IP) is a proto-oncogene by virtue of its upregulation in thyroid cancer. It is multifunctional protein involved in cell cycle modulation and genetic instability (Smith et al. 2011). In thyroid cancer it reduces the plasma membrane localisation of NIS, which causes a reduction in radioiodide effectiveness (Smith et al. 2011, Read et al. 2011). Further, PBF also destabilises the tumour suppressor p53 (Manzella et al. 2017, Read et al. 2017), facilitating thyroid cancer progression.

1.2.2.6 p53

Mutations of tumour protein p53 are found in cancers in a multitude of malignancies, and in thyroid cancer they are seen predominantly in anaplastic thyroid cancer (Fagin et al. 1993). Tumour protein p53 functions as an interesting tumour suppressor, where a mutation in one allele is enough for the action of p53 to be suppressed; these mutations are referred to as dominant negative mutants (Willis et al. 2004). p53 appears to be a late-stage ‘gatekeeper’ in thyroid cancer, with deregulation of p53

facilitating dedifferentiation of thyroid carcinoma into anaplastic thyroid cancers (McFadden et al. 2014) (Landa et al. 2016).

1.2.2.7 Telomerase-reverse-transcriptase promoter mutation

Telomerase-reverse-transcriptase (TERT) is a subunit of the telomerase enzyme that maintains telomeres. Normal cells undergo telomere shortening related to cell age, which cancer cells can evade by reactivating telomerase. The TERT promotor mutations C228T and C250T were first described in thyroid cancer in 2013 (Liu et al. 2013). TERT promotor mutations are activating and result in the maintenance of telomere length and tumour cell immortality (Gaspar et al. 2018) and are associated with a poorer outcome in papillary and follicular thyroid carcinomas, with a stronger prognostic value than BRAF V600E (Muzza et al. 2015). These mutations have been associated with transformation from differentiated thyroid carcinoma to anaplastic cancer (Oishi et al. 2017) and with radio-iodine resistance (Yang et al. 2017). Overall, the presence of a TERT promotor mutation is associated with a higher risk tumour, which is independent of the background BRAF status (Agarwal et al. 2014).

1.2.2.8 Eukaryotic Translation Initiation Factor 1A X-Linked (EIF1AX)

Mutations in Eukaryotic Translation Initiation Factor 1A X-Linked (EIF1AX) have been recently discovered in thyroid cancer (Agarwal et al. 2014). EIF1AX is a component of the translation pre-initiation complex (PIC) and therefore mutations in this gene can cause difficulties with translation initiation. EIF1AX co-occurs with RAS and is associated with a higher tumour aggressiveness (Simoes-Pereira et al. 2019). EIF1AX is seen more frequently in poorly differentiated and anaplastic carcinomas (Landa et

al. 2016) but conversely has also been demonstrated in follicular adenomas (Arivarasan et al. 2016). When discovered on diagnostic fine needle aspiration cytology (FNAc) of thyroid nodules the EIF1AX mutation confers a 20% risk of malignancy.

1.2.2.9 Summary

Papillary thyroid cancers are characterised by BRAF V600E mutations, or RAS mutations in the less aggressive subtypes, and can have RET/PTC rearrangements. Follicular thyroid cancers are dominated by RAS mutations, PPARγ/Pax8 rearrangements and inactivation of PTEN. Chromosomal rearrangements are associated with ionising radiation exposure (Nikiforov and Nikiforova 2011). EIFAX1 (RAS associated) and TERT promotor (BRAF associated) mutations confer a poorer prognosis. Anaplastic thyroid cancers derive from differentiated thyroid carcinomas and dedifferentiate by acquiring p53 mutations, PTEN inactivation or other dysregulation of the PI3K/Akt pathway and other genetic abnormalities (Manzella et al. 2017, Landa et al. 2016). While the mutational profiles of different subtypes of thyroid cancer are outlined here, there is not a well-defined mutational profile for recurrence in differentiated thyroid cancer.

1.3 Thyroid cancer management

1.3.1 Diagnosis of thyroid cancer

1.3.1.1 Clinical diagnosis

Thyroid cancer normally presents as a single nodule increasing in size, and symptomatically it presents as a painless enlarging anterior neck mass. However, thyroid nodules are common and are palpable on examination in 3-7% of all patients, with the majority of nodules discovered incidentally on radiological investigation for other conditions (Hegedus et al. 2003, Perros et al. 2014). In the UK, suspected thyroid cancer is managed according to the government 2-week wait pathway meaning urgent primary care referral for specialist investigation (Department of Health 2000). However, as a large proportion of thyroid nodules are benign, not all of these need fast-track referrals, including those with a longstanding history of goitre with no change, an incidental nodule less than one centimetre, deranged thyroid function or painful enlargement (Perros et al. 2014). These exclusion criteria do not apply in the presence of risk factors for thyroid cancer including history of neck irradiation, family history of thyroid cancer, cervical lymphadenopathy, stridor or voice change. All patients referred with suspected thyroid cancer should have a full examination of their neck and have their thyroid function checked. Patients will usually be referred for an ultrasound and if indicated a fine-needle aspiration cytology sample will be taken followed by the patient results being discussed at the multidisciplinary team (MDT) meeting.

1.3.1.2 Ultrasound

Ultrasound of the thyroid is an exceedingly sensitive test for thyroid nodules; 17 - 67 % of all patients have thyroid nodules detectable on ultrasound (Hegedus et al. 2003). The U classification system helps categorise nodules in terms of risk of malignancy, where U1 is normal, U2 is benign, U3 is equivocal/indeterminate, U4 is suspicious and U5 is malignant (Figure 1.4). A score of U3 – U5 would occasion a FNAc.

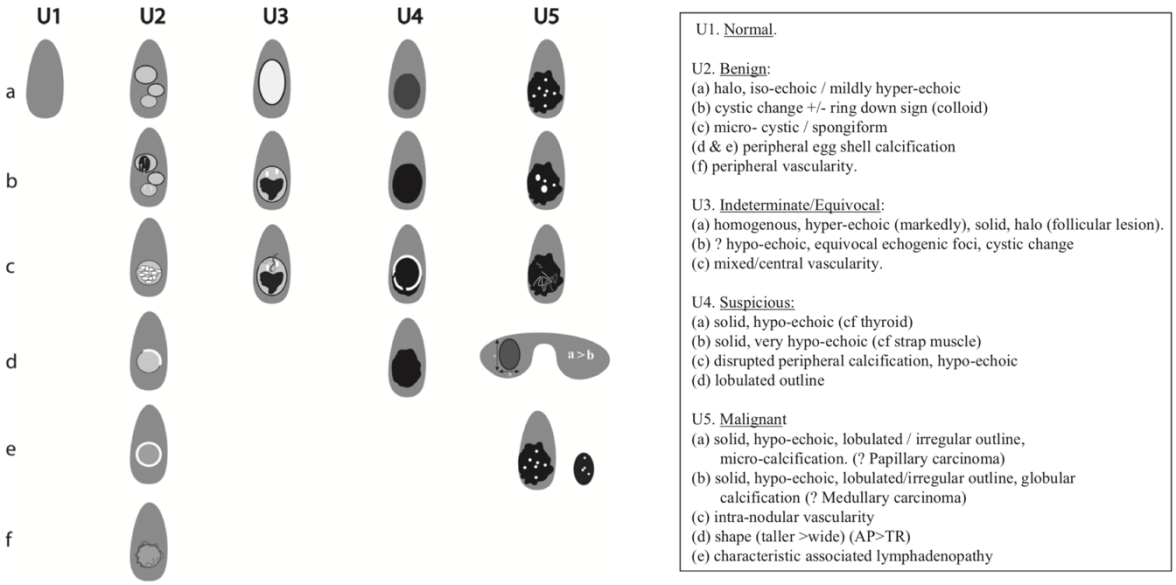

Figure 1.4: Ultrasound classification of thyroid nodules from the British Thyroid Association guidelines 2014. U1 indicates normal tissue, U2 benign tissue, U3 is equivocal/indeterminate, U4 is suspicious of malignancy and U5 indicates malignancy (Perros et al. 2014).

1.3.1.3 Fine needle aspiration cytology

Fine-needle aspiration cytology (FNAc) is performed predominantly under ultrasound guidance in Europe (Perros et al. 2014). Ultrasound helps with the decision to perform

an FNAc (section 1.3.1.2) and ultrasound guidance of FNAc improves the accuracy of sample acquisition (Cesur et al. 2006, Cai et al. 2006).

Following FNAc, the cytological report issued by the pathologist will usually include a diagnostic classification Thy category (Table 1.1). This helps determine how likely the lesion is to be malignant and determines the course of treatment decided by the multidisciplinary team meeting (MDT). In brief, a Thy1 nodule is non-diagnostic, Thy2 is benign, Thy3 is raises the possibility of malignancy, Thy4 is suspicious of malignancy and Thy5 is malignant. If a follicular lesion is seen on cytology, Thy3 is awarded, as the malignant potential of the lesion can only be diagnosed on examination of the entire neoplasm capsule (after diagnostic lobectomy).

Thy category	**Description**
Thy1	Non-diagnostic for cytological diagnosis
Thy1c	Non-diagnostic for cytological diagnosis: sample consistent with cyst fluid
Thy2	Non-neoplastic
Thy3	Neoplasm possible
Thy3a	Neoplasm possible due to cytological, nuclear or architectural atypia
Thy3f	Follicular neoplasm (cannot be distinguished as malignant or benign on cytology)
Thy4	Suspicious of malignancy
Thy5	Malignant

Table 1.1: Thy classification system for thyroid nodule cytology. From Guidance on the reporting of thyroid cytology specimens (The Royal College of Pathologists 2016).

1.3.2 Molecular markers in thyroid cancer

Molecular markers in the diagnosis of thyroid cancer is an emerging field, and currently no UK guidelines exist for this. The European Thyroid Association recommends the use of molecular markers in cytologically indeterminate nodules, but only comment on the detection of BRAF, RET/PTC, PPARγ/Pax8 and RAS mutations (Paschke et al. 2017). In the United States of America (USA) however, there is a market for predictive molecular marker testing in thyroid nodules. The American Thyroid Association (ATA) guidelines reflect this and recommend using molecular testing to supplement risk of malignancy assessment in the cytologically indeterminate lesions (Haugen et al. 2016).

Options for molecular testing in the USA include ThyroSeq3 (Steward et al. 2019), Afirma GEC (Veracyte) (Alexander et al. 2012), ThyGenX/ThyraMIR (Labourier et al. 2015) and Rosetta GX Reveal (Lithwick-Yanai et al. 2017) (Table 1.2); however, Rosetta Genomics tests are no longer available as the company filed for bankruptcy in 2018. ThyroSeq is based on targeted DNA and RNA next generation sequencing for 56 genes, combining mutations, gene fusions and gene expression. Afirma is an expression analysis of 167 mRNAs done with a two-step process, one step to screen, then a microarray for the classification step. ThyGenX/ThyrMIR is targeted sequencing for five mutations, three gene fusions and expression analysis of ten microRNAs. Rosetta GX Reveal is an expression analysis of 24 miRNAs by RT-PCR. These have limitations, including cost and a relatively low positive predictive value in cytologically indeterminate nodules. Long-term clinical outcome data is still awaited on the results of the molecular marker panels, negative predictive values are difficult to calculate as

a final histological diagnosis is not been made on lesions categorised as low risk (and not operated on). Further, for the Afirma GEC test the validation cohorts have been suggested to not be representative of the test population suggesting the sensitivity and specificity may be lower than originally reported (Valderrabano et al. 2019).

Commercially available test	Method	Sample	Sensitivity /specificity	NPV/PPV	Cost
ThyroSeq	DNA and RNA targeted NGS (56 genes)	1-2 drops from FNA	90/93 %	96/81 %	$4056
Afirma	Expression mRNAs (167 genes)	2 FNA passes	90/52 %	94/37 %	$6400
ThyGenX/ThyraMIR	Targeted NGS (8 genes) and RTqPCR (10 miRs)	1 FNA pass	89/85 %	94/74 %	$5675
Rosetta GX Reveal	Expression analysis of 24 miRNAs by qRT-PCR	1 smear or slide	74/74 %	92/43 %	$3700

Table 1.2: Commercially available molecular marker testing (in the USA) for thyroid nodules that are cytologically indeterminate. Showing the test method, sample required, sensitivity and specificity in determining malignancy in cytologically indeterminate nodules, negative predictive value (NPV) and positive predicative value (NPV) in cytologically indeterminate nodules and the cost. Table adapted from (Nishino and Nikiforova 2018).

The idea behind molecular testing is to improve the diagnostic accuracy of fine needle aspirate samples, and therefore a lot of the products focus on indeterminate cytology samples (Thy3). There has however been an application advocated for the use of molecular markers to stratify whether tumours need full therapeutic surgery over diagnostic surgery, for example in the presence of a BRAF V600E mutation, which confers a 99.3 % risk of malignancy (Nikiforov et al. 2013). BRAF V600E mutations also confer a risk of central lymph node metastasis and therefore it has been suggested that this could be used to decide on the extent of surgery (Nikiforov et al. 2013).

Individual molecular markers are not as effective as a panel of markers, evidenced by the lack of positive predictive value of BRAF V600E alone in papillary microcarcinoma (Haugen et al. 2016). A panel of clinical biomarkers could be effective, and if this took into account risk of recurrence the therapeutic impact could range from tailoring treatment to managing patient follow-up.

1.3.3 Treatment of thyroid cancer

Current first line treatment options for differentiated thyroid cancer are surgical resection and post-operative radioiodide treatment. When diagnostic surgery is indicated, as in the case of Thy3 follicular neoplasms, a lobectomy will be performed, and following a formal diagnosis further treatment will be provided, if indicated. This means that the patients with benign disease, NIFTP or very low risk disease may not need any further treatment. This avoids a total thyroidectomy, eliminating the need for lifelong treatment with thyroid hormone supplements, and circumventing the risk of hypocalcaemia. Those patients with tumours > 4 cm, multifocal disease, extra-thyroidal spread, familial disease, Hürthle cell carcinomas > 1 cm, lymph node metastasis or distant metastasis require total thyroidectomy (Perros et al. 2014). Risks of thyroidectomy include damage to the recurrent laryngeal nerve (voice hoarseness), damage to the superior laryngeal nerve (loss of voice projection), hypocalcaemia (due to damage to or loss of parathyroid glands) (Mazzaferri and Jhiang 1994), post-operative haematoma and a scar. Patients who have had a total thyroidectomy will need lifelong thyroxine to replace endogenous hormones. Surgery is a key part of the patient's therapy and the American Thyroid Association Guidelines go so far as to say

that adequate surgical resection is the most important treatment variable influencing patient outcomes (Cooper et al. 2006).

After total thyroidectomy, some patients will require postoperative radioactive iodine remnant ablation. There are considerations associated with radioiodine treatment including a hospital isolation period, need for pregnancy avoidance (6 months) or avoidance of fathering a child (4 months), and risks include painful thyroiditis, radiation cystitis, gastritis, metastasis oedema, nausea, sialadenitis and xerostomia (Perros et al. 2014). Benefits include eradication of all thyroid tissue to reduce subsequent risk of local and distant tumour recurrence and increased sensitivity of thyroglobulin as a monitoring marker (Perros et al. 2014)(section 1.3.4.1). The decision to give radioiodine treatment is an MDT decision based on the patient's staging (section 1.3.3.1), histopathology and individual circumstances, but a patient with a tumour over 4 cm, extra thyroidal extension or metastasis would have radioiodine therapy recommended. Classical papillary, follicular variant papillary or follicular tumours less than 1 cm with no angioinvasion or capsular invasion will not normally derive overall benefit from radioiodine treatment (Figure 1.5).

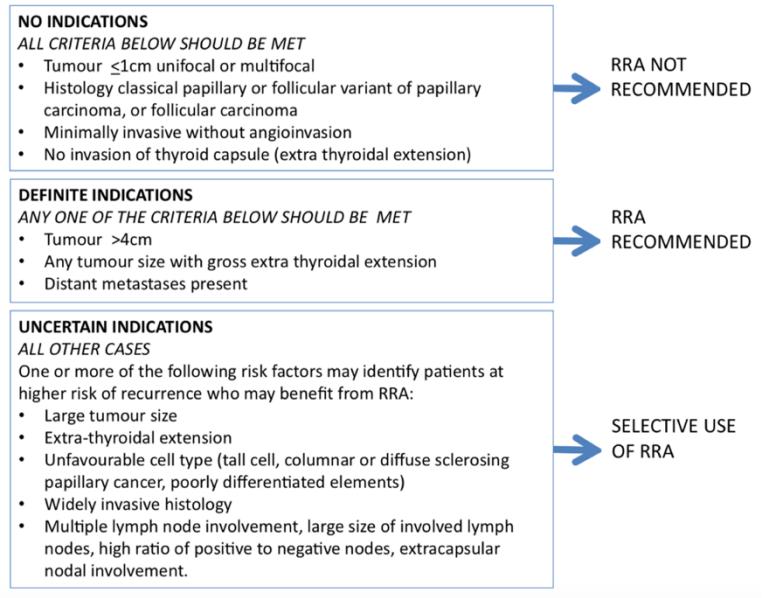

Figure 1.5: British Thyroid Association (BTA) Guidelines for the Management of Thyroid Cancer indications for radioiodine remnant ablation (RRA), image taken from BTA guidelines.

1.3.3.1 TNM staging

Tumour Node Metastasis (TNM) Classification of Malignant Tumour (Sobin 2011) is used to stage thyroid cancer in order to record the anatomical extend of the disease. This helps categorise the risk of disease progression and recurrence, and therefore determine the extent of patient treatment and the intensity of follow up (Table 1.3) (Cooper et al. 2006).

TNM Classification of Malignant Tumour	
Primary tumour	
TX	Primary tumour cannot be assessed
T0	No evidence of primary tumour
T1	Tumour ≤2 cm in greatest dimension limited to the thyroid
T1a	Tumour ≤1 cm, limited to the thyroid
T1b	Tumour >1 cm but ≤2 cm in greatest dimension, limited to the thyroid
T2	Tumour >2 cm but ≤4 cm in greatest dimension, limited to the thyroid
T3	Tumour >4 cm limited to the thyroid or gross extrathyroidal extension invading only strap muscles
T3a	Tumour >4 cm limited to the thyroid
T3b	Gross extrathyroidal extension invading only strap muscles (sternohyoid) from a tumour of any size
T4	Includes gross extrathyroidal extension into major neck structures
T4a	Gross extrathyroidal extension invading subcutaneous soft tissues, larynx, trachea, oesophagus, or recurrent laryngeal nerve from a tumour of any size.
T4b	Gross extrathyroidal extension invading prevertebral fascia or encasing carotid artery or mediastinal vessels from a tumour of any size
Regional lymph nodes	
NX	Regional lymph nodes cannot be assessed
N0	No evidence of regional lymph node metastasis
N0a	One of more cytologic or histologically confirmed benign lymph node
N0b	No radiologic or clinical evidence of locoregional lymph node metastasis
N1	Regional lymph node metastasis
N1a	Metastases to Level VI (pretracheal, paratracheal, and prelaryngeal/Delphian or upper mediastinal) lymph nodes; this can be unilateral or bilateral disease
N1b	Metastases to unilateral, bilateral, or contralateral cervical (Levels I, II, III, IV, or V) or retropharyngeal lymph nodes
Distant metastasis	
M0	No distant metastasis
M1	Distant metastasis
Residual tumour	
Rx	Cannot assess presence of residual primary tumour
R0	No residual primary tumour
R1	Microscopic residual primary tumour
R3	Macroscopic residual primary tumour

Table 1.3: TNM Classification of Malignant Tumour (8th edition).

1.3.4 Management after treatment of thyroid cancer

1.3.4.1 Thyroglobulin surveillance

Routine follow up after thyroid surgery for malignant thyroid disease includes neck examination and measurement of thyroid status, with abnormalities further investigated (usually initially with ultrasound). Thyroglobulin is checked postoperatively in patients who have had total thyroidectomy and radioiodine treatment, in order to monitor treatment outcomes and recurrence. These patients are undergo dynamic risk stratification – all patients have an initial risk stratification based on histopathological data, and those that have thyroidectomy and radioiodine treatment are reclassified according to their treatment response. Using the post treatment stimulated thyroglobulin, whole body scan and neck ultrasound they are then stratified in to the following groups: excellent response, indeterminate response or incomplete response. This then allows a more personalised approach to treatment and follow up and more information for clinician and patient about prognosis (Perros et al. 2014).

Detectable thyroglobulin after total thyroidectomy and radioiodine ablation indicates residual or recurrent thyroid tissue and an increase in thyroglobulin while on suppressive thyroxine therapy (section 1.3.4.2) is indicative of recurrence (Perros et al. 2014). Thyroglobulin is produced by thyroid cells, malignant and benign, and therefore cannot be used as a marker of progression or recurrence in patients who have undergone hemithyroidectomy only. An alternative to sequential thyroglobulin measurements is stimulated thyroglobulin, which is induced by use recombinant TSH (rhTSH) (historically done by removal of suppressive thyroxine therapy) (Robenshtok and Tuttle 2012). However, there are limitations to the use of serum thyroglobulin: the

levels are rendered unreliable in the presence of thyroglobulin antibodies (Verburg et al. 2004) and the positive predictive value is low at <40 % (Gray et al. 2018). Patients with a positive thyroglobulin are further investigated with imaging, usually an ultrasound neck and radioiodide uptake whole body scan. Thyroglobulin is currently used as a monitoring tool for recurrence, rather than as part of the risk stratification for thyroid cancer recurrence.

1.3.4.2 TSH in malignancy and post-operative TSH suppression

Thyroid stimulating hormone levels are checked during a patient's assessment for a thyroid nodule in order to assess their thyroid status. A higher TSH at presentation of a thyroid nodule or mass has been associated with an increased likelihood of a cancer diagnosis (Boelaert et al. 2006, Nieto and Boelaert 2016). Further, a higher TSH at presentation has been associated with advanced disease and lymph node metastasis but not recurrence (Fiore et al. 2009, McLeod et al. 2012). While the association of TSH and malignancy is replicated and widely accepted, it has not yet been integrated into clinical pathways (Nieto and Boelaert 2016).

Suppressing serum TSH postoperatively for patients who have had total thyroidectomies reduces the rate of thyroid cancer recurrence (Pujol et al. 1996) and improves differentiated thyroid cancer disease-specific survival (Mazzaferri and Jhiang 1994). TSH is a growth factor for the thyroid, and effects nodules in the same way. It is considered that TSH suppression can prevent formation of new nodules as well as inhibit progression of current nodules (Papini et al. 1998). Therefore, it is widely accepted for patients to have TSH suppression after treatment in the early post-operative period (Haugen et al. 2016) and some have advocated for aggressive TSH suppression in more advanced, higher stage disease (Jonklaas et al. 2006).

There are risks associated with TSH suppression; subclinical hyperthyroidism has been demonstrated to have detrimental health consequences. These repercussions include cardiovascular risks such as atrial fibrillation and coronary heart disease (Collet et al. 2012). There has also been a reported association with reduced cognitive

function and dementia (Annerbo 2013), as well as osteoporosis (Biondi et al. 2015, Polovina et al. 2015). The BTA guidelines (Perros et al. 2014) endorse utilising the Fracture Risk Assessment Tool (FRAX) score (Kanis et al. 2008) to determine fracture risk in those on suppressive therapy for longer than 5 years during follow up. Overall, the current guidelines recommend against the use of TSH suppression in those not treated with radioiodine therapy or with low risk tumours (Haugen et al. 2016, Perros et al. 2014). However, high risk tumours are still indicated for TSH suppressive therapy. Therefore, despite the potential use of TSH as an aid adjunct in a diagnostic setting, TSH will not be helpful in a post-operative disease monitoring capacity.

1.3.5 Management of thyroid cancer recurrence

Thyroid cancer recurrence is associated with increased mortality (Kruijff et al. 2014, Young et al. 2013). Early detection of thyroid cancer recurrence is thought to improve patient outcomes (Cooper et al. 2006, Perros et al. 2014). Patients with an elevated thyroglobulin should be investigated with an ultrasound scan of the neck. Fine-needle aspirate cytology should be performed on any abnormal neck masses post-treatment (Perros et al. 2014). Distant metastases occur in 5 – 23 % of differentiated thyroid cancer patients (Perros et al. 2014) so if ultrasound is negative, computed tomography (CT), ^{18}fluoro-deoxy-glucose (FDG)-positron emission tomography (PET)-CT, magnetic resonance imaging (MRI) or ^{131}I whole body scintigraphy (WBS) is indicated. WBS is dependent on the lesion being radioiodine avid, and often PET-CT positive lesions are not.

Curative surgery is the treatment of choice for recurrent disease, although particularly indolent disease can be managed by active surveillance (Perros et al. 2014). Residual disease post-surgical resection can be managed with radioiodine treatment. Distant metastasis to the lungs or soft tissues should be treated with radioiodine therapy. Pre-treatment radioiodine uptake stimulation by rhTSH is often performed to increase radioiodine uptake. After radioiodine treatment WBS should be performed, used alongside serial thyroglobulin measurement to assess the response to radioiodine treatment (Pacini et al. 2006). Disease remission can be achieved in two thirds of thyroid cancer patients with recurrence in the neck, and in a third of those with distant metastasis, and for both, remission is more likely if the tumour burden is small (Pacini et al. 2006). This supports to the argument that early detection of recurrence is important in determining patient outcomes.

1.3.6 Management of radioiodine refractory recurrence

Distant metastases of differentiated thyroid cancer are often not radioiodine avid (Perros et al. 2014), and are particularly difficult to treat. As discussed, the primary management of thyroid neck recurrence is surgical, but any residual disease is managed with radioiodine if it is radioiodine avid (Haugen et al. 2016). If not amenable to surgery, radioiodine refractory disease can be considered for high-dose external beam radiotherapy (EBRT) (Pacini et al. 2006). Sometimes radioresistant disease can be indolent and can be monitored (Haugen et al. 2016). For rapidly progressive, symptomatic or imminently threatening disease not amenable to local control, kinase inhibitor therapy can be considered (Haugen et al. 2016). Cytotoxic chemotherapy has historically been very disappointing in affecting non-radioiodine avid thyroid cancer

outcomes but VEGF targeting kinase inhibitors have emerged as a potential therapy (Anderson et al. 2013). A phase III trial of sorafenib (the DECISION trial) demonstrated an increase in disease-free survival from 5.8 months to 10.8 months (compared to placebo HR 0.59, $p<0.0001$) (Brose et al. 2014), although grade 1 or 2 adverse effects were frequent (50.2 – 76.3 %). This is an exciting development for this subset of patients who otherwise have a life expectancy of 3 – 5 years and limited treatment options (Schlumberger et al. 2014). The SELECT trial (Schlumberger et al. 2015) led to the multikinase inhibitor lenvatinib becoming the other National Institute for Health and Care Excellence (NICE) approved treatment for progressive, locally advanced or metastatic differentiated thyroid cancer that is resistant to radioiodine (National Institute for Health and Care Excellence 2018). Lenvatinib inhibits vascular endothelial growth factor receptors 1, 2, and 3, fibroblast growth factor receptors 1, 2. 3 and 4, platelet-derived growth factor receptor α, RET, and KIT (Schlumberger et al. 2015). Both lenvatinib and sorafenib delay disease progression, but there is a higher response rate and an improvement in symptoms with lenvatinib; the survival benefit for sorafenib is 13 months and for lenvatinib is 25 months (National Institute for Health and Care Excellence 2018).

Despite this progress, most patients eventually stop responding to sorafenib (Dadu et al. 2014) and almost all patients on either drug had an adverse event (Schlumberger et al. 2015, Brose et al. 2014). Data for the use of cytotoxic chemotherapy in differentiated thyroid carcinoma is disappointing (Haugen et al. 2016). Further development of therapies for radioiodine refractory patients is required. Targeted therapy on an individual patient molecular make up or therapy to boost radioiodide

responsiveness may be key to this. Understanding which thyroid carcinomas are going to recur, and the functional reasons behind the recurrence is important in improving patient care.

1.4 Recurrence in thyroid cancer

1.4.1 Recurrence in cancer

1.4.1.1 Definition of cancer recurrence

Cancer recurrence is presence of disease after the patient has been in a disease-free state. The American Thyroid Association define disease-free status in thyroid cancer as no clinical evidence of tumour, no radiological evidence of tumour (RAI or ultrasound) and no biochemical evidence of disease (unstimulated thyroglobulin <0.2ng/mL or stimulated <1ng/mL) (Haugen et al. 2016). This is an important distinction from residual disease, which is thyroid tissue left behind post-operatively, either due to proximity to important structures (such as the recurrent laryngeal nerve) or by omission.

1.4.1.2 Mechanisms of recurrence

For a malignancy to recur, the primary disease must evade treatment. Tumour cell dormancy has been postulated as a means by which cancer cells achieve this (Paez et al. 2012). The most common site of recurrence in papillary thyroid carcinoma is the cervical lymph nodes (Cooper et al. 2009) and it is considered that metastatic dormancy is a key component of how cancer cells survive but do not progress immediately in a metastatic environment (Ringel 2011). The identification of cancer

cells in adequately treated patients lends support to the dormancy theory, and it could contribute to explaining how some thyroid cancer patients recur many years after their primary disease (Ringel 2011). An important concept then, is how dormant cancer cells activate to cause such recurrence.

There have been several theories presented about escape from dormancy for the thyroid cancer cell, and these include: metastasis suppressors (genes that maintain quiescence in single metastatic cells), instigation of angiogenesis, modulation of immune surveillance and changes in the extracellular matrix (Ringel 2011). Limitations on angiogenesis has been proposed as a natural defence against cancer occurrence and progression (Folkman and Kalluri 2004). The theory of angiogenesis factors limiting dormant cell growth is supported by the use of vascular endothelial growth factor (VEGF; an angiogenic factor) inhibitors to stabilise metastatic thyroid disease (Brose et al. 2014, Ringel 2011). VEGF immunostaining has been associated with thyroid cancer recurrence and decreased survival, adding weight to the importance of angiogenesis in thyroid cancer recurrence (Lennard et al. 2001). The immune system is also implicated in thyroid cancer recurrence, attacking malignant cells with cytotoxic T cells supported by T helper cells. However, T regulatory (T-reg) cells prevent autoimmunity, and in the context of solid tumours can protect cancer cells from being recognised as foreign (Beyer and Schultze 2006). Further, Forkhead box (FOX) P3 T regulatory cells have also have been shown to induce dormancy (Farrar et al. 1999). This is mediated by T-reg cell secretion of interferon gamma (IFNγ) and tumour necrosis factors (TNF) as potent anti-angiogenic factors, and disruption to this can cause tumour progression (Wieder et al. 2008). T reg cells have been positively

correlated with recurrence free survival in non-small cell lung cancer (Shimizu et al. 2010) and higher frequencies of T reg cells in papillary thyroid cancer recurrence (French et al. 2012). It has been suggested that the presence of T reg cells in thyroid cancer patient lymph nodes (upon excision) can be used to screen suspicious nodes (French et al. 2012). However, this would be dependent on excision biopsy, which is a major drawback to using these as a recurrence biomarker. The role of the immune system in cancer recurrence is well summarised by the elimination, equilibrium, and escape model (Phay and Ringel 2013, Oleinika et al. 2013), with T reg cells facilitating the equilibrium or dormant phase. The escape phase then represents the further proliferation of tumours cells that manifests as recurrence.

Dormancy is an interesting theory in the context of thyroid cancer, supported by a subgroup of patients with indolent disease, who are evidenced by the discovery of malignant thyroid nodules on autopsy (Phay and Ringel 2013). Dormancy is often explained as tumour cells achieving quiescence and thereby avoiding cancer treatments. An alternative explanation is that micrometastases are present and are kept in equilibrium by equal proliferation and apoptosis rates (Wikman et al. 2008). As thyroid cancer is treated differently to most other malignant disease this limits the extent to which tumour cell quiescence can explain recurrence in thyroid cancer. Chemotherapeutic agents are normally effective because of their ability to select tumour cells which have high turnover (Oleinika et al. 2013), thus a dormant cancer cell may evade this. However, in the case of ablative therapy for thyroid cancer, the radioactive iodine targets all thyroid cells, both malignant and benign. This means that if tumour cell dormancy is aiding treatment evasion, the cells must have considerable

metabolic shutdown, for example not be taking up iodine. Otherwise, the recurrent cancer cells must also be able to escape RAI treatment through another pathway. This provides a possible explanation for why most lymph node metastases in recurrence are non-RAI avid (Perros et al. 2014), but does not explain how this occurs.

One further factor is the tumour cell interaction with its microenvironment, which has been recognised as a key regulator in cancer progression (Fidler 2002). The extracellular matrix (ECM) affects tumour dormancy, with cells that fail to adhere to the ECM entering a state of dormancy (Barkan et al. 2010). In order to escape dormancy, cells need to adhere to the ECM via integrin receptors, which induces cell proliferation, and changes in the ECM components, such as an increase in production of type I collagen and fibronectin (Barkan et al. 2010). In breast cancer cells a study demonstrated the transition from quiescence to proliferation to be dependent on fibronectin signalling through integrin β1, which binds to integrin α1, α2 or α3 to form an integrin heterodimer receptor (Barkan et al. 2008). Activation of the integrin receptor has a downstream effect on transforming growth factor β, focal adhesion kinase (FAK) and Src kinase (SRC), which may be part of the dormancy-progression switch (Ringel 2011). Previously, FAK activation has been implicated in lung metastasis (Shibue and Weinberg 2009). Overall, this demonstrates that activation of tumour cells, a likely component of recurrence in thyroid cancer, is dependent on ECM-tumour interaction.

Cellular invasion is a component of thyroid cancer recurrence, and epithelial to mesenchymal transition (EMT) has been implicated in thyroid cancer invasion (Vasko et al. 2007). EMT produces a change in the morphology and the motility of cells, where

cells become fibroblast-like, lose cell-cell contact receptors, have increased activity of cell movement adhesion molecules and increased proteolysis of ECM components (Shakib et al. 2019) (Figure 1.6). Conversely, some ECM proteins such as periostin and fibronectin (FN1), appear to be upregulated in EMT with FN1 being more highly expressed in PTC patients with lymph node metastasis and advanced stage PTC (Shakib et al. 2019). In follicular thyroid cancer, it has been shown that hypoxia drives hypoxia inducible factor-1α (HIF-1α) production, which in turn can induce EMT (Yang et al. 2015). Furthermore, the c-Met/PI3K/Akt signalling pathway has also been implicated as part of the EMT (Gao and Han 2018) (Figure 1.6). The EMT process has been shown to confer stem cell-like properties to cancer cells, and cancer stem cells (CSCs) have been suggested as a possible pathway to recurrence and metastatic thyroid disease (Shakib et al. 2019).

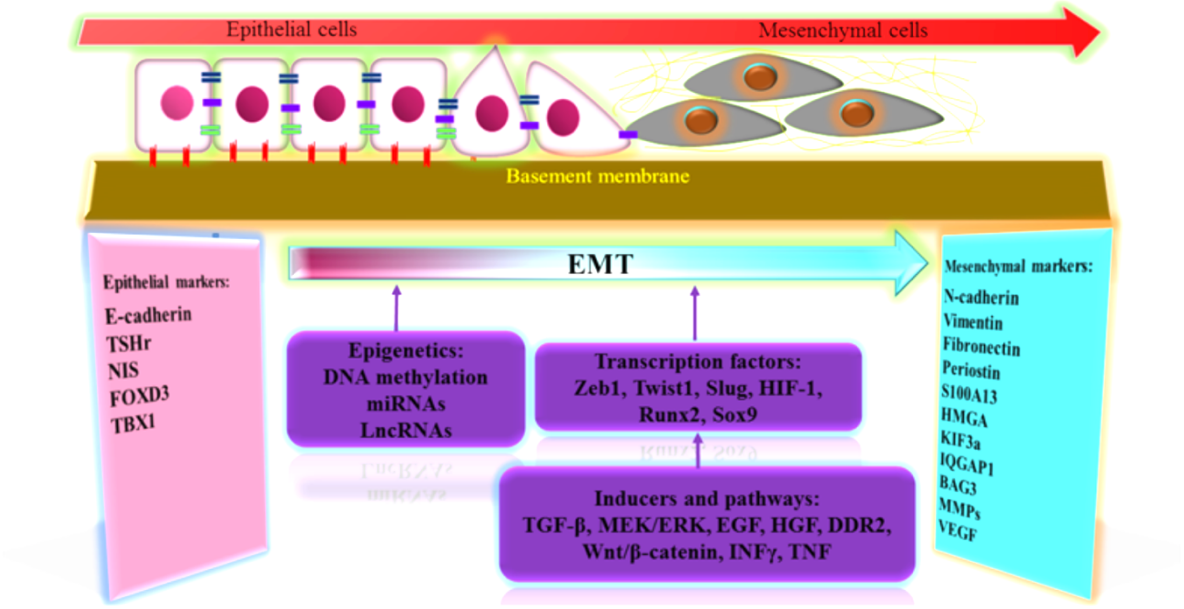

Figure 1.6: The progression through the epithelial-mesenchymal transition. Implicated pathways including MEK/ERK, HGF (c-MET) and Wnt are highlighted and mesenchymal markers listed. Taken from Shakib et al. 2019.

There are several mechanisms that are likely to contribute to thyroid cancer recurrence. Increased angiogenesis, escape from the immune system, and changes in the extracellular matrix are three components that are likely to be implicated. Investigating the mutations and pathways involved in thyroid cancer recurrence to identify significant biomarkers is important due to the significant morbidity and mortality associated with recurrence. In this thesis, next generation sequencing was employed to investigate the mutational profile and gene expression of thyroid cancer recurrence.

1.5 Next-generation sequencing

1.5.1 Next generation sequencing

Next generation sequencing (NGS) describes either whole genome sequencing (WGS) or whole exome sequencing (WES) of DNA and represents high-throughput sequencing. NGS platforms sequence millions of small fragments of DNA in parallel and are both faster and more efficient than the original Sanger sequencing (Sanger et al. 1977), which uses a chain termination method. The human genome was sequenced for the first time simultaneously by two parallel groups, one US government-funded group led by Francis Collins, the other a private group led by Craig Venter, using the shotgun sequencing approach that accelerated mapping the whole genome (Venter et al. 2001, Lander et al. 2001). It was following this that high-throughput sequencing systems began to revolutionise genomic research.

1.5.2 Next generation sequencing platforms

Next generation sequencing can be performed on multiple different modern sequencing platforms. NGS platforms are available from Illumina, Ion torrent and Roche 454, and long read sequencers are available from Oxford Nanopore and PacBio. Each of these platforms performs high-throughput sequencing using different techniques for sequence reading, with each modality providing different benefits. Illumina sequencing works by adhering short DNA fragments to a slide, which are amplified by PCR, then addition of fluorescently labelled bases to a complimentary nucleic acid chain which creates a fluorescent signal which can be detected by the sequencing computer. This technique is quick, efficient and therefore competitively priced, but produces short reads. Ion torrent utilises proton signalling for detecting the addition of bases as the pH is lowered by the release of a proton (H^+) on base addition. The bases are flooded in sequentially, one base at a time, so the sequencing computer can read which base is next in the sequence. Roche 454 again uses fragmented reads of DNA, but these are longer (1kB), and adhered to beads. The addition of a dNTP to the template DNA causes pyrophosphate group release, which produces ATP, which then activates fluorescein molecules causing fluorescence, again read by the sequencing computer software. Each base is added sequentially, so fluorescence only occurs when the correct base is added. For each of these methods bioinformatic techniques are then used to map the short reads to the human genome. Long read sequencers use nanopores to sequence long reads by reading the light or electrical signal produced as each base goes through a pore, creating much longer strands of DNA, especially useful in mapping a novel genome (Mardis 2013, Liu et al. 2012).

Due to technological advancements and market competition, the cost of sequencing has decreased rapidly over the last decade (Carlson 2009), meaning next generation sequencing is becoming more accessible (National Human Genome Research Institute 2016). More recently, RNA sequencing has been driven forward in advancement by the high throughput technology, as once RNA is converted to cDNA the process is the same as DNA sequencing. Whole exome sequencing is predominantly used in a research context, but clinical application of targeted gene sequencing is widening. However, whole exome sequencing must be interpreted carefully as results are not yet always clinically meaningful due to the lack of functional understanding of many genes. Therefore, further investigations into somatic mutations are helpful in a wider context.

1.5.3 NGS databases

1.5.3.1 The Cancer Genome Atlas (TCGA)

The Cancer Genome Atlas (TCGA) is a landmark cancer genomics program and is a collaboration between the National Cancer Institute (NCI) and the National Human Genome Research Institute (NHGRI). Most data are open access, although the raw data are under controlled access. The data present have propagated growth in computational biology, and have led to the development of many analysis tools, including cBioportal (Cerami et al. 2012), Broad GDAC Firehose (http://gdac.broadinstitute.org) (Broad Institute TCGA Genome Data Analysis Center 2019a) and Broad GDAC FireBrowse (http://firebrowse.org) (Broad Institute TCGA Genome Data Analysis Center 2019b).

1.5.3.2 The Catalogue of Somatic Mutations in Cancer (COSMIC) database

The Catalogue of Somatic Mutations in Cancer (COSMIC) is a database of somatic mutations in human cancer, predominantly hand-curated from both papers and other databases. This collates all information about somatic mutations and their implications for human disease. Currently the database includes over six million exonic mutations and over a million tumour samples and incorporates many bioinformatic scoring tools to help determine the pathogenicity of somatic mutations (Tate et al. 2018). The availability of such open access databases has advanced the understanding of somatic mutations and can aid the validation of findings in research.

1.5.4 Future role of NGS in precision medicine

Historically, only a few diseases with highly specific gene mutations, such as cystic fibrosis (CF) and mutations in the cystic fibrosis transmembrane conductance regulator (CFTR) gene, were compatible with genetic sequencing (Brittain et al. 2017). Diseases such as CF are compatible with highly targeted sequencing, however not many diseases have such a clear single causative gene. Targeted sequencing has also been applied in cancer therapy, where the presence of mutations on the genes BRCA1 and BRCA2 can help individualised risk reduction (Brittain et al. 2017). Therapies in breast cancer may also be tailored to the individual, for example trastuzumab, a humanised IgG1 monoclonal antibody, can be used if the breast cancer tumour overexpresses the oncogene HER2 (Jackson and Chester 2015). This is the beginning of precision medicine, where therapy is tailored to the individual patient.

Next generation sequencing can now provide much more mutational data than was previously accessible. This is useful in cancer genomics where there is a complexity of mutations but is currently limited by the functional and clinical information available on mutations. There are now therapies in other cancers that are being adopted as potential personalised therapies, the most prominent being vemurafenib in melanoma and thyroid cancer (BRAF/MAPK pathway inhibitor), cetuximab in colorectal cancer (monoclonal EGFR antibody), and imatinib in chronic myeloid leukaemia (CML) and gastrointestinal stomal tumours (receptor tyrosine kinase inhibitor) (Jackson and Chester 2015). Future clinical application of NGS in cancer will potentially mean each patient has a tumour signature diagnosed, leading to targeted treatment options and accurate classification of risk of tumour progression and recurrence (Jackson and Chester 2015).

1.6 Aims and Hypothesis

Thyroid cancer is the most common endocrine cancer and is rising in incidence. It is generally a treatable disease, with excellent survival rates of over 90% at 10 years (Sipos and Mazzaferri 2010). However, there is a high recurrence rate and patients with surgically inoperative recurrence or radioiodine resistant differentiated thyroid carcinoma have a very poor prognosis and high mortality rate, as do those with anaplastic thyroid cancer (Katoh et al. 2015). Increased understanding of the molecular pathogenesis of thyroid cancer has led to new possible treatment strategies for these difficult to treat patients (Brose et al. 2014, Dadu et al. 2014). Treatment for thyroid cancer can be tailored to the individual patient, to make sure they get adequate treatment, and also are not overtreated, important for both the patient and the

healthcare system. Currently this is achieved via clinical risk factors, but with an expanding understanding of molecular markers it is possible that these could be adopted for risk stratification. Alongside radioiodine-resistant thyroid cancer, the poor outcomes associated with thyroid cancer recurrence means selecting out high-risk patients is the most important challenge in thyroid cancer (Katoh et al. 2015).

Overall, the objectives of this thesis are to complete the first full NGS appraisal of recurrent thyroid cancers to identify new biomarkers which predict tumour recurrence, to perform in vitro investigations to determine function of these biomarkers, and to discover how these biomarkers relate to the clinical outcome of thyroid cancer patients.

I hypothesise that thyroid tumours which subsequently recur display a distinct pattern of driver mutations, or RNA and microRNA expression patterns, and that the molecular characterisation of these alterations will reveal novel mechanisms involved in thyroid tumour recurrence. In the longer term, the pathways of recurrence will aid clinicians and patients with accurate prognosis, facilitating the tailoring of individual patient treatments.

Chapter 2 Materials and Methods

2 Materials and Methods

2.1 Cell culture

Three cell lines were cultured for cell line based assays: the human differentiated papillary thyroid cancer TPC-1 cell line, human anaplastic thyroid cancer SW1736 cell line and human de-differentiated thyroid cancer Cal-62 cell line. The TPC-1 and SW1736 cell lines were kindly provided by Dr Rebecca Schweppe (University of Colorado; Colorado, USA). TPC-1 cells are derived from a moderately differentiated human papillary thyroid carcinoma, with mutational rearrangement on chromosome 10 causing the RET/PTC1 chimera (Ribeiro et al. 2008, Ishizaka et al. 1990) with wildtype BRAF and RAS. The SW1736 cell line is derived from an anaplastic thyroid tumour and contains the BRAF (V600E) mutation (Lee et al. 2007, Schweppe et al. 2008). The Cal-62 cell line was kindly provided by Professor James Fagin (Memorial Sloan Kettering Cancer Centre; New York, USA). Cal-62 cells are derived from undifferentiated human thyroid cancer cells and harbour a RAS mutation (KRAS G12R) (Gioanni et al. 1991). These cell lines were cultured in Roswell Park Memorial Institute (RPMI)-1640 media with L-glutamine (Life Technologies, ThermoFisher Scientific; Massachusetts, USA) supplemented with 1 % Penicillin (10^5 U/l)/Streptomycin (100 mg/l) (Life Technologies) and 10 % heat-inactivated foetal bovine serum (FBS) (Life Technologies).

For immunofluorescence the human cervical carcinoma HeLa cell line was also used. HeLa cells are derived from a cervical epidermoid carcinoma and provide a malignant epithelial cell line (Landry et al. 2013). The HeLa cell line was sourced from the

European Collection of Authenticated Cell Cultures (Salisbury, UK). HeLa cells were cultured in Dulbecco Modified Eagle's Media (DMEM) supplemented with 1 % Penicillin (10^5 U/l)/Streptomycin (100 mg/l) (Life Technologies), 10 % heat-inactivated foetal bovine serum (FBS) (Life Technologies and 1 % L-glutamine (200 mM) (Life Technologies).

Cells were cultured in a monolayer in sterile 75cm^2 flasks with media as documented above. Cell cultures were maintained in a humidified incubator in 5 % carbon dioxide at 37 °C. Cells were split once reaching 80 % confluency. Experiments were carried out at low passage numbers (below passage number 40).

2.2 Plasmid DNA Transfection

2.2.1 Plasmid preparation

Mammalian expression vectors containing the gene of interest were sourced from multiple sites, detailed in Table 2.1 below. Genes of interest were housed in different expression vectors; all contained the CMV promoter sequence and inserts for antibiotic-resistance for selection after bacterial transformation. Vector content was confirmed with Sanger sequencing after transformation, prior to transfection.

Vector name	Expression vector	Gene ID and supplier information	Gene of interest
VO	pCMV6-XL5	#PCMV6XL5 Origene Technologies; Rockville, USA	Empty vector
IMPDH2 WT	pCMV6-XL5	#SC119585 Origene Technologies; Rockville, USA	IMPDH2 (NM_000884)
IMPDH2 S280C	pCMV6-XL5	Original IMPDH2 WT vector with site-directed mutagenesis (Chapter 4)	IMPDH2 (NM_000884) with missense mutation S280C
PFKFB4 WT	pCMV6-XL5	#SC110972 Origene Technologies; Rockville, USA	PFKFB4 (NM_004567)
PFKFB4 Y366C	pCMV6-XL5	Original PFKFB4 WT vector with site-directed mutagenesis (Chapter 4)	PFKFB4 (NM_004567) with missense mutation Y366C
DICER1	pCMV-flag	Prof. P Santisteban, the Autonomous University of Madrid, Spain	DICER1
DICER1 D1810H	pCMV-flag	Original DICER WT vector with site-directed mutagenesis (Chapter 5)	DICER1 with missense mutation D1810H
DICER1-HA	pCMV3-ORF-HA	#HG11350-CY Sino Biological; Pennsylvania, USA	DICER1 (NM_030621.3)
MET	CMV3-ORF	#HG10692-UT Sino Biological; Pennsylvania, USA	MET (NM_000245.2)
FN1	pPM-N-D-C-HA	#PV355032 abm; Vancouver, Canada	FN1 (BC117176)

Table 2.1: List of mammalian expression vectors and corresponding information

2.2.2 Bacterial transformation

Bacterial transformation was performed using subcloning efficiency DH5α competent *E. coli* cells (Invitrogen, ThermoFisher Scientific; Massachusetts, USA). Ten nanograms (ng) of plasmid were added to 50 µl of DH5α cells, which were swirled then rested on ice for 30 minutes. Following this, the cells were heat-shocked at 42 °C for 30 seconds then rested on ice for a further two minutes. Nine-hundred and fifty microlitres (µl) of warmed Super Optimal broth with Catabolite repression (S.O.C.)

media (Invitrogen) were added and the sample was shaken at 225 revolutions per minute (RPM) for an hour at 37 °C in an orbital shaker. The sample was centrifuged at 13,000 RPM for three minutes then the supernatant discarded, and cells resuspended in the remaining ~50 µl S.O.C. media. The resuspended cells were spread onto two Lysogeny broth (LB) agar plates with appropriate antibiotic added according to vector antibiotic resistance (ampicillin (100 microgram per millilitre (µg/ml)) or kanamycin (50 µg/ml)). The plates were incubated overnight at 37 °C for 16 hours. Two of the colonies that grew were picked and transferred to 5 millilitre (ml) LB broth for plasmid amplification.

2.2.3 Plasmid purification and amplification

DNA amplification was performed using GenElute HP Plasmid MaxiPrep Kit (Sigma-Aldrich, Merck; Darmstadt, Germany), following the manufacturer's protocol unless otherwise stated. The 5 ml LB starter broth was warmed at 37 °C and shaken at 225 RPM in an orbital shaker for 6 hours. The starter culture was transferred into 150 ml of LB broth with antibiotic (either ampicillin (100 µg/ml) or kanamycin (50 µg/ml) depending on vector antibiotic resistance) for 16 hours. This culture was centrifuged at 4,000 RPM for 10 minutes. The bacterial pellets were then resuspended in 12 ml resuspension solution (with added RNase). The bacterial cells were lysed with the addition of 12 ml lysis solution, inverted six times then incubated for 5 minutes. Twelve millilitres of neutralisation solution were added then the solution was inverted 4-6 times. Nine millilitres of binding solution were added, then the solution was inverted twice and transferred to a filter syringe and left for five minutes. A binding column was prepared by spinning at 3,000 x g with 12 ml column preparation solution. The DNA containing

solution was pushed through the syringe into the prepared binding column, which was then spun again at 3,000 x g for 2 minutes. The column was then washed twice using two wash solutions and the same spin method. The DNA was eluted in 3 ml of nuclease free water with a final spin of 3,000 x g for 5 minutes. DNA concentration was quantified using the NanoDrop 1000 Spectrophotometer (ThermoFisher Scientific).

2.2.4 Plasmid sequencing

After amplification with the MaxiPrep kit (Sigma-Aldrich), the DNA was sequenced using Sanger Sequencing by Source Bioscience (Nottingham, UK). For plasmid sequencing 5 µl of 100 ng/µl vector was sent with 5 µl of 3.2 pmol/µl primer, or Source Bioscience provided primers were used. The primers used are documented in Table 2.2 below.

Sequencing primer name	Sequence	Target plasmid
BGH Reverse	5' TAGAAGGCACAGTCGAGG 3'	VO (pCMV6-XL5), MET
pCMV forward	5' GAGCTCGTTTAGTGAACCGTC 3'	FN1
pCMV reverse	5' CAAGGCCAGGAGAGGCACTG 3'	VO (pCMV6-XL5)
T7 promoter (F)	5' TAATACGACTCACTATAGGG 3'	MET
IMPDH2 forward	5' GATCTGGAAGATGCAATTTCCCTGGGAAGAGTCC 3'	IMPDH2 WT and IMPDH2 S280C
IMPDH2 reverse	5' GGACTCTTCCCAGGGAAATTGCATCTTCCAGATC 3'	IMPDH2 WT and IMPDH2 S280C
PFKFB4 forward	5' GCCTTGTCGAGGAAGCAGGCCAGCAGGC 3'	PFKFB4 WT and PFKFB4 Y366C
PFKFB4 reverse	5' GCCTGCTGGCCTGCTTCCTCGACAAGGC 3'	PFKFB4 WT and PFKFB4 Y366C
DICER1 forward	5' CTTAGGAGATCTGAGGAGGATG 3'	DICER1 WT and DICER D1810H
DICER1 reverse	5' CCCACTATCCATGTAAATGGC 3'	DICER1 WT and DICER D1810H

Table 2.2: Table of sequencing primer sequences. BGH Reverse, pCMV forward, pCMV reverse and T7 promoter (F) are stock primers from Source Bioscience. All other primers were designed and were ordered at a scale of 0.05 µmole, dried via Polyacrylamide gel electrophoresis (PAGE) purification from Sigma-Aldridge.

2.2.5 Site-directed mutagenesis

Mutagenesis of the plasmids was performed using the Quick-Change II XL site directed mutagenesis kit (Agilent Technologies; California, USA). Oligonucleotide mutagenesis primers were designed and ordered (Sigma-Aldrich) to replicate the mutations isolated from the TCGA database. All primers were designed and ordered at 0.05 µmole, dried via PAGE purification. These all fit to the Agilent guidelines for guanine-cytosine

content (GC content) and melting temperature and are described in Chapter 4 for IMPDH2 and PFKFB4 and Chapter 5 for DICER1.

Site-directed mutagenesis was initiated by adding 10 ng of the wild type double stranded deoxyribonucleic acid (dsDNA), 125 ng of each oligonucleotide primer (forward and reverse), to 5 µl of ten times reaction buffer, 1 µl of deoxyribonucleotide triphosphate (dNTP) mix and 3 µl of QuickSolution (all Agilent Technologies). Then the solution was made up to a total volume of 50 µl with nuclease free water. One microlitre of 2.5 U/µl PfuUltra HF DNA polymerase was added to the solution just prior to the Polymerase chain reaction (PCR) cycle in Table 2.3.

Cycles	Temperature	Time
1	95 °C	1 minute
18	95 °C	50 seconds
	60 °C	50 seconds
	68 °C	1 minute/kb of plasmid length*
1	68 °C	7 minutes

*Table 2.3: PCR thermocycling parameters for site-directed mutagenesis. *8 minutes for IMPDH2 and PFKFB4, and 7 minutes 40 seconds for DICER1.*

Next, a Dpn I digestion was performed by adding 1 µl of 10 U/µl Dpn I restriction enzyme (Agilent Technologies) to the PCR amplification reaction and incubating at 37 °C for an hour. Transformation of XL10-Gold Ultracompetent cells (Agilent Technologies) was performed by adding 2 µl of β-mercaptoethanol (Agilent Technologies) to 45 µl of the XL10-Gold Ultracompetent cells and incubating on ice for ten minutes, swirling every 2 minutes. Two microlitres of the dpn I treated DNA was added to the ultracompetent cells, swirled and incubated for 30 minutes. The tubes

were then heated in a 42 °C waterbath for 30 seconds and then incubated back on ice for 2 minutes. Five hundred microlitres of S.O.C. media (Invitrogen) were added and the tubes incubated at 37 °C for an hour in an orbital shaker at 225 RPM. The cell mixture was then plated out onto two agar plates containing the relevant antibiotic to match the vector resistance. These plates were then incubated at 37 °C for 16 hours and colonies were picked and amplified as discussed in Chapter 2.2.3.

2.2.6 Cell line transfection with plasmids

Cells were seeded into a 6-well plate (Corning, New York, USA) and incubated at 37 °C with 5 % CO_2 for 24 hours. Cell lines were transfected with plasmids using transfection reagent *Trans*IT®-LT1 (LT1) (GeneFlow; Lichfield, UK) at a ratio of 3 µl to 1 µg DNA (6 µl LT1:2 µg plasmid DNA per well). DNA and LT1 were added to Opti-MEM® I reduced serum medium (Life Technologies) making up a total volume of 200 µl per well. Following this 200 µl of the Opti-MEM transfection mix was added to the media in each well and incubated at 37 °C with 5 % CO_2 for 48 hours unless otherwise indicated. Transfection was confirmed with Western Blotting.

2.3 Small interfering RNA knockdown

Cells were seeded into a 6-well plate (Corning) and incubated at 37 °C with 5 % CO_2 for 24 hours. Cell lines were transfected with siRNA using lipofectamine RNAiMAX (Invitrogen). One millilitre of Opti-MEM® I reduced serum medium (Life Technologies) was mixed with 6 µl lipofectamine RNAiMAX and allowed to stand for 5 minutes. Then siRNA was added to the Opti-MEM® mix to a final concentration of 100 nM. This was left to allow complex formation for 20 - 30 minutes at room temperature. For

transfection, the media was removed from the well and replaced with 1 ml of the Opti-MEM®/siRNA mixture and incubated at 37 °C with 5 % CO_2 for 5 hours, at which point the media was changed back to RPMI-1640 media (Life Technologies) supplemented with 1 % Penicillin (10^5 U/l)/Streptomycin (100 mg/l) (Life Technologies) and 10 % heat-inactivated foetal bovine serum (FBS) (Life Technologies). Protein knock-down was confirmed with Western Blotting.

2.4 Western Blotting

2.4.1 Protein extraction

Cells were rinsed with phosphate buffered saline (PBS) 48 hours after transfection and then radioimmunoprecipitation assay buffer (RIPA) lysis buffer (50 mM Tris-HCl pH 7.4, 150 mM sodium chloride, 1 % (v/v) Igepal CA-630, 6 mM sodium deoxycholate and 1 mM ethylenediaminetetraacetic acid (EDTA)) with 60 µl/ml protease inhibitor cocktail (Sigma-Aldrich) was added to the cells. These were subjected to one freeze thaw cycle to lyse the cells. After centrifugation at 13,000 RPM for 30 mins at 4 °C these then underwent a bicinchoninic acid assay (BCA) assay for protein quantification.

2.4.2 Protein quantification

Control standards of Bovine Serum Albumin (BSA) protein (Sigma Aldrich) in RIPA buffer were used at 0, 0.125, 0.25, 0.5, 0.75, 1, 1.5, 2, 2.5 and 5 mg/ml. Using the Pierce Bicinchoninic acid assay (BCA) assay (ThermoFisher Scientific), samples and standards were added (4 µl) to a flat bottomed 96-well plate (Corning, New York, USA) and 80 µl of Reagent A and B mix (ratio of 1 ml to 20 µl) was added. All samples and

standards were added in duplicate. The plate was incubated at 37 °C for 30 minutes and then colorimetric absorbance was measured at 560 nM on a Wallac 1420 Victor^3 Multilabel Counter plate reader (Perkin-Elmer, Massachusetts, USA). Protein quantification was then calculated by comparison of samples against the standard curve produced by the BSA standards.

2.4.3 Western blotting

Protein samples (15 – 30 µg) were prepared with five times protein loading buffer (10 % Sodium dodecyl sulfate (SDS) (Sigma-Aldrich), 250 mM 2M Tris-HCl, 50 % glycerol (Sigma-Aldrich), 0.02 % bromophenol blue (Bio-Rad Laboratories, California, USA) and 12.5 % β-mercaptoethanol (Sigma-Aldrich)) and heated for either 5 minutes at 95 °C or for 30 minutes at 37 °C depending on the size of the protein of interest. These were then loaded onto either a 10 % resolving gel (375 mM Tris pH 8.8, 10 % acrylamide (Geneflow), 3.5 mM SDS, 0.1 % (v/v) tetramethylethylenediamine (TEMED) (Sigma-Aldrich) and 4.4 mM ammonium persulphate (APS) (Sigma-Aldrich)) or a preformed Novex WedgeWell 4-12 % Tris-Glycine Mini Gel (Invitrogen, ThermoFisher Scientific) depending on the protein probed for. Samples were separated by running at 140 V gel electrophoresis in running buffer (24.8 mM Tris (Sigma-Aldrich), 192 mM glycine and 3.5 mM SDS). Alongside, 5µl of BLUeye protein ladder (Geneflow) was run as a molecular weight marker. These proteins were transferred onto a methanol (VWR International limited, Leicestershire, UK) activated Polyvinylidene difluoride (PVDF) membrane (ThermoFisher Scientific) in transfer buffer (25 mM Tris, 192 mM glycine (Sigma-Aldrich) and 20 % methanol) at 360 mA for an hour and fifteen minutes, unless stated differently. Membranes were then

blocked with 5 % w/v skimmed milk powder (5 % milk) (Marvel; London, UK) in Tris-buffered saline with Tween®20 (TBS-T) (20 mM Tris pH 7.6, 137 mM sodium chloride (Sigma-Aldrich), 0.00025 % v/v Tween-80® (Sigma-Aldrich)) for an hour. The PVDF membrane was then incubated with the primary antibody in 5 ml of 5 % milk in TBS-T overnight, rocked at 5 °C. Three TBS-T washes were used to rinse the membrane before incubation with the secondary antibody (horseradish peroxidase-conjugated polyclonal goat anti-rabbit or rabbit anti-mouse immunoglobulin (Agilent Technologies)) 1:2000 v/v in 5 ml of 5 % milk in TBS-T for an hour at room temperature. After three further ten-minute TBS-T washes the PVDF membrane was then developed with Pierce ECL2 chemiluminescent substrate (GE Healthcare, Amersham, UK) and captured on radiographic film (Scientific Laboratory Supplies; Nottingham, UK). β-actin was used a protein loading control and was probed for using the same technique and a mouse monoclonal β-actin primary antibody (Sigma Aldrich) 1:10,000 v/v, incubated for one hour only, not overnight. The β-actin was developed with Pierce ECL chemiluminescent substrate (GE Healthcare). Antibodies used are listed below (Table 2.4).

Antibody	Type	Catalogue number	Company	Dilution
anti-IMPDH2	rabbit polyclonal	12948-1-AP	Proteintech	1:1000
anti-PFKFB4	rabbit polyclonal	ab71622	Abcam	1:200
anti-DICER1	mouse monoclonal	ab14601	Abcam	1:1000
anti-ITGα3	mouse monoclonal	66070-1-Ig	Proteintech	1:1000
anti-HA	mouse monoclonal	16B12	BioLegend	1:2000
anti-NIS	rabbit polyclonal	24324-1-AP	Proteintech	1:1000
anti-β-actin	mouse monoclonal	AC-15 A5441	Sigma Aldrich	1:10,000

Table 2.4: Table of antibodies including catalogue number and dilution

2.5 Immunofluorescent Microscopy

Cells were seeded onto a glass coverslip within a 6-well plate and transfected 24 hours after seeding. They were then incubated at 37 °C with 5 % CO_2 for 48 hours and following this, the cells were washed with PBS and fixed with 800 µl fixing solution (0.1 M phosphate buffer, 2 % paraformaldehyde, 2 % glucose, 0.02 % sodium azide) for 20 minutes. After rinsing, the cells were then permeabilised with 800 µl 100 % chilled methanol for ten minutes. After further rinsing, they were then blocked with 800 µl 10 % new born calf serum (NCS) (ThermoFisher Scientific). Following this, the coverslips were placed facedown onto 80 µl of 1 % bovine serum albumin (BSA) in PBS with primary antibody and incubated for an hour. These were rinsed again three times with PBS and then placed facedown onto 80 µl of 1 % BSA in PBS with 1 % NCS and 1:250 Alexa Fluor 488-conjugated goat anti-mouse IgG (Invitrogen), 1:250 Alexa Fluor 594-conjugated goat anti-rabbit IgG (Invitrogen) and 1:1000 Hoechst stain (Sigma-Aldrich) for an hour in the dark. Coverslips were mounted onto slides with Dako Fluorescent Mounting Medium (Agilent Technologies) then stored at 4 °C.

2.6 Proliferation assays

2.6.1 Aqueous soluble tetrazolium (MTS) assay

Cells were seeded into 96-well plates in 100 µl of media 24 hours after transfection with six replicates of each condition. After a further 24 hours 20 µl of CellTiter 96® AQueous One Solution Cell Proliferation Assay solution (Promega, UK) was added to each well. The MTS tetrazolium compound is reduced by NADPH or NADH in metabolically active cells into a coloured formazan product. The plate was incubated at 37 °C with 5 % CO_2 for one hour and then colorimetric absorbance was measured

at 490 nM on the Wallac 1420 Victor^3 Multilabel Counter plate reader (Perkin-Elmer). The background absorbance from media only wells was subtracted from the sample readings.

2.7 Cell invasion assay

Four hours after transfection, normal (10 % FBS) media on the cells was replaced with 2 % FBS media. The following day, Corning BioCoat growth factor reduced Matrigel invasion chambers (Corning; New York, USA) were warmed from -20 °C to room temperature for 20 minutes. Warmed 2 % FBS media was then added to the chambers, which were returned to the 37 °C 5 % CO_2 to rehydrate for 2 hours. 750 µl of warmed 10 % complete media were added to each well (outside the chamber) in the 24 well plate. This acted as a chemoattractant for the cells, which are trypsinised, re-suspended in 2 % FBS media and seeded inside the chambers. They were incubated at 37 °C with 5 % CO_2 for 24 hours. After this the media, Matrigel insert and any excess non-invasive cells were removed from inside the chamber and a series of steps are undertaken to stain and fix the cells that have invaded through the Matrigel to the membrane. After being washed in PBS, the cells were dehydrated in 95 % ethanol for 5 minutes, incubated in Mayer's haematoxylin solution (Sigma-Aldrich) solution for 10 minutes, then briefly rinsed in tap water and placed in Scott's tap water (3.5 gramme (g) $NaHCO_3$, 20 gm $MgSO_4$ and 1 litre (L) water) as a blueing solution for 5 minutes. They were then placed in 95 % ethanol for 2 minutes and then Eosin Y solution (Sigma-Aldrich) for 5 minutes, followed by a brief wash in tap water and rehydration in 70 % ethanol then 95 % ethanol for 2 minutes each. Cells were then photographed on an

EVOS XL Core Imaging System (ThermoFisher Scientific) and then analysed with open source software Image J (Schneider et al. 2012).

2.8 Cell migration assay

Cells were seeded into a 6-well plate (Corning) and incubated at 37 °C with 5 % CO_2 for 24 hours, then transfected with the gene of interest. A further 24hr - 48hrs later, depending on the gene studied, a scratch wound assay was performed. The media were changed to 2 % FBS to control for cell proliferation and then a linear vertical scratch was made through the centre of the well with a 200 µl pipette tip. Photographs were taken at the same point along the scratch wound on the EVOS XL Core Imaging System (ThermoFisher Scientific) at 0, 4, 8 and 24 hours, unless otherwise stated. These images were then analysed in the open source software Image J to determine the percentage wound healing at each time point.

2.9 Statistical analysis

For laboratory work, statistical analysis was carried out in GraphPad Prism (version 8) on data sets with a minimum of 3 independent experimental replicates. Significance was taken to be $p < 0.05$. For normally distributed data a Student's t-test was performed, or for grouped data an Analysis of variance (ANOVA) was performed. Tukey's multiple comparisons test was performed post hoc if the ANOVA was deemed significant. The mean and standard error of the mean were demonstrated in histograms unless otherwise documented. For non-parametric data the Mann-Whitney U test was performed, or when there was grouped analysis the Kruskal-Wallis one-way analysis of variance. For the bioinformatic analysis the statistical analysis is

referred to in individual chapters and was predominantly performed in the open source software R (www.r-project.org) using R Studio (www.rstudio.com).

Chapter 3 Thyroid cancer and The Cancer Genome Atlas

3 Thyroid cancer and The Cancer Genome Atlas

3.1 Introduction

3.1.1 The Cancer Genome Atlas (TCGA) outlook

The Cancer Genome Atlas (TCGA) is a collaboration between the National Cancer Institute (NCI) and the National Human Genome Research Institute (NHGRI) which began in 2006. Thirty-three cancer types have been studied, with over 20,000 normal and tumour specimens collated from across the USA analysed. Most data are open access, although the raw data and non-validated mutations are controlled access data.

3.1.2 The Cancer Genome Atlas in Differentiated Thyroid Cancer

The Cancer Genome Atlas contains data on 516 papillary thyroid cancer patients, with matched normal tissue (either matched normal thyroid tissue or blood). The data available include whole exome sequencing (n = 503), somatic mutations (n = 496), messenger RNA (mRNA) expression (n = 500), microRNA (miRNA) expression (n = 502), protein expression (n = 222) and clinical data (n = 508). In 2014, a study on 496 papillary thyroid cancer patients' data (Agarwal et al. 2014) demonstrated oncogenic driver events in 96.5 % of the tumours, bringing down the unknown thyroid cancer driver events from 25 % to 3.5 %. One of the study's main findings is that the majority of papillary thyroid tumours can be categorised as BRAF V600E-like or RAS-like, and in the study a score is attributed for each tumour from most BRAF V600E-like (-1) to most RAS-like (+1). This score is associated with histological subtype, tumour differentiation, mRNA and miRNA profiles as observed in Figure 3.1 below.

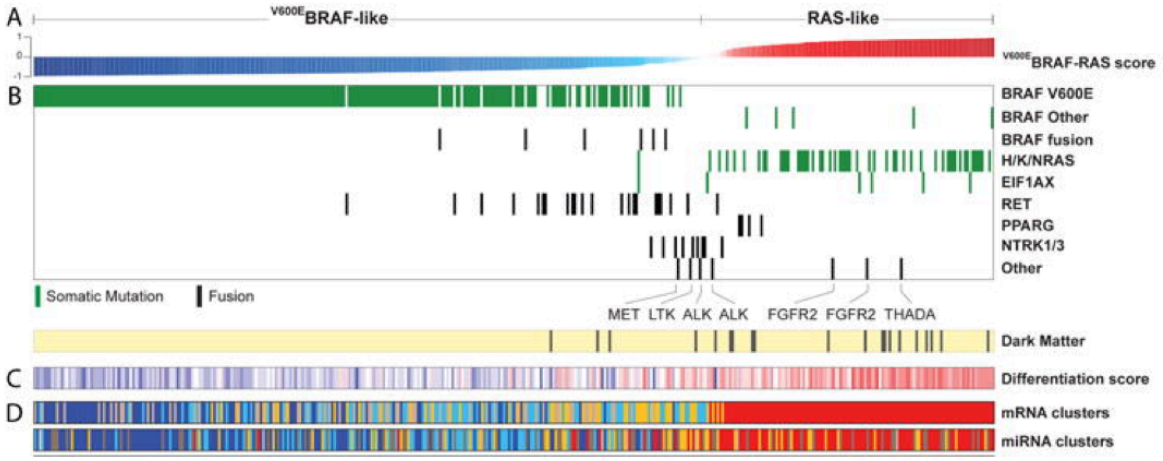

Figure 3.1: BRAF V600E-like and RAS-like score illustrating the tumour differentiation score of BRAF V600E-like and RAS-like tumours. The expression profile of mRNA/miRNA associated with BRAF V600E-like and RAS-like status is also presented. Figure adapted from Agarwal et al. 2014.

The authors advocate that differentiated thyroid cancer should be recategorised, with follicular-variant papillary thyroid cancer, currently categorised under papillary thyroid cancer, redefined as a subtype of follicular thyroid cancer.

BRAF V600E-like tumours escape the ERK/RAF feedback loop as the BRAF V600E functions as a constitutively active monomer, resulting in marked activation of the MAPK signaling pathway. Furthermore, it is suggested that due to the distinct genotypic pattern of these tumours, such as the suppression of thyroid-specific genes in BRAF tumours (Durante et al. 2007), these categories may be associated with responsiveness to therapy, including radioiodine uptake and targeted therapy.

The authors state that this study has reduced the 'dark matter' of differentiated thyroid cancer (those tumours with unknown mutational status) and has identified most oncogenic driver mutations. However, it is suggested that within the $BRAF^{V600E}$ driven tumours the heterogeneity of gene expression means further subcategorisation would be prognostically useful.

3.1.3 Thyroid Cancer Recurrence in The Cancer Genome Atlas

For assessment of recurrence in the sentinel TCGA paper the authors used risk of recurrence, calculated on the American Thyroid Association 2009 guidelines (Cooper et al. 2009) as a surrogate for recurrence. Lymph node metastasis, patient aged over 45 years old, extracapsular spread of tumour, aggressive histology and tumour size all convey an increased risk of recurrence (Cooper et al. 2009). The prognostic scoring system including metastasis, age, completeness of resection, invasion, and size of tumour (MACIS) (Hay et al. 1993) was also included in the analysis. The Cancer Genome Atlas analysis demonstrated that TERT promotor mutations were associated with a higher risk of thyroid cancer recurrence, although for both wild type and mutant TERT promotor tumours the number of patients in the low/intermediate group was higher than the high-risk group (Agarwal et al. 2014). MicroRNA 146b was demonstrated to be variably expressed in different miRNA clusters and expression was associated with low tumour differentiation score and low $BRAF^{V600E}$-like or RAS-like score and risk of recurrence. This association with aggressive PTC behaviour is in keeping with previous studies (Chou et al. 2013). Mutation density was also associated with increased likelihood of tumour recurrence.

The Cancer Genome Atlas dataset also has associated clinical data, including the patient's disease-free status, indicating if the disease has recurred or progressed following treatment. The recurrence status from this metadata was not used in the primary analysis of TCGA data. While the risk of recurrence was discussed, the actual associations with recurrence were not analysed. The potential to identify biomarkers for recurrence present at the diagnosis of the original disease is critical. Therefore, the aim of this Chapter was to derive mutational biomarkers from the TCGA thyroid dataset which predicted risk of recurrence.

3.2 Methods

3.2.1 Whole exome sequences

The Cancer Genome Atlas next generation sequencing (NGS) for the thyroid carcinoma cohort was originally performed on the Illumina Genome Analyzer sequencing platform at the Broad Institute (Agarwal et al. 2014). The samples analysed were primary tumour samples with matched normal tissue (either blood or normal thyroid tissue, the latter of which was used preferentially when available). These steps were performed by TCGA teams.

Access to TCGA data was granted after application via the NIH CGHub portal to controlled access data, which were downloaded via GeneTorrent onto the University of Birmingham High Performance Cluster [Data Access Request number: 41353-5 Project identification: 10051 'The Identification of Novel Biomarkers in Recurrent Thyroid Cancer'].

Clinical details for the 43 patients included in the somatic mutational analysis can be found in Appendix 1: Table 10.1.

3.2.2 Analysis pathways

TCGA data were originally analysed by the TCGA group using the DNA-Seq Analysis Pipeline (https://docs.gdc.cancer.gov/Data/Bioinformatics_Pipelines/DNA_Seq_Variant_Calling_Pipeline/). This pipeline uses one of two Burrows Wheeler Algorithms (BWA) to align the data to the reference genome, creating Binary Alignment Map (BAM or .bam) files. The reference genome used was GRCh38.d1.vd1 (https://gdc.cancer.gov/about-data/data-harmonization-and-generation/gdc-reference-files).

Mutation calling was performed by the TCGA using a Mutect pipeline (Cibulskis et al. 2013). The Mutect pipeline variant call format (vcf) files were downloaded as outlined above. These were then were annotated using the software Annovar (Wang et al. 2010) on the university linux 24 core, 128Gb, broadwell-class Intel High Performance Cluster BlueBEAR (www.birmingham.ac.uk/bear). Annotated vcfs were then filtered in the programming language Python by quality score and dbSNP, and then by a series of bioinformatic scoring tools by hand (discussed below in Figure 3.3).

A second analysis was performed using an in-house pipeline. For this, all patients who went on to have thyroid cancer recurrence had tumour and matched normal BAM files downloaded. Platypus variant calling (Rimmer et al. 2014b) was performed on these data as a group analysis. Annovar annotation (Wang et al. 2010) was again performed

on the vcf files, and the annotated vcf files were filtered using the same tools as the Mutect vcf analysis.

3.2.3 Filtering variants

After removal of low-quality variants (QUAL = PASS) and those with synonymous mutations, in-silico mutation prediction was performed using several bioinformatic tools: Sorting Intolerance From Tolerance (SIFT) score (Sim et al. 2012), Polymorphism Phenotyping version 2 (PolyPhen2) score (Adzhubei et al. 2010), MutationTaster (Schwarz et al. 2010) and MutationAssessor (Reva et al. 2011) score, were all used for further filtering of the variants. Scores were combined to highlight the most harmful mutations. SIFT score assesses the effect of amino acid substitution on protein function using sequence homology and ranks the variant as 'tolerated' or 'deleterious' and assigns a score. PolyPhen2 score by comparison uses the physical properties that a change in amino acid sequence inflicts upon the protein to predict altered function. The changes were ranked as 'probably damaging', 'possibly damaging' or 'benign'. MutationTaster integrates a number of data sources including Ensembl, UniProt, ClinVar and the 1000 Genomes Project to predict the effects of amino acid changes on functional protein domains, protein length, splicing and regulation of protein function. MutationAssessor is another tool based on evolutionary conservation of amino acids, and outputs a score and a category of 'high', 'medium', 'low' or 'neutral' functional impact. A summary table of the scoring tools used is below in Table 3.1.

Scoring tool				
SIFT	Tolerated (T) > 0.05 ◄——►			Damaging (D) < 0.05
PolyPhen2	Benign (B) < 0.15	Possibly damaging (P) 0.15 – 0.85		Probably damaging (D) > 0.85
MutationTaster	Polymorphism automatic (P)	Polymorphism (N)	Disease causing (D)	Disease causing automatic (A)
MutationAssessor	Neutral 0 ◄——►	Low	Medium	High 1

Table 3.1: Bioinformatic pathogenicity scoring tools SIFT, PolyPhen2, MutationTaster and MutationAssessor demonstrating the numerical score and the associated disease impact.

Finally, the variants were investigated by literature review to infer to biological significance. The mutations were manually reviewed on the TCGA cBioPortal web browser (Cerami et al. 2012, Gao et al. 2013) and opened on Integrative Genomics Viewer (IGV) (Robinson et al. 2011) to ensure that the mutation represented true somatic mutation (Figure 3.2).

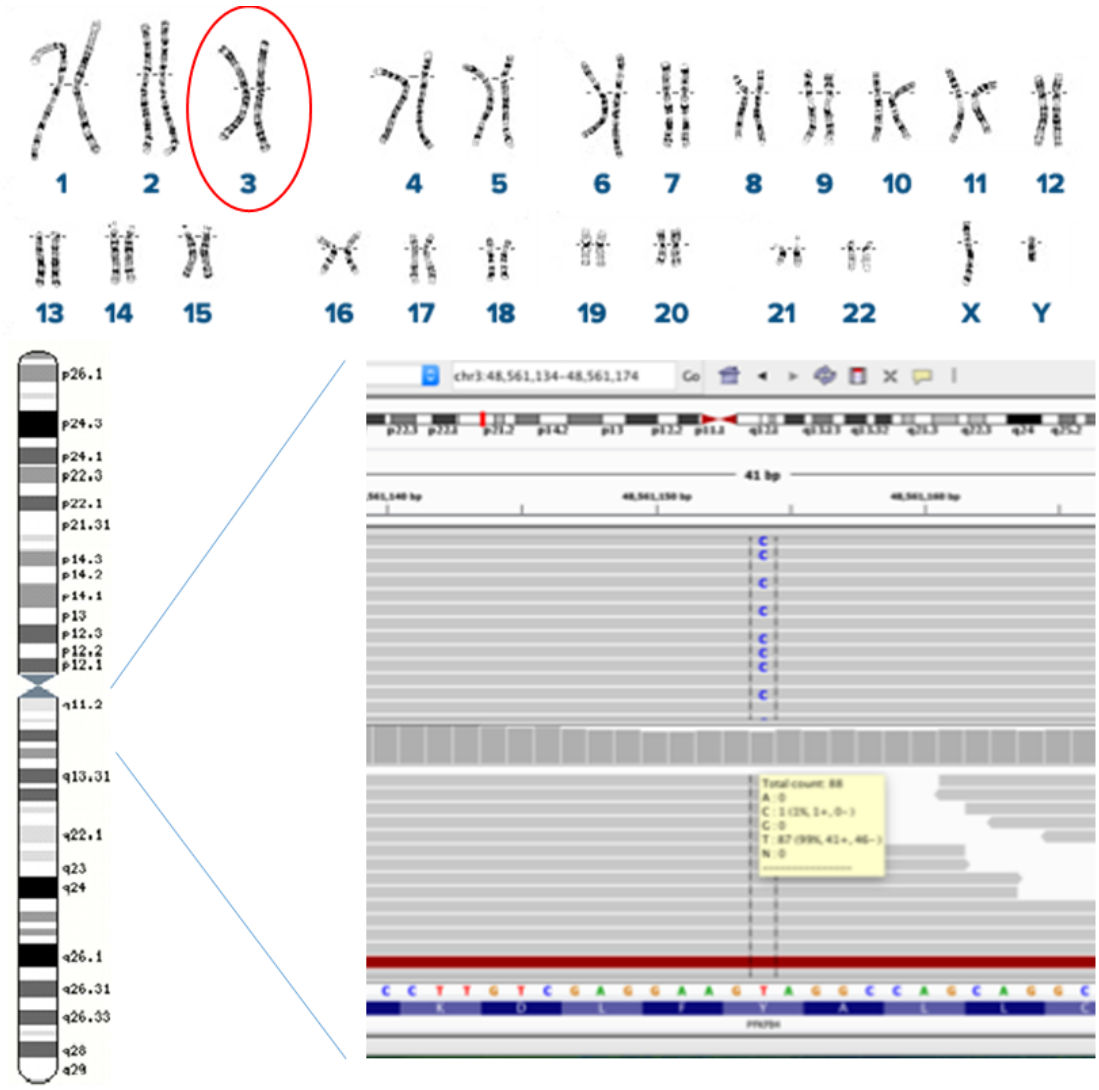

Figure 3.2: IGV review of PFKFB4 gene in sample with the Y366C variant. This demonstrates a T>C missense mutation that causes an amino acid Y366C substitution in the PFKFB4 gene located on chromosome 3.

3.2.4 RNA and miRNA analysis

The RNA and miRNA analyses were performed on open-access TCGA data, on the same patient group as the mutation analysis above. The normalised expression data from the TCGA was used for the RNA sequencing (RNA seq) analysis. The RNA count reads were downloaded from the Firebrowse portal (http://firebrowse.org) and had undergone upper quartile normalisation. MicroRNA data were also downloaded from

the Firebrowse portal and the 'reads per million miRNA mapped' value was used as the expression value of each miRNA. The methods and results from these analyses are discussed further in Chapter 6 (RNA expression) and Chapter 7 (miRNA expression). The median differential expression was calculated for each of 20,532 genes between the group of recurrent thyroid cancer patients (n = 43) and the non-recurrent (n = 459), then a Mann-Whitney U test was applied to assess significance.

3.3 Results

Paired sequencing data for 43 recurrent thyroid cancer patients was retrieved from the TCGA and analysed as described in section 3.2. Initial DNA sequencing analyses identified hundreds of variants. In order to distinguish the clinically informative variants linked to recurrence from genetic population variance and non-pathogenic variants, post-calling filtering steps were required. The filtering used for this analysis is summarised in Figure 3.3 below.

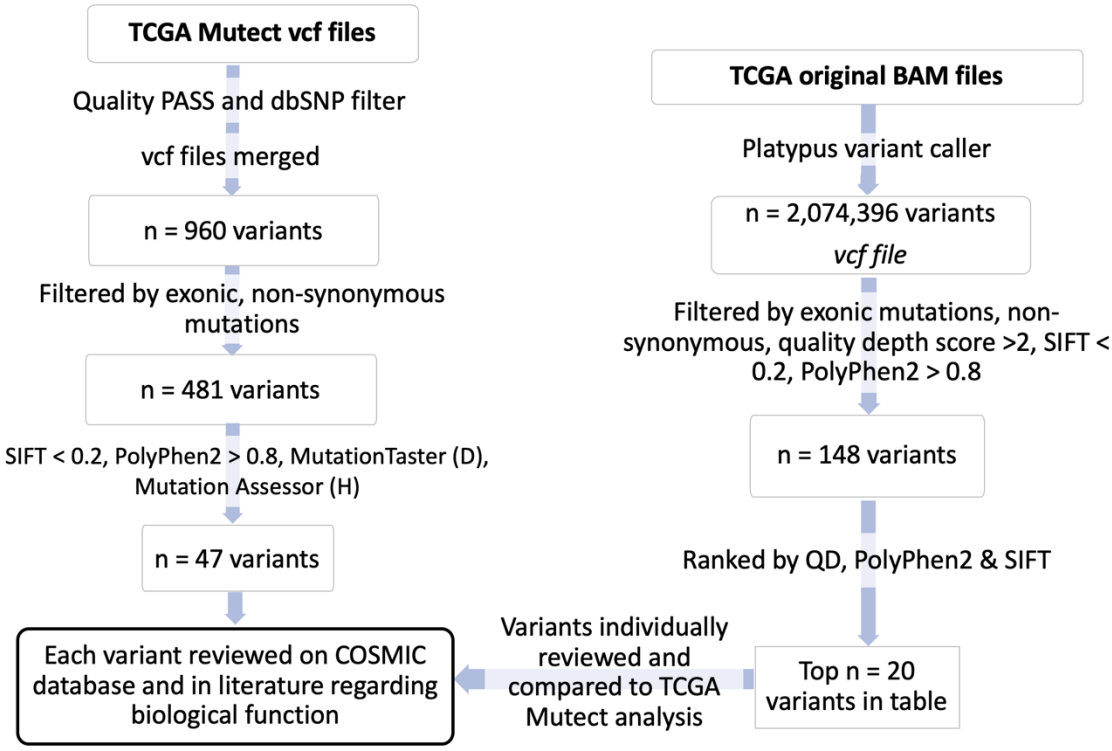

Figure 3.3: Steps in filtering the variants for the two analyses. The same bioinformatic tools were used for the filtering steps and the analyses results were cross compared for overlap and consistency.

The initial analysis from the TCGA Mutect vcf files raised 47 putative mutations (Appendix 1; Table 10.2). These were reviewed in the literature and searched for in the Catalogue Of Somatic Mutations In Cancer (COSMIC) database. After investigation into the described biological function of each of these genes, a shortlist of the variants in genes DICER1, PFKFB4 and IMPDH2 was decided upon, with the selected results displayed seen in Table 3.2 below.

Chr	**Position**	**Ref**	**Alt**	**Quality**	**Gene**	**COSMIC gene**	**COSMIC mutation spec**	**AA change**
14	95557639	C	G	312	DICER1	Y	novel	D1810H
3	49064023	G	C	11	IMPDH2	Y	novel	S280C
3	48561154	T	C	136	PFKFB4	Y	novel	Y366C

Table 3.2: List of final selected variants. The mutation on chromosome 14 causes a D1810H amino acid change, while the mutations on chromosome 3 caused a S280C and Y366C amino acid change on IMPDH2 and PFKFB4 genes respectively.

These mutations were non-familial heterozygous mutations found in the tumour tissue but not in the matched normal tissue. SIFT scores for the mutations were all 0 (D/'Damaging') and the mutations PFKFB4 and DICER1 had a PolyPhen2 score of 1 (D/'Probably damaging'), with IMPDH2 a PolyPhen2 score of 0.999 (D/'Probably damaging'), signifying high likelihood of a deleterious effect of the mutations. The variants were: IMPDH2 S280C, PFKFB4 Y366C and DICER1 D1810H. (Figure 3.4). Each mutation was present in one patient, each of whom had recurrent thyroid cancer. Another IMPDH2 mutation was observed in a 66 year old female recurrent thyroid cancer patient at R355W, implicating the gene as a potential driver of recurrence. On review of the other socring systems applied in the Annovar annotation, the Functional Analysis Through Hidden Markov Models (FATHMM) score (Shihab et al. 2013) was high for the mutation S280C indicating it was deleterious, and was low for R355W indicating it was tolerated. Consequently, the mutation S280C was selected for functional modelling.

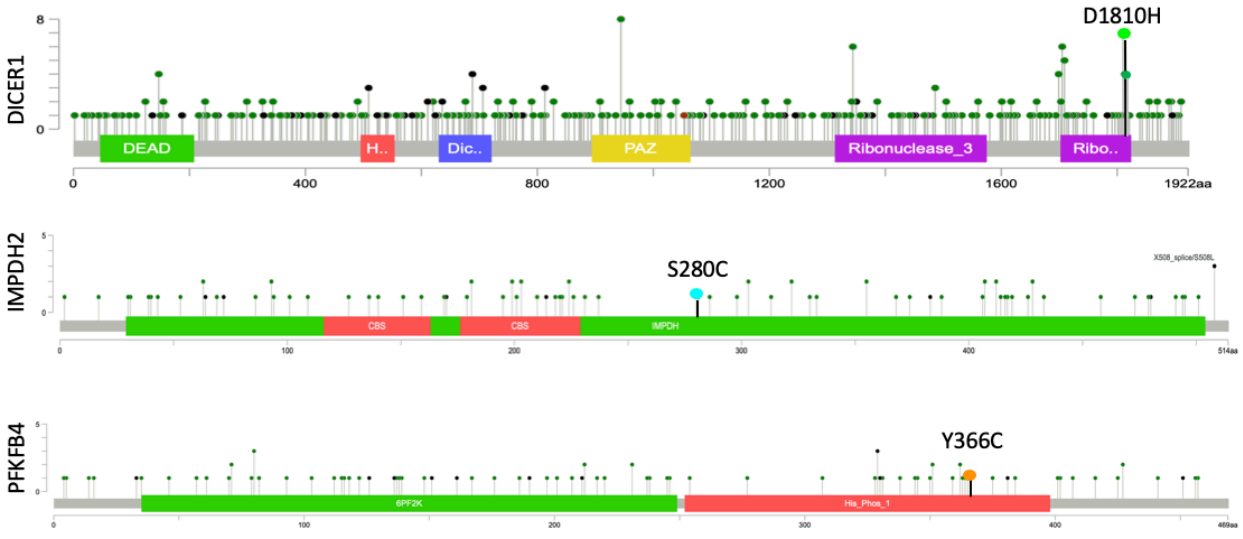

Figure 3.4: Variants as lollipop-diagram adapted from cBioPortal. Highlighted lollipops represent the mutation of interest, present in a recurrent thyroid cancer patient. Other lollipops are other mutations across the TCGA including other cancer types. Figures from TCGA cBioPortal (Cerami et al. 2012, Gao et al. 2013).

In the second analysis, variant calling was performed on the original TCGA BAM files, after the generation of vcf files as described in Chapter 3.2.2. The variants were filtered as shown in Figure 3.3 and ranked according to quality score normalised by allele depth (QD), PolyPhen2 score and SIFT score. The top twenty variants are depicted in Table 3.3.

CHROM	POS	REF	ALT	FILTER	Gene	Function	FR	QD	SIFT	Polyphen2
14	95557639	C	G	PASS	DICER1	exonic	0.0058	22.9230954	0	1
5	1232375	G	A	PASS	SLC6A18	exonic	0.0058	22.8804153	0	1
3	48561154	T	C	PASS	PFKFB4	exonic	0.0058	22.8674726	0	1
17	73055633	T	A	PASS	KCTD2	exonic	0.0058	22.2511165	0	1
12	53457578	G	A	PASS	TNS2	exonic	0.0058	20.9007657	0	1
2	46803383	G	A	PASS	RHOQ	exonic	0.0058	20.797383	0	1
3	133558368	G	A	PASS	RAB6B	exonic	0.0058	20.6424652	0	1
17	34340319	C	T	PASS	CCL23	exonic	0.0058	20.3224387	0	1
1	248512767	G	T	PASS	OR14C36	exonic	.	20	0	1
17	47246163	T	C	PASS	B4GALNT2	exonic	0.0988	20	0	1
7	77973161	C	T	PASS	MAGI2	exonic	0.0058	20.5051172	0	0.999
6	29910371	C	T	PASS	HLA-A	exonic	0.0719	20	0	0.999
3	38889182	G	A	PASS	SCN11A	exonic	0.0058	22.7650674	0	0.996
X	46359996	G	A	PASS	ZNF674	exonic	0.0238	23.5997063	0	0.987
7	140453136	A	T	PASS	BRAF	exonic	0.1744	20	0	0.971
9	100845135	A	C	PASS	NANS	exonic	0.0058	29.9603617	0	0.969
11	1275535	A	T	PASS	MUC5B	exonic	0.0058	21.8373543	0	0.961
2	219503377	G	C	PASS	ZNF142	exonic	0.0058	22.8313294	0	0.952
1	160054053	T	A	PASS	KCNJ9	exonic	0.0058	23.6581931	0	0.906
7	100549967	C	T	PASS	MUC3A	exonic	0.1438	20	0.01	.

Table 3.3: List of variants from vcf generated from the second analysis using in-house Platypus pipeline, ranked by PolyPhen2 score. DICER1 D1810H mutation and PFKFB4 Y366C mutations are highlighted in red and the BRAF V600E mutation in orange.

This new analysis, which was a grouped analysis of the 43 patients who later recurred, compared their primary thyroid cancers and matched normal tissue. A number of variants that came up in this analysis were already well characterised, including the BRAF V600E mutation and NRAS Q61K. Two of the mutations observed in the TCGA Mutect analysis were also present: DICER1 D1810H and PFKFB4 Y366C.

3.3.1 Genetic variants associated with thyroid cancer recurrence

In silico predictions of mutational drivers in cancer always require further validation by study of functional effects. The novel missense mutations IMPDH2 S280C, PFKFB4 Y366C and DICER1 D1810H were taken forward for functional validation.

IMPDH2 is the rate limiting enzyme in guanine nucleotide synthesis and has been associated with tumour progression (Zhou et al. 2014). It is thought to be related to cellular proliferation and therefore tumourigenesis (He et al. 2018). PFKFB4 regulates glycolysis by synthesis of fructose-2, 6-bisphosphate (Sun et al. 2016). It is over-expressed in hypoxic conditions and is thought to aid malignant cells evade apoptosis. High expression is associated with multiple different malignancy types (Zhang et al. 2016). DICER1 codes for the protein dicer, which is an RNAse III enzyme integral to small interfering RNA (siRNA) gene regulation. Dicer cleaves pre-microRNA into mature microRNA. Dicer is also a component of the RNA-induced silencing complex (RISC) which loads siRNA and miRNA onto mRNA, facilitating their post-transcriptional gene regulation (Foulkes et al. 2014)

It is important to note that the patient with an IMPDH2 S280C mutation also had a background driver mutation of BRAF V600E. The PFKFB4 mutation occurred on a background NRAS Q61K mutation. The DICER1 D1810H mutation occurred with no BRAF/RAS mutation. Consequently, a range of cell lines was utilised in the functional work described in Chapters 4 and 5, to ensure mirroring of the background mutational profile of the original patients.

3.3.2 RNA Analysis

In addition to considering qualitative change in gene expression via mutations found in DNA sequencing, quantitative changes in gene expression levels may be apparent in RNA data. The most differentially expressed genes in recurrent vs non-recurrent thyroid cancer were highlighted from the TCGA RNA data. The top 40 differentially expressed genes from this analysis are depicted in a heatmap in Figure 3.5 and the individual genes that were most differentially expressed are discussed further in Chapter 6.

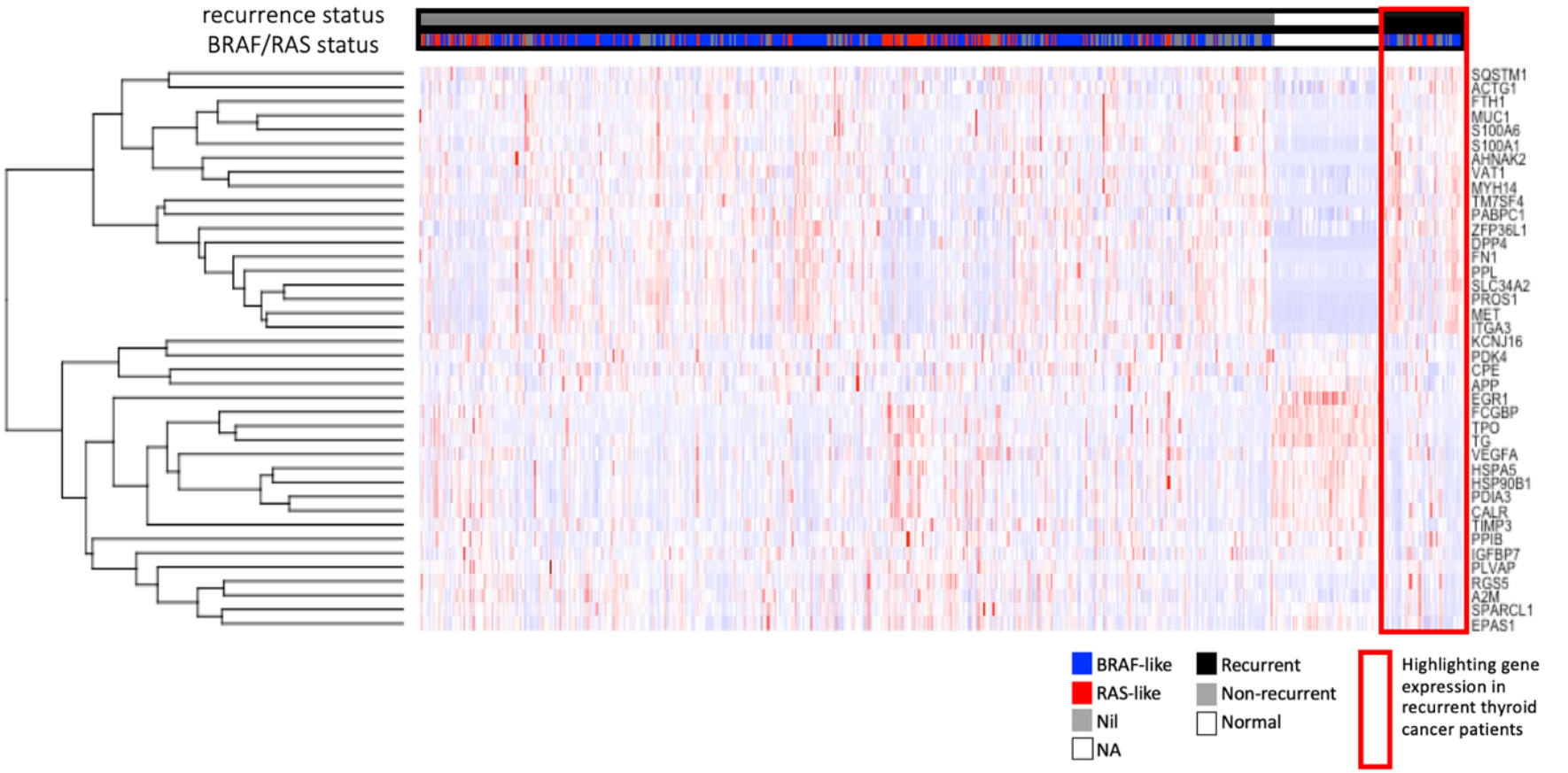

Figure 3.5: Top 40 differentially expressed genes in recurrent vs non-recurrent patients. Differential expression was calculated using median expression values for the recurrent group compared to the non-recurrent. The gene expression for the top 40 genes were plotted into the heatmap using heatmap.3 (Zhao et al. 2014) in R. BRAF-like or RAS-like status and recurrence status was incorporated from the TCGA clinical data.

The heatmap illustrates that although differential expression does look distinct in the recurrent thyroid cancer patients, the background BRAF-like and RAS-like status is also important in the way it relates to gene expression patterns. It appears that there is a pattern showing the RAS-like phenotype to be more similar to the normal phenotype which is apparent across both the recurrent and non-recurrent patient groups. The genes also appear to be clustered, with expression patterns similar across different genes, indicating that they may be involved in similar or overlapping pathways.

3.4 Discussion

3.4.1 TCGA Whole exome sequencing

Using TCGA data for a novel analysis provided a large volume of sequencing data with matching clinical data. This was of particular interest in the context of thyroid cancer recurrence as a prospective dataset would necessarily take a long time to collate, and one performed in retrospect may not provide access to good quality sequencing data. For example, identifying samples retrospectively would inevitably require sequencing from formalin-fixed paraffin-embedded (FFPE) tumour blocks, which is very challenging due to DNA breakdown and cross-linking in the preservation process (Do and Dobrovic 2015). However, as the TCGA dataset has now been completed, and is anonymised, any extra clinical details required above what is currently available will not be accessible, so the data is dependent on those entering the information, which is one drawback of using an established database.

The ideal experiment to analyse recurrence would have been to compare mutation data from recurrent patient primary tumours to non-recurrent patient primary tumours. This would have the value of highlighting the potential drivers for recurrence rather than tumour initiation. A drawback of any study of recurrence is the limit on the follow up for patients, so non-recurrent patients could go on to recur in the future. Thus, variants present in the non-recurrent tumours may in fact be wrongly categorised, as we are considering variants present on initial histology. Therefore, subtracting variant files of non-recurrent patients from recurrent patients would potentially remove variants of interest. The recurrent group of patients were therefore considered and analysed as a group, and their matched normal tissue was used as the control. Also considered was the data volume: with original bam files between 5 and 20 Gb each, this would mean storing then processing 2.5 – 10 terabytes of data.

The planned pipeline for the analysis of the TCGA data was to use Stampy (Lunter and Goodson 2011) to map the reads and Platypus (Rimmer et al. 2014a) as a variant caller ready for file annotation. Stampy has the advantage of being more sensitive than other read mapping software such as Burrows-Wheeler Aligner (BWA) and works well for divergent sequences (Pattnaik et al. 2012). However, the analysis on the University High Performance Cluster (HPC) repeatedly had segmentation faults when running Stampy, despite troubleshooting with Dr Albert Menezes a University of Birmingham bioinformatician, and the relevant team on Github (https://github.com/andyrimmer/Platypus). Therefore, after many iterations, the Platypus software was run directly on BWA aligned files. Platypus has been tested on BWA as an aligner as well as Stampy and works reliably with both aligners. It uses

local realignment to increase accuracy and has been demonstrated to have performed well for whole genome and whole exome data, particularly exonic variants (Rimmer et al. 2014a). The benefit of this analysis was that the TCGA have also performed another analysis on the same bam files, using a different pipeline using Mutect as the variant caller. The Mutect vcf files from the TCGA analysis were then also annotated and filtered as described, meaning that the data had been analysed using two different sets of software, which increases the confidence in variants called in both analyses, such as the variants seen in DICER1 and PFKFB4.

3.4.2 Shortlisting driver mutations in recurrence

Shortlisting genes from Next Generation Sequencing analyses is challenging – analysis creates a list of variants that inevitably need filtering. In a whole exome there might be 30 - 50,000 single nucleotide variants (SNVs) and 30 % of these are likely to be non-synonymous – not all of these can be investigated functionally, therefore filtering is required. Filtering itself has limitations: if too stringent it will exclude true positive results and it is dependent upon the value and applicability of the tools applied. dbSNP (https://www.ncbi.nlm.nih.gov/snp/) is a database of collection of common genetic polymorphisms, which was utilised in the Mutect analysis pipeline (Figure 3.3) to select out novel variants. However, dbSNP does not always take into account the pathogenicity of single nucleotide polymorphisms, and an alternative approach is to use a population frequency cut off. Those variants found commonly in the studied population are unlikely to be a pathogenic driver mutation. Interestingly, dbSNP has an annotation for the mutation $BRAF^{V600E}$, which means that this mutation was filtered out as a polymorphism in this analysis – a mutation that is clearly of profound

importance in thyroid cancer. Due to this significant limitation the dbSNP filtration step was not included in the second (Platypus) analysis.

The tools selected for filtering were included in the annotation software Annovar and are both commonly applied and well validated tools. Each prediction tool uses different means to predict pathogenicity and therefore a combination of these increases the likelihood of selecting for pathogenic variants. SIFT, for example, is a sequence homology-based tool that presumes that the more readily conserved an amino acid site is, the more important it is, and therefore more damaging a mutation at that site is. It is highly sensitive but can overcall neutral variants as pathogenic. PolyPhen2 uses structural information to see if there is a likelihood of significant change to the coded protein and uses the UniProtKB/Swiss-Prot database to look up the annotation for that site. It uses this annotation to predict the functional impact the mutation is likely to have. MutationAssessor, like SIFT, uses protein homology to predict the pathogenicity of the mutation. MutationTaster searches for the genotypes in HapMap, Ensembl and other tools and if it is a true single nucleotide polymorphism (SNP), present a population level it is considers it non-pathogenic. This tool was important to include as it can also score mutations that are not single nucleotide variants (SNVs), but limitations are it cannot manage indels that are over 12 base pairs (bp) or alterations that span the intron-exon border.

Deciding which tools to use and the parameters to set them to (see Chapter 3.3) does not end the selection process. There can be a substantial list of variants (see Appendix

1; Table 10.2) even after filtering. Other databases, such as the COSMIC database, and the field of literature can then be used to shortlist candidate mutations.

Pathway analysis softwares, such as Cytoscape (Shannon et al. 2003) are another way to consider a list of variants – to see if any of the proposed variants are linked by similar or different pathways. As the hypothesis here was to find the drivers of recurrence in each tumour, it was useful to see that each of the putative driver mutations appeared to be separate to each other in the pathway analysis (Figure 3.6). Of note, they all appeared separate in pathway and cluster analysis to BRAF, which is known to be key to tumour initiation.

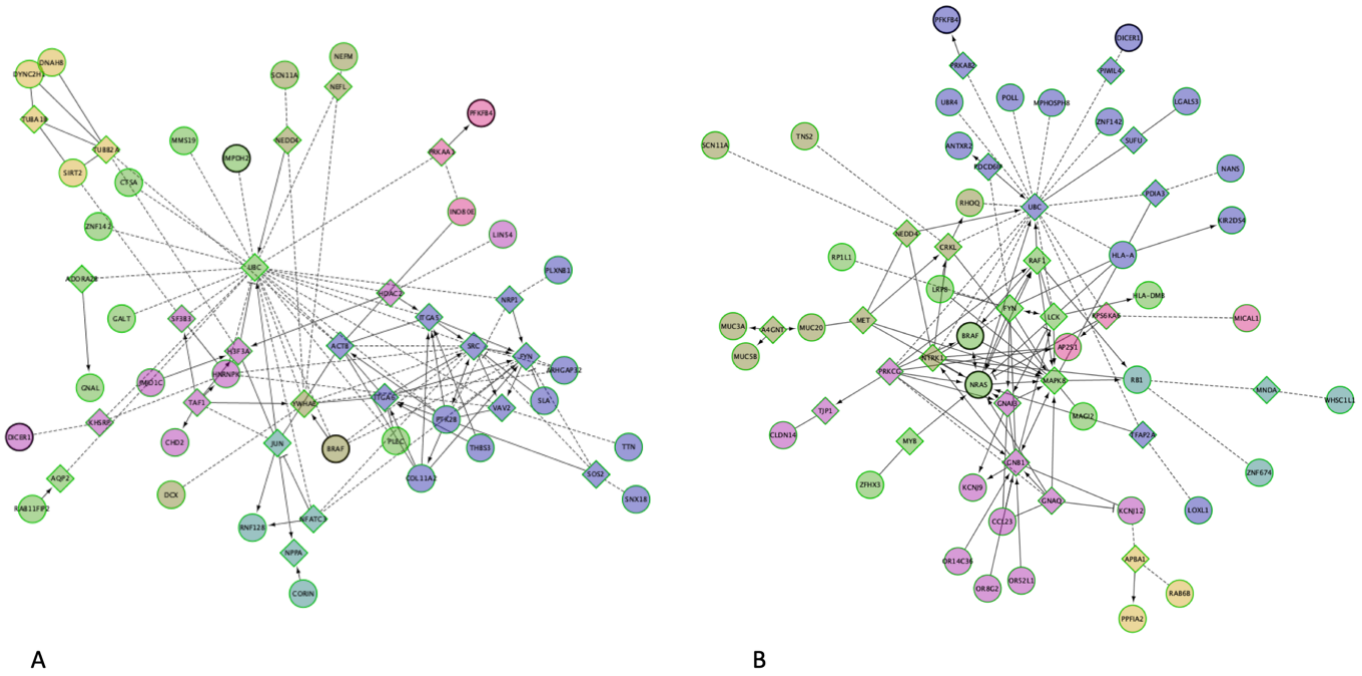

Figure 3.6: Pathway analysis using FI Reactome (Wu and Haw 2017) in Cytoscape (Shannon et al. 2003). This analysis uses linker genes (shown in diamonds) and coloured according to FI Reactome clusters. A) Mutect analysis: Top five significant networks on pathway enrichment, ranked by number of proteins in network: Integrin signaling pathway (p = 0.009), Focal adhesion (p = 0.01), Endothelins (p = 0.01), Signaling events mediated by VEGFR1 and VEGFR2 (p = 0.01), ECM-receptor interaction (p = 0.02). B) Platypus analysis. Top 5 significant networks on pathway enrichment: Neurotransmitter Receptor binding and Downstream Transmission (p = 0.0006), Natural killer cell mediated cytotoxicity (p = 0.0007), Viral carcinogenesis (p = 0.003), Bladder cancer (p = 0.0002), Non-small cell lung cancer (p = 0.0006).

Furthermore, this analysis provides an insight into gene groups that are not necessarily apparent from considering variants individually. This is observed in the analysis of the Mutect mutated genes, as the networks of integrin signalling pathways, focal adhesions and ECM-receptor interaction have been highlighted, suggesting that cell adhesion and migration are key factors in recurrence. Certainly integrins have been implicated before in metastasis (Ganguly et al. 2013), and similar cell survival and migration arguments might hold for recurrence. This is of interest as it is a theme that recurs later in the RNA expression gene analysis (Chapter 6).

The individual genes highlighted by the NGS WES analysis - IMPDH2, PFKFB4 and DICER1 - are all interesting in the context of cancer. Each has a role that may propagate tumour aggressiveness and ability to recur, explored in full in Chapters 4 and 5. DICER1 is also associated with thyroid disease as DICER1 syndrome is caused by a germline mutation in the DICER1 gene. This leads to a susceptibility to pleuropulmonary blastoma, ovarian or testicular tumours, other endocrine tumours and multinodular goitre (MNG). There is also an increased association with differentiated thyroid cancer. However, despite the in-silico validation of these gene variants as pathogenic, it is widely recognised that these need functional validation before they can be employed clinically. Therefore, we took the selected gene variants and recapitulated the mutations using site-directed mutagenesis. These were then transfected into multiple thyroid cancer cell lines and functional studies on the cells were performed, as described in Chapters 4 and 5.

3.4.3 RNA analysis

The heatmap illustrating the overview of the RNA analysis (Figure 3.5) demonstrates the homogeneous nature of the normal tissue phenotype, and the complexity of the tumour phenotype. This has been partly extricated by the addition of the background mutation status (Braf-like, Ras-like or nil). The background mutational profile appears to have an influence over the recurrent and non-recurrent tumours alike. Within the recurrent patient group, it does appear that there is a pattern across the gene expression profile with certain genes more often up- or down-regulated. These results are considered further in Chapter 6, where the RNA expression levels of recurrence versus non-recurrence is explored in more detail, and on an individual gene basis.

3.4.4 Concluding remarks

This chapter has outlined two means of analysis of TCGA data, one using files with variants already called by the TCGA analysis team, one using a novel pipeline from the original 'raw data' files. The results demonstrate a number of potentially pathogenic variants, which may drive a thyroid tumour to recur. Three potential mutational drivers of recurrence in thyroid cancer - IMPDH2 S280C, PFKFB4 Y366C and DICER1 D1810H - have been selected for further investigation and functional validation. This chapter has also introduced the potential for other analyses, such as RNA expression data, which are explored further later in the thesis.

Chapter 4 IMPDH2 and PFKFB4 as mutational drivers of recurrence in thyroid cancer

4 IMPDH2 and PFKFB4 as mutational drivers of recurrence in thyroid cancer

4.1 Introduction

4.1.1 IMPDH2 normal function

Inosine monophosphate dehydrogenase (IMPDH) catalyses the rate-limiting step of guanine nucleotide synthesis, converting inosine monophosphate (IMP) to xanthosine monophosphate (XMP) (Keppeke et al. 2018). XMP is further converted by guanosine monophosphate synthetase (GMPS) into guanosine 5′-monophosphate (GMP) (Jackson et al. 1975). Further processing converts GMP into the nucleotide guanine (Figure 4.1).

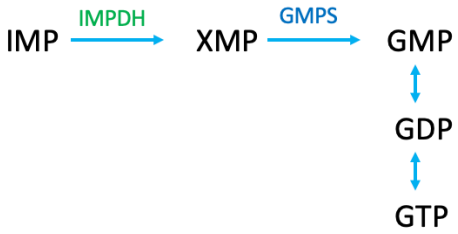

Figure 4.1: Inosine monophosphate dehydrogenase synthesis of guanine pathway. Adapted from (Jackson et al. 1975).

There are two isoforms of inosine monophosphate dehydrogenase: IMPHD1 and IMPDH2 (Natsumeda et al. 1990). These each have a different genetic locus and appear to have different functions; mutations in IMPDH1 causes the ophthalmic disease retinitis pigmentosa, but IMPDH2 mutations do not (Bowne et al. 2002). The IMPDH enzyme is linked to malignancy and proliferation in hepatic disease (Jackson et al. 1975). Expression levels of IMPDH2 in different tissues is variable, and the

activity of IMPDH2 does not always correlate with the expression level, suggesting post-transcriptional modifying events alter enzyme activity (Senda and Natsumeda 1994). It is understandable that IMPDH2 would have a relationship with cellular proliferation, due to the increased demand for nucleotide synthesis required. A recent study suggested that IMPDH2 has a role in PI3K/AKT signalling pathways, showing increased phosphorylated FOXO1 and increased phosphorylated TOR when IMPDH2 was overexpressed (Duan et al. 2018). Phosphorylation of FOXO1 by Akt via IκB kinase (IKK) leads to increased degradation of the tumour suppressor FOXO1 (Massague 2004), suggesting a pathway through which IMPDH2 may implement its proliferative effects. Phosphorylation of TOR results in increased ribosomal protein translation (Massague 2004), (Bjornsti and Houghton 2004), also facilitating increased proliferation. As the PI3K/AKT signalling pathway is implicated in thyroid cancer progression (Petrulea et al. 2015), (Matson et al. 2017), IMPDH2 may be involved here.

4.1.2 IMPDH2 S280C mutation

The IMPDH2 gene is approximately 5.8 kb long and has 14 exons (Zimmermann et al. 1995). The IMPDH2 protein forms a tetramer of identical monomers (Colby et al. 1999). There are two cystathionine beta synthase (CBS) domains, the second of which is within the catalytic domain. Increased expression of IMPDH2 has an impact on cellular proliferation and tumour progression and this would suggest that an oncogenic mutation in IMPDH2 would be likely to be an activating mutation (He et al. 2018). The nearest annotated active sites to the IMPDH2 S280C mutation described in Chapter 3 are serine 276 (highly conserved) (Sintchak et al. 1996) and phenylalanine 282. There has been no investigation of the functional effect of a mutation at site serine 280. There

is no literature on IMPDH2 in thyroid cancer, so functional studies in thyroid cancer cell lines will help consider IMPDH2 function in the context of thyroid cells.

4.1.3 PFKFB4 normal function

The PFKFB family of proteins includes four enzymes all encoded by different genes. They were originally discovered in different tissue types but have been found to have widespread expression. Each protein has a kinase in the N-terminal region and phosphatase domain in the C-terminal region. The kinase domain catalyses fructose-6-phosphate (F-6-P) into fructose 2,6-bisphosphate (F-2,6-BP), which is converted into phosphofructokinase 1 (Pfk1) (Pegoraro et al. 2013). Phosphofructokinase is a key enzyme regulator of glycolysis (Goncalves and Cantley 2018). The phosphatase domain catalyses the destruction of F-2,6-BP, inhibiting the activation of the glycolysis pathway by Pfk1. Thereby, the PFKFB family regulate glycolysis activation by both production and degradation of F-2,6-BP. The four isoforms have highly conserved enzymatic domains and differ mostly in their regulatory regions (Cavalier et al. 2012). Post-transcriptional modification can also alter the function of the protein as can mutations that cause a functional impact.

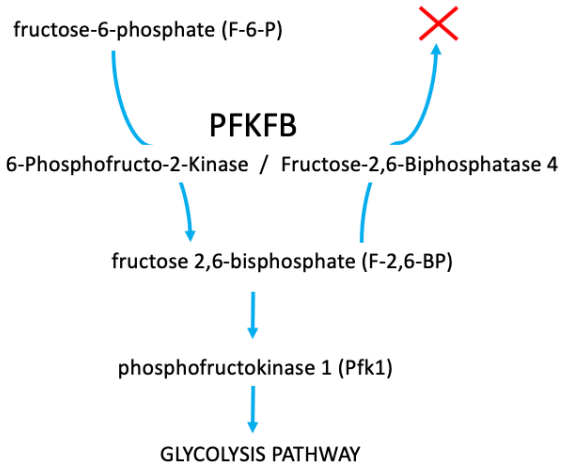

Figure 4.2: The 6-Phosphofructo-2-Kinase/Fructose-2,6-Biphosphatase 4 family regulate glycolysis by both production and degradation of fructose 2,6-bisphosphate (F-2,6-BP).

Cells use the citric acid cycle and oxidative phosphorylation to produce energy in the form of adenosine triphosphate (ATP). Conversely, metabolism in tumours primarily depends on glycolysis, even in aerobic conditions. This is known as the Warburg effect (Vander Heiden et al. 2009). PFKFB4 is also shown to be increased in tumour cell lines exposed to hypoxia (Bobarykina et al. 2006, Minchenko et al. 2014) indicating PFKFB4 could be a key component in helping cancer cells survive.

4.1.4 PFKFB4 Y366C mutation

PFKFB4, like the other PFKFB isoforms, is a homodimeric bifunctional enzyme. Each 55 kDa monomer contains the kinase and phosphatase region. PFKFB4 has been demonstrated to be overexpressed in other cancers, including bladder cancer and has been considered as a prognostic biomarker (Yun et al. 2012). In prostate cancer, it has been shown to be integral to proliferation, invasion and migration (Li et al. 2017). This would indicate that it is possible that a driver mutation in PFKFB4 could be an activating

mutation, especially if it occurs in an active biological domain. However, considering the bifunctional nature of the protein, and that the mutation PFKFB4 Y366C is in the fructose-2,6-bisphosphatase domain it could be that an oncogenic mutation reduces the function of the phosphatase domain, which destroys F-2,6-BP and reduces effective glycolysis.

4.1.5 PFKFB4 in The Cancer Genome Atlas (TCGA)

TCGA data reveal there is another thyroid cancer patient with a different PFKFB4 mutation (Y401C) in a patient who did not have documented recurrence by the close of the study – a 75-year-old man living at 44 months after diagnosis. This was again seen on a background mutation of NRAS Q61K. Overall in TCGA, there was a 0.8 % somatic mutation frequency in PFKFB4 across the PanCancer Atlas study (Cerami et al. 2012, Gao et al. 2013). The most common PFKFB4 mutations were observed in the lymphoid neoplasm Diffuse Large B-cell Lymphoma (8.3 %), melanoma (4 %) and uterine carcinoma. The survival curve for those with mutations compared to those without is equivocal (Figure 4.3), which fits with the potentially opposing nature of the mutation effect on the glycolysis pathway.

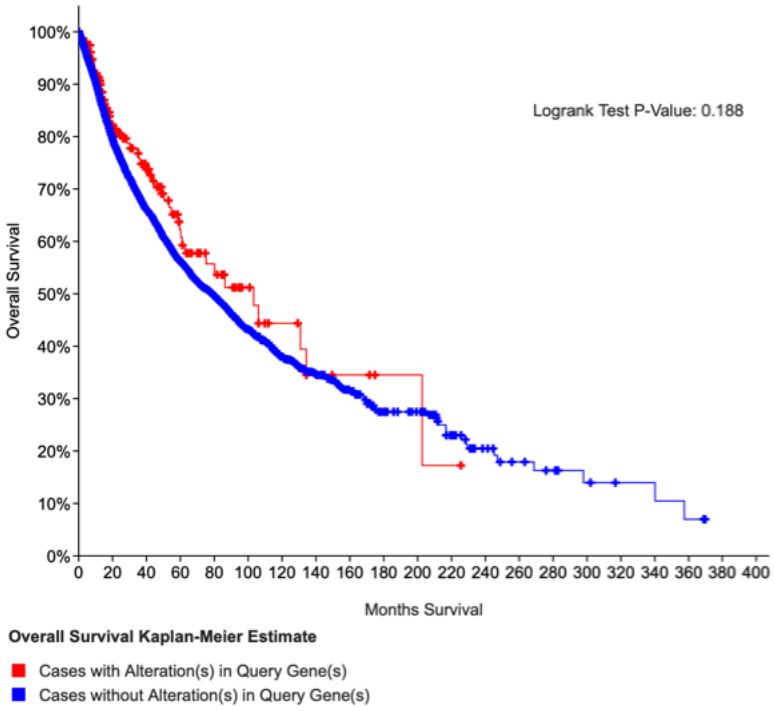

Figure 4.3: Kaplen-Meier estimates of overall survival against time (months) retrieved from TCGA cbioportal PanCancer Atlas for PFKFB4 mutations for all cancers. There is no significant difference in survival between those with and without PFKFB4 mutations (Cerami et al. 2012, Gao et al. 2013).

4.1.6 IMPDH2 in The Cancer Genome Atlas (TCGA)

There are two thyroid cancer patients in the TCGA with recurrent disease that have IMPDH2 mutations – S280C and R355W. The FATHMM score (Shihab et al. 2013) was deleterious for the mutation S280C and tolerated for R355W hence S280C was taken forward for futher investigation. Overall in the PanCancer Atlas, there was a somatic mutation rate of 0.3 % in IMPDH2. The association with survival is shown below in Figure 4.4 and while survival is initially better, patients with IMPDH2 mutations die younger than those without.

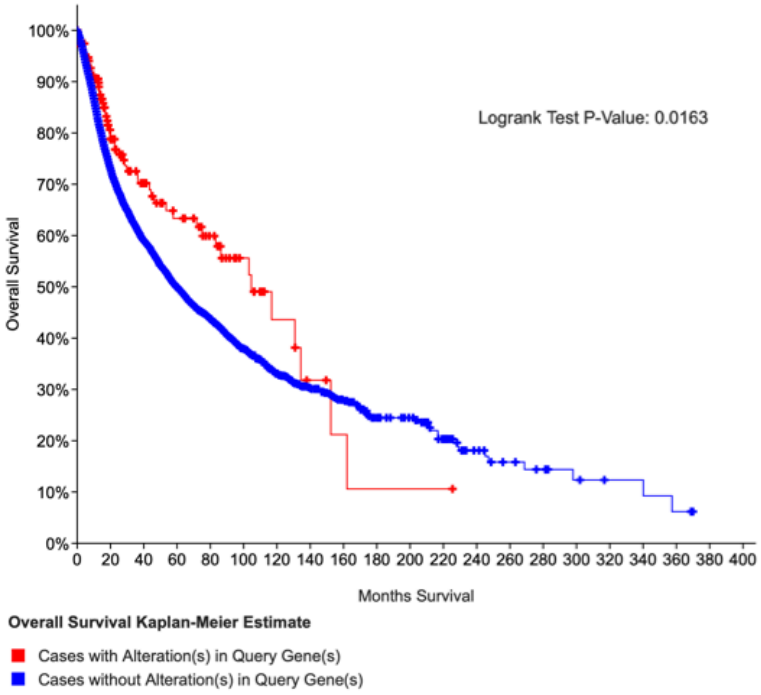

Figure 4.4: Kaplan-Meier estimates of overall survival against time (months) retrieved from TCGA cbioportal PanCancer Atlas survival graph for IMPDH2 mutations (Cerami et al. 2012, Gao et al. 2013).

4.1.7 IMPDH2 and PFKFB4 in Iterative Threading ASSEmbly Refinement (I-TASSER)

Both the wildtype and mutant of each protein were put through the online I-TASSER portal, which is a platform for prediction of protein structure and function (Roy et al. 2010) and the STRUM portal (Quan et al. 2016), which uses i-TASSER as part of its prediction of protein structure stability. Here it was used to assess the effects of the missense mutations, as a significant impact on protein stability is likely to confer a larger functional effect. IMPDH2 wildtype and mutation is shown in Figure 4.5 below.

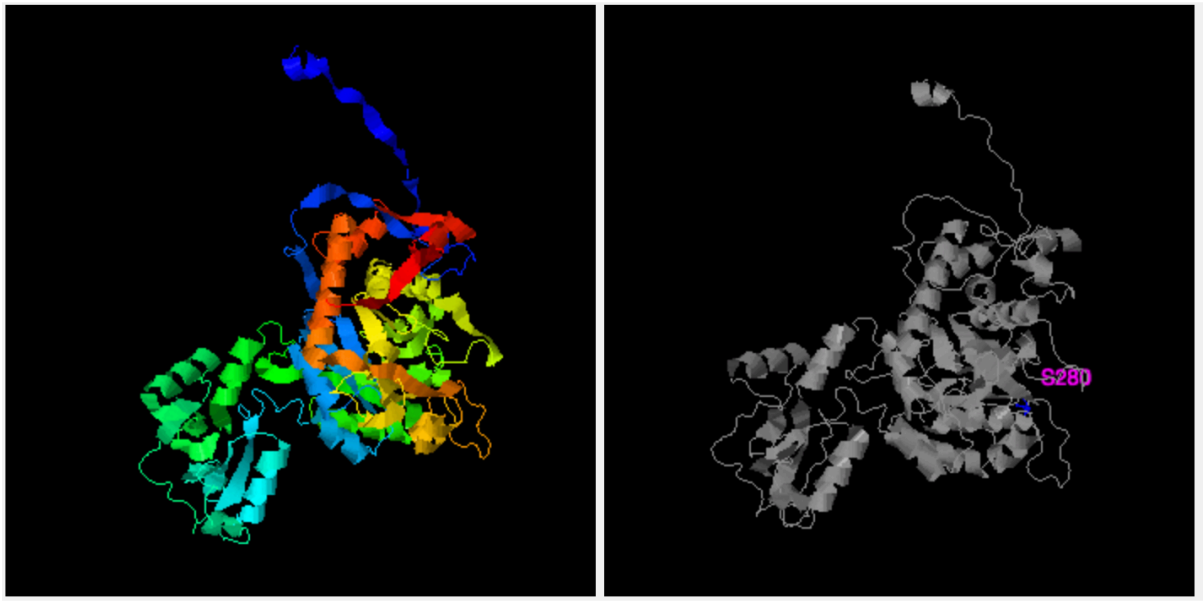

Figure 4.5: STRUM structure stability prediction for IMPDH2 wildtype and S280C mutation. Coloured image shows protein structure predicted by iTASSER and colours represent different domains. Grey image demonstrates location of missense mutation. Stability change (ddG) score -0.35 (score < 0 indicative of mutation causing destabilisation (Quan et al. 2016)).

PFKFB4 mutation on the prediction software also demonstrated a change in protein stability, as seen in Figure 4.6 below.

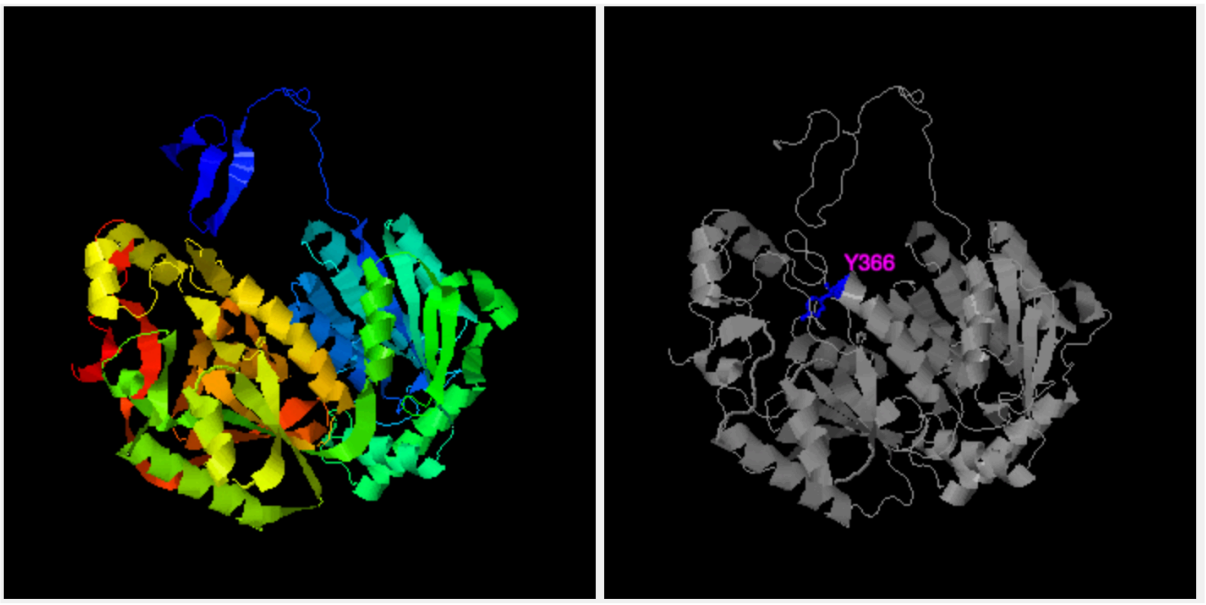

Figure 4.6: STRUM structure stability prediction for PFKFB4 wildtype and Y366C mutation. Coloured image shows protein structure predicted by iTASSER and colours represent each protein domain. Grey image demonstrates location of missense mutation. ddG score -0.08 (Quan et al. 2016).

4.2 Materials and Methods

4.2.1 Cell culture

TPC-1 cells, SW1736 cells and Cal-62 cells were cultured in RPMI in 75 cm² flasks and seeded into 6 well plates as described in section 2.1. After 24 hours in the 6-well plate cells were transfected with vectors containing IMPDH2 and PFKFB4 as detailed in section 2.2.6.

4.2.2 Protein extraction and Western blotting

Protein extraction and Western blotting was performed according to section 2.4. Protein was denatured for 5 minutes at 95 °C. Samples were run on a 10 % resolving gel and transfer was for 1 hour 15 minutes. Western blots were probed with rabbit polyclonal anti-IMPDH2 antibody (12948-1-AP) (Proteintech, Illinois, USA) 1:1000 v/v and rabbit polyclonal anti-PFKFB4 antibody (ab71622) (Abcam, Cambridge, UK) 1:200 v/v.

4.2.3 Cell invasion and migration assays

Cell invasion assay was performed as per section 2.7 with reseeding after 24 hours and invaded cell fixing at 48 hours. Cell migration scratch wound assay was performed in 10 % RPMI media after 48 hours incubation. The time points were 4, 8, 12 and 24 hours and details are documented in section 2.8.

4.2.4 Quantification of immunofluorescent microscopy findings

Immunofluorescent slides were created as per section 2.5. In order to quantify the length of intracellular bodies Image J was used to convert the image scale from pixels to μM. Mean number of bodies and mean length were calculated and analysed in GraphPad Prism.

4.3 Results

4.3.1 Cell invasion

In order to investigate the effect of IMPDH2 and PFKFB4 mutations on cellular invasion, cell invasion assays were performed. Wildtype IMPDH2 transfection appeared to cause an increase in cell invasion in transfected cells in the TPC-1 cell line but only the mutant did significantly enhance invasion compared to VO (Figure 4.7). There was no significant difference between WT and mutant. A similar trend was seen in the SW1736 cell line where both the wild type and the mutant transfected IMPDH2 showed increased invasion, although findings were non-significant. The Cal-62 cell line did not show any significant difference between VO, WT and mutant IMPDH2. The accompanying Western blot confirms overexpression of IMPDH2 WT and mutant. The results suggests that while over-expression of the IMPDH2 protein may drive some invasion, mutation of the S280C residue per se is not associated with increased cell invasiveness.

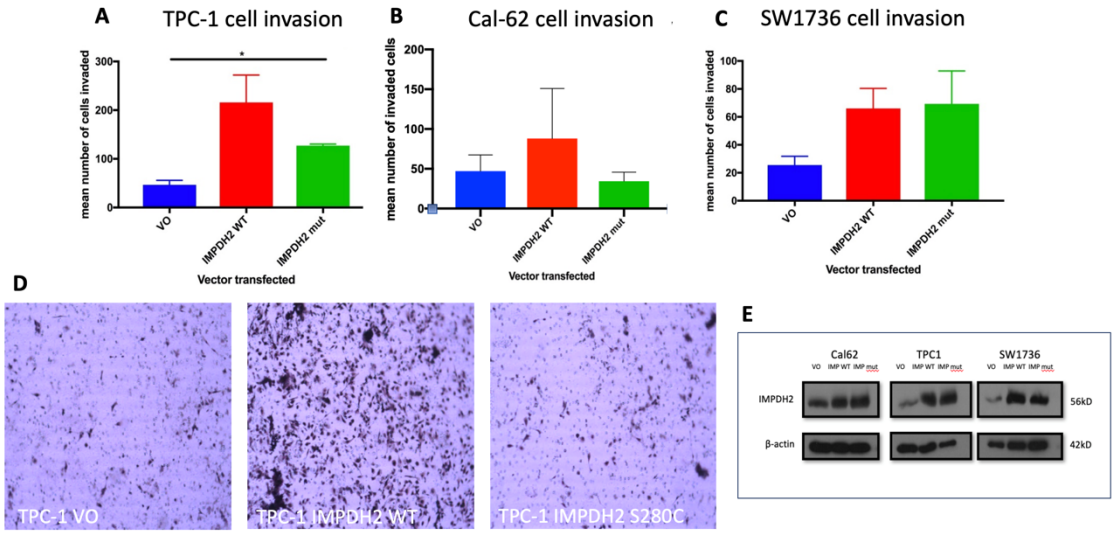

*Figure 4.7: A, B & C: Cell invasion assay comparing vector only (VO), IMPDH2 wildtype (WT) and IMPDH2 missense mutation S280C (mut) in three cells lines (TPC-1, Cal-62 and SW1736). D: Representative microscopy images below demonstrate cell invasion through the Matrigel matrix and membrane. 10x magnification. D) Western blot demonstrates successful transfection of IMPDH2 wild type (WT) and IMPDH2 mutant S280C (mut) in three cell lines. n = 3 separate experiments, * $p < 0.05$.*

The cell invasion assay for PFKFB4 demonstrated no change in cell invasiveness between VO, WT and mutant (Figure 4.8) in any cell lines.

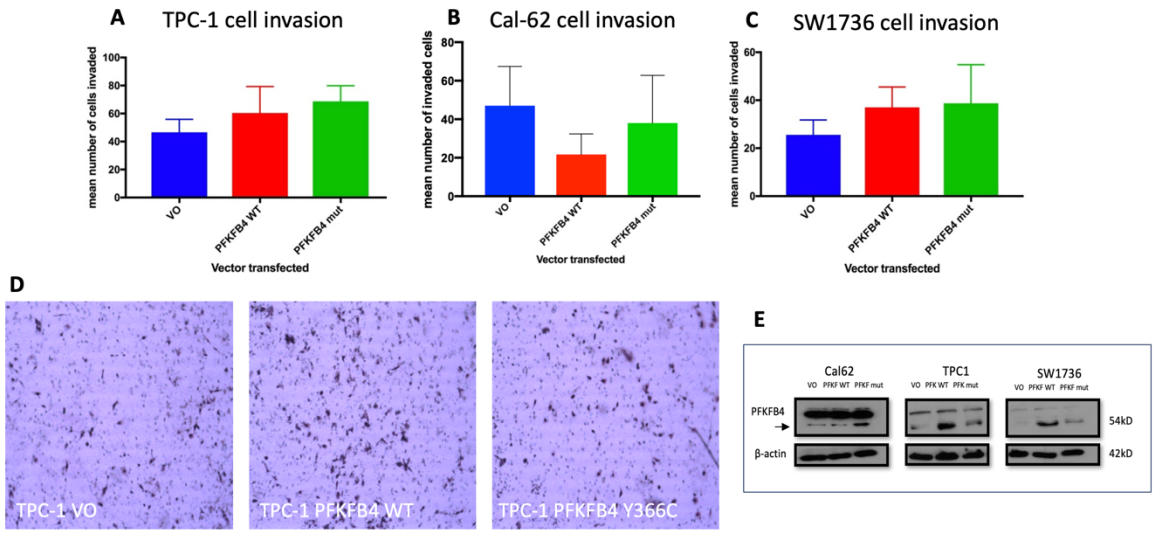

Figure 4.8: A, B & C: Cell invasion assay comparing vector only (VO), PFKFB4 wildtype (WT) and PFKFB4 missense mutation Y366C (mut) in three cells lines (TPC-1, Cal-62 and SW1736). D: Representative microscopy images below demonstrate cell invasion through the Matrigel matrix and membrane. 10x magnification. E: Western blot demonstrates successful transfection of PFKFB4 wild type (WT) and PFKFB4 mutant Y366C (mut) in three cell lines. n = 3 separate experiments, all not significant.

4.3.2 Cell migration

Cell migration is another useful marker of altered cellular behaviour and if gene mutations are implicated in recurrence it is probable that expression of these mutations in cell lines might result in a pro-migratory phenotype. Overexpression of IMPDH2 in TPC-1 cells resulted in an increase in migration of the IMPDH2 mutant compared to both VO and wild type IMPDH2 (Figure 4.9) ($p < 0.05$). There was no significant difference between VO and WT, demonstrating this is likely due to the mutation rather

than overexpression. This was seen at all time points (4 hours, 8 hours and 24 hours). However, the overexpression of IMPDH2 WT and mutant in the Cal-62 cell line and SW1736 cell line did not significantly alter cellular migration.

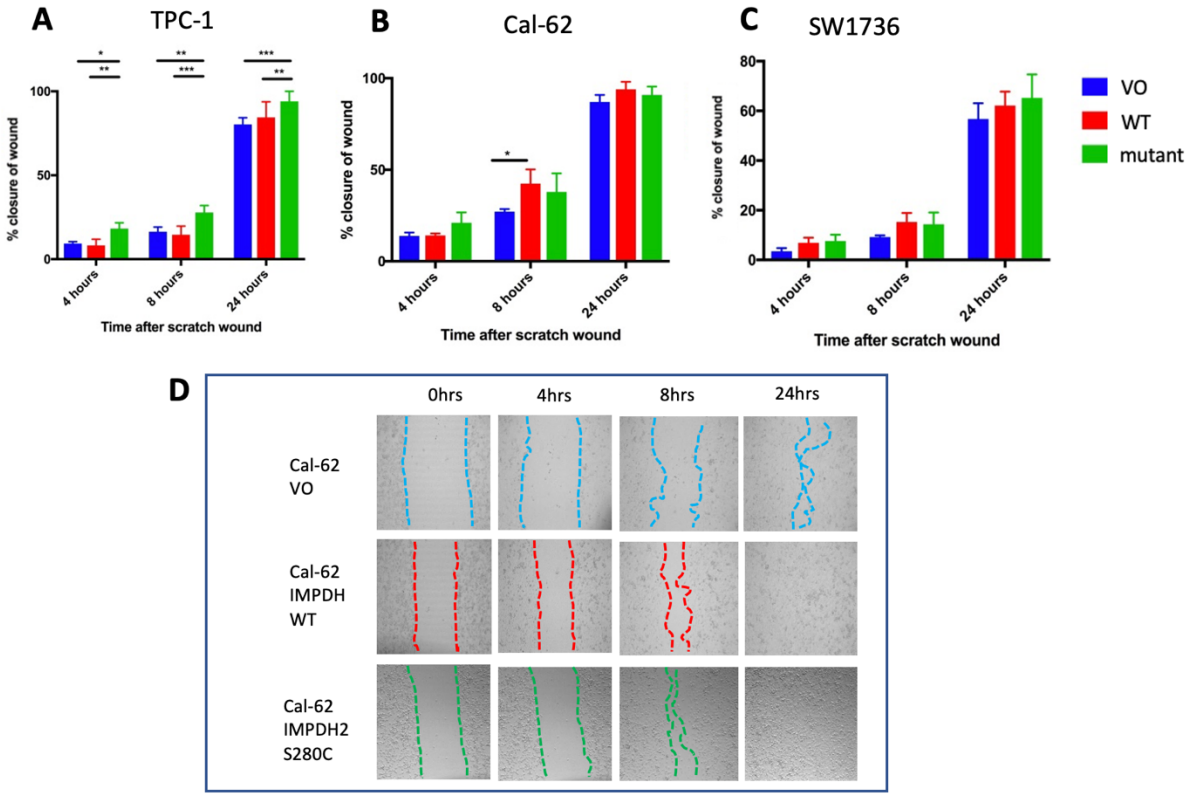

*Figure 4.9: A, B & C: Cell migration assay comparing vector only (VO), IMPDH2 wildtype (WT) and IMPDH2 missense mutation S280C (mutant) in three cells lines (TPC-1, Cal-62 and SW1736). D: Light microscopy images show representative healing of scratch wounds over time in different conditions, 10x magnification. n = 3, * p < 0.05, ** p < 0.01, *** p < 0.001.*

For PFKFB4 WT and mutant expression, the cell migration assay was not significant at any timepoint in any of the cell lines.

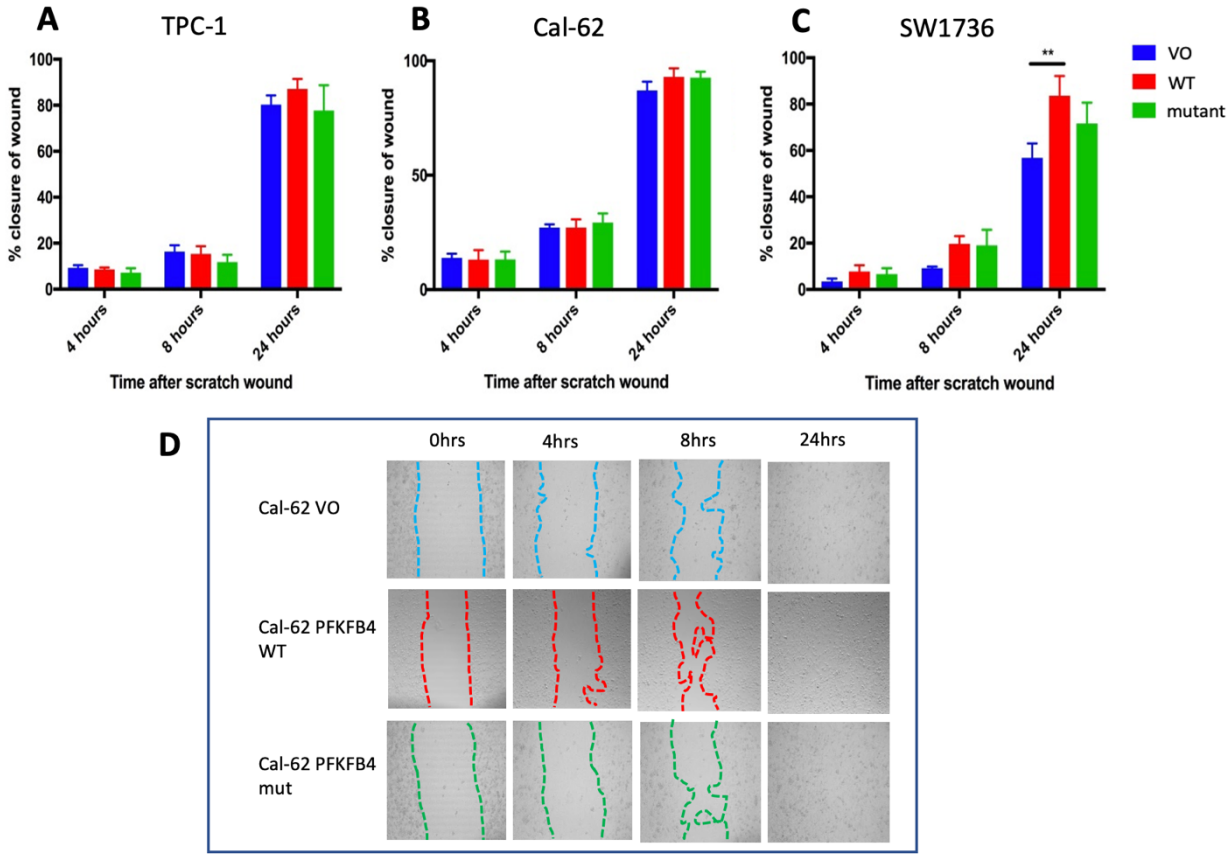

*Figure 4.10: A, B & C: Cell migration assay comparing vector only (VO), PFKFB4 wildtype (WT) and PFKFB4 missense mutation Y366C (mutant) in three cells lines (TPC-1, Cal-62 and SW1736). D Light microscopy images show representative healing of scratch wounds over time in different conditions, with no difference seen in the different conditions. 10x magnification. n = 3, ** p < 0.01.*

4.3.3 Immunofluorescent imaging examining subcellular localisation of IMPDH2 and PFKFB4

Immunofluorescent imaging was performed on cells transfected with VO, IMPDH2 WT and IMPDH2 S280C, and stained for IMPDH2 using anti-IMPDH2 antibody (12948-1-AP) (Proteintech) 1:50 v/v. The same procedure was performed for PFKFB4 WT and

the Y366C mutant using the anti-PFKFB4 antibody (ab71622) (Abcam) 1:50 v/v. For PFKFB4 there was no difference in subcellular localisation between the wild type and mutant proteins (Figure 4.11), with diffuse cytoplasmic staining seen with more intensity in the perinuclear region. The VO images have been adjusted to make the cells visible, the endogenous (and VO) cells were much less bright than the transfected cells (both wild type and mutant).

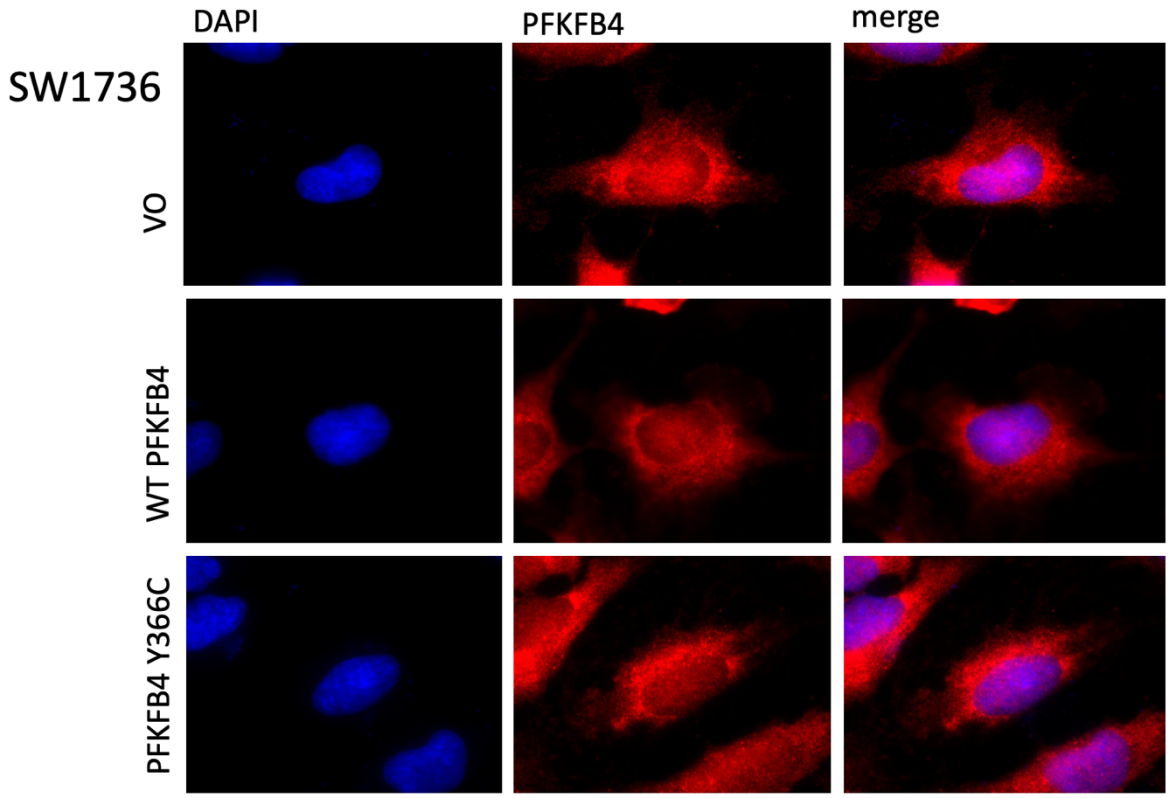

Figure 4.11: Immunofluorescent images demonstrating PFKFB4 WT and mutant over-expression in SW1736 cells. Stained with DAPI (blue) and anti-PFKFB4 (red). 40x magnification.

Upon IMPDH2 transfection (described in section 2.5) intracellular bodies were apparent (Figure 4.12).

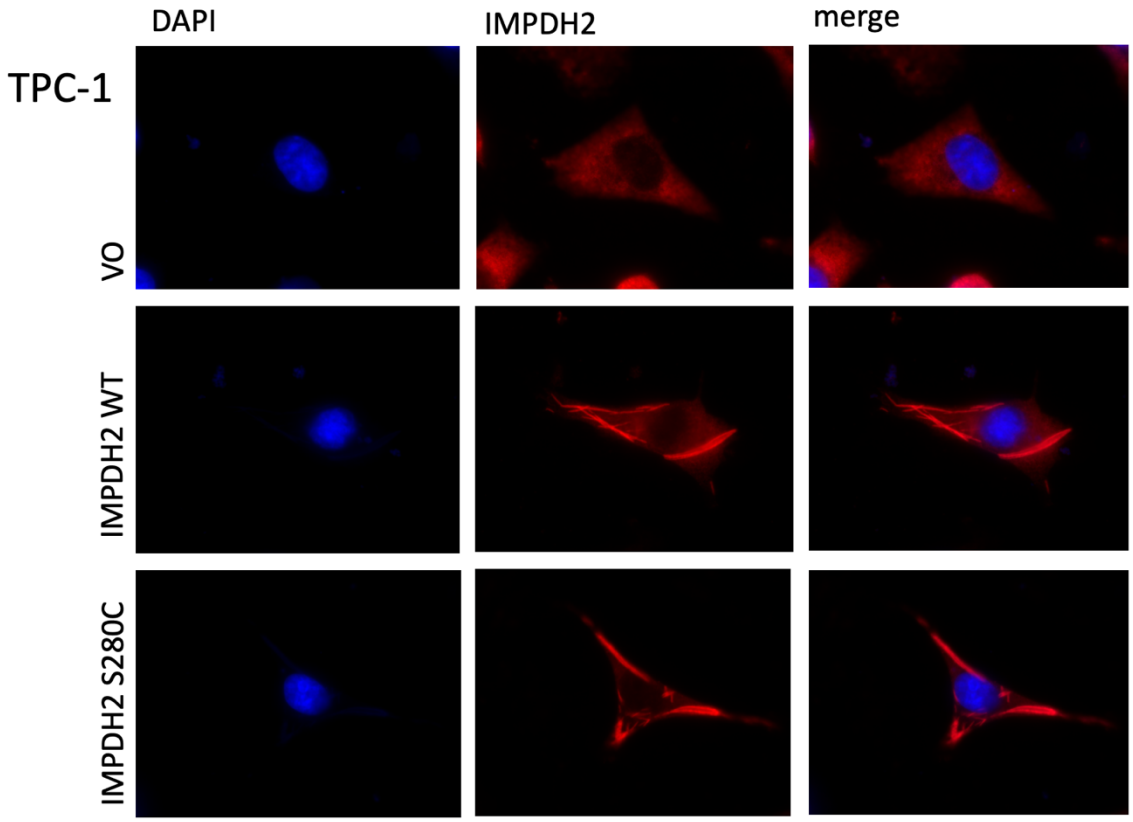

Figure 4.12: Immunofluorescent images demonstrating IMPDH2 WT and mutant over-expression in IMPDH2 cells. Stained with DAPI (blue) and anti-IMPDH2 (red). 40x magnification.

Further images were taken with the ZEN confocal microscope (Zeiss; Oberkochen, Germany) following staining with an ER marker (anti-PDI antibody; Figure 4.13), which suggested these to be cytoophidia or ‘rods and rings’, previously described in hepatic cell lines (Chang et al. 2015). The intracellular bodies were located independently from the ER.

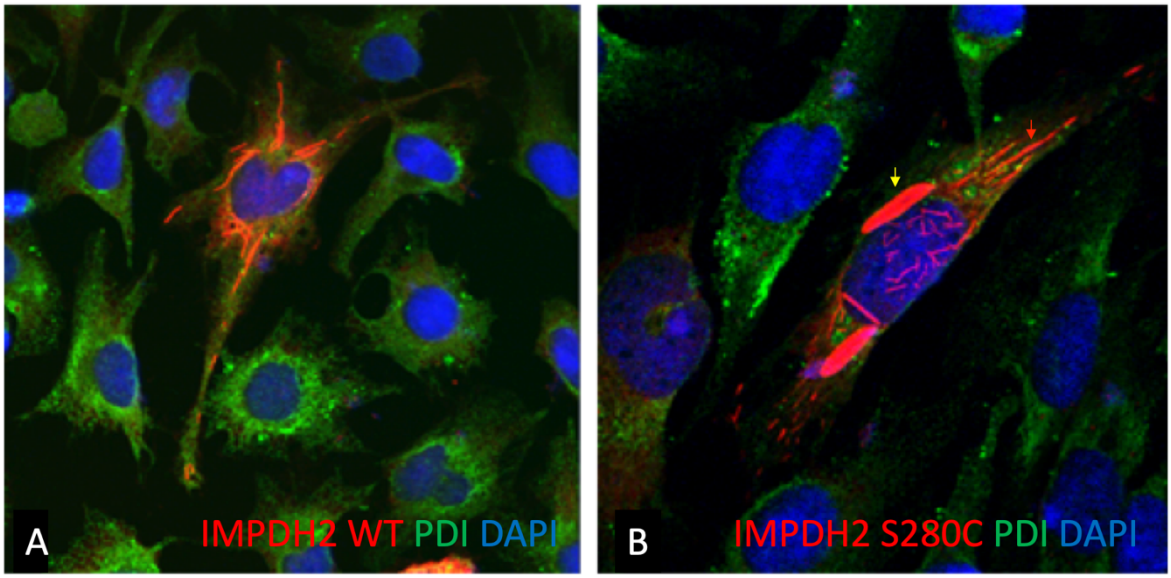

Figure 4.13: Immunofluorescent image demonstrating 'rods and rings' in SW1736 cell line taken on confocal microscope. A) IMPDH2 WT stained with anti-IMPDH2 antibody (red), DAPI (blue) and PDI (green). B) IMPDH2 S280C. Red arrow rod, yellow arrow ring.

The cytoophidia were observed both when wildtype or mutant IMPDH2 were over-expressed in all cell lines examined – TPC-1, SW1736 and HeLa cells. They were not seen in the VO transfected cells. In order to quantify whether the rods and rings were different between the wild type and mutant groups the number and length of the rods and rings were measured using Image J. The size and number of rods and rings (n = 5 cells) was not significantly different (Figure 4.14).

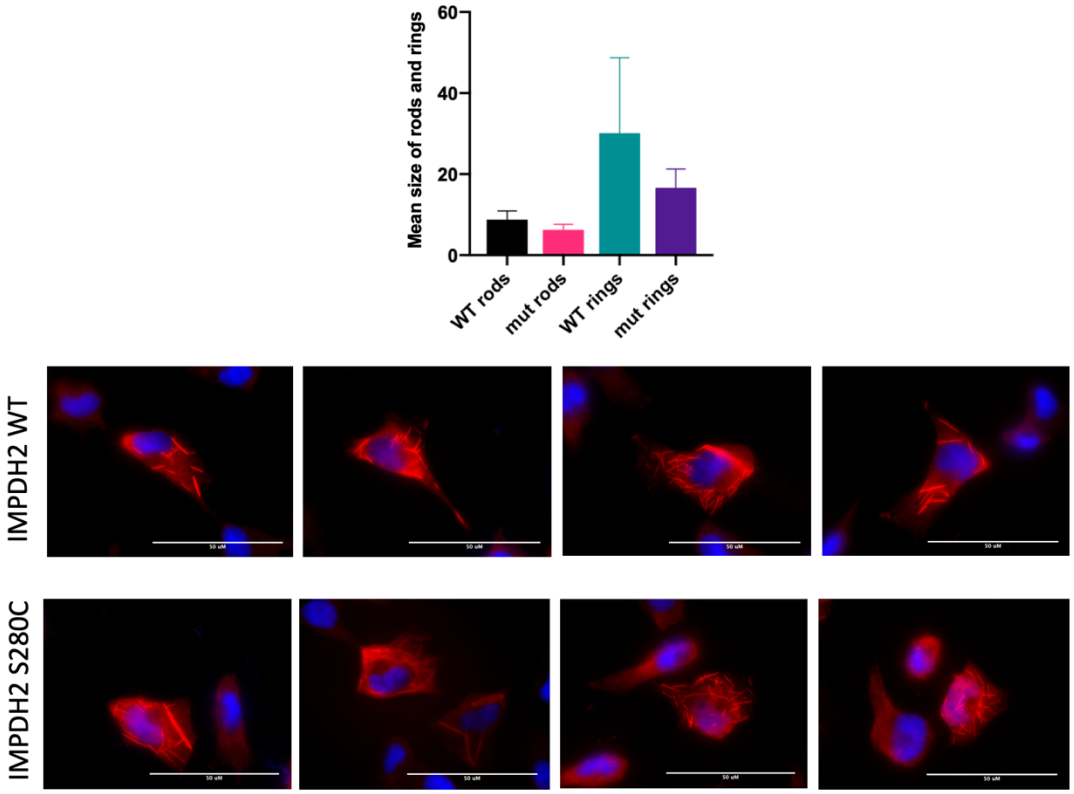

Figure 4.14: Immunofluorescence images for cytoophidium quantification and graph depicting mean size of rods and rings counted in wildtype (WT) vs IMPDH2 S280C (mut) TPC-1 cells. Immunofluorescent images of representative pictures (40x magnification, n = 5). Scale bar = 50 μM, all not significant.

4.3.4 Effect of IMPDH2 mutation on cell proliferation

As the presence of cytoophidia can be associated with altered cell turnover, MTS assays were performed to assess the effect of both wildtype and mutant IMPDH2 on cell proliferation. No significant changes in proliferation were apparent following transfection with wild type compared to mutant in either cell line (Figure 4.15).

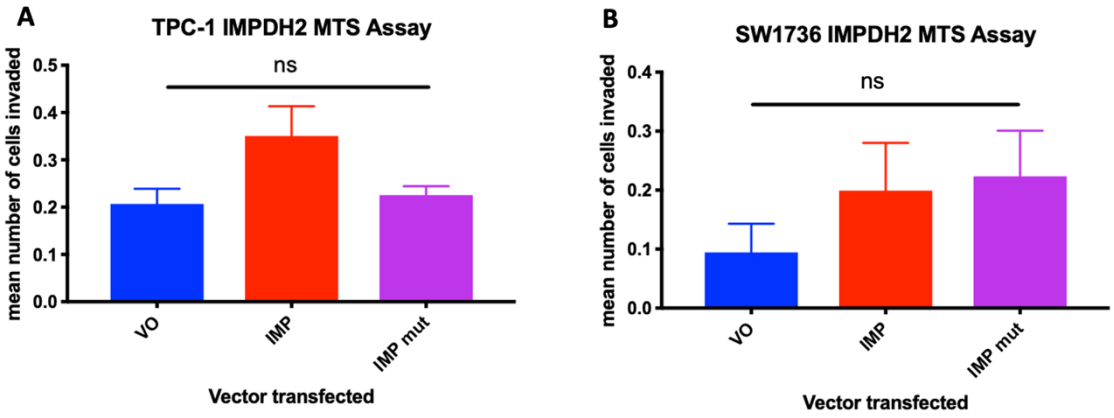

Figure 4.15: Cell proliferation assay (MTS) comparing vector only (VO), IMPDH2 wildtype (WT) and IMPDH2 missense mutation S280C (mut) in A) TPC-1 and B) SW1736 cell lines. n = 3, ns = not significant.

4.4 Discussion

4.4.1 IMPDH2

IMPDH2 demonstrated an increase in invasion and migration in one cell line (TPC-1). The TPC-1 cell line has a RET/PTC1 rearrangement and is $BRAF^{V600E}$ negative, whereas the IMPDH2 mutations observed in the patients were on a background of a $BRAF^{V600E}$ mutation. The proliferation assay showed only a modest, non-significant, increase in proliferation in the context of the $BRAF^{V600E}$ mutation (SW1736 cell line). Therefore, the summation of the data from the overexpression of WT and S280C mutant IMPDH2 was that there was no significant difference between the wildtype and mutant for cell turnover.

The cytoophidia observed in immunofluorescence (IF) studies have been demonstrated before but this is a novel finding in thyroid cancer cell lines (Chang et al.

2018). They are enzymatic macrostructures within the cell, comprising superstructures of the enzyme IMPDH2 and of its pyrimidine-synthesis counterpart cytidine 5′-triphosphate (CTP) synthase (Liu 2011). Cytoophidia are highly conserved across species and can be induced by specific treatment in other cell lines, such as glucose deprivation (Liu 2011). They are thought to be induced by the metabolically active cell and play a role in proliferation and metabolism (Keppeke et al. 2018). This is in keeping with the induction of formation of the cytoophidia in the transfected cells, as it might be expected in conjunction with an increase in proliferation, as would be found in aggressive tumours. However, when the MTS proliferation assay was performed only a moderate, non-significant increase in proliferation was demonstrated, suggesting that cytoophidia do not directly drive cell turnover in thyroid cells. There is a possibility that this is a limitation of the MTS assay itself, which is commonly used as a viability assay too, and alternative assays such as a Bromodeoxyuridine/5-bromo-2'-deoxyuridine (BrdU) assay may examine this more effectively.

To further investigate the effect of the IMPDH2 S280C mutation, which showed functional effects on the cells in the TPC1 cell line, a pathway analysis could be undertaken in the future. A simple way to investigate this further would be to examine the levels of Akt and phosphorylated FOXO1 by Western blotting, as this might help us understand if the mutant is having an impact via the PI3K/AKT signalling pathway.

IMPDH2 overexpression has been observed in many cancers, and induction of cytoophidia in metabolically active cells may signify that this could be a potential therapeutic target. However, to date IMPDH2 inhibitors (such as azathioprine,

mycophenolic acid and ribavirin) have not shown much potential in cancer therapy and are used in immunosuppression (and viral disease in the case of ribavirin). Conceivably, the assembly and disassembly of IMPDH2 into suprastructures could be a future drug target (Calise et al. 2018), but much more would need to be known and understood in cytoophidia function before this could be a realistic option and have a therapeutic impact. One reasonable step to determine more accurately if this is an activating mutation would be to use clustered regularly interspaced short palindromic repeats (CRISPR)-Cas9 gene editing to create a cell line with the mutation but with no change in expression levels.

4.4.2 PFKFB4

While the results for PFKFB4 overexpression in thyroid cancer cell lines did not demonstrate an increase in cell invasion or migration, this may be because the cell line cells were under relatively little stress. As a key component of the glycolysis pathway PFKFB4 helps tumour cells evade apoptosis during hypoxia (Chesney et al. 2014). It has been shown that PFKFB4 mRNA expression increases in cell spheroid formation compared to monolayers (Gao et al. 2018) – this may be because once a sphere is formed the centre is in a relatively hypoxic environment where glycolysis and the PFKFB4 pathway are more important (Zhang et al. 2016). Future work with PFKFB4 in organoids would be very interesting and may demonstrate more effectively whether this is an activating mutation. Organoids were created during this study (Figure 4.16) but the model was not established enough by the end of the PhD to examine the PFKFB4 mutation.

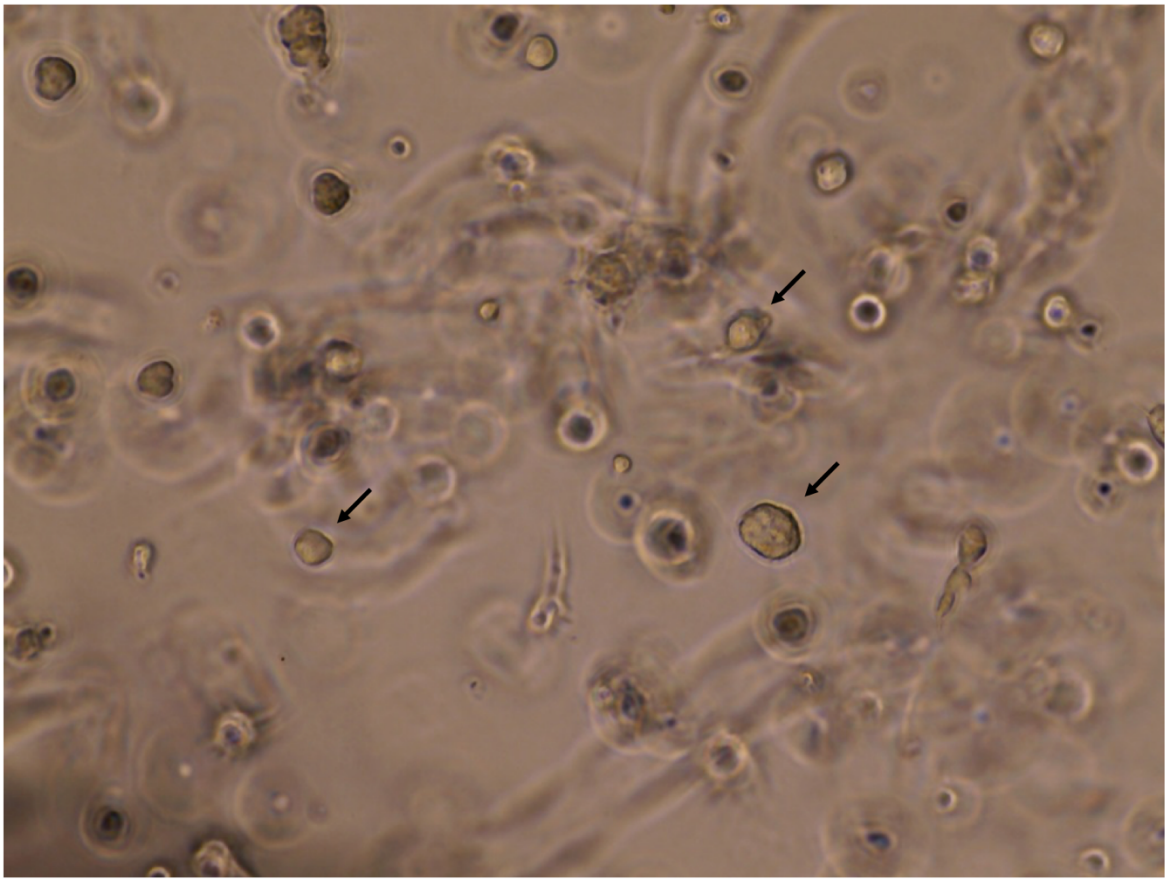

Figure 4.16: Light microscopy image of Cal-62 cells growing in 3D formation in Matrigel. Cells were resuspended in RPMI media at 5,000 cells/µl. 1 µl of cell medium was added to 49 µl of 10 % Matrigel. This was pipetted into a dome in the centre of a 6-well plate and placed into the incubator for 30 minutes at 37 °C with 5 % CO_2. Organoid media was added after the 30 minute incubation around the Matrigel dome in the well. Organoid media were created using: Advanced RPMI (Thermo Fisher Scientific), N-acetyl-l-cysteine 2.5 mM (Sigma-Aldrich), Epidermal growth factor (EGF), 50 ng/ml (Pepro Tech, New Jersey, USA), Fibroblast growth factor 10 (FGF10) 100 ng/ml (Pepro Tech), R-spondin-1 200 ng/ml (R&D Systems), Noggin 100 ng/ml (Pepro Tech), Wnt-3a 30 ng/ml (Wako Pure Chemical Industries, Virginia, USA), Thyroid-stimulating hormone (TSH) 16 mIU/ml Sigma-Aldrich, GlutaMax 2 mM (Invitrogen), HEPES buffer 10 mM (Sigma-Aldrich), penicillin-streptomycin (Invitrogen) – 1ml/100ml. Arrows highlight organoids in focus in this plane.

Further to this, another way to investigate the role of PFKFB4 would be to stress the cells, in a similar way to might be found in a tumour environment. This could include measures such as FBS deplete media, or a hypoxic cell culture chamber and measuring the cell response between vector only, wildtype and mutant transfected cells. Assays such as a Seahorse XF24 Extracellular Flux Analyzer (Seahorse Bioscience, Massachusetts) can determine the oxygen consumption, glycolysis rates and ATP consumption and therefore give a quantifiable account of the metabolism in cell lines, and might further our understanding of how PFKFB4 might alter cell glycolysis. However, there is the possibility that the PFKFB4 variant investigated is not an oncogenic driver in thyroid cancer, which highlights the importance of functional validation of bioinformatic analyses.

4.4.3 Concluding remarks

Neither the IMPDH2 mutation nor the PFKFB4 mutation demonstrated a profound effect on cell invasion or migration or proliferation, three assays often used to appraise oncogenic driver events. This may in part be due to the modelling used for the gene mutations, as discussed in this chapter. The overexpression of the wildtype gene and mutant is done on the background of a normal expression of endogenous protein, and this will potentially limit effects seen. If these somatic mutations were profound driver mutations it might be expected that more obviously aggressive behaviour would be observed. It may be that these mutations only confer a survival advantage to tumours, enabling recurrence, under certain settings. For example, hypoxia for PFKFB4. Interactions with the tumour microenvironment are complex and difficult to model, however. The reason tumours recur is complex and multifactorial. Although these

somatic mutations possibly contribute to recurrence a clearer demonstration of a functional link would need to be exhibited in order to consider them as key biomarkers.

Chapter 5 DICER1 in thyroid cancer

5 DICER1

5.1 Introduction

5.1.1 DICER1 normal function

DICER1 is located on chromosome 14q32.13 and consists of 27 exons. It has 1922 amino acids and encodes the ribonuclease Dicer, which is a key component in post-transcriptional gene modification. Dicer cleaves pre-microRNAs into microRNAs (miRs) and also cleaves non-coding double stranded RNA segments into small interfering RNAs (siRNAs). Dicer also forms part of the RNA-induced silencing complex (RISC), which uses miRNA or siRNA to identify the target complementary mRNA (Foulkes et al. 2014). Dicer loads these RNAs onto the Argonaute protein Ago 2 for formation of the RISC and is part of the RISC itself, alongside the human immunodeficiency virus transactivating response RNA-binding protein (TRBP). These dicer functions are demonstrated in Figure 5.1 below, which shows the pathway of miRNA from their primary status to their active function in gene silencing.

The dicer protein is thought to form an L structure, with the helicase domain in the base, adjacent to the RNAse IIIa and IIIb regions. The helicase may have a role in clamping the substrate RNA, and the two RNAse domains form a catalytic core, which cleaves RNA (Foulkes et al. 2014). Aside from the role in small interfering RNA function, Dicer also has an antiviral function, where it cleaves the viral RNA into viral siRNA so that it can be loaded onto the RISC complex. The viral siRNA then facilitates targeting and breakdown of the viral mRNA (Berkhout and Haasnoot 2006).

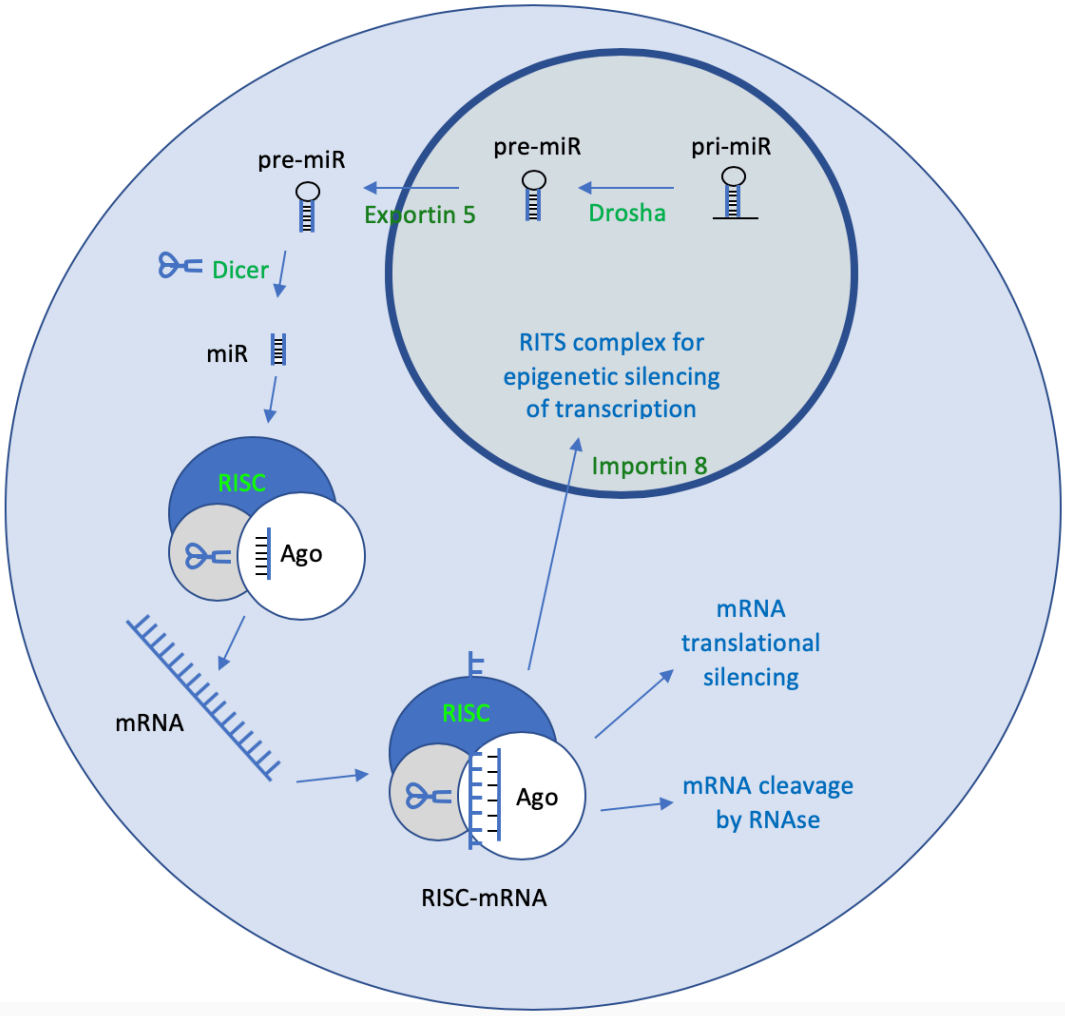

Figure 5.1: MicroRNA function and interaction with Dicer. Three types of gene silencing are demonstrated: mRNA cleavage by the RNAse activity of Argonaute 2 (Ago), mRNA translational silencing, and migration of the miRNA-Ago complex to the nucleus to form an RNA-induced transcriptional silencing (RITS) complex. Translational silencing can occur via deadenylation and degradation, 5' decapping and reduced stability, or inability of ribosomal attachment due to Ago binding. Figure based on diagrams and information from (Pratt and MacRae 2009), (Carthew and Sontheimer 2009) and (Liu et al. 2018). miR, microRNA; Pri-miR, primary miRNA; pre-miR, miR precursor; RISC, RNA-induced silencing complex; Ago, Argonaute 2; mRNA, messenger RNA; RITS, RNA-induced transcriptional silencing.

DICER-induced post-transcriptional modifications impact oncogenes and tumour suppressor genes, which may explain the complex role Dicer has in carcinogenesis (Solarski et al. 2018). In general, reduced expression of DICER1 is associated with cancer, but this varies between tissue type (Foulkes et al. 2014). For example, lower levels of DICER1 expression have been associated with a poorer prognosis in lung, breast, skin, endometrial and ovarian cancer, whereas metastatic prostate cancers showed overexpression of DICER1 (Foulkes et al. 2014).

5.1.2 DICER1 somatic mutations

DICER1 mutations can occur anywhere in the gene, and germline mutations are found throughout the gene. Interestingly, somatic mutations in tumours tend to cluster in the RNAse IIIb region, which corresponds to the catalytic core of the Dicer protein. Specifically, they are observed most frequently in six metal ion binding spots: p.E1705, p.D1709, p.D1713, p.G1809, p.D1810 and p.E1813 (de Kock et al. 2019). These mutations appear to be often associated with another DICER1 mutation in the other allele, suggesting a loss of heterozygosity (LOH) two-hit hypothesis. However, contrary to the LOH hypothesis, the mutations seen in the metal ion binding regions do not appear to cause Dicer a complete loss of function, but rather change the function (de Kock et al. 2019, Foulkes et al. 2014). For example, a mutation in the RNAse IIIa region appears to reduce the cleavage and production of 3p miRs and the common hotspot mutations on the RNAse IIIb region affect cleavage of the 5p miRs. As a result of this the RNAse IIIb mutations cells have increased 3p miR expression and reduced 5p miR expression (Anglesio et al. 2013).

5.1.3 DICER1 and the thyroid

Familial DICER1 syndrome is a condition where patients with pleuropulmonary blastoma and other related tumours have an underlying germline DICER1 mutation. It is known to be associated with thyroid disease, with multinodular goitre and a predisposition to differentiated thyroid cancer. DICER1 syndrome related tumours include sex cord stromal tumours, cystic nephroma and renal sarcoma, nasal chondromesenchymal hamartomas, rhabdomyosarcoma, pituitary blastomas and pineoblastomas (Solarski et al. 2018). Presentation is normally with diagnosis of pleuropulmonary blastoma in a paediatric patient. Originally DICER1 was considered to be a haploinsufficient tumour suppressor, as most germline mutations were found in one allele only. It is now postulated that it could be more complex, as often DICER1 syndrome patients with a tumour will have a somatic RNAse IIIb mutation acquired too, but not necessarily associated with complete loss of function as previously described in the literature (Robertson et al. 2018).

Mutations of DICER1 in follicular adenomas have also been found and mutations are not always associated with malignant disease (Poma et al. 2019). This suggests that the impact of different mutations varies depending on the background mutational profile of that patient and potentially environmental factors too.

5.1.4 DICER1 in The Cancer Genome Atlas (TCGA)

Three thyroid cancer patients in the TCGA database had DICER1 mutation. One had recurrent disease and was identified in the analysis above (D1810H missense mutation). Another patient had the missense mutation E1813G and the third patient

had a R1906S mutation. The two missense mutations in the RNase III domain had no RAS or BRAF mutation, whereas the R1906S mutation in the double strand RNA-binding domain had a NRAS Q61R mutation (Cerami et al. 2012, Gao et al. 2013, Poma et al. 2019).

The role of this chapter was to explore the effect of these DICER1 mutations discovered in recurrent papillary thyroid cancer on aspects of cellular function, and to investigate the effects of loss of functional DICER1 expression.

5.2 Materials and Methods

5.2.1 Protein extraction and Western blotting

Protein was extracted and quantified in keeping with section 2.4. The protein was denatured for 30 minutes at 37 °C. The Western blot protocol was performed as described in the same section. The protein was run on a preformed Novex WedgeWell 4-12 % Tris-Glycine Mini Gel (Invitrogen), and transfer was for 1 hr 25 mins. The membrane was probed with mouse monoclonal antibody anti-DICER antibody (ab14601) (Abcam) 1:1000 v/v.

5.2.2 Cell invasion and migration assays

Cell invasion and migration assays were performed as outlined in section 2.7 and 2.8 in three cell lines TPC-1, Cal-62 and SW1736. pCMV-flag vectors containing DICER1 WT or DICER1 D1810H were transfected in, and vector-only used as a control. The

DICER1 vector was kindly provided by Prof. P Santisteban (the Autonomous University of Madrid, Spain).

5.2.3 Clustered Regularly Interspaced Short Palindromic Repeat (CRISPR): Design of guide RNAs

In order to abrograte DICER1 function, a CRISPR knockout cell line was produced. CRISPR was selected over siRNA knockdown because DICER1 is intricately involved in siRNA production and processing, which may have compromised experimental design. Overexpression of the mutant DICER1 D1810H and other germline DICER1 mutants was initially planned in the DICER1 depleted cells, so a stable cell line was also preferred. Concomitant siRNA knockdown of wildtype DICER1, plus transient transfection of a DICER1 mutant would likely cause cross-knockdown of the mutant of interest.

In order to create a CRISPR cell line guide RNAs (gRNA) were designed. There are several web-based tools which help design guide sequences for the CRISPR/Cas9 system. In order to knock down all isoforms of Dicer, the first exon common to all validated isoforms (exon 4) was selected. The exon fasta sequence was entered into multiple gRNA design tools including CRISPOR (Haeussler et al. 2016), the Wellcome Trust Sanger Institute Genome Editing database (Hodgkins et al. 2015), CRISPR Design by the MIT Zhang lab (Hsu et al. 2013) and The Broad Institute Genetic Perturbation Platform (Doench et al. 2016, Sanson et al. 2018). The results were catalogued into a spreadsheet, and concordant results noted. Each gRNA was checked for the number and location of predicted off-target effects, and the proximity

of these areas to the seed region (Protospacer adjacent motif (PAM)-proximal 10-12 nucleotides (Jiang and Doudna 2017)). Any exonic off-target effects were investigated. The three guide RNAs with the best predictive scores and minimal off-target effects were selected, with a view to transfect cell lines with three gRNAs and exclude the least efficient at DNA cutting at a later step (T7 Endonuclease 1 mismatch assay). The gRNAs selected were the top three in Table 5.1 below.

Ranking	gRNA (including PAM)	No of tools generating gRNA	MIT specificity score (CRISPOR)	Potential off-target effects in 12bp next to PAM 0-1-2-3-4 mismatches
1	ATGCTGAGGGGTTGCAAAGC AGG	4	72	0 - 0 - 1 - 0 - 2
2	TTGCAACCCCTCAGCATGGC AGG	3	66	0 - 0 - 0 - 4 - 6
3	AGTCCAAAGAAAGGACCCAT TGG	4	76	0 - 0 - 0 - 1 - 3
4	TCACCAATGGGTCCTTTCTT TGG	3	75	0 - 0 - 0 - 1 - 4
5	ACCCCTGCTTCCTCACCAAT GGG	3	71	0 - 0 - 0 - 2 - 3

Table 5.1: Table of guide RNA sequences with adjacent Protospacer adjacent motif (PAM) sequence. Off-target prediction for the 12 bp adjacent to the PAM is included and MIT specificity score generated by the CRISPOR gRNA design tool. The MIT specificity score ranges measure how unique in the genome a guide RNA is on a scale of 0-100 – the higher the score, the lower the off-target effects.

5.2.4 CRISPR: gRNA cloning and vector preparation

The gRNA oligonucleotides were prepared with T4 ligase buffer (New England Biolabs, Massachusetts, United States) and T4 Polynucleotide Kinase (New England Biolabs) and transferred to the thermocycler for 30 mins at 37 °C then five mins at 95 °C, followed by a 15-minute hold at 25 °C. This was to phosphorylate the 5' end of the gRNA oligonucleotides and anneal the gRNAs. The gRNA preparation was then diluted 1:200 in double distilled water (ddH_20).

The pLenti-CRISPR plasmid, kindly supplied by Dr V Smith (University of Birmingham, UK) (Figure 5.2) was prepared with a BsmBI digestion using Fast digest BsmBI (Esp31) (ThermoFisher Scientific) and 10x Fast digest buffer (ThermoFisher Scientific) at 37 °C for an hour. This was then run on a 1% agarose gel and gel purified using the QIAquick Gel Extraction Kit (Qiagen, Hilden, Germany) to extract the 11 kb fragment. (Figure 5.2).

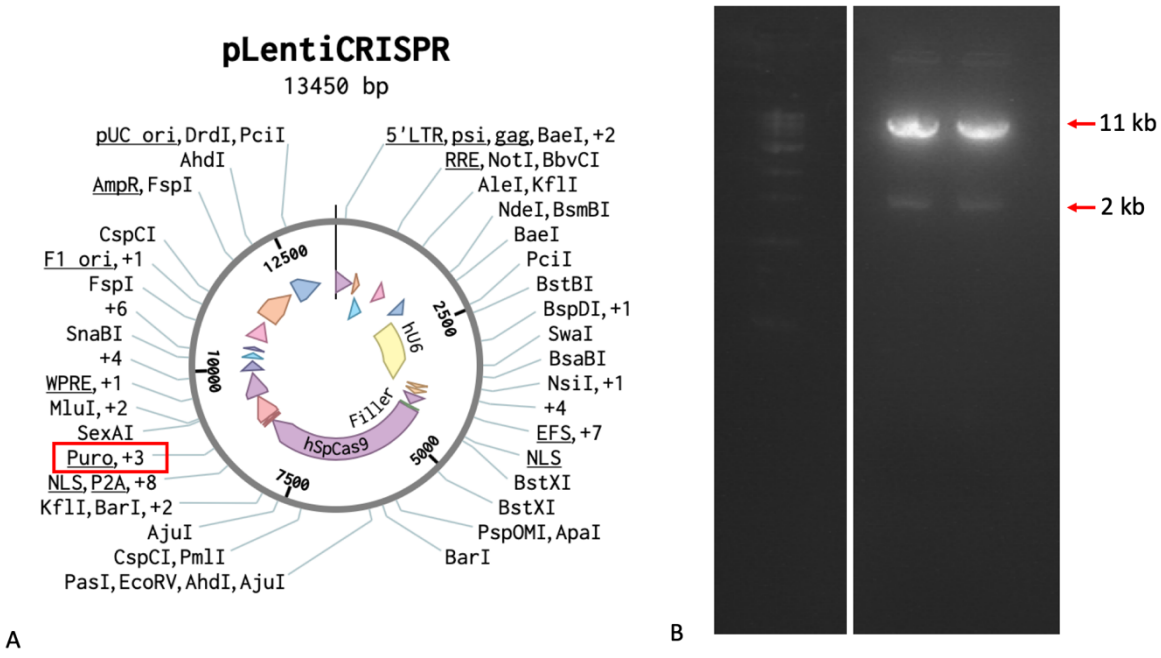

Figure 5.2: pLenti-CRISPR plasmid and agarose electrophoresis gel demonstrating cut vector. A) pLenti-CRISPR plasmid, including puromycin resistance. B) Gel electrophoresis of the pLenti-CRISPR plasmid with the filler cut out. Gel shows 11 kb fragment (cut vector) and 2 kb fragment (filler). The 11 kb fragment was cut out and gel purified. Run with 1 kb DNA ladder (New England Biolabs).

The plasmid was then Alkaline Phosphatase, Calf Intestinal (CIP)-treated with CIP (New England Biolabs) and CutSmart buffer 10x (New England Biolabs) to remove the 5' phosphatase. This was to prevent circularisation of the linearised vector. The CIP treated vector was then column purified using the QIAquick PCR Purification Kit (Qiagen).

Finally, the gRNA oligonucleotides were ligated into the digested pLenti-CRISPR vector using T4 DNA ligase in T4 DNA ligase buffer, which was left at 16 °C overnight. The ligation reaction was then transformed into DH5α competent *E. coli* cells as described in section 2.2.2 and amplified with the QIAprep Spin Mini Prep kit (Qiagen). These were then Sanger sequenced (Source Bioscience) to confirm removal of the vector filler and insertion of the gRNA in the correct locus (Figure 5.3).

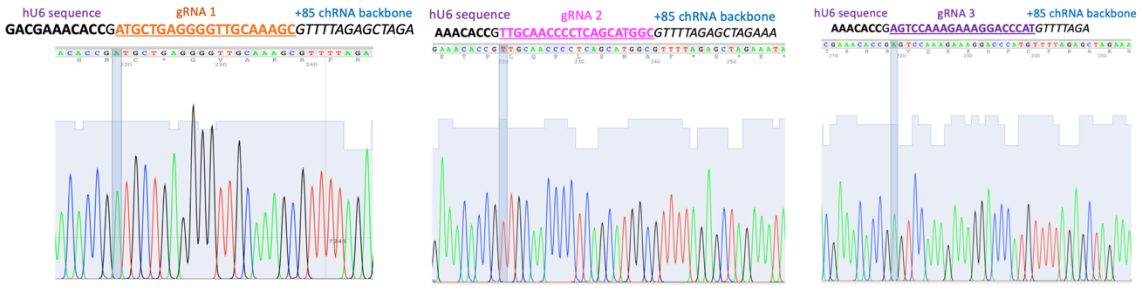

Figure 5.3: DNA sequence trace demonstrating successful cloning of gRNA 1, 2 and 3 into the pLenti-CRISPR plasmid.

5.2.5 CRISPR: Transfection

TPC-1 and Cal-62 cell lines were all tested with a mycoplasma detection kit (Jena Bioscience, Jena, Germany) and were clear of mycoplasma. Cells were transfected

with the pLenti-CRISPR vectors with gRNAs 1, 2 and 3 (Table 5.1) and one control non-transfected well. After 24 hours incubation at 37 °C with 5 % CO_2 the medium on the cells was changed to RPMI with 1 µg/ml puromycin for a 48-hour incubation. At this point all the cells in the untransfected well had died and the medium was changed back to RPMI only.

Repeat wells were seeded, transfected and incubated for DNA extraction (described below in section 5.2.8) without single cell sorting. This DNA was run on a T7E mismatch assay (described below in section 5.2.10) to assess cutting efficiency of the gRNAs (Figure 5.7).

5.2.6 CRISPR: Single cell sorting

Once confluent in 75 cm^2 flasks, the transfected cells were single cell sorted by fluorescence-activated cell sorting (FACS) (Figure 5.4). Cells were washed in PBS, trypsinised and resuspended in PBS then centrifuged at 300 x g for 5 minutes at 4 °C. The cells were then resuspended in MACS buffer (0.5% BSA and 1 mM ethylenediaminetetraacetic acid (EDTA) in PBS) and transferred into a FACS tube. Dr A Flores-Langarica (University of Birmingham) kindly performed the cell sorting using the BD FACSAria Fusion Machine with FACSDiva version 8.0.1 software, with gating for single cells into 96 well plates, prepared with 100 µl RPMI per well.

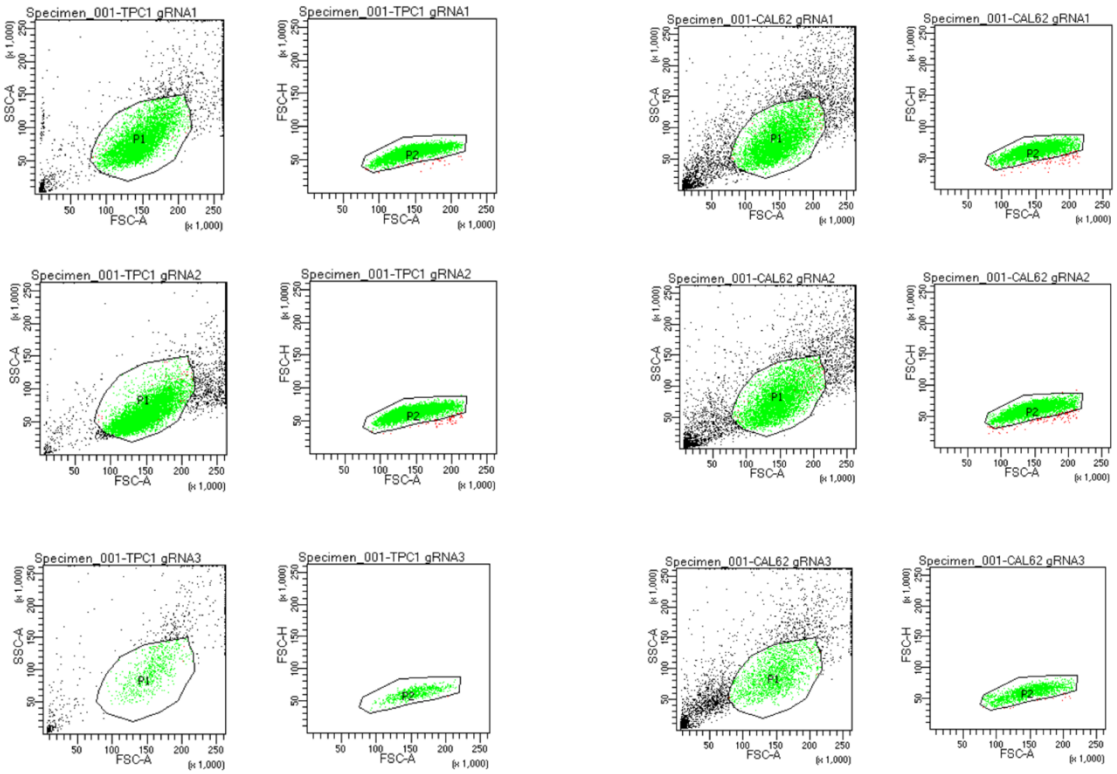

Figure 5.4: Fluorescence-activated cell sorting (FACS) flow cytometry for single cell sorting. Sequential gating of SSC-A versus FSC-A to identify cells of interest (p1) and FSC-A versus FSC-H to identify singlets (p2). Left column are TPC-1 cells and the right are Cal-62 cells, with each line a different gRNA. SSC-A, Side SCatter Area (granularity); FSC-A, Forward Scatter Area (size); FSC-H, Forward Scatter Height. FACS kindly performed by Dr A Flores-Langarica (University of Birmingham).

5.2.7 CRISPR: Cell culture

Cells were incubated at 37 °C with 5 % CO_2 in RPMI with media changes every two to three days as required. Once the cells were 80% confluent, they were harvested with a PBS wash and trypsinisation and resuspension in RPMI. A third of the cells were then seeded into a 24-well plate and the remaining two thirds into a 6-well plate. These were labelled according to their cell line, gRNA and original plate position. When confluent, the 6-well plate cells were washed with PBS, trypsinised and resuspended

in RPMI media. They were then centrifuged at 125 x g for 3 minutes. The supernatant was removed, and cells were resuspended in RPMI media with 10% DMSO. They were placed in a cryovial and frozen at -80 °C.

5.2.8 CRISPR: DNA extraction

When the 24-well plates were confluent the cells were washed with PBS, trypsinised and resuspended in RPMI. They were then centrifuged at 125 x g for 3 minutes and Genolysis buffer (1.5M Tris-HCl pH 8, 0.5M EDTA pH 8, 5M NaCl, 10 % SDS, Igepal (Sigma-Aldrich), Tween®20) was added, then the cells were incubated at -20 °C for over 24 hours. Following this the samples were brought to room temperature, and 75 µl 5M NaCl was added to the sample, which was rocked at room temperature for 5 minutes. This was then centrifuged at 13,000 RPM for 10 minutes at room temperature. The supernatant was then transferred to a clean Eppendorf. Glycoblue 1.2 µl (Ambion, Texas, USA) and 350 µl isopropanol (Sigma Aldrich) were then added and the tube inverted five times. This was left for an hour and then centrifuged at 13,000 RPM for 20 minutes at 15 °C. The supernatant was removed, and the pellet washed with 70 % ethanol and spun again at 13,000 RPM for 15 minutes at 15 °C. The ethanol supernatant was removed and then the pellet air-dried before resuspension in nuclease free water at 55 °C for 2 hours.

5.2.9 CRISPR: PCR

DICER1 CRISPR cut site PCR primers were designed and ordered at 0.05 µmole, dry, with polyacrylamide gel electrophoresis (PAGE) purification (Sigma) (Table 5.2).

Sequencing primer	Sequence
DICER1 cut site F design 1	5' GGTAAGGTACAGAATGCTTGACTCC 3'
DICER1 cut site R design 1	5' CCAGCTCACTAGGACAGACAC 3'
DICER1 cut site F design 2	5' TCTTGTTTCTGTGCTTTCTTTGT 3'
DICER1 cut site R design 2	5' CAGAAGTGGGAGGCCTGAAA 3'

Table 5.2: PCR sequencing primers for DICER1 CRISPR cut site. Original primers (1) and new primers (2).

PCR was performed using Q5 High-Fidelity DNA Polymerase kit (New England Biolabs). This included 5x Q5 Reaction buffer, 5x Q5 high GC enhancer and Q5 DNA polymerase with 10mM dNTPs and forward and reverse DICER1 cut site sequencing primers, created as a mastermix and added to 300 ng of template DNA. This was then run on the PCR protocol in Table 5.3. Wildtype DNA was also extracted and amplified alongside the CRISPR cut DNA to run on the T7E mismatch assay. The original PCR primers were not very efficient, and as a result were redesigned using Primer3 (Koressaar and Remm 2007), which improved the PCR efficiency. Both original and new primers are shown in Table 5.2.

Cycles	Temperature	Time
1	95 °C	5 minutes
35	95 °C	30 seconds
	60 °C	30 seconds
	72 °C	2 minutes
1	72 °C	5 minutes

Table 5.3: PCR thermocycling parameters for CRISPR cut site amplification

5.2.10 CRISPR: T7 Endonuclease 1 mismatch assay

The T7 Endonuclease 1 (T7E) mismatch assay was performed by combining clone PCR product with wildtype PCR product and incubating for 5 minutes at 95 °C. This was cooled slowly over an hour, then T7E (New England Biolabs) was added to each clone with NEB2 buffer (New England Biolabs) and incubated for 1 hour at 37 °C. A 5 µl sample of the product was then loaded onto a 2% agarose gel with GelRed (Biotium, California, USA), each clone sample adjacent to the corresponding wildtype DNA PCR product. This gel was run at 100 V for 30 minutes, and assay interpretation is discussed in section 5.3.3 below.

5.2.11 CRISPR: Sequencing

Once the T7E mismatch was run, if the T7E gel bands were potentially indicative of mutation, then the samples were sequenced. Prior to being sent for sequencing, the PCR product was cleaned using ExoSap. Shrimp Alkaline Phosphatase (rSAP) (New England Biolabs) was added to Exonuclease I (New England Biolabs) in a two to one ratio. This was added to the PCR product and incubated for 20 minutes at 37 °C then inactivated at 80 °C for 15 minutes on the thermocycler. Samples were sequenced using Sanger Sequencing service by Source Bioscience (Nottingham, UK). A positive result for a clone would consist of clean sequencing then a divergence to two wave forms, where the cut had been made. This sequencing would then have to be reviewed by hand using recognition of wildtype regions to qualify the mutation site as an insertion or deletion and whether it had a frameshift impact or not. Once the sequence for each allele had been derived, both sides were checked on ExPASy (Artimo et al. 2012) to determine the impact of the nucleotide mutation on the amino acid sequence. If an

early stop mutation was noted for both alleles, then this was considered to be a homozygous knock out. Once a knockout clone had been identified through the DNA extraction and sequencing described, the cells were thawed and cultured as previously described (2.1). Knockout effects were confirmed with Western Blotting.

5.3 Results

5.3.1 Cell invasion

Cell invasion assays were performed in three cell lines after transient transfection of DICER1 wildtype and the D1810H mutant into the parental cell lines TPC-1, Cal-62 and SW1736. Trends were seen in an increase in cell invasion, especially apparent in the TPC-1 cell line, but there was no significant difference observed between wildtype and mutant DICER1 (Figure 5.5), only significance being seen between VO and wildtype DICER1 overexpression in the SW1736 cell line.

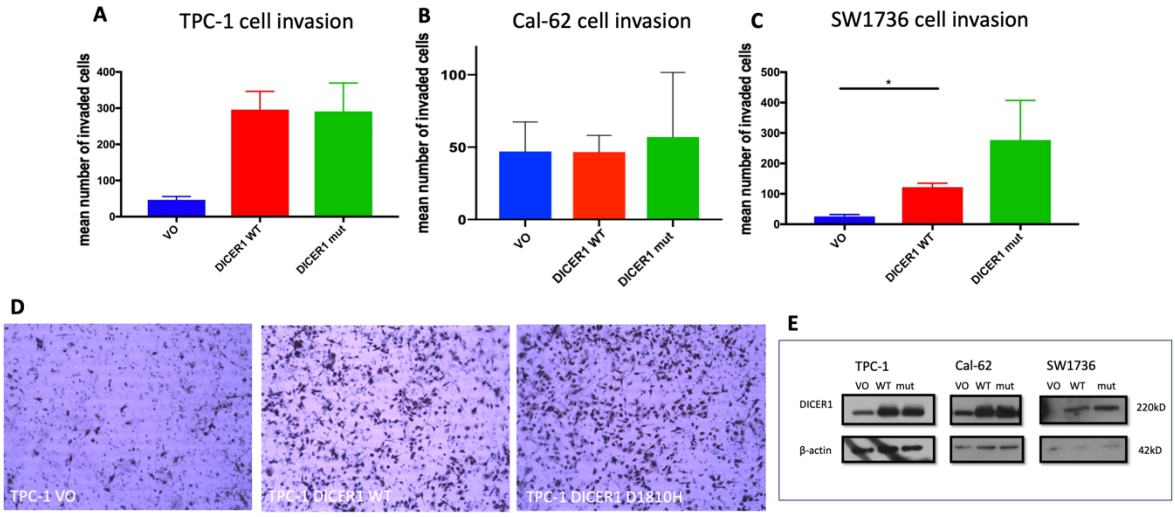

*Figure 5.5: A, B & C: Cell invasion assay comparing vector only (VO), DICER1 wildtype (WT) and DICER1 missense mutation D1810H in three cells lines (A: TPC-1 B: Cal-62 and C: SW1736). n = 3 separate experiments. D: Light microscopy images show representative invasive cells in TPC-1 cells. * p < 0.05. E: Western blot demonstrating transfection of cell lines with VO, DICER1 wildtype and DICER1 D1810H.*

5.3.2 Cell migration

Cell migration was again performed in three cell lines after transient transfection with DICER1 WT and DICER1 D1810H and showed no marked differences between the wildtype and mutant overall (Figure 5.6), with the only significant difference shown between VO and mutant in the TPC-1 cell line (no significance between wildtype and mutant).

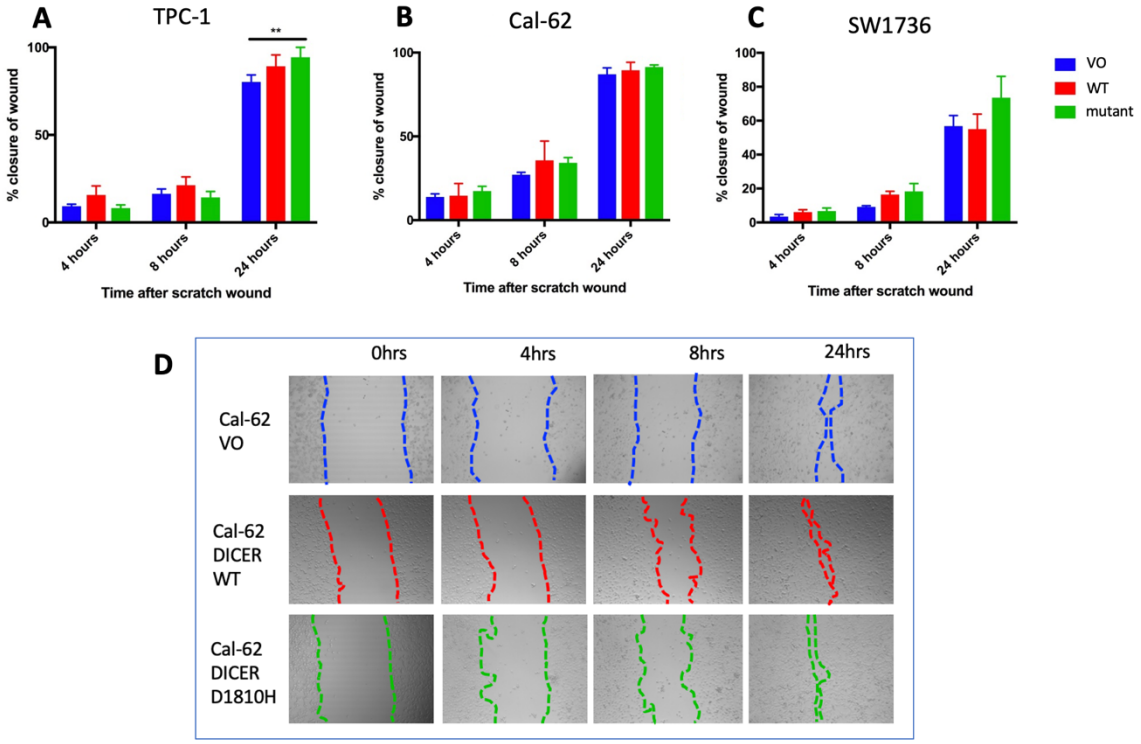

*Figure 5.6: A, B & C: Cell migration assay comparing vector only (VO), DICER1 wildtype (WT) and DICER1 missense mutation D1810H (mutant) in three cells lines (A: TPC-1, B: Cal-62 and C: SW1736). D: Light microscopy images show representative cell scratch wounds and healing over time course in Cal-62 cells. Magnification 10x, n=3, ** p < 0.01.*

5.3.3 CRISPR T7 Endonuclease 1 mismatch assay

In order to identify positive clones (with successful CRISPR knockout) for sequencing the T7E mismatch assay was performed. The T7E assay demonstrates a double band if there is a mutation on one strand of the double stranded DNA. The CRISPR-cut DNA is annealed with wildtype DNA, and if there is an imperfection in the DNA-matching (due to the CRISPR-derived mutation on one side) this region of imperfection is cut by the T7E enzyme. The T7E mismatch assay performed before single cell sorting demonstrated gRNA 1 and 2 to be the most efficient at cutting (Figure 5.7). For gRNA

3 the amount of DNA extracted was much lower and the additional bands in the T7E lane were not as clear.

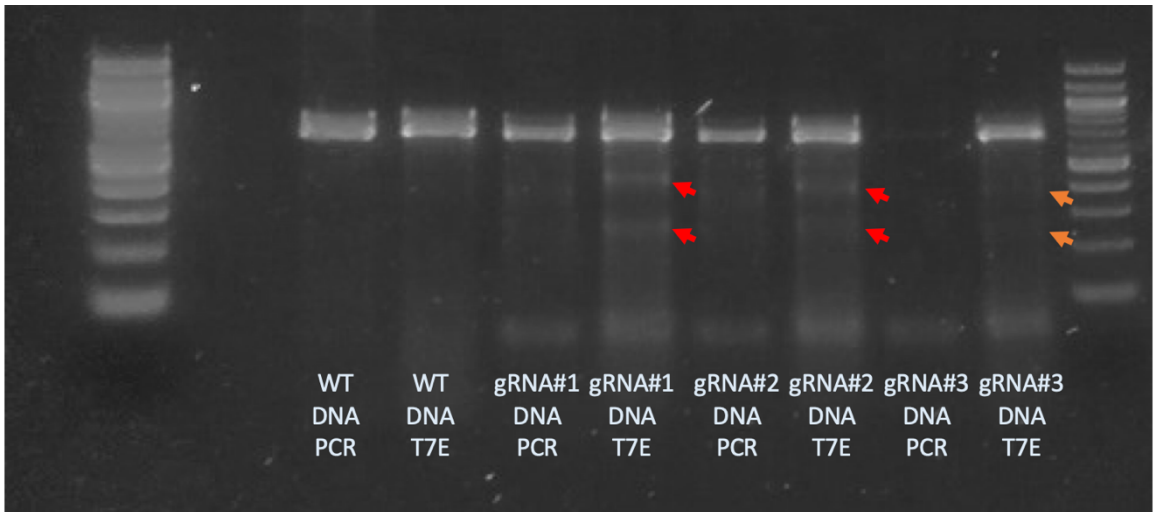

Figure 5.7: Initial T7E performed on heterogenous DNA from transfected cells before single cell sorting to demonstrate cutting efficiency of the gRNAs. PCR products (control) are loaded next to T7E products. Cal62 cell line. Efficient cutting gRNA 1 and 2 bands are shown in red arrows, the gRNA 3 bands shown in orange arrows.

An example of the T7E mismatch assay for the single cell clones is shown below (Figure 5.8).

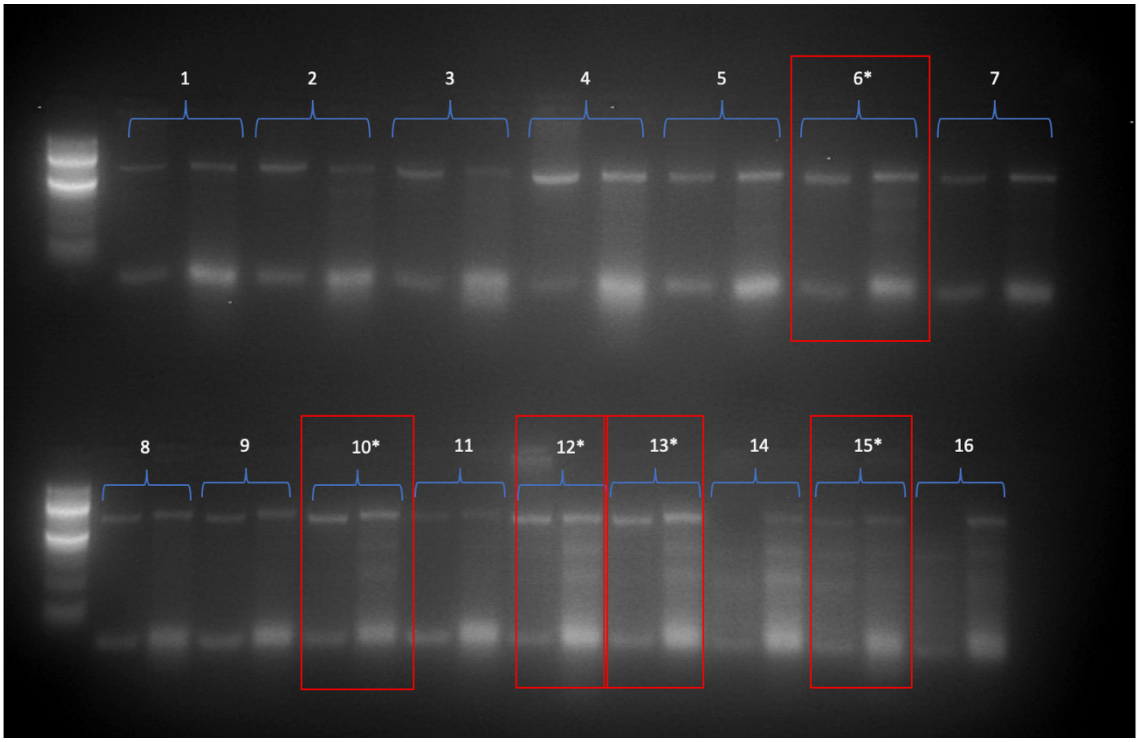

*Figure 5.8: T7E mismatch assay for the first 16 CRISPR clones. Positive results are annotated with * in a red box and and were sent for Sanger sequencing.*

Due to the nature of the T7E assay, some mutations are not picked up using this screening tool. If a mutation contains a very large indel then the imperfection in the DNA annealing can be too large for the enzyme to recognise. Similarly, if there is a one base pair missense mutation, the imperfection is very small and the efficiency of the T7E cutting this can be low. Therefore, the T7E assay was initially used as a screening tool to select clones for sequencing, although several non-positive T7E clones were also sequenced and were CRISPR knockout clones.

5.3.4 CRISPR sequencing results

The sequencing results identified multiple clones that were heterozygous knock outs for DICER1 and some that were homozygous knock outs. The knockout rate was much

higher for the TPC-1 cell line than the Cal-62 where there was a high incidence of wild type DICER1. Homozygous knockout clones from gRNA 1 and 2 were identified in the TPC-1 cell line, but there was only one homozygous knockout clone generated in the Cal-62 cell line. Therefore, this cell line was not taken forward. There can be off-target effects generated by the CRISPR process, so it is good practice to have multiple clones per cell line each generated from different gRNAs. Each gRNA has different potential off-target effects so selecting clones generated by different gRNAs should control for this during experiments.

Sequencing revealed a variety of different results, with one homozygous knock out clone manifesting from a single base pair insertion in both alleles (Figure 5.9). The heterozygous knockouts could be recognised by the division into two wave forms but with the preservation of wildtype on one allele. The homozygous knockouts with different mutations on each allele divided into two wave forms with no preservation of wild type (Figure 5.10). These figures (Figure 5.9 and Figure 5.10) represent the clones from gRNA 1 and 2 that were taken forward.

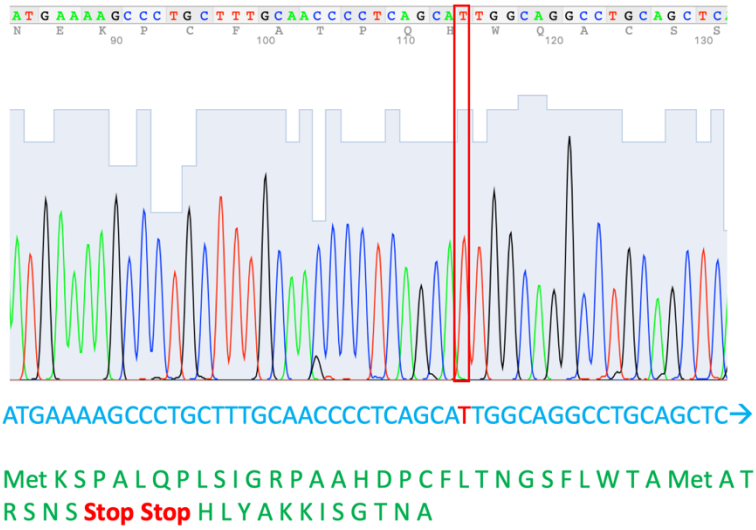

Figure 5.9: DNA sequence trace of TPC-1 gRNA 1 clone 1 demonstrating insertion of an extra T nucleotide in both alleles. Nucleotide sequence is shown with the corresponding amino acid sequence beneath demonstrating early stop codons induced by this mutation.

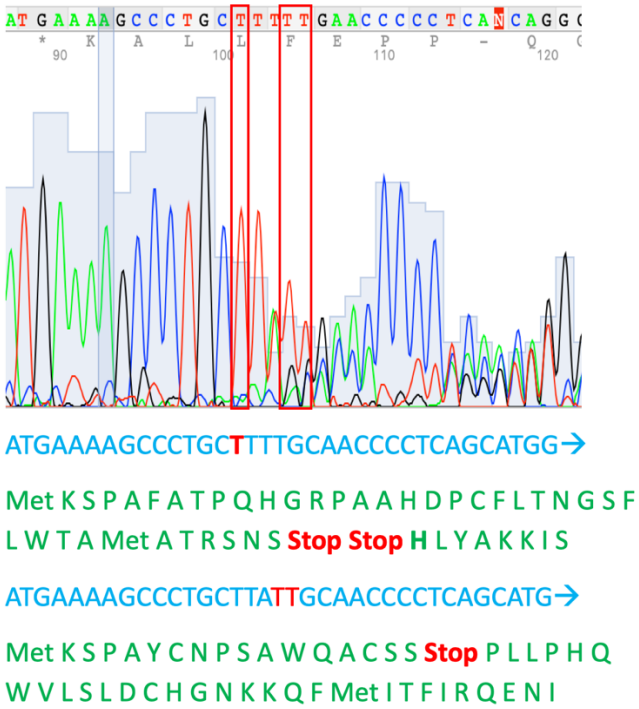

Figure 5.10: DNA sequence trace of TPC-1 gRNA 2 clone 1 demonstrating insertion of an extra T nucleotide in allele one and an extra TT insertion in allele two. Nucleotide sequence is shown with the corresponding amino acid sequence demonstrating early stop codons induced by these mutations.

5.3.5 CRISPR cell line Western blot

In order to assess knockdown of the DICER1 gene protein expression levels were checked and demonstrated successfully abrogated expression (Figure 5.11) in clones from gRNA 1 (one clone shown) and gRNA 2 (two clones shown). There was however residual protein in all clones selected.

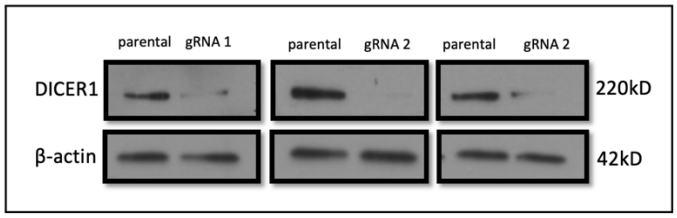

Figure 5.11: Knock down of dicer protein in DICER1 KO CRISPR clones in the TPC-1 cell line. Control parental cells are TPC-1 wildtype cells. From left to right TPC-1 gRNA 1 clone 1, TPC-1 gRNA 2 clone 1, TPC-1 gRNA 2 clone 2.

5.3.6 CRISPR DICER1 KO functional assessment

After confirmation of DICER1 knockdown it was important to see if the knock down of DICER1 affected cellular function. To assess this cell scratch wound migration assays (described in section 2.8.8) and MTS cell proliferation (as described in section 2.6.1) were performed using gRNA 1 clone 1 and gRNA 2 clone 1. Cell migration was induced at 24 hours in both of the CRISPR cell lines compared to parental (Figure 5.12). The proliferation assay revealed no significant difference between the parental cell line and the CRISPR cell lines (Figure 5.13). This defines the wound scratch assay results as a truly migratory phenomenon by excluding the contribution of proliferation to the movement of the cells.

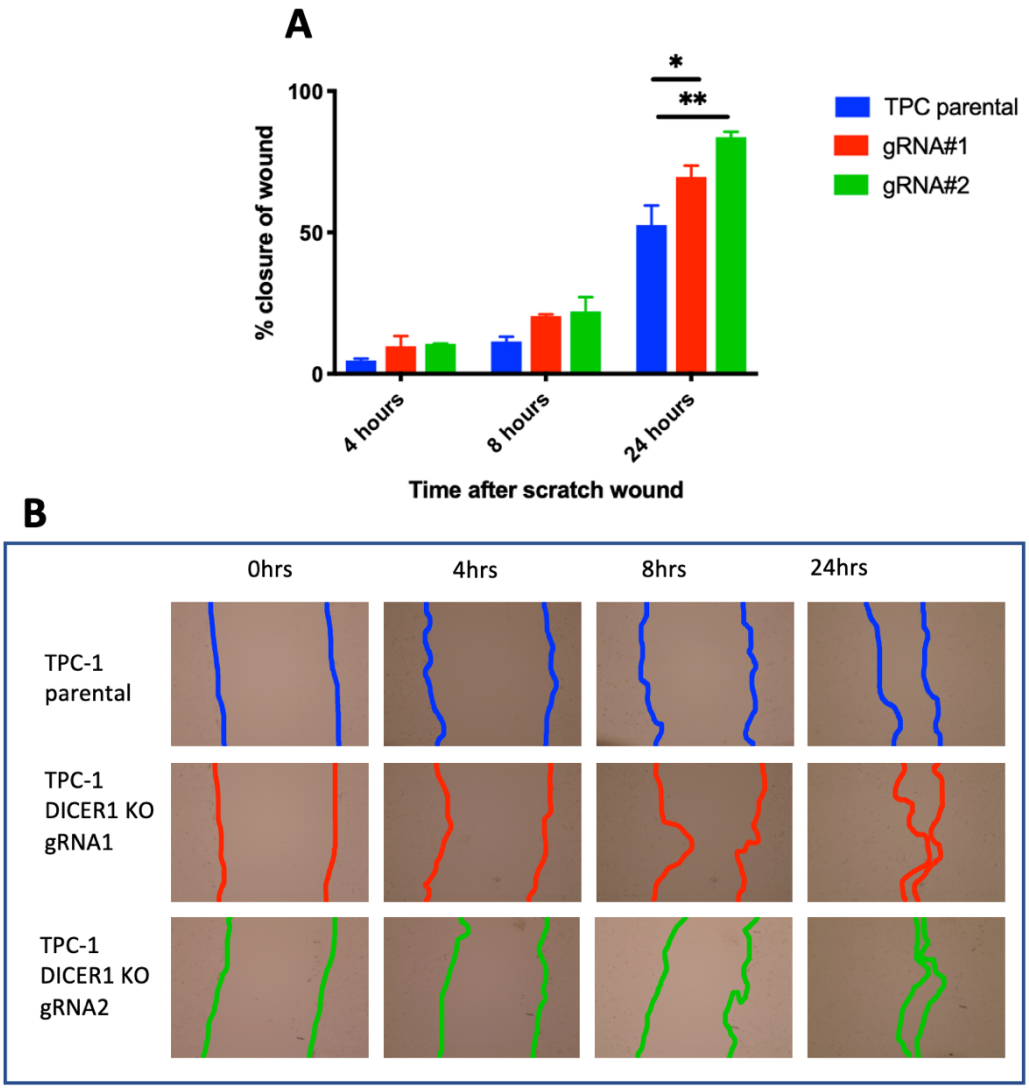

*Figure 5.12: A) Cell scratch wound assay comparing CRISPR TPC-1 gRNA 1 and gRNA 2 to parental TPC-1 cells. B) Representative light microscopy images showing scratch wound healing. 10x magnification, n = 3, * $p < 0.05$, ** $p < 0.01$. n = 3.*

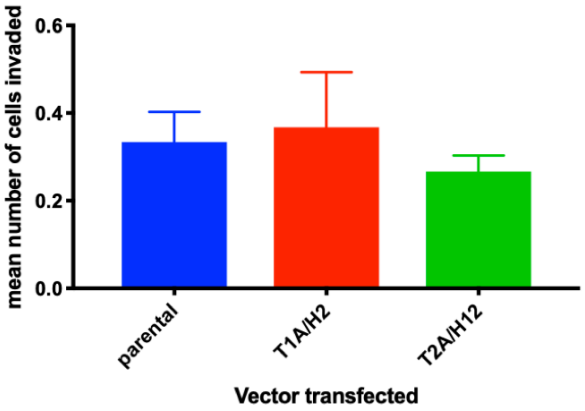

Figure 5.13: Cell proliferation (MTS) assay comparing CRISPR TPC-1 DICER1 KO gRNA 1 and gRNA 2 to parental TPC-1 cells. n = 3. T1A/H2, gRNA1 clone 1; T2A/H12, gRNA2 clone 1. All not significant.

5.4 Discussion

5.4.1 DICER1 D1810H

The overexpression of DICER1 WT and the DICER1 D1810H mutant failed to significantly modulate cell migration or proliferation. This is possibly to be due to the model used to examine the mutant D1810H, or could potentially be because the mutation is not a driver. Overexpression of a gene has limitations, and if the effect of a mutant is to change the function of the gene then this effect might be masked by the presence of the endogenous wild type DICER1 that is already present in the cell line. This is particularly of note in tumour suppressor genes where the gene mutation reduces the efficacy of that gene. Overexpressing a non-functional gene, on top of the normal gene already present in the cell, is unlikely to have a significant effect. An interesting way to explore this further would be to examine the miR expression after transfection as this would demonstrate a potential mechanism of action for any changes too.

DICER1 has been suggested to be a haploinsufficient tumour suppressor (Foulkes et al. 2014) and there are multiple ways in which these can act, challenging the traditional two-hit model for tumour suppressor genes (Comings 1973). Knocking out gene function on one allele can have an impact on protein function simply by depletion of gene expression (Inoue and Fry 2017). Alternatively, tumour suppressors can have a dominant negative effect, such as the tumour suppressor p53, where, in certain cases, the protein generated from the mutated allele interferes with the wildtype protein function (Willis et al. 2004). Using the overexpression model, an effect would be expected to be seen if the tumour suppressor DICER1 had a dominant negative effect, as the overexpressed mutant would interact with the inherently expressed wildtype, which was not observed in the experiments performed. However, the mutation considered in DICER1 in the ribonuclease IIIb region may not be a complete loss of function mutant, as some DICER1 function is still preserved with missense mutations in this region (Foulkes et al. 2014). Mutations in a metal ion binding residue or in the catalytic core of the ribonuclease IIIb region have been predominantly associated with a reduction in the production of mature 5p miRNAs (Wang et al. 2015). The effective production of 3p miRNAs in these tumours implies that some DICER1 function is preserved in ribonuclease IIIb region hotspot mutations such as D1810H.

Due to the complications of the model used to examine the DICER1 mutation, a DICER1 KO CRISPR cell line was generated to investigate the functional effects of DICER1 knockout further.

5.4.2 DICER1 CRISPR knockout model

The CRISPR-Cas9 system development (Jinek et al. 2012) enabled gene editing in a manner that was more efficient, more cost-effective and therefore more accessible than the techniques available before it (Nemudryi et al. 2014). The CRISPR-Cas9 system is adapted from the innate defensive response to invading viruses and plasmids. For use in vitro, a vector containing the Cas9 protein and a sequence guide RNA (gRNA) is transfected into a cell, and the Cas9 identifies a region of DNA next to a Protospacer adjacent motif (PAM) that matches the gRNA. A PAM sequence is a region containing a common sequence of base pairs; Cas9 will only cut if this is present and this protects non-target DNA. In this case, the PAM for the Cas9 protein was NGG. When DNA matches the gRNA a double stranded cut is made in the DNA by Cas9 approximately three base pairs upstream to the PAM sequence. Error-prone DNA repair to the double stranded break will often incorporate insertions or deletions. These have the potential to cause an early stop codon, or to cause a frameshift thereby inducing an early stop codon. This then disrupts the translation of the gene protein. If an error causing an early stop codon is integrated into both alleles early on in the gene sequence, then the gene will not be expressed at the protein level. This is referred to as a homozygous knockout.

Designing gRNAs to create CRISPR KO cell lines has the potential to generate off target effects. When generating the DICER1 gRNA sequences, the web-based tools that were used also produced predictions for off-target effects. In order to mitigate this any gRNAs with off-target effects on known thyroid oncogenes or tumour suppressors

were excluded. For example, one gRNA had potential off-target effects on BRAF and was eliminated from the shortlist.

Off-target effects are annotated as regions which match other areas in the genome, either perfectly, or with a small number of mismatches. For the gRNAs selected, all of the predicted off-target effects where there were 3 mismatches or fewer were either non-exonic, or they contained mismatches in the seed region which are not well tolerated (Hua Fu et al. 2014) or they were effects on genes not expressed in the thyroid gland. It has been previously shown that more than two mismatches in the gRNA are not well tolerated, with 96% of CRISPR RNA not functioning when two mismatches were present, and virtually none functioning with three mismatches (Anderson et al. 2015).

It is important to use more than one gRNA for generating CRISPR clones, as each gRNA will produce different potential off target effects. Therefore, if experiments include cell lines generated by different gRNAs, if the results are concordant it is more likely that the effects seen are due to the targeted gene editing than any off-target effects. In the Cal-62 cell line the CRISPR treated clones were successfully selected for by puromycin treatment, compared to the untransfected control well. However, upon sequencing, very few knockout clones were located. This indicates that of the viable clones, the cells had likely been transfected with the CRISPR-gRNA plasmid but either not cut or were repaired accurately. Therefore, the Cal-62 CRISPR-KO cell line was unfortunately not taken forward, as clones from multiple gRNAs were not established.

5.4.3 DICER1 CRISPR cell line functional effects

The DICER1 knockout cell line was established in TPC-1 cells from gRNA 1 and gRNA2, with knock down confirmed on Western blot. Using the CRISPR knockout system, protein detection and functional assessment are the best way to confirm knockdown, after genetic sequencing. The Western blot for the CRISPR DICER1 KO cell line (Figure 5.11) showed successful knockdown, though with a trace of protein in the KO wells in both clones. As confirmation of knockdown in both alleles was apparent on sequencing, it would be expected that all the protein would have been knocked out, and therefore no band visible at all. It is unlikely to be non-specific binding due to the antibody, as this is mouse monoclonal antibody shown to produce clean Western blots. There are several different transcript variants of DICER1, and one of the computationally predicted isoforms (XM_011536605.2) does not express exon 4 and it may well be that this transcript has therefore escaped the CRISPR process.

Despite this, a functional effect was observed in the two knockout cell lines compared to the parental cell line – the cells were more migratory (Figure 5.12). This migratory response is in keeping with the idea that lower DICER1 expression is associated with a worse cancer outcome (Ramírez-Moya et al. 2019) and fits with DICER1 functioning as a tumour suppressor.

5.4.4 Concluding remarks

This chapter has demonstrated the functional effect of the reduction of DICER1 in a thyroid cell line. However, due to the complexity of the effect of the hotspot mutation,

the complete knockout of the DICER1 function does not fully represent the impact of the mutation. Future work to transfect in the DICER1 D1810H mutant, and other non-hotspot mutations, into the DICER KO cell lines, would be interesting. The functional effects of this mutation could thereby be more accurately defined, and the impact on the 5-p microRNA profile would also be interesting to review.

Chapter 6 RNA gene expression levels in thyroid cancer recurrence

6 RNA gene expression levels in thyroid cancer recurrence

6.1 Introduction

6.1.1 RNA expression in thyroid cancer

Messenger RNA (mRNA) expression profiles in thyroid cancer are known to be influenced by the underlying mutational burden. The BRAF V600E mutation, for instance, results in activation of the MAPK/Raf/Ras pathway, with resultant effects on the gene expression profile (Rusinek et al. 2011). Importantly, the presence of BRAF V600E is known to downregulate the sodium/ iodide symporter (NIS), along with other thyroid differentiation markers including the thyroid stimulating hormone receptor (TSHR), apical iodide transporter (SLC5A8), thyroid peroxidase (TPO) and thyroglobulin (TG) (Durante et al. 2007). From these, NIS is of particular importance because of its role in thyroid cancer therapeutics. Radioiodine treatment of thyroid cancer is dependent on the ability of NIS to uptake radioactive iodine into target cells. Compounding this, NIS that is expressed is more likely to be abnormally located in the cytoplasm (Durante et al. 2007). Diminished expression and mislocation of NIS protein are the principle mechanisms attributed to poorer clinical outcomes associated with BRAF V600E tumours; this treatment evasion makes the tumour more difficult to treat. However, not all patients receive radioiodine therapy and this does not fully explain the incidence of thyroid cancer recurrence.

A previous study aimed to understand the aggressive nature of BRAF driven tumours, and undertook a gene set enrichment analysis in BRAF V600E tumours (Nucera et al. 2010). A significant association with particular genes was identified, including tumour

extracellular thrombospondin 1 (TSP-1), transforming growth factor beta 1 (TGF-β1), integrin alpha-3 (ITGα3), fibronectin (FN1), cathepsin B (CTSB) and other ECM proteins (Nucera et al. 2010). The Cancer Genome Atlas explored the effects of gene expression profiles as well as mutational effects in order to explore this further.

6.1.2 The Cancer Genome Atlas and RNA expression levels in recurrence

Genetic drivers in PTC have distinct signalling consequences and have been subcategorised by TCGA analysis into BRAF V600E-like (BRAF-like) and RAS-like PTC, according to distinct gene signatures (Agarwal et al. 2014). Both BRAF-like and Ras-like tumours are MAPK driven, but the constitutively active BRAF V600E monomer escapes the ERK negative feedback loop, meaning that there is much greater signalling of the MAPK pathway (Figure 6.1). Similar to previous studies, the genes for iodine metabolism were significantly downregulated in BRAF-like tumours, whereas in Ras-like tumours expression of these genes remained preserved (Agarwal et al. 2014). Subsequently, sixteen genes related to thyroid function and metabolism were selected to create a Thyroid Differentiation Score (TDS), which correlates with the differentiation of the tumour and also corresponds with several cancer-related genes. However, the predominant conclusion was that the iodine metabolism related genes were downregulated by the results of the overactivation of the MAPK pathway (Agarwal et al. 2014). Importantly, the Thyroid Differentiation Score was considered to be correlated with both risk of recurrence and MACIS (Metastasis, patient Age, Completeness of resection, local Invasion, and tumour Size) score (Agarwal et al. 2014). This was the initial analysis of the mRNA expression of the TCGA data. The

objectives of this chapter were to further define the gene expression profile in the patients in the TCGA who have recurrent thyroid cancer.

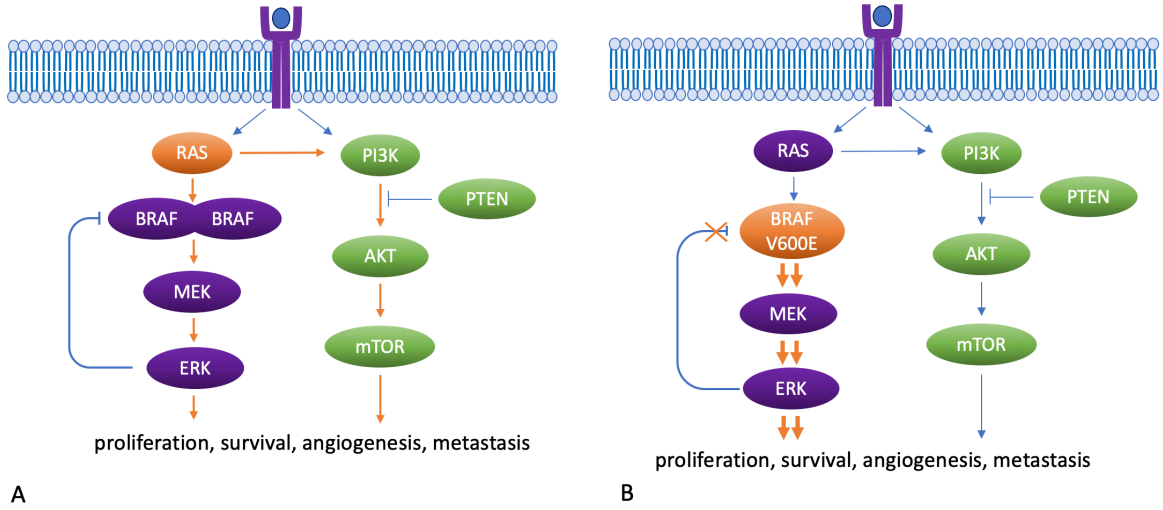

Figure 6.1: MAPK and PI3K-AKT signaling pathways. A) RAS-driven tumour pathway B) BRAF V600E-driven tumour pathway, with significantly more MEK/ERK signaling. (Caronia et al. 2011, Agarwal et al. 2014).

6.2 Methods

6.2.1 Bioinformatic analyses

RNA expression analysis was performed by downloading the TCGA RNA sequencing data (RNA-Seq by Expectation Maximization (RSEM) normalised RNA data files) through the FireHose portal (https://gdac.broadinstitute.org). The TCGA RNA sequencing (RNA-seq) data have been upper quartile normalised. The total RNA-seq data for 500 PTC samples were analysed including 457 non-recurrent and 43 recurrent tumour specimens. Sixty patients had matched normal tissue samples (normal thyroid tissue from the same patients who had contributed tumour samples), which were also

analysed. For each of the 20,532 genes the absolute median differential expression between recurrent and non-recurrent patients was calculated. The Mann-Whitney U value was calculated in R, and the genes were then ranked by median differential expression.

6.2.2 Bacterial Transformation

A vector was sourced for FN1 (PV355032) (ABM) and transformed into DH5α competent *E. coli* cells as described in section 2.2.2. Plasmid DNA (including VO) was purified and amplified using an endonuclease-free EndoFree Plasmid Maxi Kit (Qiagen) prior to transfection into cell lines.

6.2.3 Transfection

Thyroidal cell lines (TPC-1, Cal-62 and SW1736) were seeded into 6-well plates for 24 hours. Transfection with expression vector VO or FN1 were performed 24 hours before functional assays. Transfection was carried out according to section 2.2.6.

6.2.4 Cell migration and proliferation assays

Classical scratch wound healing assays were performed to assess cell migration as described in section 2.8. The media was changed from standard RPMI with 10 % FBS to RPMI with 2 % FBS just before the scratch was made, to minimise the effects of cellular proliferation on the assay. Cell proliferation MTS assay was performed as previously described (section 2.6.1).

6.2.5 Small interfering RNA (siRNA) knockdown

Endoribonuclease-prepared siRNA (esiRNA) was purchased specific to ITGα3 (EHU133981) (Sigma Aldrich) in order to ablate expression of ITGα3 and reduce the function of the whole integrin receptor (ITGα3/β1).

In brief, cells were seeded into a 6-well plate (Corning) and incubated at 37 °C with 5 % CO_2 for 24 hours. Cell lines were transfected with ITGα3 esiRNA using the transfection reagent RNAiMAX (Invitrogen). One millilitre per well of Opti-MEM (Life Technologies) was added to 6 µl lipofectamine RNAiMAX and incubated for 5 minutes, then esiRNA was added to a final concentration of 100 nM. After 20 minutes, RPMI media was removed from cells and replaced with one millilitre of the Opti-MEM, esiRNA, transfection reagent mix. Following incubation at 37 °C with 5 % CO_2 for 4-6 hours the Opti-MEM transfection mix was replaced with RPMI and cells were incubated for a further 20 hours. ITGα3 knockdown was assessed via Western Blotting (conducted as in outlined section 2.4.3) probed with mouse monoclonal antibody anti-ITGα3 (66070-1-Ig).

6.2.6 MET inhibitor treatment

The MET inhibitor SU11274 (Sigma-Aldrich) was used to treat the three thyroid cell lines TPC-1, Cal-62 and SW1736 seeded into 6-well plates. Each inhibitor dose (0.5 µM, 1 µM, 2 µM, 5 µM) was prepared in DMSO (final concentration 0.05 %) and both no treatment and DMSO-only were used as controls. Treated cells were incubated at 37 °C with 5 % CO_2 for 24 hours. The media was then changed to RPMI with 2% FBS and the cell scratch wound assay performed to assess cell migration (section 2.8). To

confirm cell viability, trypan blue was used to quantify the number of dead cells. Cells were washed with PBS, trypsinised and then resuspended in RPMI. The 0.4% Trypan Blue (Life Technologies) was added at a 1:1 ratio to the cell suspension and incubated for 1-2 minutes. Cells were then counted in a haemocytometer and a percentage of blue (dead) to normal cells calculated.

6.3 Results

6.3.1 Most differentially expressed genes in recurrent thyroid cancer

The differential expression profile of recurrent thyroid cancer tumours versus non-recurrent thyroid cancer tumours was compared by calculating median differential expression (and significance) for each gene. Of the top 100 median differentially expressed genes 40 were statistically significantly different (Appendix 1; Table 10.3). This included thyroglobulin (TG), thyroid peroxidase (TPO), fibronectin (FN1), integrin alpha 3 (ITGα3) and the proto-oncogene MET. The genes FN1, ITGα3 and MET are all recognised as potentially oncogenic and FN1 and MET have already been implicated in thyroid cancer (Huang et al. 2001).

6.3.2 Enrichment analysis of differentially expressed genes.

Gene set enrichment analysis is performed to identify groups of proteins that are overexpressed in certain disease pathways. In order to perform pathway analysis on the most differentially expressed genes, the DAVID database (Huang da et al. 2009) was used to perform a Kyoto Encyclopaedia of Genes and Genomes (KEGG) pathway analysis and the Gene Ontology (GO) GOTERM BP DIRECT analysis (Figure 6.2).

A

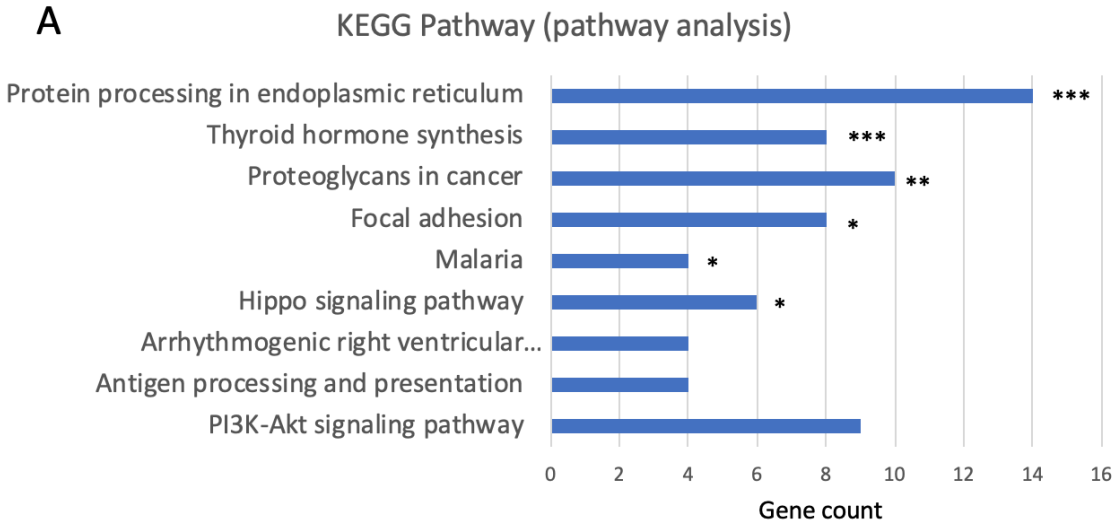

B

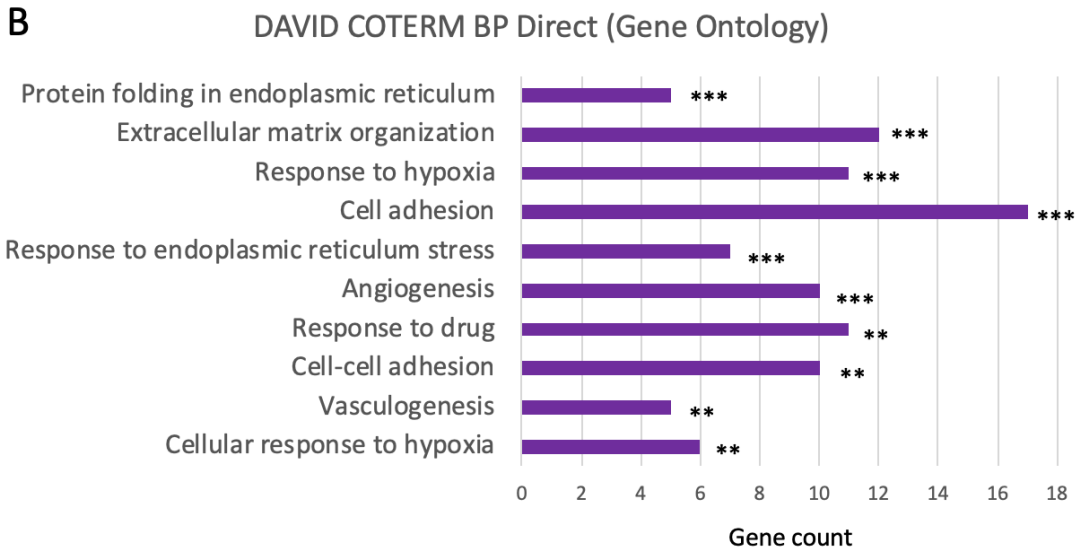

C

KEGG Pathway Term	Genes
Protein processing in endoplasmic reticulum	P4HB, HERPUD1, PDIA3, RRBP1, CRYAB, PDIA6, PDIA4, CALR, CANX, HYOU1, HSP90B1, HSPA5, RPN2, DDOST
Thyroid hormone synthesis	SLC26A4, TG, HSP90B1, TPO, HSPA5, PDIA5, PDIA4, LRP2, CANX
Proteoglycans in cancer	ACTG1, ERBB3, VEGFA, MET, HSPG2, ITGA2, TIMP3, SDC2, KDR, FN1
Focal adhesion	ACTG1, FLT1, VEGFA, MET, ITGA2, ITGA3, KDR, FN1
Malaria	ICAM1, CD81, MET, SDC2
Hippo signaling pathway	ACTG1, YWHAZ, CTGF, TGFBR2, AMOT, DVL1
Arrhythmogenic right ventricular cardiomyopathy	ACTG1, DSG2, ITGA2, ITGA3
Antigen processing and presentation	PDIA3, CTSS, CALR, CANX
PI3K-Akt signaling pathway	HSP90B1, YWHAZ, FLT1, VEGFA, MET, ITGA2, ITGA3, KDR, FN1

D

DAVID COTERM BP Direct Term	Genes
Protein folding in endoplasmic reticulum	CANX, CALR, HSP90B1, HSPA5, PDIA3
Extracellular matrix organization	APP, COL14A1, CYR61, FN1, HSPG2, ITGA2, ITG3A, ICAM1, KDR, NID2, TMPRSS6, VWA1
Response to hypoxia	APOLD1, CAT, CRYAB, DPP4, EGR1, EPAS1, HSP90B1, ITGA2, MUC1, TGRBR2, VEGFA
Cell adhesion	ARF6, APP, BCAM, CTGF, CYR61, DSG2, EMILIN2, FN1, IGFBP7, ITGA2, ITGA3, ICAM1, NEDD9, NID1, PODXL, RHOB, SORBS2
Response to endoplasmic reticulum stress	HSP90B1, HERPUD1, HYOU1, P4HB, PDIA3, PDIA4, PDIA6
Angiogenesis	APOLD1, CTGF, EPAS1, FN1, FLT1, HSPG2, KDR, RHOB, TMPRSS6, VEGFA
Response to drug	CALR, CAT, POR, ITGA2, ITGA3, ICAM1, LCN2, PARP4, RPN2, SREBF1, TGFBR2
Cell-cell adhesion	PARK7, SLC9A3R2, EIF3E, FMNL2, HSPA5, HDLBP, PPL, PFKP, RPL14, YWHAZ
Vasculogenesis	ZFP36L1, AMOT, KDR, TGFBR2, VEGFA
Cellular response to hypoxia	ZFP36L1, EPAS1, HYOU1, ICAM1 P4HB, VEGFA

*Figure 6.2: DAVID pathway analysis (KEGG) (A) and gene ontology analysis (GOTERM BP DIRECT) analysis (B) (top ten terms) of top 200 differentially expressed genes in recurrent patients versus non-recurrent patients. X axis – gene count, y-axis DAVID term. C) Genes in the KEGG pathway analysis D) Genes in the COTERM BP Direct analysis. Arrhythmogenic right ventricular…; Arrhythmogenic right ventricular cardiomyopathy. * $p < 0.05$, ** $p < 0.01$, *** $p < 0.001$, rest ns not significant.*

Cell adhesion, ECM organization and endoplasmic reticulum (ER) protein processing were highlighted by the enrichment analysis (Figure 6.2). The proteoglycans in cancer category was significant in the KEGG pathway analysis (Figure 6.2

A

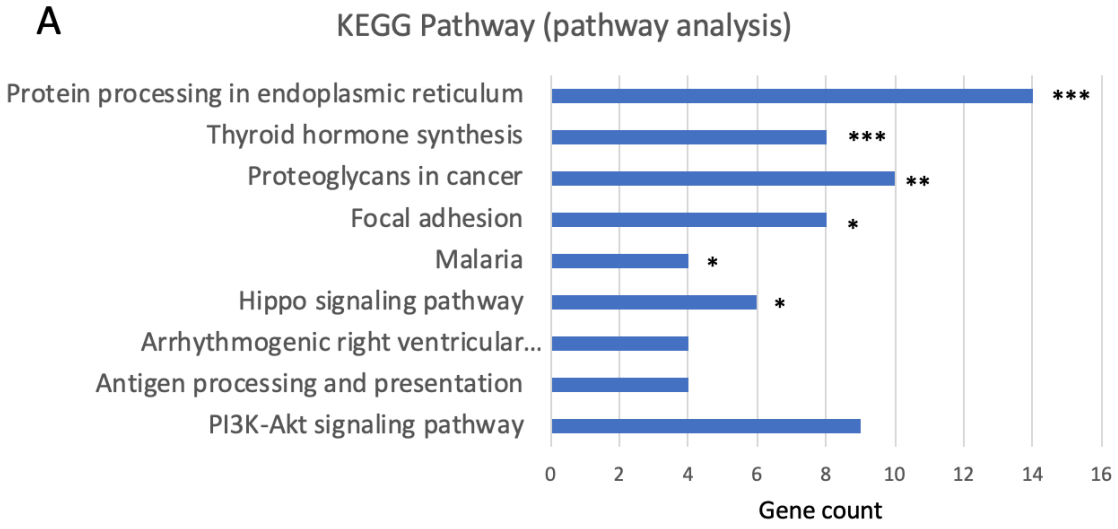

B

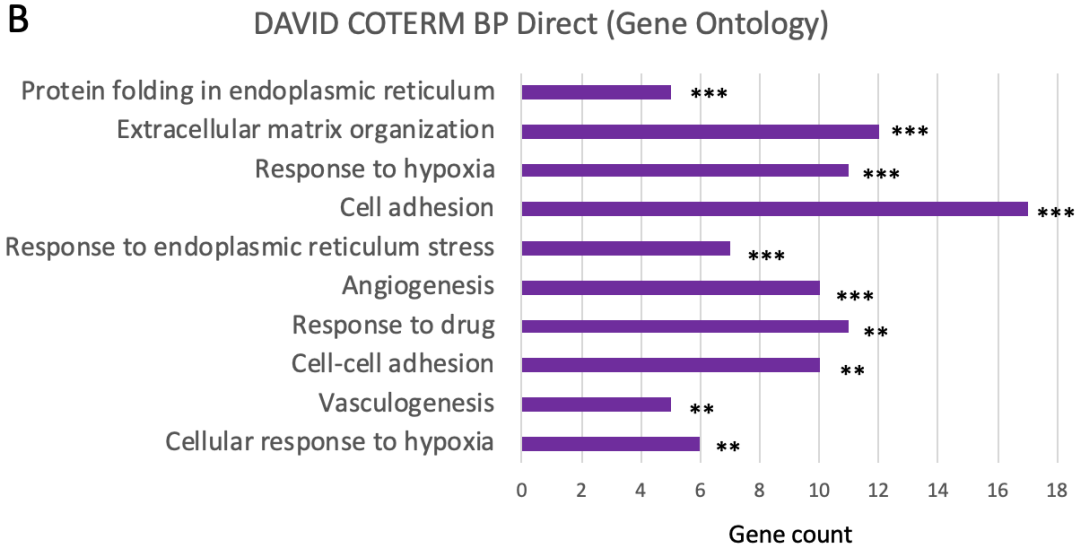

C

KEGG Pathway Term	Genes
Protein processing in endoplasmic reticulum	P4HB, HERPUD1, PDIA3, RRBP1, CRYAB, PDIA6, PDIA4, CALR, CANX, HYOU1, HSP90B1, HSPA5, RPN2, DDOST
Thyroid hormone synthesis	SLC26A4, TG, HSP90B1, TPO, HSPA5, PDIA5, PDIA4, LRP2, CANX
Proteoglycans in cancer	ACTG1, ERBB3, VEGFA, MET, HSPG2, ITGA2, TIMP3, SDC2, KDR, FN1
Focal adhesion	ACTG1, FLT1, VEGFA, MET, ITGA2, ITGA3, KDR, FN1
Malaria	ICAM1, CD81, MET, SDC2
Hippo signaling pathway	ACTG1, YWHAZ, CTGF, TGFBR2, AMOT, DVL1
Arrhythmogenic right ventricular cardiomyopathy	ACTG1, DSG2, ITGA2, ITGA3
Antigen processing and presentation	PDIA3, CTSS, CALR, CANX
PI3K-Akt signaling pathway	HSP90B1, YWHAZ, FLT1, VEGFA, MET, ITGA2, ITGA3, KDR, FN1

D

DAVID COTERM BP Direct Term	Genes
Protein folding in endoplasmic reticulum	CANX, CALR, HSP90B1, HSPA5, PDIA3
Extracellular matrix organization	APP, COL14A1, CYR61, FN1, HSPG2, ITGA2, ITG3A, ICAM1, KDR, NID2, TMPRSS6, VWA1
Response to hypoxia	APOLD1, CAT, CRYAB, DPP4, EGR1, EPAS1, HSP90B1, ITGA2, MUC1, TGRBR2, VEGFA
Cell adhesion	ARF6, APP, BCAM, CTGF, CYR61, DSG2, EMILIN2, FN1, IGFBP7, ITGA2, ITGA3, ICAM1, NEDD9, NID1, PODXL, RHOB, SORBS2
Response to endoplasmic reticulum stress	HSP90B1, HERPUD1, HYOU1, P4HB, PDIA3, PDIA4, PDIA6
Angiogenesis	APOLD1, CTGF, EPAS1, FN1, FLT1, HSPG2, KDR, RHOB, TMPRSS6, VEGFA
Response to drug	CALR, CAT, POR, ITGA2, ITGA3, ICAM1, LCN2, PARP4, RPN2, SREBF1, TGFBR2
Cell-cell adhesion	PARK7, SLC9A3R2, EIF3E, FMNL2, HSPA5, HDLBP, PPL, PFKP, RPL14, YWHAZ
Vasculogenesis	ZFP36L1, AMOT, KDR, TGFBR2, VEGFA
Cellular response to hypoxia	ZFP36L1, EPAS1, HYOU1, ICAM1 P4HB, VEGFA

A; p = 0.0012) and this encompasses MET, the MAPK and PI3K-Akt pathways, which are responsible for thyroid cancer progression. Key genes that came up in multiple pathways included MET, FN1, ITGα2, ITGα3, ICAM1, VEGFA, CALR and HSP90B1. This analysis highlights the importance of cell adhesion and tumour cell interaction with the extracellular matrix, the ER and hypoxia and angiogenesis in thyroid tumour recurrence.

6.3.3 Volcano plot of differential expression of recurrent versus non-recurrent thyroid cancer patients

To further investigate potential changes in the mRNA expression signature, a volcano plot of the fold change (FC) of differential expression was plotted (Figure 6.3). An advantage of using this approach was that it highlighted certain genes with a high fold change of mRNA expression in recurrent patients compared to non-recurrent patients. Examples include Frizzled homolog protein 9 (FZD9; log fold change (FC) 1.91, p < 0.0001), Collagen Type XIX Alpha 1 Chain (COL19A1; FC -2.3, p = 0.0003),

Pregnancy Specific Beta-1-Glycoprotein 3 (PSG3; FC -2.52, p = 0.0005), glutamate ionotropic receptor kainate type subunit 4 (GRIK4; FC 2.11, p < 0.0001), Potassium Voltage-Gated Channel Subfamily J Member 13 (KCNJ13; FC 1.88, p -= 0.0002), Transmembrane protein 139 (TMEM139; FC 1.71, p = 0.0005), Limb and CNS Expressed 1 (LIX1; FC 1.62, p = 0.0009) and SLC5A5 (NIS; FC 2.13, p < 0.0001). FZD9 has been implicated as a potential tumour marker but has variable effects in the presence of Wnt (Ueno et al. 2013). LIX1 appears to be an indicator of poor prognosis in endometrial cancer in the open source online omics project Protein Atlas (Uhlen et al. 2015), and TMEM139 is implicated in renal and pancreatic cancer in the same database. NIS is one of the key iodine metabolism proteins in the thyroid and expression has already been linked to poor prognosis. This is thought to be causative as the lower NIS expression results in decreased susceptibility to radioiodine therapy, although TCGA data suggest that lower expression may also favour a more aggressive phenotype (Agarwal et al. 2014).

Figure 6.3: Volcano plot of log fold change of mRNA expression (x axis) versus log p-value (y axis). Teal dots at p < 0.001. Labelled genes are p < 0.001 and log fold change > 1.5. Positive log fold change represents lower expression, negative represents higher expression.

6.3.4 Selected differentially expressed genes

After assessing the mRNA expression data through a number of analyses, a shortlist of the most biologically interesting differentially expressed genes was made. These were selected from the median differential expression analysis as the most effective representative of the difference between recurrent and non-recurrent disease.

FN1, ITGα3 and MET were all significantly differentially expressed in recurrent versus non-recurrent patient thyroid carcinoma tissues and all genes were already implicated in oncogenesis. In order to determine the direction of differential expression (higher or lower in the recurrent patients) and to compare to the median expression level in normal tissue, the genes FN1, ITGα3 and MET were plotted as log transformed data (Figure 6.4).

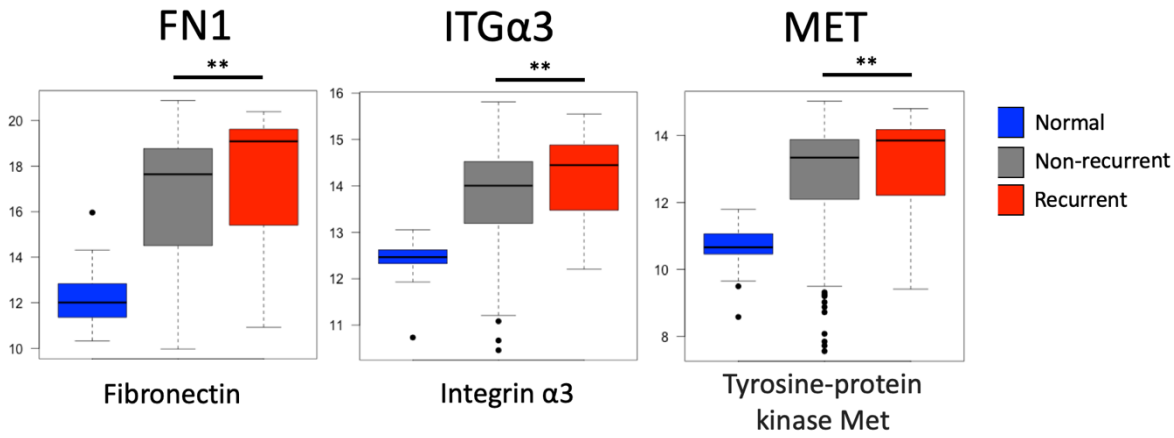

*Figure 6.4: Comparison of median mRNA expression levels of FN1, ITGα3 and MET in normal tissue against non-recurrent patient primary tumour tissue and recurrent patient primary tumour tissue. Non-recurrent patients n = 461, recurrent n = 43 and normal n = 58. Boxplot generated in R (boxplot) demonstrates median, upper and lower quartiles in the box and the whiskers correspond to data points up to 1.5 multiplied by the interquartile range beyond the quartile. Data points outside this are represented by dots. * p < 0.05, ** p < 0.01, *** p < 0.001.*

6.3.5 Gene expression and BRAF-like or RAS-like tumour status

Altered fibronectin (FN1) expression is associated with thyroid cancer (Huang et al. 2001, Takano et al. 1998a) and has been associated with BRAF V600E status, but its expression is not dependent on BRAF V600E mRNA expression (Watanabe et al. 2009). To investigate the association apparent between FN1 and BRAF V600E status a heatmap was generated of FN1, ITGα3 and MET expression and BRAF status in the 43 recurrent patients in the TCGA (Figure 6.5). Interestingly, this shows that FN1, ITGα3 and MET expression all closely correlate with BRAF V600E status.

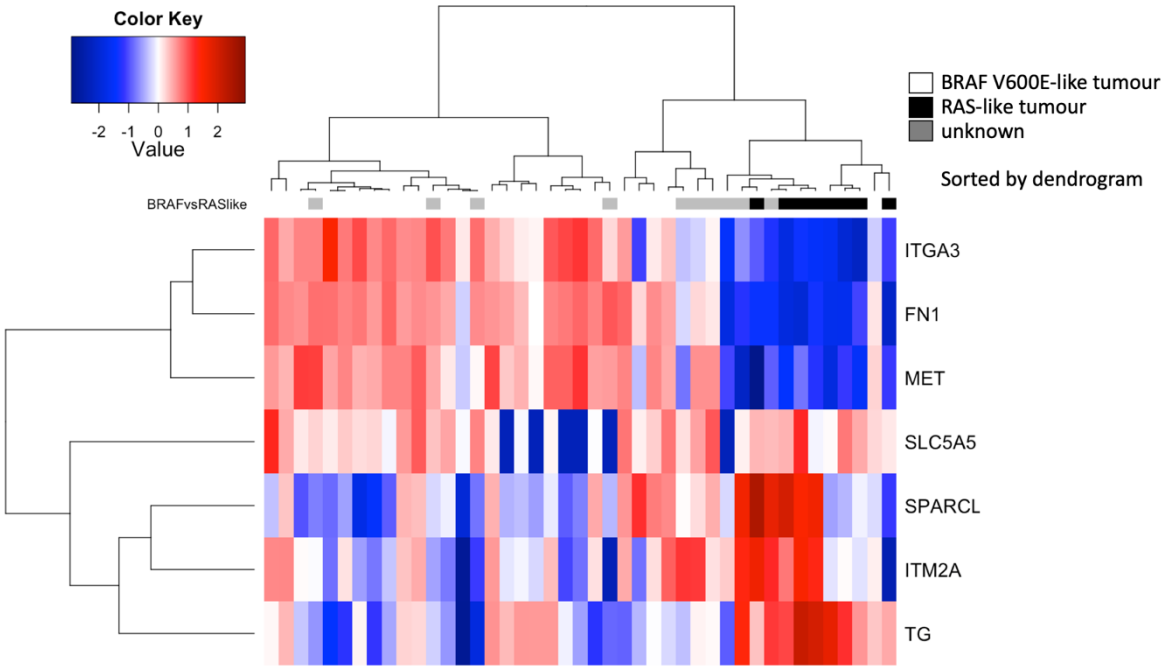

Figure 6.5: Heat map of selected most differentially expressed genes between recurrent and non-recurrent patients, recurrent patients only (n = 43). BRAF-like and RAS-like status also shown (top bar; white – BRAF V600E-like, grey – unknown, black – Ras-like). Sorted by dendrogram.

The genes FN1, ITGα3 and MET were nominated for further analysis via cellular functional studies.

6.3.6 Fibronectin, ITGα3 and MET functional analysis

Having identified potential genes implicated in thyroid cancer recurrence via altered mRNA expression the next objective was functional analysis of these genes in cell lines, to delineate the role of these genes in the recurrence pathway.

6.3.6.1 Fibronectin

Cell proliferation assays were not affected by FN1 transfection (Figure 6.6). Cell migration assays showed an increase in migration on transfection of fibronectin (Figure 6.7). Proof of transfection by Western blot is shown (Figure 6.6).

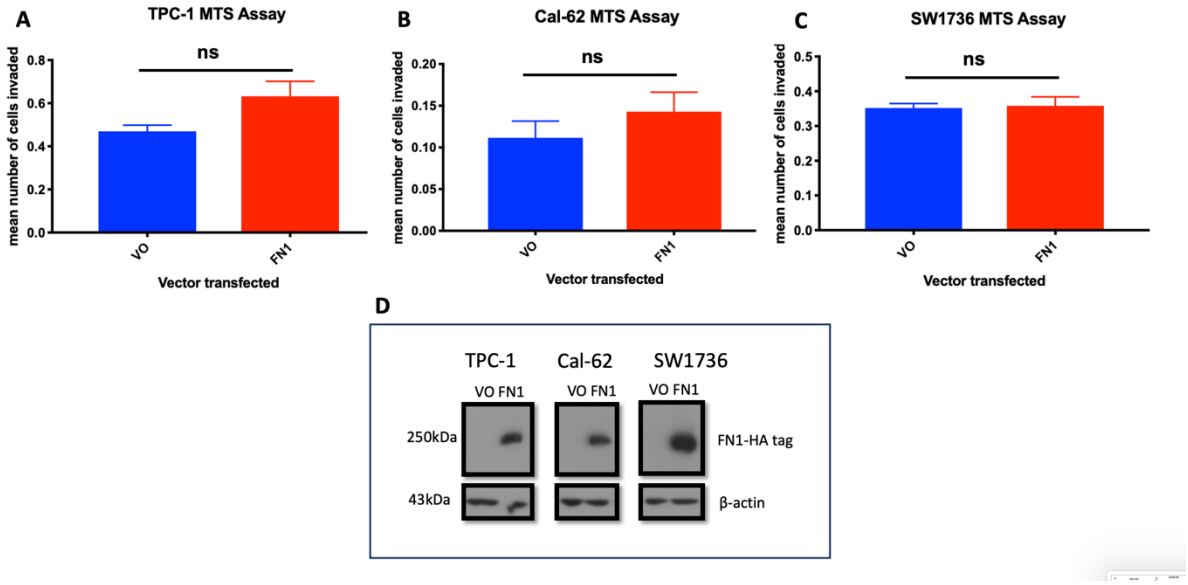

Figure 6.6: A, B & C: Cell proliferation assay (MTS) comparing vector only (VO) and fibronectin (FN1) in three cells lines (A: TPC-1, B: Cal-62 and C: SW1736). D: Western blot analysis of FN1 in thyroidal cell lines (TPC-1, Cal-62 and SW1736) transfected with FN1 or vector only (VO) and probed with mouse monoclonal anti-HA antibody (16B12) (BioLegend). n = 3, ns not significant.

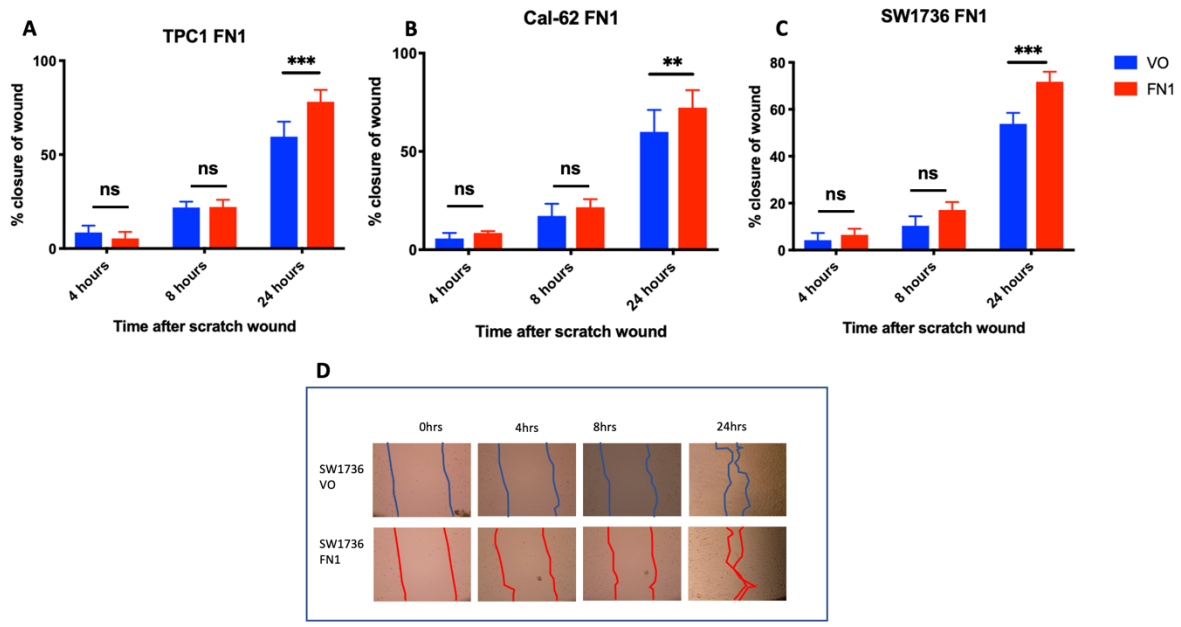

*Figure 6.7: A, B & C: Cell migration assay comparing vector only (VO) to fibronectin transfection (FN1) in three cells lines (A: TPC-1, B: Cal-62 and C: SW1736). D: Representative images of the cell scratch wound closing shown (10x). n = 3. * p < 0.05, ** p < 0.01, *** p < 0.001, ns not significant.*

6.3.6.2 ITGα3

As RNA-seq analysis showed that ITGα3 was increased in recurrent tumours (Figure 6.4), the next step was to determine if modulating ITGα3 expression affected the tumourigenic potential of cancer cells. Cell proliferation assays showed a modest decrease in turnover as assessed via MTS assay in the ITGα3 knockdown. There was a significant difference in proliferation in ITGα3 knockdown compared to scrambled siRNA control in the Cal-62 cell line (scr versus ITGα3 KD p = 0.034) and also TPC-1 cell line between mock transfection and ITGα3 knockdown (mock versus ITGα3 KD p = 0.05, Figure 6.8).

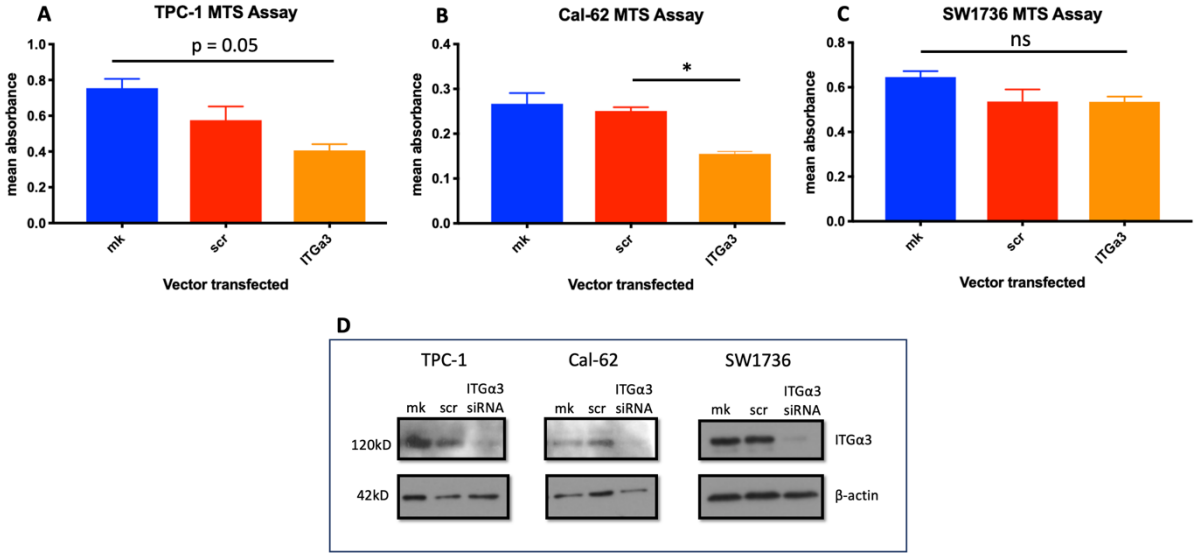

*Figure 6.8: A, B & C: Cell proliferation assay (MTS) comparing mock transfection (mk), scrambled siRNA (scr) and ITGα3 knockdown in three cells lines (A: TPC-1, B: Cal-62 and C: SW1736). D: Western blot shows knock down of ITGα3 in three cell lines, with controls mock (mk) and scrambled siRNA (scr). n = 3, * p < 0.05, ** p < 0.01, *** p < 0.001, ns non-significant.*

Scratch-wound cell migration assays demonstrated that ITGα3 ablation using siRNA markedly reduced the cell migratory properties of TPC-1 (scrambled siRNA (scr) versus ITGα3 knockdown (KD), p = 0.007), Cal-62 (scr versus ITGα3 KD, p = 0.0036) and SW1736 (scr versus ITGα3 KD, p = 0.0012) cells at 24 hours (Figure 6.9). Evidence of knock down is demonstrated in Figure 6.8.

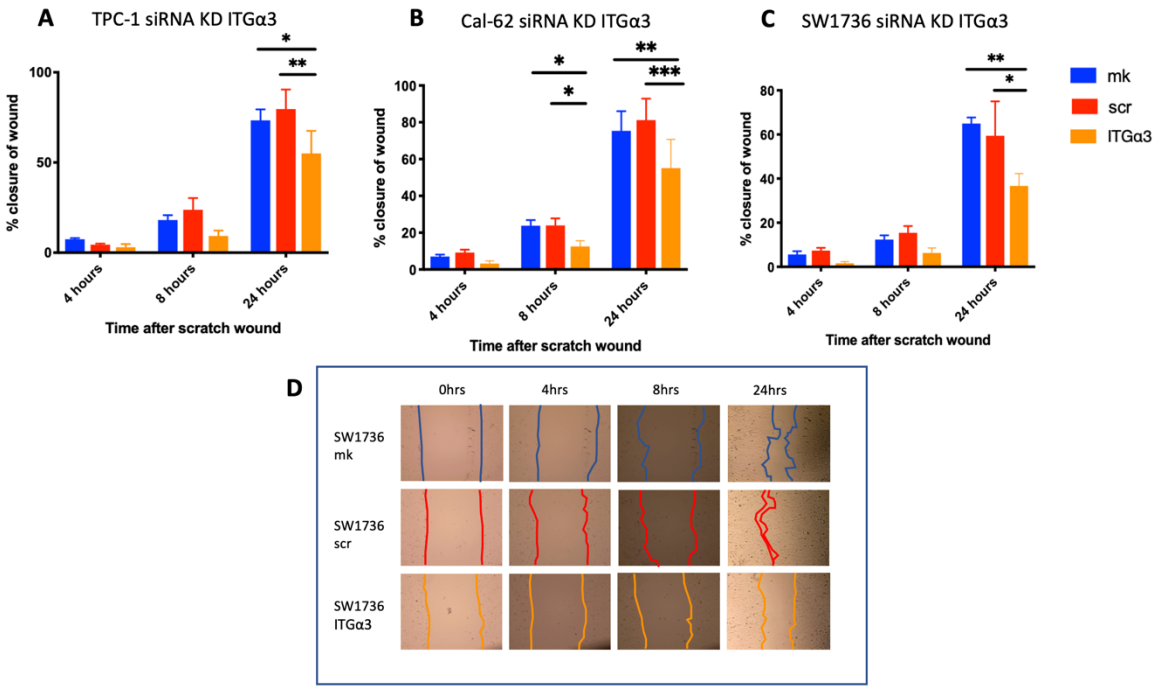

*Figure 6.9: A, B & C: Cell scratch wound migration assay comparing mock transfection (mk), scrambled siRNA (scr) and ITGα3 siRNA knockdown in three cells lines (A: TPC-1, B: Cal-62 and C: SW1736). D: Representative images of the cell scratch wound closing shown (10x). n = 4, Cal-62 n = 3. * p < 0.05, ** p < 0.01, *** p < 0.001.*

6.3.6.3 MET inhibition

MET is well recognised as an oncogene and is known for its effects on proliferation, migration and cell survival (Trusolino et al. 2010). MET activates multiple pathways including the MAPK and PI3K/Akt pathway. It has been implicated in thyroid cancer recurrence (Inaba et al. 2002) and has been postulated as a drug target in numerous cancers (Gherardi et al. 2012). Given the availability of MET inhibitors, treatment with the well characterised drug SU11274 was performed on three thyroid cancer cell lines. In both TPC-1 and SW1736 cells there was a dose dependent effect on the cells reducing the migratory phenotype observed in Figure 6.10. In particular, the wound

closure rate was reduced by ~50 % when using the MET inhibitor at a dose of 2 μM in the TPC-1 and SW1736 cell lines (Figure 6.10), whereas Cal-62 cells were relatively resistant to SU11274 treatment.

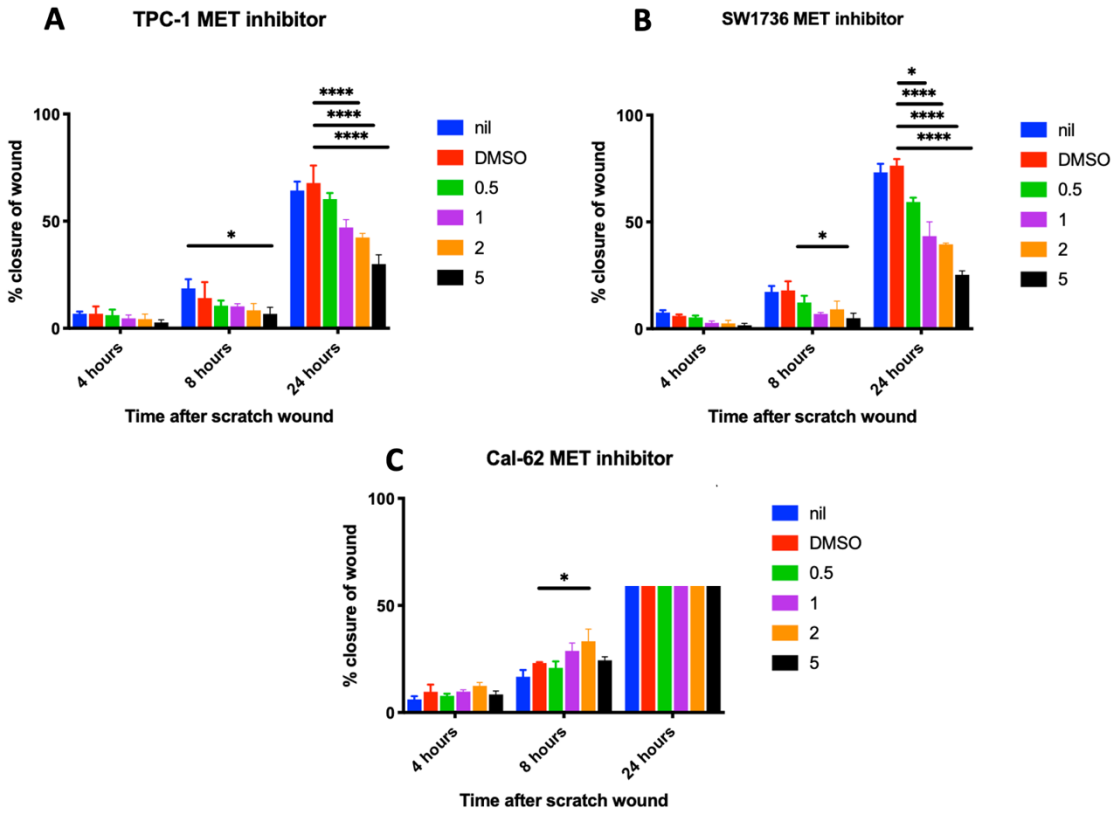

*Figure 6.10: A, B & C: Cell scratch wound assay assessing impact of MET inhibitor SU11274 treatment on cancer cell migration. MET inhibitor (SU11274, increasing doses, shown in legend in μM) compared to no treatment (nil) or DMSO treatment in three cells lines (A: TPC-1, B: Cal-62 and C: SW1736) in a cell scratch wound migration assay with time points at 0hrs, 4hrs, 6hrs and 24hrs. Dose dependent response seen in A: TPC-1 and B: SW1736 cell lines, not in C: Cal-62 cell line. n = 3. * p < 0.05, ** p < 0.01, *** p < 0.001, **** p < 0.0001.*

In order to assess whether this effect was true, and not a non-specific manifestation of cell death on addition of the drug, a trypan blue stain was added to quantify cell death

(Figure 6.11). Cell death was less than 10 % in each cell line and did not markedly increase between different drug doses, thereby attributing the decreasing migration to drug-specific effects.

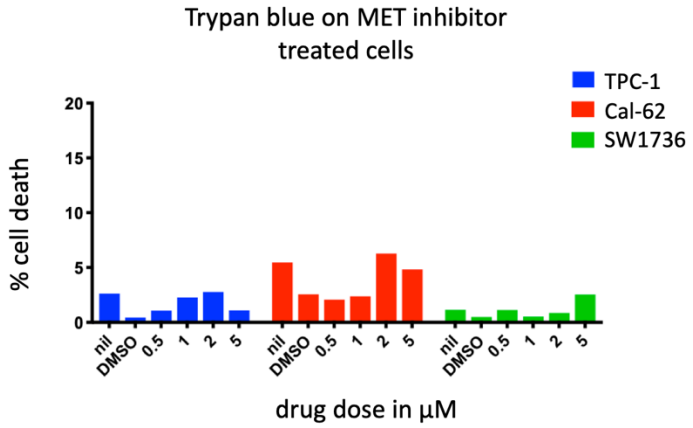

Figure 6.11: MET inhibitor SU11274 at doses 0 – 5 µM does not induce significant cell death on trypan blue staining. MET inhibitor (increasing doses) treatment with trypan blue added to discern the percentage of dead cells. n = 1.

Thus, the overexpression of FN1 induced an increase in cell migration but had no effect on proliferation. The knockdown of ITGα3 reduced the migratory and proliferative phenotype of the thyroid cancer cells appraised. Treatment with the MET inhibitor SU11274 demonstrated a dose response affecting cell migration. Each of these genes may therefore have a functional role in thyroid oncogenesis.

6.4 Discussion

6.4.1 Most differentially expressed genes and enrichment

RNA expression signatures can be a powerful way of exploring cancer cell phenotypes. RNA data can be processed in a number of ways; conventionally often fold change between different values is applied. This helps compare mRNA expression to the gene baseline expression. This analysis compared the expression of genes in a group of recurrent thyroid cancer patients to a group of non-recurrent thyroid cancer patients, rather than their normal tissue baseline. This was because the true interest in this analysis lay in the difference between the recurrent tumours and the non-recurrent tumours. Because the patient true baseline (normal tissue) was therefore not used in this analysis, both absolute values and fold change were examined. Assessment of the median differentially expressed genes (absolute values) came up with thousands of significantly differentially expressed genes, and two approaches to assess this data were taken. The top fifteen most differentially expressed genes were examined to select any thyroid iodine metabolism proteins, oncogenes, tumour suppressors or other genes of interest for further examination (Appendix 1; Table 10.3). The data were also assessed by enrichment using the DAVID database, highlighting pathways in the top 200 significantly differentially expressed genes. The volcano plot (Figure 6.3) demonstrates genes that have the largest fold change in expression, and the most interesting of these is NIS, the sodium iodide symporter. Of particular significance, this demonstrates that decreased NIS expression, and therefore potential radioiodine treatment evasion, is apparent in recurrent tumours on the initial histology.

DAVID enrichment analysis further highlighted cell adhesion and ECM organization, and endoplasmic reticulum (ER) protein processing. The ER is responsible for protein folding and maturation, and ER stress activates the unfolded protein response (UPR). The UPR either activates apoptosis or restores homeostasis, and adaptations of this can facilitate cancer cells evading appropriate cell death (Yadav et al. 2014). Cell adhesion, focal adhesion and the extracellular matrix interactions are also involved in tumourigenesis and have been implicated in recurrent disease. The association with recurrence ranges from implicating integrins in the switch to cancer cell dormancy, treatment evasion and co-operative signaling with receptor tyrosine kinases for cell survival (Eke and Cordes 2015). Proteoglycans in cancer came up in both arms of the analysis. This encompasses both MET and the MAPK and PI3K-Akt pathways, all implicated in thyroid cancer progression and aggressiveness.

After the assessment of all the RNA data analyses, the proteins FN1, ITGα3 and MET from the differentially expressed genes were considered genes with potential importance in thyroid cancer recurrence (Zhai et al. 2019) and were selected for functional experiments.

6.4.2 FN1 and ITGα3

Fibronectin 1 (FN1) has a role in cell adhesion and cell motility, upregulation of which would potentially generate the ability for tumours to both metastasise and recur. FN1 has also been linked with cancer aggressiveness previously, both generally and in the context of thyroid cancer (Sponziello et al. 2016, da Silveira Mitteldorf et al. 2011).

Fibronectin has been postulated as a marker for thyroid cancer on FNAc (Takano et al. 1998b) and as a means of identifying residual disease or monitoring patients (Hesse et al. 2005). Fibronectin is also a marker of mesenchymal status in the epithelial mesenchymal transition (EMT). EMT is a progression from a set of polarised epithelial cells to a motile mesenchymal state, and is recognised as part of the development of cells from primary tumour to invasion, metastasis and recurrence (Huber et al. 2005, Wang and Zhou 2013). This is activated by a number of different pathways, including the tyrosine kinase receptor Raf/Ras pathway. The results observed in this Chapter are consistent with this, with overexpression of FN1 conferring a migratory advantage to the cells. No change in proliferation was seen, and these findings may suggest that motility is the main oncogenic component of FN1. Previous studies have demonstrated an association between FN1 expression and the invasive, migratory and proliferative nature of thyroid cancer cell lines (Xia et al. 2017, Sponziello et al. 2016). What is especially interesting here from the TCGA data is that the increased FN1 level was apparent at the patients' initial histology, highlighting this as a potential prognostic biomarker.

FN1 and ITGα3 have been previously identified as differentially expressed genes in thyroid cancer compared to normal tissue, and also appear to influence the expression of each other (Han et al. 2018). They interact directly under certain conditions, with fibronectin binding to ITGα3/β1 (Brown et al. 2015, Elices et al. 1991) and ITGα3/β1 increasing the deposition of fibronectin into the pericellular matrix (Wu et al. 1995). The results from this chapter clearly show a dependence on ITGα3 for the pro-migratory status of the cells. Integrin α3 has been demonstrated to be present in invadopodia in

breast cancer cells (Coopman et al. 1996) and recruits ECM degrading proteases (Mueller et al. 1999, Morini et al. 2000). This breakdown of the ECM helps tumour cells invade and even metastasise.

Integrins are not only involved in tumour invasiveness, but also are implicated in cancer cells' dormancy post-treatment and consequent recurrence (Eke and Cordes 2015). The activation of ITGα3/β1 causes phosphorylation of FAK, leading to increased kinase activity, including interaction with Src and cortactin (Eke and Cordes 2015). Cortactin has been previously associated with the thyroid proto-oncogene PTTG1-binding factor (PTTG1IP/PBF), which occurs at the leading edge of migratory tumour cells (Watkins et al. 2016), increasing tumour invasiveness. In a mouse model of lung metastasis, ITGα3/β1 was implicated in adherence in metastasis and also cell signalling to induce colony formation (Wang et al. 2004). Further to this, an ITGα3/β1 specific binding ligand has recently been presented as a potential means of delivering targeted treatment to non-small cell lung cancer cells (Xiao et al. 2019).

The results in this chapter highlight ITGα3 as an important integrin in thyroid cancer, emphasising its potential for a therapeutic role.

6.4.3 MET

MET is an established oncogene, and is known to be implicated in thyroid cancer, specifically in lymph node metastasis and worsening stage (Trovato et al. 2017, Chen et al. 1999). The expression of MET has been associated with thyroid cancer

recurrence, and due to the oncogenic nature of the protein it has been suggested that it has a pathological role too (Inaba et al. 2002).

In anaplastic thyroid cancers, RAF-kinase inhibitor treatment demonstrated initial disease response and then recurrence; the recurrent tumours had MAPK signalling reactivated, predominantly via MET amplification (Knauf et al. 2018). Anaplastic thyroid cancer is thought to be a continuum from differentiated thyroid cancer through dedifferentiation to anaplastic thyroid cancer (Landa et al. 2016) and so this information could potentially be translated to differentiated thyroid cancer. The recurrent anaplastic tumours that escaped blockade of MAPK signalling via MET amplification were highly sensitive to MET inhibitors (Knauf et al. 2018).

In these experiments, the migration of thyroid cancer cell lines was markedly reduced in a dose dependent manner, independent of cell death in the TPC-1 and SW1736 cell lines, but not in the Ras dependent Cal-62 cell line. The MET inhibitor SU11274 has been used in cell lines to demonstrate responsiveness to treatment (Kenessey et al. 2010), but this can be inhibited by mutations in the MET gene (Berthou et al. 2004). Treatment of a melanoma cell line with SU11274 has previously demonstrated cell plasticity and adaptivity to targeted MET inhibition (Kucerova et al. 2016). In addition, inhibition of RAF and MET in thyroid cancer cell lines has shown to effective at tumour suppression (Byeon et al. 2016). The effectiveness of SU11274 in the thyroid cancer cell lines further implicates MET as a driver of thyroid cancer, and as a prospective treatment in recurrent resistant tumours. Further studies are required however to confirm that the effects of the MET inhibitors do take place by their action upon MET,

as off-target effects could also contribute to their actions upon cell migration. Preliminary steps towards this could be accomplished using Western blots examining phosphorylation of Akt and levels of MET and phosphorylated MET.

6.4.4 Concluding remarks

Several pathways have been implicated by this analysis in the pathogenesis of thyroid cancer recurrence. The interaction of the cell with the ECM seems to be key, and the novel validation of ITGα3 as a tumourigenic factor in thyroid cancer cell lines is intriguing. Further exploration of this in ECM protein-lined cell culture plates may help us further understand the tumour-ECM interaction. MET is also a key driving force in thyroid oncogenesis and appears to be a factor in thyroid cancer treatment resistance and recurrence. Further work on radioiodine resistant cell lines and MET inhibitors would be interesting. More pressingly, mathematical modelling combining these three biomarkers to generate cut-off values for clinical application would be very useful. This would generate a tool that when validated, could direct the assertiveness of follow up for thyroid cancer patients.

Chapter 7 MicroRNA expression levels in thyroid cancer recurrence

7 MicroRNA expression levels in thyroid cancer recurrence

7.1 Introduction

7.1.1 MicroRNAs

MicroRNAs (miRs) are small non-coding RNAs that modify post-transcriptional gene expression. MicroRNAs silence mRNA by binding to their complementary sequence and causing cleavage, reduced translation of the mRNA or epigenetic silencing of transcription (Figure 5.1). The role of miRs in cancer can be complex. MicroRNAs can act as oncomiRs or tumour suppressors, depending on their end actions (Esquela-Kerscher and Slack 2006), but these often vary in different tissue types or environments. This is thought to be due to the miRs targeting multiple sites and having both oncogenic and suppressive effects, depending on their interactions with cancer genes, the immune system and their environment (Svoronos et al. 2016).

7.1.2 MicroRNAs in thyroid cancer

There are several examples of miRs with well-defined roles in thyroid cancer (Table 1.1). One of the most prominent is Let-7, which targets the RAS gene, reduces MAPK expression and tumour growth (Ricarte-Filho et al. 2009). MiR-146b is the most frequently upregulated miR in thyroid cancer and is considered a poor prognostic indicator (Ramírez-Moya and Santisteban 2019). In particular, miR-146b inhibits the actions of PTEN, which regulates the PI3K/Akt pathway. DICER1 expression is also reduced by expression of miR-146b, which forms a negative feedback loop (Ramírez-Moya et al. 2019). MiR-146b and several other thyroid cancer associated miRs such as miR-221 and miR-222 are particularly associated with the BRAF V600E mutation

(Chou et al. 2010)(Table 7.1). RAS-like tumours have their own associated miR including miR-183 and miR-182. Additionally, miR-221 and miR-222 have been associated with lymph node metastasis and grade of tumour (Sun et al. 2013). The miR-221 has also been postulated as a marker of recurrence (Dai et al. 2017). The study showed that of eight miRs studied, miR-221 and miR-222 were significantly associated with PTC recurrence, alongside several clinical factors such as TNM stage. MicroRNA-221 was the only independent risk factor for PTC in a multivariate Cox proportional hazard analysis. However, a detailed analysis of miRs implicated in thyroid cancer recurrence has not been undertaken.

	BRAF-like	RAS-like
Signalling	High MAPK signalling	Low MAPK signalling, PI3K/Akt signalling
Genetic alterations	BRAF V600E mutation, RET fusions, BRAF fusions	NRAS, HRAS, KRAS, EIF1AX PAX8/PPAR, NTRK22q-del mutations
Histological variants	Classical, tall cell	Follicular variant
miR profile	miR-21, miR-146b, miR-204, miR-221/222	miR-183-5p, miR-182-5p

Table 7.1: MicroRNA profile of RAS-like and BRAF-like thyroid tumours, from (Riesco-Eizaguirre and Santisteban 2016). In BRAF-like tumours miR-21, miR-146b, miR-221, miR-222 are upregulated and miR-204 is downregulated; in RAS-like tumours miR-182 and miR-183 are upregulated.

7.1.3 MicroRNAs and TCGA

Thyroid cancer specific analysis of TCGA data has so far identified six miR clusters associated with BRAF- or Ras- like status and mRNA expression (Agarwal et al. 2014).

Interestingly, two BRAF associated clusters (5 and 6) were associated with recurrence. Cluster 5 had high expression of miR-146b and miR-375 and low expression of miR-204 whereas Cluster 6 had high expression of miR-21 and low expression of miR-204. However, the possible functional role of miRs implicated in recurrence has not been examined. The objective of this chapter was to investigate the profile of miRs differentially expressed in recurrent compared to non-recurrent patients. From these, several of the most differentially expressed miRs were selected for further study *in vitro*. In particular, the role of candidate miRs was studied by transfection of miR mimics or inhibitors in thyroid cancer cell lines.

7.2 Materials and Methods

7.2.1 Bioinformatic analysis of differential expression of microRNAs in recurrent versus non-recurrent patients

The median differential expression of each miR was conducted in the same manner as for the RNA data (section 6.2.1) computed in R. Downloaded TCGA data were normalised to reads per million counts. The absolute differential expression data generated a list of 62 miRs that were significantly differentially expressed (Appendix 1; Table 10.4). From these, the most relevant miRs in thyroid cancer were selected, using a literature review of miR expression in thyroid cancer. The expression level of the miR in normal tissue, non-recurrent patient primary tumour tissue and recurrent patient primary tumour tissue was plotted (Figure 7.1).

7.2.2 Transfection and knock down of microRNAs

TPC-1, Cal-62 and SW1736 thyroidal cell lines were seeded into 6-well plates for 24 hours. They were then transfected with the miR negative control mimic (CN-001000-01-05), miR-221-5p mimic (C-301163-01-0002), miR-486-5p inhibitor (IH-300746-05-0002) or miR-1179 inhibitor (IH-301320-01-0002) (Dharmacon, Colorado, USA). To transfect cells, one millilitre per well of Opti-MEM (Life Technologies) was added to 6 µl lipofectamine RNAiMAX (Invitrogen) and incubated for 5 minutes. The microRNA mimic or inhibitor was then added to a final concentration of 100 nM. The RPMI medium was removed from cells and replaced with the Opti-MEM-transfection mix. Cells were then incubated for 4-6 hours prior to the RPMI media being replaced. Subsequent assays were then typically performed 20 hours later. Transfection and knockdown were confirmed with microRNA Real Time quantitative PCR (RTqPCR).

7.2.3 MicroRNA extraction

The cells were seeded in a 6 well plate and transfected with either miR mimic or inhibitor. After 48 hours incubation miR extraction was performed. Medium was removed from the confluent cells and cells were washed with PBS. Cells were lysed by addition of 700 µl Qiazol Lysis Reagent (Qiagen). The following steps are based on the miRNeasy Micro Kit (Qiagen) protocol. The cell lysate was transferred to a microcentrifuge tube and vortexed for one minute. The sample was then incubated at room temperature for five minutes, then 140 µl of chloroform were added and mixed for 15 seconds. This was then incubated at room temperature for a further five minutes. The sample was then centrifuged at 13,000 x g at 4 °C for 25 minutes. The sample had separated into three phases, and the upper colourless aqueous phase was moved

into a new collection tube and mixed with 525 µl of 100% ethanol. The sample-ethanol mix was then spun through a RNeasy MinEute spin column (Qiagen) for 15 seconds at 10,000 rpm at room temperature. The column was then washed with 500 µl Buffer RPE and spun for 15 seconds at 10,000 rpm at room temperature. A second wash was performed with 80% ethanol, spun for 2 minutes at 10,000 rpm at room temperature. Another 10,000 RPM five-minute spin was then performed to dry the column. The miR sample was then eluted in 14 µl of nuclease free water and quantified using the NanoDrop 1000 Spectrophotometer (ThermoFisher Scientific).

7.2.4 Real time PCR of microRNAs

The RT-PCR was preceded by polyadenylation to add a poly(A) tail to extracted miRs, addition of an adapter ligand, and then reverse transcription. A complementary DNA (cDNA) amplification step was then taken prior to the RTqPCR. These steps were performed using the TaMan Advanced miRNA Assay (ThermoFisher Scientific) and TaqMan Advanced miRNA cDNA Synthesis Kit (ThermoFisher Scientific). The poly(A) tailing reaction was performed by adding 3 µl of Poly(A) Reaction Mix (0.5 µl 10X Poly(A) Buffer, 0.5 µl ATP, 0.3 µl Poly(A) Enzyme and 1.7 µl RNase-free water) to 2 µl of miR sample (diluted to 5 ng/µl). The samples were vortexed briefly and then centrifuged before being placed in the thermocycler (Table 7.2).

Step	Temperature	Time
Polyadenylation	37 °C	45 minutes
Stop reaction	65 °C	10 minutes
Hold	4 °C	hold

Table 7.2: Thermocycler parameters for poly(A) tailing reaction

The adaptor ligation step was performed by adding 10 µl of Ligation Reaction Mix (3 µl 5X DNA Ligase Buffer, 4.5 µl 50% PEG 8000, 0.6 µl 25X Ligation Adaptor, 1.5 µl RNA Ligase, 0.4 µl RNase-free water) to the 5 µl from the poly(A) tailing step. The samples were vortexed briefly and then centrifuged before being placed in the thermocycler (Table 7.3).

Step	Temperature	Time
Ligation	16 °C	60 minutes
Hold	4 °C	Hold

Table 7.3: Thermocycler parameters for Adaptor ligand reaction.

The reverse transcription reaction was performed by adding 15 µl of the Real Time Reaction Mix (6 µl 5X RT Buffer, 1.2 µl 25mM dNTP Mix, 1.5 µl 20X Universal RT Primer, 3 µl 10X RT Enzyme Mix, 3.3 µl RNase-free water) to the adaptor ligand reaction sample. The samples were vortexed briefly and centrifuged before being placed in the thermocycler (Table 7.4).

Step	Temperature	Time
Reverse transcription	42 °C	15 minutes
Stop reaction	85 °C	5 minutes
Hold	4 °C	hold

Table 7.4: Thermocycler parameters for reverse transcription reaction.

The miR-amplification step (miR-Amp) was performed by adding 45 µl of miR-Amp Reaction Mix (25 µl 2X miR-Amp Master Mix, 2.5 µl 20X miR-Amp Primer Mix, 17.5 µl

RNase-free water) to 5 µl of the reverse transcription reaction sample. The samples were vortexed briefly and centrifuged before being placed in the thermocycler (Table 7.5).

Step	Cycles	Temperature	Time
Enzyme activation	1	95 °C	5 minutes
Denature	14	95 °C	3 seconds
Anneal/Extend		60 °C	30 seconds
Stop	1	99 °C	10 minutes
Hold	1	4 °C	Hold

Table 7.5: Thermocycling parameters for miR amplification reaction.

A one in ten dilution of the cDNA from the miR-Amp step was prepared. A PCR Reaction Mix (10 µl 2X TaqMan Fast Advanced Master Mix, 1 µl 20X TaqMan Advanced miRNA Assay and 4 µl RNase-free water) was prepared for each miR. 20X TaqMan Advanced miRNA Assay probes used were: hsa-miR-221-5p TaqMan™ Advanced miRNA Assay (A25576/478778_mir), hsa-miR-1179 TaqMan™ Advanced miRNA Assay (A25576/478626_mir), hsa-miR-486-5p TaqMan™ Advanced miRNA Assay (A25576/478128_mir), hsa-miR-24-3p TaqMan™ Advanced miRNA Assay (A25576/477992_mir), and hsa-miR-25-3p TaqMan™ Advanced miRNA Assay (A25576/477994_mir). MicroRNA 24 and 25 were used as controls, selected as recommended by the ThermoFisher technical guide (ThermoFisher Scientific 2016); miR-24 was a miR reported to have stable expression across most human tissues, and miR-25-3p was recommended as a tissue-specific miRNA normaliser for cancer cell lines. Five microlitres of the diluted cDNA sample was added to 15 µl of the PCR Reaction Mix in the PCR reaction plate. The samples were vortexed briefly and centrifuged before being placed in the thermocycler for the real time PCR (RTqPCR)

(Table 7.6). Each TaqMan probe contained the fluorescent reporter 6-carboxyfluorescein (FAM) at the 5' end and a 3' non-fluorescent quencher minor groove binder (NFQ-MGB).

Step	Cycles	Temperature	Time
Enzyme activation	1	95 °C	20 seconds
Denature	40	95 °C	3 seconds
Anneal/Extend		60 °C	30 seconds
Hold	1	4 °C	Hold

Table 7.6: PCR thermocycling parameters for miR real-time PCR reaction.

7.3 Results

7.3.1 MicroRNA analysis of TCGA data

The microRNA analysis of TCGA data demonstrated that 62 miRs were significantly ($p < 0.05$) differentially expressed in recurrent versus non-recurrent thyroid cancer patients (Appendix 1; Table 10.4). The expression levels of these miRs in the recurrent thyroid cancer patient tumours were plotted compared to the non-recurrent patient tumours and the normal thyroid tissue (Figure 7.1).

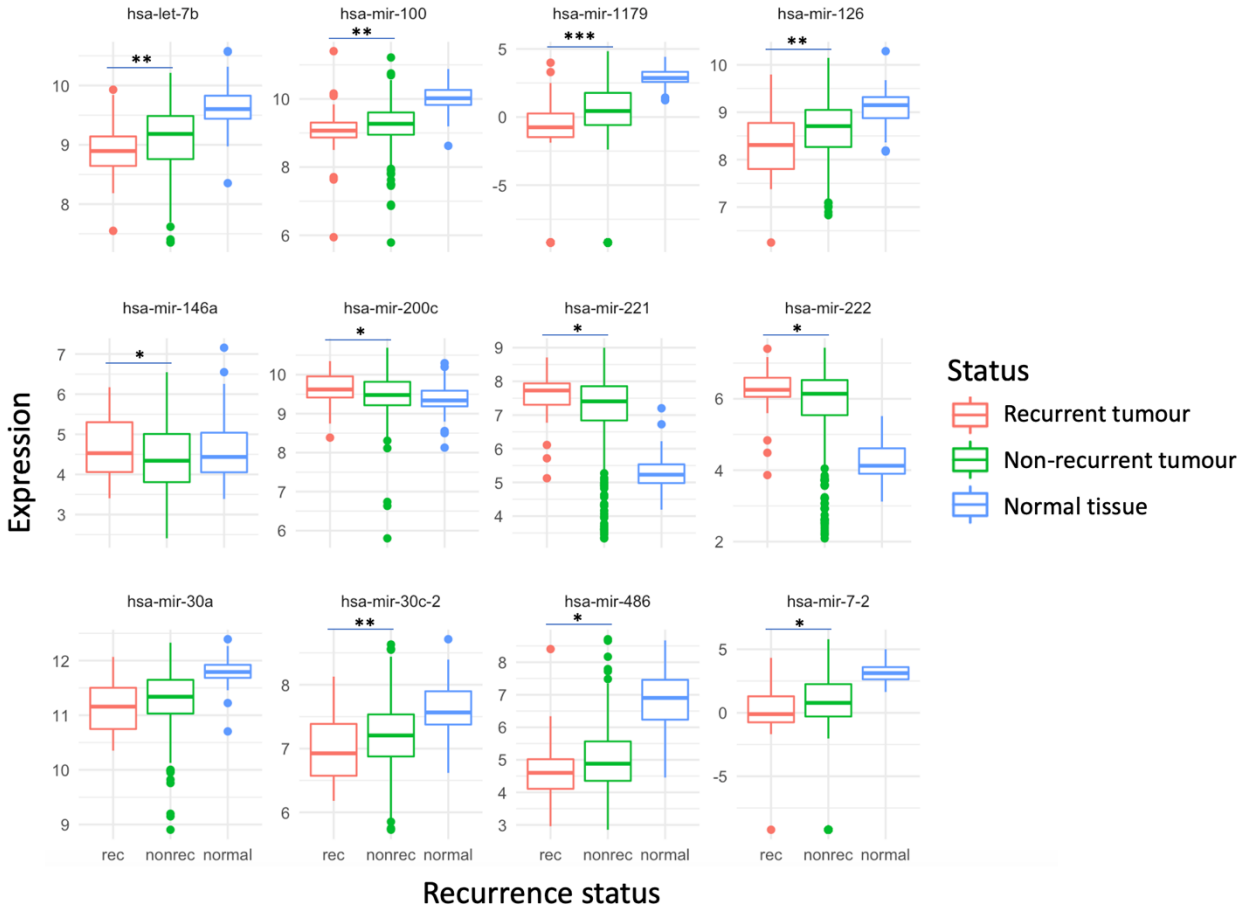

*Figure 7.1: Differential expression of selected miRs in recurrent patient primary tissue compared to non-recurrent patient primary tissue. * p < 0.05, ** p < 0.01, *** p < 0.001.*

An enrichment analysis was performed to assess the biological processes and molecular functions affected by the group of 62 miRs and a pathway analysis was performed (Figure 7.2). The biological process analysis pointed overwhelmingly towards gene silencing (as expected) and angiogenesis related processes. The molecular function analysis predominantly highlighted RNA binding and RNA polymerase binding mechanisms, which would again be expected in a study on the effects of miRs. In the pathway analysis miRNAs in cancer was highlighted by the KEGG pathway analysis, and RNA silencing pathways from BioSystems: REACTOME

(Figure 7.3). However, the false discovery rate (FDR) increased for all the pathways except the miRNAs in cancer, so this is the only pathway accepted as reliable and significant. In terms of novel information these results highlight a link between miR and angiogenesis that would not have been highlighted by investigation of each miR alone.

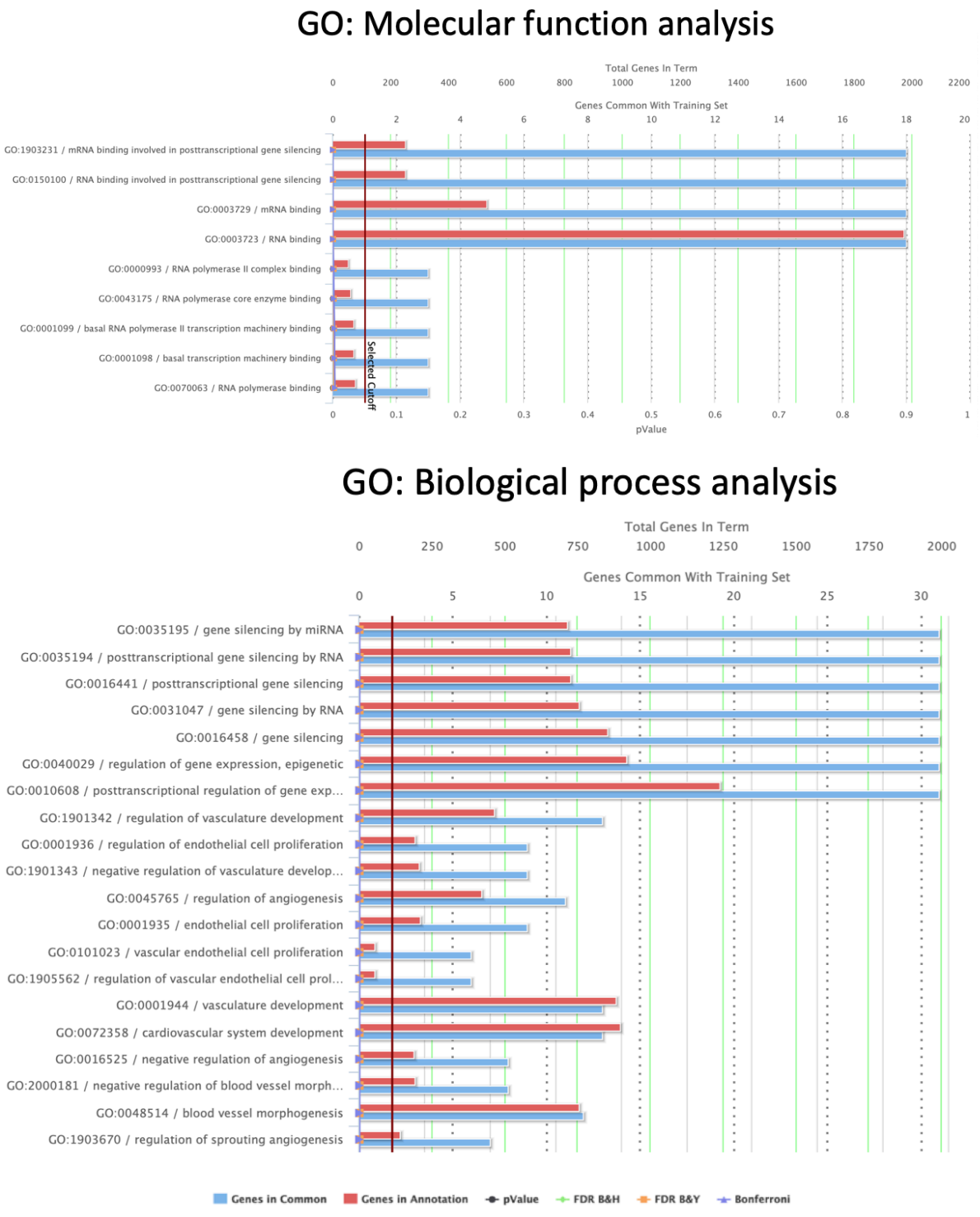

Figure 7.2: Enrichment analysis of 62 significantly differentially expressed miRs from the open source online enrichment portal ToppGene (https://toppgene.cchmc.org) by Gene Ontology analysis. GO: Molecular function analysis and GO: Biological Process Analysis. All bars p < 0.0001 (****).

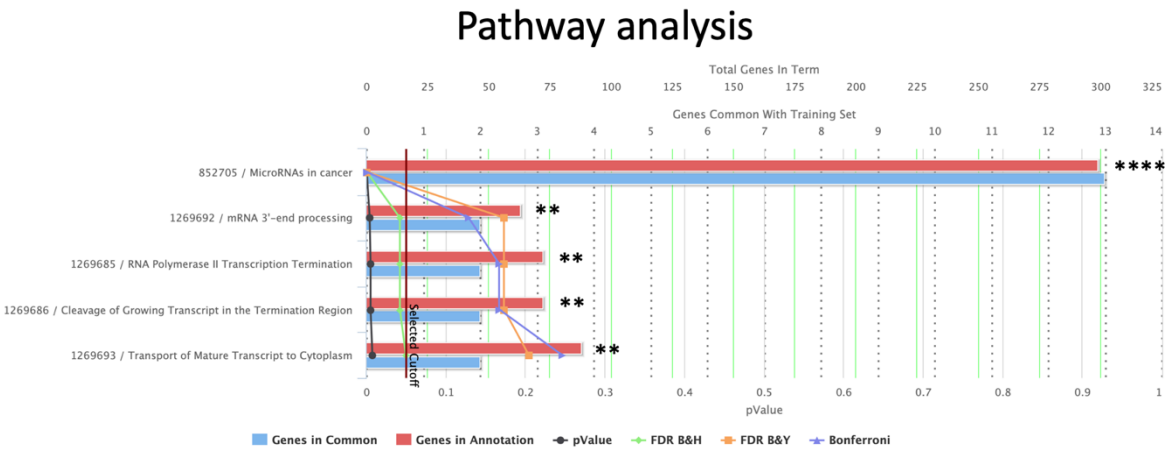

*Figure 7.3: Enrichment analysis of 62 significantly differentially expressed miRs using open source online enrichment portal ToppGene (https://toppgene.cchmc.org) by miR pathway analysis. For Pathway analysis the pathway 'MicroRNAs in cancer' from KEGG analysis, and pathways 'mRNA 3' -end processing', 'RNA Polymerase II Transcription Termination', 'Cleavage of Growing Transcript in the Termination Region', 'Transport of Mature Transcript to Cytoplasm' from BioSystems: REACTOME analysis. * p < 0.05, ** p < 0.01, *** p < 0.001, **** p < 0.0001.*

The top fifteen differentially expressed miRs in recurrent thyroid cancer were examined in the literature in relation to thyroid disease and cancer. MiR-221 is well defined as a oncomiR in thyroid cancer, and inhibition confers a less aggressive cell behaviour in thyroid cell lines (Diao et al. 2017). Reduced expression of miR-486 and miR-1179 have been linked to thyroid cancer, but not implicated to date in recurrence (Hu et al. 2016, Rosignolo et al. 2017). In order to examine differentially expressed miR function

the three candidate oncomiRs miR-221, miR-486 and miR-1179 were selected for functional experiments.

7.3.2 Significant change in miR expression in transfected cells

In order to assess successful miR delivery, relative miR level were determined in TPC-1 and SW1736 cells transfected with miR mimics and inhibitors by PTqPCR (Figure 7.4).

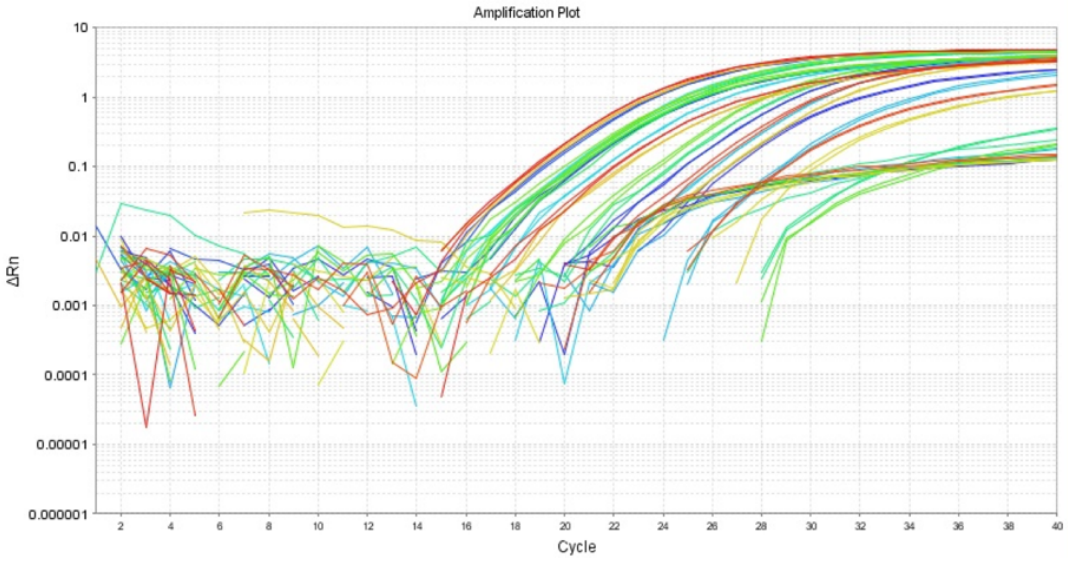

Figure 7.4: Example of RTqPCR amplification plots for miRNA expression. TPC-1 parental cell line with miR 24 and 25 (controls) and miRs 221, 486 and 1179 amplifying successfully.

Importantly, there was a significant increase in miR-221 levels ($p < 0.0001$) in miR-221 mimic transfected cells, and a decrease in both miR-486 ($p < 0.05$) and miR-1179 ($p < 0.05$) in TPC-1 cells transfected with each miR inhibitor respectively (Figure 7.5A). A similar trend was observed in SW1736 cells (Figure 7.5B). This demonstrates successful overexpression and knockdown of the miRs respectively.

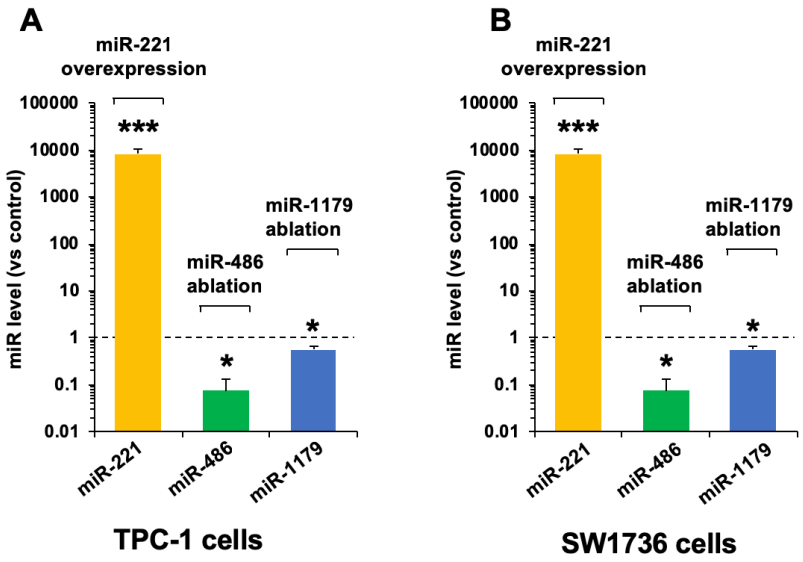

*Figure 7.5: Transfection (miR-221) and knockdown (miR-486 and miR-1179) illustrated by real time PCR (RTqPCR). A) TPC-1 cell line B) SW1736 cell line. Fold change compared to control miR-25, one-tailed t-test performed. n = 3, * p < 0.05, ** p < 0.01, *** p < 0.001.*

The effect of miR transfection and knockdown on expression of the other miRs was also examined, in order to try to discern if any of the miRs were potential regulators of each other. It appears that miR-221 and miR-486 had a reciprocal effect on expression observed in the SW1736 cells (Figure 7.6B) whilst miR-1179 only significantly impacted miR-486 expression in the TPC-1 cell line.

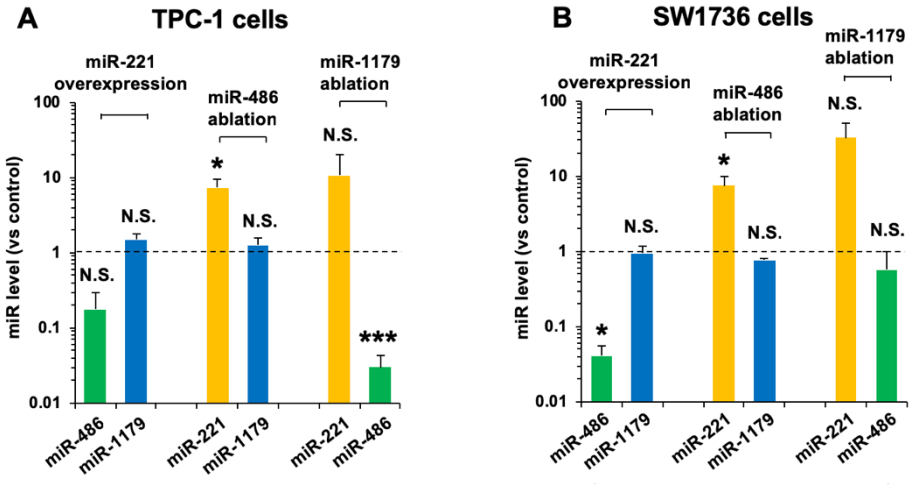

*Figure 7.6: Effect of miR transfection (miR-221) and knockdown (miR-486 and miR-1179) on expression levels of other miRs assessed by RTqPCR. A) TPC-1 cell line B) SW1736 cell line. Fold change, two tailed t-test performed. n = 3, * p < 0.05, ** p < 0.01, *** p < 0.001.*

7.3.3 Interaction of miR transfection on other miR expression

The expression of miR-221, miR-486 and miR-1179 from the TCGA data were plotted against each other (Figure 7.7).

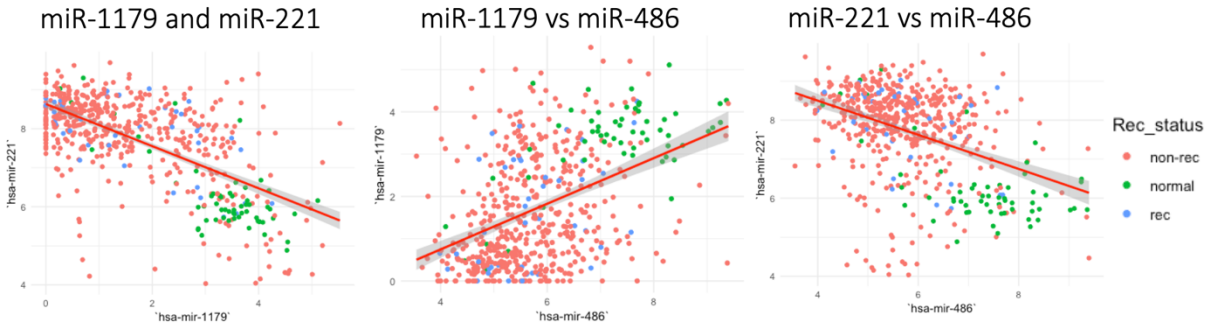

Figure 7.7: Bioinformatic prediction of the miR expression interaction between miRs from the TCGA data.

This consolidates the links between the miRs' expression but does not demonstrate causation beyond what was observed in the RTqPCR data. It appears likely that miR-

1179 affects miR-486 expression and the relationship between miR-486 and miR-221 is reciprocal. It may be therefore that the link between miR-1179 and miR-221 expression is due to the effects of miR-486. Repeated measures of this RTqPCR data at different timepoints would be required to examine the causality of these effects in more detail.

7.3.4 Functional assays in microRNA transfected cells

Having successfully demonstrated miR transfection (Figure 7.5), a cell migration assay (cell scratch wound) was performed using miR-transfected TPC-1 and SW1736 cells (Figure 7.8). Of particular significance was an increase in migration in cells with miR-486 and miR-1179 knockdown at 24 hours in TPC-1 cells ($p < 0.001$) (Figure 7.8), but not in those with miR-221 overexpression (p = ns). A similar trend was observed in SW1736 cells ($p < 0.01$), although a significant increase in cell migration was evident at an earlier time point of 8 hours in miR-486 ablated cells compared to controls ($p < 0.05$; Figure 7.8).

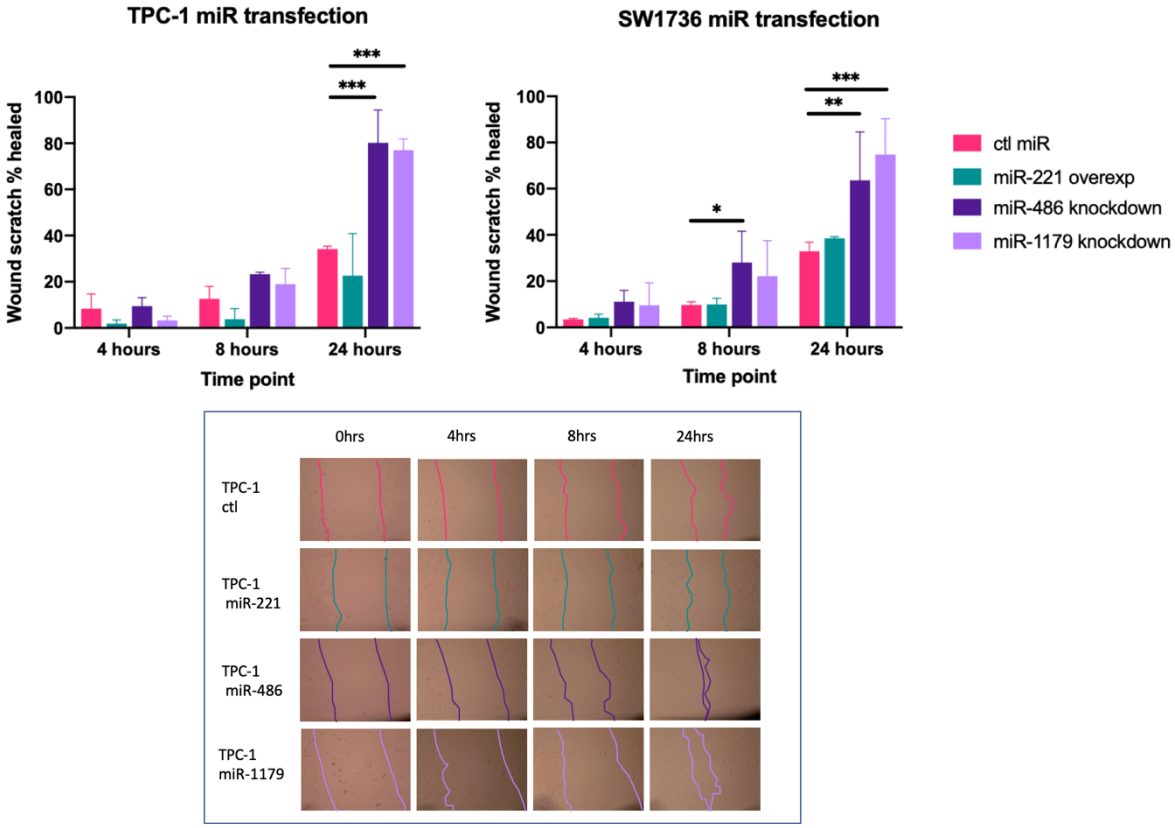

Figure 7.8: Cell migration assay comparing control miR (negative control mimic), miR-221 mimic, miR-486 inhibitor and miR-1179 inhibitor transfected cells in two cells lines (TPC-1 and SW1736). Representative images of the scratch wound healing shown, 10x magnification. n = 2.

Cell proliferation assays were also performed with an MTS assay but did not demonstrate a significant difference between miR-transfected cells and controls (Figure 7.9). This demonstrates that the effect on migration apparent in Figure 7.8 is a true migratory effect not due to cellular proliferation.

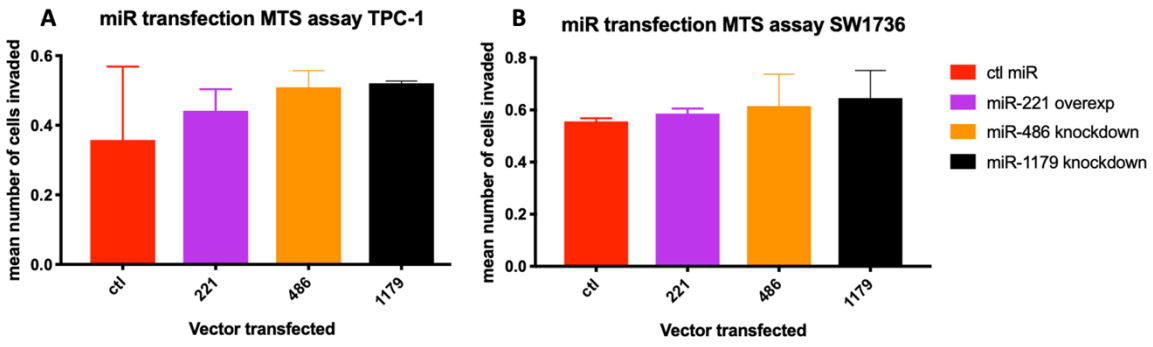

Figure 7.9: A & B: Cell proliferation assay (MTS) comparing control miR (negative control mimic), miR-221 mimic transfection, miR-486 inhibitor transfection and miR-1179 inhibitor transfection (A: TPC-1 cell line and B: SW1726 cell line) All non-significant, n = 2.

7.3.5 Effect of miR transfection on NIS expression

MicroRNAs bind mRNA to effect post-translational changes in protein expression. To examine if the selected miRs had an effect on thyroid iodine metabolism, protein was extracted from the transfected cells as described in section 2.4. The protein was quantified, and a Western blot performed, which was probed for NIS. Over-expression of miR-221 and inhibition of miR-1179 caused a reduction in NIS protein in both cell lines (TPC-1 and SW1736).

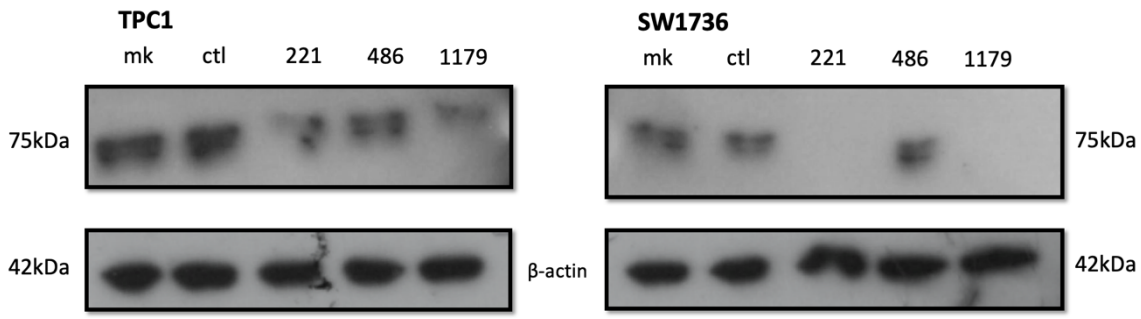

Figure 7.10: Overexpression of miR-221 and knockdown of miR-1179 reduces NIS expression. MiR transfection (mock transfection, control miR, miR-221 mimic, miR-486 and miR-1179 inhibitor) effect on NIS expression in two cell lines (TPC-1 and SW1736). Western blot probed for NIS with anti-NIS rabbit polyclonal antibody (ProteinTech) 24324-1-AP 1:1000 v/v. N = 1.

7.4 Discussion

7.4.1 MicroRNA analysis of TCGA data

The miRs miR-221, miR-486 and miR-1179 were highlighted as of potential importance in recurrent thyroid cancer by the analysis of the most differentially expressed miRs in TCGA data in thyroid cancer recurrence. Therefore, their functional properties were investigated *in vitro*. MiR-221 was selected for further investigation as expression of miR-221 is upregulated in differentiated thyroid cancer consistently across different studies (Leonardi et al. 2012). Several target genes have been postulated as the target of miR-221 including the proto-oncogene tyrosine-protein kinase KIT, the matrix metalloproteinase Tissue Inhibitor Of Metalloproteinase 3 (TIMP3) (Diao et al. 2017, He et al. 2005) and the metastasis suppressor Reversion-inducing-cysteine-rich protein with kazal motifs (RECK) (Wei et al. 2019). It has been highlighted as a miR

differentially expressed in cancer versus normal tissue, and even proposed as a prognostic biomarker for tumour recurrence (Dai et al. 2017). A study looking at recurrence risk factors (including a limited number of miRs) in thyroid cancer showed miR-221 was the only independent risk factor for recurrence (HR 1.41; 95%CI 1.14–1.95, P = 0.007) (Dai et al. 2017). In that analysis miR-486 and miR-1179 were not assessed.

MicroRNA 486 was of interest as it has been demonstrated to be under expressed in differentiated thyroid cancer (Wojcicka et al. 2016) and associated with cancer stage, survival and recurrence (Wen et al. 2018). Interestingly, it has also been proposed as one of the miRs in a two-miR-marker for carcinoma in follicular thyroid nodules (Stokowy et al. 2015); this is important as cytological analysis is unable to differentiate between benign and malignant in follicular neoplasms.

Similarly, miR-1179 is also under-expressed in thyroid cancer (Hu et al. 2016, Wojcicka et al. 2016). It was of particular interest in this study as it was the most differentially expressed miR in terms of median differential expression. Also, functional studies of the effects of miR-1179 have not been conducted. One study identified all three miRs (miR-221, miR-476 and miR-1179) as potential biomarkers for thyroid cancer but did not associate them with recurrence, while miR-146 and miR-222 were associated with risk of recurrence (Rosignolo et al. 2017). A key difference was that the study by Rosignolo et al. used clinical factors to predict risk of recurrence, whereas here the available TCGA data had patients with confirmed instances of thyroid cancer recurrence.

7.4.2 Functional effects of miR transfection

Despite several preceding studies demonstrating the oncogenic nature of miR-221 in thyroid cancer, the results were not replicated here (Diao et al. 2017, Wei et al. 2019). One of these studies was conducted in the TPC-1 cell line but used miR-221 knockdown and reduced cell proliferation and migration as markers of miR-221 oncogenic activity (Diao et al. 2017). An important finding was that miR-486 and miR-1179 demonstrated significantly increased wound healing at 24 hours in two thyroidal cell lines, indicating that they are not just passengers with reduced expression in thyroid cancer recurrence, but have an active role in oncogenesis. This is even with a relatively modest knockdown of miR-1179 as seen in the RTqPCR quantification (Figure 7.5).

To investigate the potential targets of miR-486 by pathway analysis the miR pathway prediction software DIANA miRpath v3.0 (Vlachos et al. 2015) was used. A list of the significantly mutated genes from the TCGA thyroid bioportal (Cerami et al. 2012) was entered into the DIANA database, along with miR-486. This generated five predicted KEGG pathways: arrhythmogenic right ventricular cardiomyopathy, lysine degradation, central carbon metabolism in cancer, glycosphingolipid biosynthesis and microRNAs in cancer. The genes in the microRNAs in cancer are MET, NRAS and PTEN (matched in Tarbase) – these are all drivers in thyroid cancer and are possibilities as targets of miR-486. One target of miR-486 that has been validated in cell lines is the extracellular matrix protein fibrillin-1 (Ma et al. 2016). This may have an impact on thyroid carcinogenesis, but it is likely that miR-486 has multiple targets (Saiselet et al. 2016).

In functional investigations of miR-1179, one study found that the circular RNA hsa_circ_0039411 affected cell growth, migration and invasion by acting as a sponge for miR-1179 in papillary thyroid cancer (Yang et al. 2019). To further investigate how miR-1179 has its functional effect, the same pathway analysis in DIANA miRpath v3.0 was performed. This came up with six pathways: ECM-receptor interaction, mismatch repair, pathways in cancer, endometrial cancer, colorectal cancer and adherens junction. The largest pathway was Pathways in cancer, with four genes: the cell-cell adhesion gene CTNNB1, the transcription factor E2F3, the DNA mismatch repair gene MSH2 and the ECM protein gene LAMC1. It is evident that the role of miR-1179 in PTC is complex and further work is required.

7.4.3 miR expression in different cell lines

An intriguing observation was the apparent interaction of miR-486 with the other two miRs. MiR-221 and miR-486 seem to both regulate each other, with miR-486 influencing miR-221 expression in both cell lines, which is of interest when considering the established importance of miR-221 in thyroid cancer. MiR-486 expression was also reduced by the knockdown of miR-1179 which interestingly was the most differentially expressed miR between recurrent and non-recurrent patient tumour samples (Appendix 1; Table 10.4). It would be interesting to explore these interactions further to see which pathways they impart their effect through.

7.4.4 Conclusions & future directions

Current treatment of thyroid cancer recurrence is particularly difficult when disease becomes radioiodine refractory (Yang et al. 2017). The loss of NIS protein expression

by miR-221 overexpression and miR-1179 knockdown may therefore be important. Surprisingly, neither miR-221 or miR-1179 appear to impact NIS expression directly according to the bioinformatic prediction software mirPath or TargetScan (data not shown). NIS expression can be influenced by many different pathways and the miR-1179 and miR-221 effect may act by affecting one of these. It would be critical in future work to confirm the precise relationship between NIS with these miRs by using functional assays, such as radioiodine uptake assays. It would also be useful to better define this potentially novel pathway associated with NIS knockdown, in case it can be exploited clinically.

Another consideration is that miRs may have a significant role in prognostics as they are better preserved in FFPE tissue than DNA and RNA are, have been successfully detected in diagnostic FNAc (Pallante et al. 2006) and also have been evaluated with some success as potential serum markers of recurrence (Gómez-Pérez et al. 2019, Zhang et al. 2017). MicroRNAs are complex in their interactions with genes, as they normally have multiple gene targets, which makes their interactions difficult to differentiate and validate (Saiselet et al. 2016). This brings about complexity in using miRs in cancer therapeutics. However, there is a more immediate potential role for miRs such as miR-221, miR-486 and miR-1179 as prognostic indicators.

Chapter 8 Conclusions and future directions

8 Conclusions and future directions

8.1 The challenge of recurrent thyroid cancer

Thyroid cancer recurrence is associated with increased morbidity and mortality (Kruijff et al. 2014, Young et al. 2013). Differentiated thyroid cancer recurrence is more challenging to treat than primary disease (Perros et al. 2014) and can be both surgically irresectable and radioiodine resistant (Haugen et al. 2016). If this is the case, there are limited treatment options, with significant associated morbidity (Pacini et al. 2006, Haugen et al. 2016). Early detection of recurrent disease is thought to impact favourably on patient outcomes (Cooper et al. 2006, Perros et al. 2014). Prediction of recurrence can therefore aid patients by both tailoring their treatment to their disease risk and increasing their post-treatment recurrence surveillance.

8.2 Mutations as drivers of thyroid cancer recurrence

The Cancer Genome Atlas provided a large volume dataset of somatic mutations (and raw sequencing data files) with matching clinical information, and an analysis of the patients who had recurred was undertaken to identify somatic mutations as markers of recurrence. Three potential mutational drivers identified were IMPDH2 S280C, PFKFKB4 Y366C and DICER1 D1810H which were taken forward into functional cell line studies. Neither the IMPDH2 S280C mutation nor the PFKFB4 Y366C mutation demonstrated a profound effect on cell line behaviour. While this may have been limited to an extent by the models used, no associated aggressive phenotype was seen. A functional effect was seen on knockdown of DICER1 in the CRISPR DICER1 knockout cell line, possibly representative of a loss-of-function mutation. However, the

complete knockout of the DICER1 function does not represent the complexity of the impact of the hotspot mutation, and further studies into the effect of the hotspot mutations on cellular function and miR profile would be interesting.

While the mutational profile of thyroid cancer is becoming more transparent (Agarwal et al. 2014) the somatic mutations highlighted by this NGS analysis of recurrent thyroid cancer did not appear to highlight new and distinct drivers of recurrence. This may well be because the initiating mutations are well defined and recurrence is dominated by acquisition of further mutations, similar to the mechanism behind dedifferentiation of thyroid cancer (Landa et al. 2016), and therefore these mutations are not apparent on the patient's initial histology, which is what the analysis in this PhD was centred on.

8.3 Gene expression in thyroid cancer recurrence

RNA expression analysis is a useful way to explore a cancer cell phenotype. The mRNA expression analysis performed highlighted important pathways in thyroid cancer recurrence including cell adhesion, ECM organisation, response to hypoxia, angiogenesis and the endoplasmic reticulum. Particularly overexpressed individual genes included FN1, ITGα3 and the proto-oncogene MET. FN1 has been long associated with cancer aggressiveness (Sponziello et al. 2016, da Silveira Mitteldorf et al. 2011) and its effect on both cell adhesion and cell motility potentially generate the ability for tumours to metastasise and recur. The interaction of the cancer cell with the ECM is clearly important, and the novel validation of ITGα3 as an oncogenic factor in thyroid cancer cell lines is interesting. The final gene MET appears to be a driver in thyroid oncogenesis and a factor in thyroid cancer treatment resistance and

recurrence. Cell work on radioiodine resistance and the use of MET inhibitors would potentially be useful to determine applicability of these drugs in thyroid cancer to help inform clinical trials of targeted therapy.

Combining these three genes as biomarkers for the clinical application of determining recurrence risk could be beneficial for patients. In the case of MET, knowing that MET is overexpressed in an individual patient's tumour may open up therapeutic options if required in the future.

8.4 MicroRNA expression in thyroid cancer recurrence

There is variable expression of miRs in thyroid cancer at presentation in patients that recurred compared to those that did not. The variable expression of miR-221, miR-486 and miR-1179 was investigated here by replicating overexpression or knockdown in thyroid cancer cell lines. Certainly, it appears that the knockdown of miR-486 and miR-1179 affects the migratory nature of the thyroid cancer cell lines, suggesting that they may be functionally linked to cancer progression. The use of miR therapeutically is somewhat limited by the off target and differing effects on different tissues, although some targeted miR therapeutics are being considered in ATC (Wojcicka et al. 2016). Targeted delivery can also be challenging, especially in recurrent thyroid cancer. Therefore this new information might be more suited to being exploited as a diagnostic tool, especially if it is combined with information from the mRNA expression data.

Treatment of thyroid cancer recurrence is especially difficult when the disease becomes radioiodine refractory (Yang et al. 2017) so the repression of NIS protein

expression by the miR-221 mimic and the miR-1179 inhibitor is interesting (n = 1) but needs replication. The pathways by which this occurs have not been explored in this PhD but may provide further understanding of how to restore radioactive iodine avidity.

8.5 Future directions

Knockdown of NIS with miR-1179 knockdown and miR-221 overexpression and correlation with functional studies such as radioiodine activity would confirm the effect of the miRs on NIS. Further to this, reversal of this effect in less radioiodine avid cell lines would be experimentally interesting in terms of addressing potential new therapies. Further investigation of MET inhibition as a targeted therapy, possibly in combination with other targeted drugs may be of clinical use in patients with very difficult aggressive disease.

Creation of a clinical prediction biomarker tool using the overexpressed genes FN1, ITGα3 and MET in combination with miR-221, miR-486 and miR-1179 levels could help to determine the risk of disease recurrence for patients with thyroid cancer. This in turn could be developed clinically to quantify risk of recurrence and help allocate patients to more or less invasive treatment and to an appropriate level of post-treatment surveillance.

8.6 Concluding remarks

While the impact of driver mutations in genes such as BRAF, RAS, EIF1AX and the TERT promotor in thyroid cancer is clear, there does not appear to be an obvious set

of driver mutations common to patients with recurrent thyroid cancer. This may be due to the acquisition of a higher mutational burden with time, as seen in the model of progressive dedifferentiation to anaplastic thyroid cancer. Alternatively, it may be that the important mutations in thyroid cancer are already known, and yet are not ideal as predictive markers of thyroid cancer recurrence. However, the expression levels of both RNA and miRs on initial patient presentation appear to correlate with thyroid cancer recurrence. Particularly interesting are the genes FN1, ITGα3 and the miR 486 and 1179, with the association between expression and cellular migration established. If these varied expression levels can be harnessed as a clinical tool, this could potentially help direct individualised patient care.

Chapter 9 **References**

9 References

Adzhubei, I. A., Schmidt, S., Peshkin, L., Ramensky, V. E., Gerasimova, A., Bork, P., Kondrashov, A. S. and Sunyaev, S. R. (2010) 'A method and server for predicting damaging missense mutations', *Nat Methods,* 7(4), 248-9.

Agarwal, A. R., Aksoy A, Ally A, et al. (2014) 'Integrated genomic characterization of papillary thyroid carcinoma', *Cell,* 159(3), 676-90.

Alexander, E. K., Kennedy, G. C., Baloch, Z. W., Cibas, E. S., Chudova, D., Diggans, J., Friedman, L., Kloos, R. T., LiVolsi, V. A., Mandel, S. J., Raab, S. S., Rosai, J., Steward, D. L., Walsh, P. S., Wilde, J. I., Zeiger, M. A., Lanman, R. B. and Haugen, B. R. (2012) 'Preoperative diagnosis of benign thyroid nodules with indeterminate cytology', *N Engl J Med,* 367(8), 705-15.

Anderson, E. M., Haupt, A., Schiel, J. A., Chou, E., Machado, H. B., Strezoska, Z., Lenger, S., McClelland, S., Birmingham, A., Vermeulen, A. and Smith, A. (2015) 'Systematic analysis of CRISPR-Cas9 mismatch tolerance reveals low levels of off-target activity', *J Biotechnol,* 211, 56-65.

Anderson, R. T., Linnehan, J. E., Tongbram, V., Keating, K. and Wirth, L. J. (2013) 'Clinical, safety, and economic evidence in radioactive iodine-refractory differentiated thyroid cancer: a systematic literature review', *Thyroid,* 23(4), 392-407.

Anglesio, M. S., Wang, Y., Yang, W., Senz, J., Wan, A., Heravi-Moussavi, A., Salamanca, C., Maines-Bandiera, S., Huntsman, D. G. and Morin, G. B. (2013) 'Cancer-associated somatic DICER1 hotspot mutations cause defective miRNA processing and reverse-strand expression bias to predominantly mature 3p strands through loss of 5p strand cleavage', *J Pathol,* 229(3), 400-9.

Annerbo, S. L., Johan (2013) 'A Clinical Review of the Association of Thyroid Stimulating Hormone and Cognitive Impairment', *ISRN Endocrinology,* 2013, 6.

Arivarasan, K., Federica, P., Susan, J. H., Jennie, V., Marina, N. N., Simion, C. and Yuri, E. N. (2016) 'Prevalence and phenotypic correlations of EIF1AX mutations in thyroid nodules', *Endocrine-Related Cancer,* 23(4), 295-301.

Artimo, P., Jonnalagedda, M., Arnold, K., Baratin, D., Csardi, G., de Castro, E., Duvaud, S., Flegel, V., Fortier, A., Gasteiger, E., Grosdidier, A., Hernandez, C., Ioannidis, V., Kuznetsov, D., Liechti, R., Moretti, S., Mostaguir, K., Redaschi, N., Rossier, G., Xenarios, I. and Stockinger, H. (2012) 'ExPASy: SIB bioinformatics resource portal', *Nucleic Acids Res,* 40(W1), W597-W603.

Barkan, D., Green, J. E. and Chambers, A. F. (2010) 'Extracellular matrix: a gatekeeper in the transition from dormancy to metastatic growth', *Eur J Cancer,* 46(7), 1181-8.

Barkan, D., Kleinman, H., Simmons, J. L., Asmussen, H., Kamaraju, A. K., Hoenorhoff, M. J., Liu, Z. Y., Costes, S. V., Cho, E. H., Lockett, S., Khanna, C., Chambers, A. F. and Green, J. E. (2008) 'Inhibition of metastatic outgrowth from single dormant tumor cells by targeting the cytoskeleton', *Cancer Res,* 68(15), 6241-50.

Beadnell, T. C., Nassar, K. W., Rose, M. M., Clark, E. G., Danysh, B. P., Hofmann, M.-C., Pozdeyev, N. and Schweppe, R. E. (2018) 'Src-mediated regulation of the PI3K pathway in advanced papillary and anaplastic thyroid cancer', *Oncogenesis,* 7(2), 23.

Berkhout, B. and Haasnoot, J. (2006) 'The interplay between virus infection and the cellular RNA interference machinery', *FEBS Lett,* 580(12), 2896-902.

Berthou, S., Aebersold, D. M., Schmidt, L. S., Stroka, D., Heigl, C., Streit, B., Stalder, D., Gruber, G., Liang, C., Howlett, A. R., Candinas, D., Greiner, R. H., Lipson, K. E. and Zimmer, Y. (2004) 'The Met kinase inhibitor SU11274 exhibits a selective inhibition pattern toward different receptor mutated variants', *Oncogene,* 23(31), 5387-5393.

Beyer, M. and Schultze, J. L. (2006) 'Regulatory T cells in cancer', *Blood,* 108(3), 804-11.

Biondi, B., Bartalena, L., Cooper, D. S., Hegedüs, L., Laurberg, P. and Kahaly, G. J. (2015) 'The 2015 European Thyroid Association Guidelines on Diagnosis and Treatment of Endogenous Subclinical Hyperthyroidism', *Eur Thyroid J,* 4(3), 149-163.

Bjornsti, M.-A. and Houghton, P. J. (2004) 'The tor pathway: a target for cancer therapy', *Nature Reviews Cancer,* 4(5), 335-348.

Bobarykina, A. Y., Minchenko, D. O., Opentanova, I. L., Moenner, M., Caro, J., Esumi, H. and Minchenko, O. H. (2006) 'Hypoxic regulation of PFKFB-3 and PFKFB-4 gene expression in gastric and pancreatic cancer cell lines and expression of PFKFB genes in gastric cancers', *Acta Biochim Pol,* 53(4), 789-99.

Boelaert, K., Horacek, J., Holder, R. L., Watkinson, J. C., Sheppard, M. C. and Franklyn, J. A. (2006) 'Serum Thyrotropin Concentration as a Novel Predictor of Malignancy in Thyroid Nodules Investigated by Fine-Needle Aspiration', *The Journal of Clinical Endocrinology & Metabolism,* 91(11), 4295-4301.

Bowne, S. J., Sullivan, L. S., Blanton, S. H., Cepko, C. L., Blackshaw, S., Birch, D. G., Hughbanks-Wheaton, D., Heckenlively, J. R. and Daiger, S. P. (2002) 'Mutations in the inosine monophosphate dehydrogenase 1 gene (IMPDH1) cause the RP10 form of autosomal dominant retinitis pigmentosa', *Hum Mol Genet,* 11(5), 559-68.

Braun, E. M., Windisch, G., Wolf, G., Hausleitner, L. and Anderhuber, F. (2007) 'The pyramidal lobe: clinical anatomy and its importance in thyroid surgery', *Surg Radiol Anat,* 29(1), 21-7.

Brittain, H. K., Scott, R. and Thomas, E. (2017) 'The rise of the genome and personalised medicine', *Clin Med (Lond),* 17(6), 545-551.

Broad Institute TCGA Genome Data Analysis Center (2019a) 'Analysis-ready standardised TCGA data from Broad GDAC Firehose', [online], available: http://gdac.broadinstitute.org].

Broad Institute TCGA Genome Data Analysis Center (2019b) 'A tool to explore and visualize cancer data generated by Broad GDAC Firehose', [online], available: http://firebrowse.org].

Brose, M. S., Nutting, C. M., Jarzab, B., Elisei, R., Siena, S., Bastholt, L., de la Fouchardiere, C., Pacini, F., Paschke, R., Shong, Y. K., Sherman, S. I., Smit, J. W., Chung, J.,

Kappeler, C., Pena, C., Molnar, I. and Schlumberger, M. J. (2014) 'Sorafenib in radioactive iodine-refractory, locally advanced or metastatic differentiated thyroid cancer: a randomised, double-blind, phase 3 trial', *Lancet,* 384(9940), 319-28.

Brown, A. C., Dysart, M. M., Clarke, K. C., Stabenfeldt, S. E. and Barker, T. H. (2015) 'Integrin alpha3beta1 Binding to Fibronectin Is Dependent on the Ninth Type III Repeat', *J Biol Chem,* 290(42), 25534-47.

Byeon, H. K., Na, H. J., Yang, Y. J., Kwon, H. J., Chang, J. W., Ban, M. J., Kim, W. S., Shin, D. Y., Lee, E. J., Koh, Y. W., Yoon, J.-H. and Choi, E. C. (2016) 'c-Met-mediated reactivation of PI3K/AKT signaling contributes to insensitivity of BRAF(V600E) mutant thyroid cancer to BRAF inhibition', *Molecular Carcinogenesis,* 55(11), 1678-1687.

Cai, X. J., Valiyaparambath, N., Nixon, P., Waghorn, A., Giles, T. and Helliwell, T. (2006) 'Ultrasound-guided fine needle aspiration cytology in the diagnosis and management of thyroid nodules', *Cytopathology,* 17(5), 251-6.

Calise, S. J., Abboud, G., Kasahara, H., Morel, L. and Chan, E. K. L. (2018) 'Immune Response-Dependent Assembly of IMP Dehydrogenase Filaments', *Frontiers in immunology,* 9, 2789-2789.

Cameselle-Teijeiro, J. M. and Sobrinho-Simoes, M. (2018) 'New WHO classification of thyroid tumors: a pragmatic categorization of thyroid gland neoplasms', *Endocrinol Diabetes Nutr,* 65(3), 133-135.

Carlson, R. (2009) 'The changing economics of DNA synthesis', *Nat Biotech,* 27(12), 1091-1094.

Caronia, L. M., Phay, J. E. and Shah, M. H. (2011) 'Role of BRAF in Thyroid Oncogenesis', *Clinical Cancer Research,* 17(24), 7511.

Carthew, R. W. and Sontheimer, E. J. (2009) 'Origins and Mechanisms of miRNAs and siRNAs', *Cell,* 136(4), 642-655.

Cavalier, M. C., Kim, S.-G., Neau, D. and Lee, Y.-H. (2012) 'Molecular basis of the fructose-2,6-bisphosphatase reaction of PFKFB3: Transition state and the C-terminal function', *Proteins: Structure, Function, and Bioinformatics,* 80(4), 1143-1153.

Cerami, E., Gao, J., Dogrusoz, U., Gross, B. E., Sumer, S. O., Aksoy, B. A., Jacobsen, A., Byrne, C. J., Heuer, M. L., Larsson, E., Antipin, Y., Reva, B., Goldberg, A. P., Sander, C. and Schultz, N. (2012) 'The cBio cancer genomics portal: an open platform for exploring multidimensional cancer genomics data', *Cancer Discov,* 2(5), 401-4.

Cesur, M., Corapcioglu, D., Bulut, S., Gursoy, A., Yilmaz, A. E., Erdogan, N. and Kamel, N. (2006) 'Comparison of palpation-guided fine-needle aspiration biopsy to ultrasound-guided fine-needle aspiration biopsy in the evaluation of thyroid nodules', *Thyroid,* 16(6), 555-61.

Chang, C.-C., Keppeke, G. D., Sung, L.-Y. and Liu, J.-L. (2018) 'Interfilament interaction between IMPDH and CTPS cytoophidia', *The FEBS journal,* 285(20), 3753-3768.

Chang, C.-C., Lin, W.-C., Pai, L.-M., Lee, H.-S., Wu, S.-C., Ding, S.-T., Liu, J.-L. and Sung, L.-Y. (2015) 'Cytoophidium assembly reflects upregulation of IMPDH activity', *Journal of Cell Science,* 128(19), 3550-3555.

Chen, B.-K., Ohtsuki, Y., Furihata, M., Takeuchi, T., Iwata, J., Liang, S.-B. and Sonobe, H. (1999) 'Overexpression of c-Met Protein in Human Thyroid Tumors Correlated with Lymph Node Metastasis and Clinicopathologic Stage', *Pathology - Research and Practice,* 195(6), 427-433.

Cheng, L., Lopez-Beltran, A., Massari, F., MacLennan, G. T. and Montironi, R. (2018) 'Molecular testing for BRAF mutations to inform melanoma treatment decisions: a move toward precision medicine', *Modern pathology : an official journal of the United States and Canadian Academy of Pathology, Inc,* 31(1), 24-38.

Chesney, J., Clark, J., Klarer, A. C., Imbert-Fernandez, Y., Lane, A. N. and Telang, S. (2014) 'Fructose-2,6-bisphosphate synthesis by 6-phosphofructo-2-kinase/fructose-2,6-bisphosphatase 4 (PFKFB4) is required for the glycolytic response to hypoxia and tumor growth', *Oncotarget,* 5(16), 6670-86.

Cho, S. J., Suh, C. H., Baek, J. H., Chung, S. R., Choi, Y. J., Chung, K. W., Shong, Y. and Lee, J. H. (2019) 'Active Surveillance for Small Papillary Thyroid Cancer: A Systematic Review and Meta-Analysis', *Thyroid*.

Chou, C. K., Chen, R. F., Chou, F. F., Chang, H. W., Chen, Y. J., Lee, Y. F., Yang, K. D., Cheng, J. T., Huang, C. C. and Liu, R. T. (2010) 'miR-146b is highly expressed in adult papillary thyroid carcinomas with high risk features including extrathyroidal invasion and the BRAF(V600E) mutation', *Thyroid,* 20(5), 489-94.

Chou, C. K., Yang, K. D., Chou, F. F., Huang, C. C., Lan, Y. W., Lee, Y. F., Kang, H. Y. and Liu, R. T. (2013) 'Prognostic implications of miR-146b expression and its functional role in papillary thyroid carcinoma', *The Journal of Clinical Endocrinology & Metabolism,* 98(2), E196-205.

Cibulskis, K., Lawrence, M. S., Carter, S. L., Sivachenko, A., Jaffe, D., Sougnez, C., Gabriel, S., Meyerson, M., Lander, E. S. and Getz, G. (2013) 'Sensitive detection of somatic point mutations in impure and heterogeneous cancer samples', *Nat Biotechnol,* 31(3), 213-9.

Colby, T. D., Vanderveen, K., Strickler, M. D., Markham, G. D. and Goldstein, B. M. (1999) 'Crystal structure of human type II inosine monophosphate dehydrogenase: Implications for ligand binding and drug design', *Proceedings of the National Academy of Sciences,* 96(7), 3531-3536.

Collet, T. H., Gussekloo, J., Bauer, D. C., den Elzen, W. P., Cappola, A. R., Balmer, P., Iervasi, G., Asvold, B. O., Sgarbi, J. A., Volzke, H., Gencer, B., Maciel, R. M., Molinaro, S., Bremner, A., Luben, R. N., Maisonneuve, P., Cornuz, J., Newman, A. B., Khaw, K. T., Westendorp, R. G., Franklyn, J. A., Vittinghoff, E., Walsh, J. P. and Rodondi, N. (2012) 'Subclinical hyperthyroidism and the risk of coronary heart disease and mortality', *Arch Intern Med,* 172(10), 799-809.

Comings, D. E. (1973) 'A general theory of carcinogenesis', *Proc Natl Acad Sci U S A,* 70(12), 3324-8.

Cooper, D. S., Doherty, G. M., Haugen, B. R., Kloos, R. T., Lee, S. L., Mandel, S. J., Mazzaferri, E. L., McIver, B., Pacini, F., Schlumberger, M., Sherman, S. I., Steward, D. L. and Tuttle, R. M. (2009) 'Revised American Thyroid Association management guidelines for patients with thyroid nodules and differentiated thyroid cancer', *Thyroid,* 19(11), 1167-214.

Cooper, D. S., Doherty, G. M., Haugen, B. R., Kloos, R. T., Lee, S. L., Mandel, S. J., Mazzaferri, E. L., McIver, B., Sherman, S. I. and Tuttle, R. M. (2006) 'Management guidelines for patients with thyroid nodules and differentiated thyroid cancer', *Thyroid,* 16(2), 109-42.

Coopman, P. J., Thomas, D. M., Gehlsen, K. R. and Mueller, S. C. (1996) 'Integrin alpha 3 beta 1 participates in the phagocytosis of extracellular matrix molecules by human breast cancer cells', *Molecular Biology of the Cell,* 7(11), 1789-1804.

Corver, W. E. and Morreau, H. (2019) 'Unique landscape of widespread chromosomal losses in Hürthle cell carcinoma', *Endocrine-Related Cancer,* 26(3), L1-L3.

da Silveira Mitteldorf, C. A., de Sousa-Canavez, J. M., Leite, K. R., Massumoto, C. and Camara-Lopes, L. H. (2011) 'FN1, GALE, MET, and QPCT overexpression in papillary thyroid carcinoma: molecular analysis using frozen tissue and routine fine-needle aspiration biopsy samples', *Diagn Cytopathol,* 39(8), 556-61.

Dadu, R., Devine, C., Hernandez, M., Waguespack, S. G., Busaidy, N. L., Hu, M. I., Jimenez, C., Habra, M. A., Sellin, R. V., Ying, A. K., Cote, G. J., Sherman, S. I. and Cabanillas, M. E. (2014) 'Role of Salvage Targeted Therapy in Differentiated Thyroid Cancer Patients Who Failed First-Line Sorafenib', *The Journal of Clinical Endocrinology & Metabolism,* 99(6), 2086-2094.

Dai, L., Wang, Y., Chen, L., Zheng, J., Li, J. and Wu, X. (2017) 'MiR-221, a potential prognostic biomarker for recurrence in papillary thyroid cancer', *World journal of surgical oncology,* 15(1), 11-11.

de Kock, L., Wu, M. K. and Foulkes, W. D. (2019) 'Ten years of DICER1 mutations: provenance, distribution and associated phenotypes', *Hum Mutat*.

de la Fouchardière, C., Decaussin-Petrucci, M., Berthiller, J., Descotes, F., Lopez, J., Lifante, J.-C., Peix, J.-L., Giraudet, A.-L., Delahaye, A., Masson, S., Bournaud-Salinas, C. and Borson Chazot, F. (2018) 'Predictive factors of outcome in poorly differentiated thyroid carcinomas', *European Journal of Cancer,* 92, 40-47.

Department of Health, U. (2000) 'The NHS Cancer Plan', [online], available: https://www.thh.nhs.uk/documents/_departments/cancer/nhscancerplan.pdf].

Di Cosmo, C., Liao, X.-H., Dumitrescu, A. M., Philp, N. J., Weiss, R. E. and Refetoff, S. (2010) 'Mice deficient in MCT8 reveal a mechanism regulating thyroid hormone secretion', *The Journal of Clinical Investigation,* 120(9), 3377-3388.

Diao, Y., Fu, H. and Wang, Q. (2017) 'MiR-221 Exacerbate Cell Proliferation and Invasion by Targeting TIMP3 in Papillary Thyroid Carcinoma', *American Journal of Therapeutics,* 24(3), e317-e328.

Do, H. and Dobrovic, A. (2015) 'Sequence artifacts in DNA from formalin-fixed tissues: causes and strategies for minimization', *Clin Chem,* 61(1), 64-71.

Doench, J. G., Fusi, N., Sullender, M., Hegde, M., Vaimberg, E. W., Donovan, K. F., Smith, I., Tothova, Z., Wilen, C., Orchard, R., Virgin, H. W., Listgarten, J. and Root, D. E. (2016) 'Optimized sgRNA design to maximize activity and minimize off-target effects of CRISPR-Cas9', *Nat Biotechnol,* 34, 184.

Dohan, O., De la Vieja, A., Paroder, V., Riedel, C., Artani, M., Reed, M., Ginter, C. S. and Carrasco, N. (2003) 'The sodium/iodide Symporter (NIS): characterization, regulation, and medical significance', *Endocr Rev,* 24(1), 48-77.

Duan, S., Huang, W., Liu, X., Liu, X., Chen, N., Xu, Q., Hu, Y., Song, W. and Zhou, J. (2018) 'IMPDH2 promotes colorectal cancer progression through activation of the PI3K/AKT/mTOR and PI3K/AKT/FOXO1 signaling pathways', *J Exp Clin Cancer Res,* 37(1), 304.

Dunn, L. A., Sherman, E. J., Baxi, S. S., Tchekmedyian, V., Grewal, R. K., Larson, S. M., Pentlow, K. S., Haque, S., Tuttle, R. M., Sabra, M. M., Fish, S., Boucai, L., Walters, J., Ghossein, R. A., Seshan, V. E., Ni, A., Li, D., Knauf, J. A., Pfister, D. G., Fagin, J. A. and Ho, A. L. (2018) 'Vemurafenib Redifferentiation of BRAF Mutant, RAI-Refractory Thyroid Cancers', *The Journal of Clinical Endocrinology & Metabolism,* 104(5), 1417-1428.

Durante, C., Puxeddu, E., Ferretti, E., Morisi, R., Moretti, S., Bruno, R., Barbi, F., Avenia, N., Scipioni, A., Verrienti, A., Tosi, E., Cavaliere, A., Gulino, A., Filetti, S. and Russo, D. (2007) 'BRAF mutations in papillary thyroid carcinomas inhibit genes involved in iodine metabolism', *The Journal of Clinical Endocrinology & Metabolism,* 92(7), 2840-3.

Eke, I. and Cordes, N. (2015) 'Focal adhesion signaling and therapy resistance in cancer', *Seminars in Cancer Biology,* 31, 65-75.

Elices, M. J., Urry, L. A. and Hemler, M. E. (1991) 'Receptor functions for the integrin VLA-3: fibronectin, collagen, and laminin binding are differentially influenced by Arg-Gly-Asp peptide and by divalent cations', *J Cell Biol,* 112(1), 169-81.

Esquela-Kerscher, A. and Slack, F. J. (2006) 'Oncomirs — microRNAs with a role in cancer', *Nature Reviews Cancer,* 6(4), 259-269.

Fagin, J. A., Matsuo, K., Karmakar, A., Chen, D. L., Tang, S. H. and Koeffler, H. P. (1993) 'High prevalence of mutations of the p53 gene in poorly differentiated human thyroid carcinomas', *The Journal of Clinical Investigation,* 91(1), 179-184.

Farrar, J. D., Katz, K. H., Windsor, J., Thrush, G., Scheuermann, R. H., Uhr, J. W. and Street, N. E. (1999) 'Cancer dormancy. VII. A regulatory role for CD8+ T cells and IFN-gamma in establishing and maintaining the tumor-dormant state', *J Immunol,* 162(5), 2842-9.

Fidler, I. J. (2002) 'The organ microenvironment and cancer metastasis', *Differentiation,* 70(9-10), 498-505.

Fiore, E., Rago, T., Provenzale, M. A., Scutari, M., Ugolini, C., Basolo, F., Coscio, G. D., Berti, P., Grasso, L., Elisei, R., Pinchera, A. and Vitti, P. (2009) 'Lower levels of TSH are associated with a lower risk of papillary thyroid cancer in patients with thyroid nodular disease: thyroid autonomy may play a protective role', *Endocrine-Related Cancer,* 16(4), 1251-1260.

Folkman, J. and Kalluri, R. (2004) 'Cancer without disease', *Nature,* 427(6977), 787-787.

Foulkes, W. D., Priest, J. R. and Duchaine, T. F. (2014) 'DICER1: mutations, microRNAs and mechanisms', *Nat Rev Cancer,* 14(10), 662-72.

French, J. D., Kotnis, G. R., Said, S., Raeburn, C. D., McIntyre, R. C., Jr., Klopper, J. P. and Haugen, B. R. (2012) 'Programmed death-1+ T cells and regulatory T cells are enriched in tumor-involved lymph nodes and associated with aggressive features in papillary thyroid cancer', *The Journal of Clinical Endocrinology & Metabolism,* 97(6), E934-43.

Ganguly, K. K., Pal, S., Moulik, S. and Chatterjee, A. (2013) 'Integrins and metastasis', *Cell adhesion & migration,* 7(3), 251-261.

Gao, J., Aksoy, B. A., Dogrusoz, U., Dresdner, G., Gross, B., Sumer, S. O., Sun, Y., Jacobsen, A., Sinha, R., Larsson, E., Cerami, E., Sander, C. and Schultz, N. (2013) 'Integrative analysis of complex cancer genomics and clinical profiles using the cBioPortal', *Sci Signal,* 6(269), pl1.

Gao, R., Li, D., Xun, J., Zhou, W., Li, J., Wang, J., Liu, C., Li, X., Shen, W., Qiao, H., Stupack, D. G. and Luo, N. (2018) 'CD44ICD promotes breast cancer stemness via PFKFB4-mediated glucose metabolism', *Theranostics,* 8(22), 6248-6262.

Gao, W. and Han, J. (2018) 'Overexpression of ING5 inhibits HGF-induced proliferation, invasion and EMT in thyroid cancer cells via regulation of the c-Met/PI3K/Akt signaling pathway', *Biomed Pharmacother,* 98, 265-270.

Gaspar, T. B., Sá, A., Lopes, J. M., Sobrinho-Simões, M., Soares, P. and Vinagre, J. (2018) 'Telomere Maintenance Mechanisms in Cancer', *Genes,* 9(5), 241.

Gherardi, E., Birchmeier, W., Birchmeier, C. and Vande Woude, G. (2012) 'Targeting MET in cancer: rationale and progress', *Nat Rev Cancer,* 12(2), 89-103.

Gioanni, J., Zanghellini, E., Mazeau, C., Zhang, D., Courdi, A., Farges, M., Lambert, J. C., Duplay, H. and Schneider, M. (1991) '[Characterization of a human cell line from an anaplastic carcinoma of the thyroid gland]', *Bull Cancer,* 78(11), 1053-62.

Giordano, T. J. (2018) 'Genomic Hallmarks of Thyroid Neoplasia', *Annu Rev Pathol,* 13, 141-162.

Gómez-Pérez, A. M., Cornejo Pareja, I. M., García Alemán, J., Coín Aragüez, L., Sebastián Ochoa, A., Alcaide Torres, J., Molina Vega, M., Clu Fernández, C., Mancha Doblas, I. and Tinahones, F. J. (2019) 'New molecular biomarkers in differentiated thyroid carcinoma: Impact of miR-146, miR-221 and miR-222 levels in the evolution of the disease', *Clinical Endocrinology,* 91(1), 187-194.

Goncalves, M. D. and Cantley, L. C. (2018) 'A Glycolysis Outsider Steps into the Cancer Spotlight', *Cell Metab,* 28(1), 3-4.

Gray, J. L., Singh, G., Uttley, L. and Balasubramanian, S. P. (2018) 'Routine thyroglobulin, neck ultrasound and physical examination in the routine follow up of patients with differentiated thyroid cancer-Where is the evidence?', *Endocrine,* 62(1), 26-33.

Gupta, N., Dasyam, A. K., Carty, S. E., Nikiforova, M. N., Ohori, N. P., Armstrong, M., Yip, L., LeBeau, S. O., McCoy, K. L., Coyne, C., Stang, M. T., Johnson, J., Ferris, R. L., Seethala, R., Nikiforov, Y. E. and Hodak, S. P. (2013) 'RAS Mutations in Thyroid FNA Specimens Are Highly Predictive of Predominantly Low-Risk Follicular-Pattern Cancers', *The Journal of Clinical Endocrinology & Metabolism,* 98(5), E914-E922.

Haeussler, M., Schönig, K., Eckert, H., Eschstruth, A., Mianné, J., Renaud, J.-B., Schneider-Maunoury, S., Shkumatava, A., Teboul, L., Kent, J., Joly, J.-S. and Concordet, J.-P. (2016) 'Evaluation of off-target and on-target scoring algorithms and integration into the guide RNA selection tool CRISPOR', *Genome Biology,* 17(1), 148.

Han, J., Chen, M., Wang, Y., Gong, B., Zhuang, T., Liang, L. and Qiao, H. (2018) 'Identification of Biomarkers Based on Differentially Expressed Genes in Papillary Thyroid Carcinoma', *Scientific Reports,* 8(1), 9912.

Hara, H., Fulton, N., Yashiro, T., Ito, K., DeGroot, L. J. and Kaplan, E. L. (1994) 'N-ras mutation: an independent prognostic factor for aggressiveness of papillary thyroid carcinoma', *Surgery,* 116(6), 1010-6.

Haugen, B. R., Alexander, E. K., Bible, K. C., Doherty, G. M., Mandel, S. J., Nikiforov, Y. E., Pacini, F., Randolph, G. W., Sawka, A. M., Schlumberger, M., Schuff, K. G., Sherman, S. I., Sosa, J. A., Steward, D. L., Tuttle, R. M. and Wartofsky, L. (2016) '2015 American Thyroid Association Management Guidelines for Adult Patients with Thyroid Nodules and Differentiated Thyroid Cancer: The American Thyroid Association Guidelines Task Force on Thyroid Nodules and Differentiated Thyroid Cancer', *Thyroid,* 26(1), 1-133.

Hay, I. D., Bergstralh, E. J., Goellner, J. R., Ebersold, J. R. and Grant, C. S. (1993) 'Predicting outcome in papillary thyroid carcinoma: development of a reliable prognostic scoring system in a cohort of 1779 patients surgically treated at one institution during 1940 through 1989', *Surgery,* 114(6), 1050-7; discussion 1057-8.

He, H., Jazdzewski, K., Li, W., Liyanarachchi, S., Nagy, R., Volinia, S., Calin, G. A., Liu, C.-g., Franssila, K., Suster, S., Kloos, R. T., Croce, C. M. and de la Chapelle, A. (2005) 'The role of microRNA genes in papillary thyroid carcinoma', *Proc Natl Acad Sci U S A,* 102(52), 19075-19080.

He, Y., Zheng, Z., Xu, Y., Weng, H., Gao, Y., Qin, K., Rong, J., Chen, C., Yun, M., Zhang, J. and Ye, S. (2018) 'Over-expression of IMPDH2 is associated with tumor progression and poor prognosis in hepatocellular carcinoma', *American journal of cancer research,* 8(8), 1604-1614.

Hegedus, L., Bonnema, S. J. and Bennedbaek, F. N. (2003) 'Management of simple nodular goiter: current status and future perspectives', *Endocr Rev,* 24(1), 102-32.

Hesse, E., Musholt, P. B., Potter, E., Petrich, T., Wehmeier, M., von Wasielewski, R., Lichtinghagen, R. and Musholt, T. J. (2005) 'Oncofoetal fibronectin – a tumour-specific marker in detecting minimal residual disease in differentiated thyroid carcinoma', *British Journal of Cancer,* 93(5), 565-570.

Hodgkins, A., Farne, A., Perera, S., Grego, T., Parry-Smith, D. J., Skarnes, W. C. and Iyer, V. (2015) 'WGE: a CRISPR database for genome engineering', *Bioinformatics,* 31(18), 3078-3080.

Howell, G. M., Hodak, S. P. and Yip, L. (2013) 'RAS mutations in thyroid cancer', *The oncologist,* 18(8), 926-932.

Hsu, P. D., Scott, D. A., Weinstein, J. A., Ran, F. A., Konermann, S., Agarwala, V., Li, Y., Fine, E. J., Wu, X., Shalem, O., Cradick, T. J., Marraffini, L. A., Bao, G. and Zhang, F. (2013) 'DNA targeting specificity of RNA-guided Cas9 nucleases', *Nat Biotechnol,* 31(9), 827-32.

Hu, Y., Wang, H., Chen, E., Xu, Z., Chen, B. and Lu, G. (2016) 'Candidate microRNAs as biomarkers of thyroid carcinoma: a systematic review, meta-analysis, and experimental validation', *Cancer Medicine,* 5(9), 2602-2614.

Hua Fu, B. X., Hansen, L. L., Artiles, K. L., Nonet, M. L. and Fire, A. Z. (2014) 'Landscape of target:guide homology effects on Cas9-mediated cleavage', *Nucleic Acids Res,* 42(22), 13778-13787.

Huang da, W., Sherman, B. T. and Lempicki, R. A. (2009) 'Systematic and integrative analysis of large gene lists using DAVID bioinformatics resources', *Nature protocols,* 4(1), 44-57.

Huang, Y., Prasad, M., Lemon, W. J., Hampel, H., Wright, F. A., Kornacker, K., LiVolsi, V., Frankel, W., Kloos, R. T., Eng, C., Pellegata, N. S. and de la Chapelle, A. (2001) 'Gene expression in papillary thyroid carcinoma reveals highly consistent profiles', *Proceedings of the National Academy of Sciences,* 98(26), 15044.

Huber, M. A., Kraut, N. and Beug, H. (2005) 'Molecular requirements for epithelial-mesenchymal transition during tumor progression', *Curr Opin Cell Biol,* 17(5), 548-58.

Inaba, M., Sato, H., Abe, Y., Umemura, S., Ito, K. and Sakai, H. (2002) 'Expression and significance of c-met protein in papillary thyroid carcinoma', *Tokai J Exp Clin Med,* 27(2), 43-9.

Inoue, K. and Fry, E. A. (2017) 'Haploinsufficient tumor suppressor genes', *Adv Med Biol,* 118, 83-122.

Ishizaka, Y., Ushijima, T., Sugimura, T. and Nagao, M. (1990) 'cDNA cloning and characterization of ret activated in a human papillary thyroid carcinoma cell line', *Biochem Biophys Res Commun,* 168(2), 402-8.

Jackson, R. C., Weber, G. and Morris, H. P. (1975) 'IMP dehydrogenase, an enzyme linked with proliferation and malignancy', *Nature,* 256(5515), 331-3.

Jackson, S. E. and Chester, J. D. (2015) 'Personalised cancer medicine', *International journal of cancer,* 137(2), 262-6.

Jiang, F. and Doudna, J. A. (2017) 'CRISPR–Cas9 Structures and Mechanisms', *Annual Review of Biophysics,* 46(1), 505-529.

Jinek, M., Chylinski, K., Fonfara, I., Hauer, M., Doudna, J. A. and Charpentier, E. (2012) 'A programmable dual-RNA-guided DNA endonuclease in adaptive bacterial immunity', *Science,* 337(6096), 816-21.

Jonklaas, J., Sarlis, N. J., Litofsky, D., Ain, K. B., Bigos, S. T., Brierley, J. D., Cooper, D. S., Haugen, B. R., Ladenson, P. W., Magner, J., Robbins, J., Ross, D. S., Skarulis, M., Maxon, H. R. and Sherman, S. I. (2006) 'Outcomes of patients with differentiated thyroid carcinoma following initial therapy', *Thyroid,* 16(12), 1229-42.

Kanis, J. A., Johnell, O., Oden, A., Johansson, H. and McCloskey, E. (2008) 'FRAX and the assessment of fracture probability in men and women from the UK', *Osteoporos Int,* 19(4), 385-97.

Katoh, H., Yamashita, K., Enomoto, T. and Watanabe, M. (2015) 'Classification and general considerations of thyroid cancer', *Ann Clin Pathol,* 3(1), 1045.

Kenessey, I., Keszthelyi, M., Kramer, Z., Berta, J., Adam, A., Dobos, J., Mildner, M., Flachner, B., Cseh, S., Barna, G., Szokol, B., Orfi, L., Keri, G., Dome, B., Klepetko, W., Timar, J. and Tovari, J. (2010) 'Inhibition of c-Met with the specific small molecule tyrosine kinase inhibitor SU11274 decreases growth and metastasis formation of experimental human melanoma', *Curr Cancer Drug Targets,* 10(3), 332-42.

Keppeke, G. D., Chang, C. C., Peng, M., Chen, L.-Y., Lin, W.-C., Pai, L.-M., Andrade, L. E. C., Sung, L.-Y. and Liu, J.-L. (2018) 'IMP/GTP balance modulates cytoophidium assembly and IMPDH activity', *Cell division,* 13, 5-5.

Kitahara, C. M. and Sosa, J. A. (2016) 'The changing incidence of thyroid cancer', *Nature Reviews Endocrinology,* 12, 646.

Knauf, J. A., Luckett, K. A., Chen, K.-Y., Voza, F., Socci, N. D., Ghossein, R. and Fagin, J. A. (2018) 'Hgf/Met activation mediates resistance to BRAF inhibition in murine anaplastic thyroid cancers', *The Journal of Clinical Investigation,* 128(9), 4086-4097.

Kogai, T. and Brent, G. A. (2012) 'The sodium iodide symporter (NIS): regulation and approaches to targeting for cancer therapeutics', *Pharmacol Ther,* 135(3), 355-70.

Koressaar, T. and Remm, M. (2007) 'Enhancements and modifications of primer design program Primer3', *Bioinformatics,* 23(10), 1289-91.

Kruijff, S., Petersen, J. F., Chen, P., Aniss, A. M., Clifton-Bligh, R. J., Sidhu, S. B., Delbridge, L. W., Gill, A. J., Learoyd, D. and Sywak, M. S. (2014) 'Patterns of structural recurrence in papillary thyroid cancer', *World J Surg,* 38(3), 653-9.

Kucerova, L., Demkova, L., Skolekova, S., Bohovic, R. and Matuskova, M. (2016) 'Tyrosine kinase inhibitor SU11274 increased tumorigenicity and enriched for melanoma-initiating cells by bioenergetic modulation', *BMC Cancer,* 16, 308-308.

Labourier, E., Shifrin, A., Busseniers, A. E., Lupo, M. A., Manganelli, M. L., Andruss, B., Wylie, D. and Beaudenon-Huibregtse, S. (2015) 'Molecular Testing for miRNA,

mRNA, and DNA on Fine-Needle Aspiration Improves the Preoperative Diagnosis of Thyroid Nodules With Indeterminate Cytology', *The Journal of Clinical Endocrinology & Metabolism,* 100(7), 2743-2750.

Landa, I., Ibrahimpasic, T., Boucai, L., Sinha, R., Knauf, J. A., Shah, R. H., Dogan, S., Ricarte-Filho, J. C., Krishnamoorthy, G. P., Xu, B., Schultz, N., Berger, M. F., Sander, C., Taylor, B. S., Ghossein, R., Ganly, I. and Fagin, J. A. (2016) 'Genomic and transcriptomic hallmarks of poorly differentiated and anaplastic thyroid cancers', *J Clin Invest,* 126(3), 1052-66.

Lander, E. S., Linton, L. M., Birren, B., Nusbaum, C., Zody, M. C., Baldwin, J., Devon, K., Dewar, K., Doyle, M., FitzHugh, W., Funke, R., Gage, D., Harris, K., Heaford, A., Howland, J., Kann, L., Lehoczky, J., LeVine, R., McEwan, P., McKernan, K., Meldrim, J., Mesirov, J. P., Miranda, C., Morris, W., Naylor, J., Raymond, C., Rosetti, M., Santos, R., Sheridan, A., Sougnez, C., Stange-Thomann, Y., Stojanovic, N., Subramanian, A., Wyman, D., Rogers, J., Sulston, J., Ainscough, R., Beck, S., Bentley, D., Burton, J., Clee, C., Carter, N., Coulson, A., Deadman, R., Deloukas, P., Dunham, A., Dunham, I., Durbin, R., French, L., Grafham, D., Gregory, S., Hubbard, T., Humphray, S., Hunt, A., Jones, M., Lloyd, C., McMurray, A., Matthews, L., Mercer, S., Milne, S., Mullikin, J. C., Mungall, A., Plumb, R., Ross, M., Shownkeen, R., Sims, S., Waterston, R. H., Wilson, R. K., Hillier, L. W., McPherson, J. D., Marra, M. A., Mardis, E. R., Fulton, L. A., Chinwalla, A. T., Pepin, K. H., Gish, W. R., Chissoe, S. L., Wendl, M. C., Delehaunty, K. D., Miner, T. L., Delehaunty, A., Kramer, J. B., Cook, L. L., Fulton, R. S., Johnson, D. L., Minx, P. J., Clifton, S. W., Hawkins, T., Branscomb, E., Predki, P., Richardson, P., Wenning, S., Slezak, T., Doggett, N., Cheng, J. F., Olsen, A., Lucas, S., Elkin, C., Uberbacher, E., Frazier, M., et al. (2001) 'Initial sequencing and analysis of the human genome', *Nature,* 409(6822), 860-921.

Landry, J. J., Pyl, P. T., Rausch, T., Zichner, T., Tekkedil, M. M., Stütz, A. M., Jauch, A., Aiyar, R. S., Pau, G., Delhomme, N., Gagneur, J., Korbel, J. O., Huber, W. and Steinmetz, L. M. (2013) 'The genomic and transcriptomic landscape of a HeLa cell line', *G3 (Bethesda),* 3(8), 1213-24.

Lee, J. J., Foukakis, T., Hashemi, J., Grimelius, L., Heldin, N. E., Wallin, G., Rudduck, C., Lui, W. O., Hoog, A. and Larsson, C. (2007) 'Molecular cytogenetic profiles of novel and established human anaplastic thyroid carcinoma models', *Thyroid,* 17(4), 289-301.

Lennard, C. M., Patel, A., Wilson, J., Reinhardt, B., Tuman, C., Fenton, C., Blair, E., Francis, G. L. and Tuttle, R. M. (2001) 'Intensity of vascular endothelial growth factor expression is associated with increased risk of recurrence and decreased disease-free survival in papillary thyroid cancer', *Surgery,* 129(5), 552-8.

Leonardi, G. C., Candido, S., Carbone, M., Colaianni, V., Garozzo, S. F., Cina, D. and Libra, M. (2012) 'microRNAs and thyroid cancer: biological and clinical significance (Review)', *Int J Mol Med,* 30(5), 991-9.

Li, W., Qian, L., Lin, J., Huang, G., Hao, N., Wei, X., Wang, W. and Liang, J. (2017) 'CD44 regulates prostate cancer proliferation, invasion and migration via PDK1 and PFKFB4', *Oncotarget,* 8(39), 65143-65151.

Lithwick-Yanai, G., Dromi, N., Shtabsky, A., Morgenstern, S., Strenov, Y., Feinmesser, M., Kravtsov, V., Leon, M. E., Hajduch, M., Ali, S. Z., VandenBussche, C. J., Zhang, X.,

Leider-Trejo, L., Zubkov, A., Vorobyov, S., Kushnir, M., Goren, Y., Tabak, S., Kadosh, E., Benjamin, H., Schnitzer-Perlman, T., Marmor, H., Motin, M., Lebanony, D., Kredo-Russo, S., Mitchell, H., Noller, M., Smith, A., Dattner, O., Ashkenazi, K., Sanden, M., Berlin, K. A., Bar, D. and Meiri, E. (2017) 'Multicentre validation of a microRNA-based assay for diagnosing indeterminate thyroid nodules utilising fine needle aspirate smears', *J Clin Pathol,* 70(6), 500-507.

Liu, H., Lei, C., He, Q., Pan, Z., Xiao, D. and Tao, Y. (2018) 'Nuclear functions of mammalian MicroRNAs in gene regulation, immunity and cancer', *Molecular Cancer,* 17(1), 64.

Liu, J. L. (2011) 'The enigmatic cytoophidium: compartmentation of CTP synthase via filament formation', *Bioessays,* 33(3), 159-64.

Liu, L., Li, Y., Li, S., Hu, N., He, Y., Pong, R., Lin, D., Lu, L. and Law, M. (2012) 'Comparison of next-generation sequencing systems', *J Biomed Biotechnol,* 2012, 251364.

Liu, X., Bishop, J., Shan, Y., Pai, S., Liu, D., Murugan, A. K., Sun, H., El-Naggar, A. K. and Xing, M. (2013) 'Highly prevalent TERT promoter mutations in aggressive thyroid cancers', *Endocr Relat Cancer,* 20(4), 603-10.

Ljubas, J., Ovesen, T. and Rusan, M. (2019) 'A Systematic Review of Phase II Targeted Therapy Clinical Trials in Anaplastic Thyroid Cancer', *Cancers,* 11(7), 943.

Lunter, G. and Goodson, M. (2011) 'Stampy: a statistical algorithm for sensitive and fast mapping of Illumina sequence reads', *Genome Res,* 21(6), 936-9.

Ma, X., Wei, J., Zhang, L., Deng, D., Liu, L., Mei, X., He, X. and Tian, J. (2016) 'miR-486-5p inhibits cell growth of papillary thyroid carcinoma by targeting fibrillin-1', *Biomed Pharmacother,* 80, 220-226.

Manzella, L., Stella, S., Pennisi, M. S., Tirrò, E., Massimino, M., Romano, C., Puma, A., Tavarelli, M. and Vigneri, P. (2017) 'New Insights in Thyroid Cancer and p53 Family Proteins', *International journal of molecular sciences,* 18(6), 1325.

Mardis, E. R. (2013) 'Next-Generation Sequencing Platforms', *Annual Review of Analytical Chemistry,* 6(1), 287-303.

Mariotti, S. B.-P., P. (2016) *Physiology of the Hypothalamic-Pituitary-Thyroid Axis.,* Endotext [online], available: https://www.ncbi.nlm.nih.gov/books/NBK278958/ [accessed

Massague, J. (2004) 'G1 cell-cycle control and cancer', *Nature,* 432(7015), 298-306.

Matson, D. R., Hardin, H., Buehler, D. and Lloyd, R. V. (2017) 'AKT activity is elevated in aggressive thyroid neoplasms where it promotes proliferation and invasion', *Exp Mol Pathol,* 103(3), 288-293.

Mazzaferri, E. L. and Jhiang, S. M. (1994) 'Long-term impact of initial surgical and medical therapy on papillary and follicular thyroid cancer', *The American Journal of Medicine,* 97(5), 418-428.

McFadden, D. G., Vernon, A., Santiago, P. M., Martinez-McFaline, R., Bhutkar, A., Crowley, D. M., McMahon, M., Sadow, P. M. and Jacks, T. (2014) 'p53 constrains progression to anaplastic thyroid carcinoma in a Braf-mutant mouse model of

papillary thyroid cancer', *Proceedings of the National Academy of Sciences,* 111(16), E1600-E1609.

McLeod, D. S. A., Watters, K. F., Carpenter, A. D., Ladenson, P. W., Cooper, D. S. and Ding, E. L. (2012) 'Thyrotropin and Thyroid Cancer Diagnosis: A Systematic Review and Dose-Response Meta-Analysis', *The Journal of Clinical Endocrinology & Metabolism,* 97(8), 2682-2692.

Medici, M., Kwong, N., Angell, T. E., Marqusee, E., Kim, M. I., Frates, M. C., Benson, C. B., Cibas, E. S., Barletta, J. A., Krane, J. F., Ruan, D. T., Cho, N. L., Gawande, A. A., Moore, F. D., Jr. and Alexander, E. K. (2015) 'The variable phenotype and low-risk nature of RAS-positive thyroid nodules', *BMC medicine,* 13, 184-184.

Minchenko, O. H., Tsuchihara, K., Minchenko, D. O., Bikfalvi, A. and Esumi, H. (2014) 'Mechanisms of regulation of PFKFB expression in pancreatic and gastric cancer cells', *World journal of gastroenterology,* 20(38), 13705-13717.

Morini, M., Mottolese, M., Ferrari, N., Ghiorzo, F., Buglioni, S., Mortarini, R., Noonan, D. M., Natali, P. G. and Albini, A. (2000) 'The alpha 3 beta 1 integrin is associated with mammary carcinoma cell metastasis, invasion, and gelatinase B (MMP-9) activity', *International journal of cancer,* 87(3), 336-42.

Mueller, S. C., Ghersi, G., Akiyama, S. K., Sang, Q. X., Howard, L., Pineiro-Sanchez, M., Nakahara, H., Yeh, Y. and Chen, W. T. (1999) 'A novel protease-docking function of integrin at invadopodia', *J Biol Chem,* 274(35), 24947-52.

Muzza, M., Colombo, C., Rossi, S., Tosi, D., Cirello, V., Perrino, M., De Leo, S., Magnani, E., Pignatti, E., Vigo, B., Simoni, M., Bulfamante, G., Vicentini, L. and Fugazzola, L. (2015) 'Telomerase in differentiated thyroid cancer: promoter mutations, expression and localization', *Mol Cell Endocrinol,* 399, 288-95.

National Human Genome Research Institute (2016) 'Sequencing Cost Graph: Moore's law', [online], available: https://www.genome.gov/images/content/costpergenome2015_4.jpg].

National Institute for Health and Care Excellence (2018) 'Lenvatinib and sorafenib for treating differentiated thyroid cancer after radioactive iodine', *NICE guidelines* [online], available: https://www.nice.org.uk/guidance/ta535/resources/lenvatinib-and-sorafenib-for-treating-differentiated-thyroid-cancer-after-radioactive-iodine-pdf-82606902620101].

Natsumeda, Y., Ohno, S., Kawasaki, H., Konno, Y., Weber, G. and Suzuki, K. (1990) 'Two distinct cDNAs for human IMP dehydrogenase', *J Biol Chem,* 265(9), 5292-5.

Nemudryi, A. A., Valetdinova, K. R., Medvedev, S. P. and Zakian, S. M. (2014) 'TALEN and CRISPR/Cas Genome Editing Systems: Tools of Discovery', *Acta Naturae,* 6(3), 19-40.

Nieto, H. and Boelaert, K. (2016) 'WOMEN IN CANCER THEMATIC REVIEW: Thyroid-stimulating hormone in thyroid cancer: does it matter?', *Endocr Relat Cancer,* 23(11), T109-t121.

Nikiforov, Y. E. (2006) 'Radiation-induced thyroid cancer: what we have learned from chernobyl', *Endocr Pathol,* 17(4), 307-17.

Nikiforov, Y. E. and Nikiforova, M. N. (2011) 'Molecular genetics and diagnosis of thyroid cancer', *Nature Reviews Endocrinology,* 7, 569.

Nikiforov, Y. E., Yip, L. and Nikiforova, M. N. (2013) 'New strategies in diagnosing cancer in thyroid nodules: impact of molecular markers', *Clin Cancer Res,* 19(9), 2283-8.

Nishino, M. and Nikiforova, M. (2018) 'Update on Molecular Testing for Cytologically Indeterminate Thyroid Nodules', *Arch Pathol Lab Med,* 142(4), 446-457.

Nozhat, Z. and Hedayati, M. (2016) 'PI3K/AKT Pathway and Its Mediators in Thyroid Carcinomas', *Mol Diagn Ther,* 20(1), 13-26.

Nucera, C., Porrello, A., Antonello, Z. A., Mekel, M., Nehs, M. A., Giordano, T. J., Gerald, D., Benjamin, L. E., Priolo, C., Puxeddu, E., Finn, S., Jarzab, B., Hodin, R. A., Pontecorvi, A., Nose, V., Lawler, J. and Parangi, S. (2010) 'B-Raf and thrombospondin-1 promote thyroid cancer progression', *Proceedings of the National Academy of Sciences,* 107(23), 10649.

Oishi, N., Kondo, T., Ebina, A., Sato, Y., Akaishi, J., Hino, R., Yamamoto, N., Mochizuki, K., Nakazawa, T., Yokomichi, H., Ito, K., Ishikawa, Y. and Katoh, R. (2017) 'Molecular alterations of coexisting thyroid papillary carcinoma and anaplastic carcinoma: identification of TERT mutation as an independent risk factor for transformation', *Modern pathology : an official journal of the United States and Canadian Academy of Pathology, Inc,* 30(11), 1527-1537.

Oleinika, K., Nibbs, R. J., Graham, G. J. and Fraser, A. R. (2013) 'Suppression, subversion and escape: the role of regulatory T cells in cancer progression', *Clin Exp Immunol,* 171(1), 36-45.

Pacini, F., Schlumberger, M., Dralle, H., Elisei, R., Smit, J. W. and Wiersinga, W. (2006) 'European consensus for the management of patients with differentiated thyroid carcinoma of the follicular epithelium', *Eur J Endocrinol,* 154(6), 787-803.

Paez, D., Labonte, M. J., Bohanes, P., Zhang, W., Benhanim, L., Ning, Y., Wakatsuki, T., Loupakis, F. and Lenz, H. J. (2012) 'Cancer dormancy: a model of early dissemination and late cancer recurrence', *Clin Cancer Res,* 18(3), 645-53.

Pallante, P., Visone, R., Ferracin, M., Ferraro, A., Berlingieri, M. T., Troncone, G., Chiappetta, G., Liu, C. G., Santoro, M., Negrini, M., Croce, C. M. and Fusco, A. (2006) 'MicroRNA deregulation in human thyroid papillary carcinomas', *Endocr Relat Cancer,* 13(2), 497-508.

Papini, E., Petrucci, L., Guglielmi, R., Panunzi, C., Rinaldi, R., Bacci, V., Crescenzi, A., Nardi, F., Fabbrini, R. and Pacella, C. M. (1998) 'Long-Term Changes in Nodular Goiter: A 5-Year Prospective Randomized Trial of Levothyroxine Suppressive Therapy for Benign Cold Thyroid Nodules', *The Journal of Clinical Endocrinology & Metabolism,* 83(3), 780-783.

Paschke, R., Cantara, S., Crescenzi, A., Jarzab, B., Musholt, T. J. and Sobrinho Simoes, M. (2017) 'European Thyroid Association Guidelines regarding Thyroid Nodule Molecular Fine-Needle Aspiration Cytology Diagnostics', *Eur Thyroid J,* 6(3), 115-129.

Pattnaik, S., Vaidyanathan, S., Pooja, D. G., Deepak, S. and Panda, B. (2012) 'Customisation of the exome data analysis pipeline using a combinatorial approach', *PloS one,* 7(1), e30080-e30080.

Pegoraro, C., Maczkowiak, F. and Monsoro-Burq, A. H. (2013) 'Pfkfb (6-phosphofructo-2-kinase/fructose-2,6-bisphosphatase) isoforms display a tissue-specific and dynamic expression during Xenopus laevis development', *Gene Expr Patterns,* 13(7), 203-11.

Pellegriti, G., Frasca, F., Regalbuto, C., Squatrito, S. and Vigneri, R. (2013) 'Worldwide Increasing Incidence of Thyroid Cancer: Update on Epidemiology and Risk Factors', *Journal of Cancer Epidemiology,* 2013, 10.

Perros, P., Boelaert, K., Colley, S., Evans, C., Evans, R. M., Gerrard Ba, G., Gilbert, J., Harrison, B., Johnson, S. J., Giles, T. E., Moss, L., Lewington, V., Newbold, K., Taylor, J., Thakker, R. V., Watkinson, J. and Williams, G. R. (2014) 'Guidelines for the management of thyroid cancer', *Clin Endocrinol (Oxf),* 81 Suppl 1, 1-122.

Petrulea, M. S., Plantinga, T. S., Smit, J. W., Georgescu, C. E. and Netea-Maier, R. T. (2015) 'PI3K/Akt/mTOR: A promising therapeutic target for non-medullary thyroid carcinoma', *Cancer Treat Rev,* 41(8), 707-13.

Phay, J. E. and Ringel, M. D. (2013) 'Metastatic mechanisms in follicular cell-derived thyroid cancer', *Endocrine-Related Cancer,* 20(6), R307-R319.

Pizzolanti, G., Russo, L., Richiusa, P., Bronte, V., Nuara, R. B., Rodolico, V., Amato, M. C., Smeraldi, L., Sisto, P. S., Nucera, M., Bommarito, A., Citarrella, R., Lo Coco, R., Cabibi, D., Lo Coco, A., Frasca, F., Gulotta, G., Latteri, M. A., Modica, G., Galluzzo, A. and Giordano, C. (2007) 'Fine-needle aspiration molecular analysis for the diagnosis of papillary thyroid carcinoma through BRAF V600E mutation and RET/PTC rearrangement', *Thyroid,* 17(11), 1109-15.

Polovina, S., Micic, D., Miljic, D., Milic, N., Micic, D. and Popovic, V. (2015) 'The Fracture Risk Assessment Tool (FRAX score) in subclinical hyperthyroidism', *Vojnosanit Pregl,* 72(6), 510-6.

Poma, A. M., Condello, V., Denaro, M., Torregrossa, L., Elisei, R., Vitti, P. and Basolo, F. (2019) 'DICER1 somatic mutations strongly impair miRNA processing even in benign thyroid lesions', *Oncotarget,* 10(19), 1785-1797.

Pratt, A. J. and MacRae, I. J. (2009) 'The RNA-induced silencing complex: a versatile gene-silencing machine', *The Journal of biological chemistry,* 284(27), 17897-17901.

Pujol, P., Daures, J. P., Nsakala, N., Baldet, L., Bringer, J. and Jaffiol, C. (1996) 'Degree of thyrotropin suppression as a prognostic determinant in differentiated thyroid cancer', *The Journal of Clinical Endocrinology & Metabolism,* 81(12), 4318-4323.

Puxeddu, E., Moretti, S., Giannico, A., Martinelli, M., Marino, C., Avenia, N., Cristofani, R., Farabi, R., Reboldi, G., Ribacchi, R., Pontecorvi, A. and Santeusanio, F. (2003)

'Ret/PTC activation does not influence clinical and pathological features of adult papillary thyroid carcinomas', *European Journal of Endocrinology,* 148(5), 505-513.

Quan, L., Lv, Q. and Zhang, Y. (2016) 'STRUM: structure-based prediction of protein stability changes upon single-point mutation', *Bioinformatics,* 32(19), 2936-46.

Ramírez-Moya, J. and Santisteban, P. (2019) 'miRNA-Directed Regulation of the Main Signaling Pathways in Thyroid Cancer', *Frontiers in Endocrinology,* 10(430).

Ramírez-Moya, J., Wert-Lamas, L., Riesco-Eizaguirre, G. and Santisteban, P. (2019) 'Impaired microRNA processing by DICER1 downregulation endows thyroid cancer with increased aggressiveness', *Oncogene,* 38(27), 5486-5499.

Read, M. L., Fong, J. C., Modasia, B., Fletcher, A., Imruetaicharoenchoke, W., Thompson, R. J., Nieto, H., Reynolds, J. J., Bacon, A., Mallick, U., Hackshaw, A., Watkinson, J. C., Boelaert, K., Turnell, A. S., Smith, V. E. and McCabe, C. J. (2017) 'Elevated PTTG and PBF predicts poor patient outcome and modulates DNA damage response genes in thyroid cancer', *Oncogene,* 36, 5296.

Read, M. L., Lewy, G. D., Fong, J. C., Sharma, N., Seed, R. I., Smith, V. E., Gentilin, E., Warfield, A., Eggo, M. C., Knauf, J. A., Leadbeater, W. E., Watkinson, J. C., Franklyn, J. A., Boelaert, K. and McCabe, C. J. (2011) 'Proto-oncogene PBF/PTTG1IP regulates thyroid cell growth and represses radioiodide treatment', *Cancer Res,* 71(19), 6153-64.

Reva, B., Antipin, Y. and Sander, C. (2011) 'Predicting the functional impact of protein mutations: application to cancer genomics', *Nucleic Acids Res,* 39(17), e118.

Ribeiro, F. R., Meireles, A. M., Rocha, A. S. and Teixeira, M. R. (2008) 'Conventional and molecular cytogenetics of human non-medullary thyroid carcinoma: characterization of eight cell line models and review of the literature on clinical samples', *BMC Cancer,* 8, 371.

Ricarte-Filho, J. C., Fuziwara, C. S., Yamashita, A. S., Rezende, E., da-Silva, M. J. and Kimura, E. T. (2009) 'Effects of let-7 microRNA on Cell Growth and Differentiation of Papillary Thyroid Cancer', *Transl Oncol,* 2(4), 236-41.

Riesco-Eizaguirre, G. and Santisteban, P. (2016) 'ENDOCRINE TUMOURS: Advances in the molecular pathogenesis of thyroid cancer: lessons from the cancer genome', *European Journal of Endocrinology,* 175(5), R203-R217.

Rimmer, A., Phan, H., Mathieson, I., Iqbal, Z., Twigg, S. R. F., Consortium, W. G. S., Wilkie, A. O. M., McVean, G. and Lunter, G. (2014a) 'Integrating mapping-, assembly- and haplotype-based approaches for calling variants in clinical sequencing applications', *Nat Genet,* 46(8), 912-918.

Rimmer, A., Phan, H., Mathieson, I., Iqbal, Z., Twigg, S. R. F., Consortium, W. G. S., Wilkie, A. O. M., McVean, G. and Lunter, G. (2014b) 'Integrating mapping-, assembly- and haplotype-based approaches for calling variants in clinical sequencing applications', *Nat Genet,* 46(8), 912-918.

Ringel, M. D. (2011) 'Metastatic dormancy and progression in thyroid cancer: targeting cells in the metastatic frontier', *Thyroid,* 21(5), 487-492.

Robbins, H. L. and Hague, A. (2016) 'The PI3K/Akt Pathway in Tumors of Endocrine Tissues', *Frontiers in Endocrinology,* 6, 188-188.

Robenshtok, E. and Tuttle, R. M. (2012) 'Role of Recombinant Human Thyrotropin (rhTSH) in the Treatment of Well-Differentiated Thyroid Cancer', *Indian journal of surgical oncology,* 3(3), 182-189.

Robertson, J. C., Jorcyk, C. L. and Oxford, J. T. (2018) 'DICER1 Syndrome: DICER1 Mutations in Rare Cancers', *Cancers,* 10(5), 143.

Robinson, J. T., Thorvaldsdottir, H., Winckler, W., Guttman, M., Lander, E. S., Getz, G. and Mesirov, J. P. (2011) 'Integrative genomics viewer', *Nat Biotechnol,* 29(1), 24-6.

Roman, B. R., Morris, L. G. and Davies, L. (2017) 'The thyroid cancer epidemic, 2017 perspective', *Current opinion in endocrinology, diabetes, and obesity,* 24(5), 332-336.

Romei, C. and Elisei, R. (2012) 'RET/PTC Translocations and Clinico-Pathological Features in Human Papillary Thyroid Carcinoma', *Front Endocrinol (Lausanne),* 3, 54.

Rosignolo, F., Memeo, L., Monzani, F., Colarossi, C., Pecce, V., Verrienti, A., Durante, C., Grani, G., Lamartina, L., Forte, S., Martinetti, D., Giuffrida, D., Russo, D., Basolo, F., Filetti, S. and Sponziello, M. (2017) 'MicroRNA-based molecular classification of papillary thyroid carcinoma', *Int J Oncol,* 50(5), 1767-1777.

Rothenberg, S. M., McFadden, D. G., Palmer, E. L., Daniels, G. H. and Wirth, L. J. (2015) 'Redifferentiation of iodine-refractory BRAF V600E-mutant metastatic papillary thyroid cancer with dabrafenib', *Clin Cancer Res,* 21(5), 1028-35.

Roy, A., Kucukural, A. and Zhang, Y. (2010) 'I-TASSER: a unified platform for automated protein structure and function prediction', *Nature protocols,* 5(4), 725-738.

Rusinek, D., Szpak-Ulczok, S. and Jarzab, B. (2011) 'Gene expression profile of human thyroid cancer in relation to its mutational status', *Journal of Molecular Endocrinology,* 47(3), R91-R103.

Saiselet, M., Pita, J. M., Augenlicht, A., Dom, G., Tarabichi, M., Fimereli, D., Dumont, J. E., Detours, V. and Maenhaut, C. (2016) 'miRNA expression and function in thyroid carcinomas: a comparative and critical analysis and a model for other cancers', *Oncotarget,* 7(32), 52475-52492.

Sanger, F., Nicklen, S. and Coulson, A. R. (1977) 'DNA sequencing with chain-terminating inhibitors', *Proc Natl Acad Sci U S A,* 74(12), 5463-7.

Sanson, K. R., Hanna, R. E., Hegde, M., Donovan, K. F., Strand, C., Sullender, M. E., Vaimberg, E. W., Goodale, A., Root, D. E., Piccioni, F. and Doench, J. G. (2018) 'Optimized libraries for CRISPR-Cas9 genetic screens with multiple modalities', *Nature Communications,* 9(1), 5416.

Sapin, R. and Schlienger, J. L. (2003) '[Thyroxine (T4) and tri-iodothyronine (T3) determinations: techniques and value in the assessment of thyroid function]', *Ann Biol Clin (Paris),* 61(4), 411-20.

Schlumberger, M., Brose, M., Elisei, R., Leboulleux, S., Luster, M., Pitoia, F. and Pacini, F. (2014) 'Definition and management of radioactive iodine-refractory differentiated thyroid cancer', *Lancet Diabetes Endocrinol,* 2(5), 356-8.

Schlumberger, M., Tahara, M., Wirth, L. J., Robinson, B., Brose, M. S., Elisei, R., Habra, M. A., Newbold, K., Shah, M. H., Hoff, A. O., Gianoukakis, A. G., Kiyota, N., Taylor, M. H., Kim, S. B., Krzyzanowska, M. K., Dutcus, C. E., de las Heras, B., Zhu, J. and Sherman, S. I. (2015) 'Lenvatinib versus placebo in radioiodine-refractory thyroid cancer', *N Engl J Med,* 372(7), 621-30.

Schneider, C. A., Rasband, W. S. and Eliceiri, K. W. (2012) 'NIH Image to ImageJ: 25 years of image analysis', *Nat Methods,* 9(7), 671-5.

Schwarz, J. M., Rodelsperger, C., Schuelke, M. and Seelow, D. (2010) 'MutationTaster evaluates disease-causing potential of sequence alterations', *Nat Methods,* 7(8), 575-6.

Schweppe, R. E., Klopper, J. P., Korch, C., Pugazhenthi, U., Benezra, M., Knauf, J. A., Fagin, J. A., Marlow, L. A., Copland, J. A., Smallridge, R. C. and Haugen, B. R. (2008) 'Deoxyribonucleic Acid Profiling Analysis of 40 Human Thyroid Cancer Cell Lines Reveals Cross-Contamination Resulting in Cell Line Redundancy and Misidentification', *The Journal of Clinical Endocrinology & Metabolism* 93(11), 4331-41.

Senda, M. and Natsumeda, Y. (1994) 'Tissue-differential expression of two distinct genes for human IMP dehydrogenase (E.C.1.1.1.205)', *Life Sci,* 54(24), 1917-26.

Shakib, H., Rajabi, S., Dehghan, M. H., Mashayekhi, F. J., Safari-Alighiarloo, N. and Hedayati, M. (2019) 'Epithelial-to-mesenchymal transition in thyroid cancer: a comprehensive review', *Endocrine*.

Shannon, P., Markiel, A., Ozier, O., Baliga, N. S., Wang, J. T., Ramage, D., Amin, N., Schwikowski, B. and Ideker, T. (2003) 'Cytoscape: a software environment for integrated models of biomolecular interaction networks', *Genome Res,* 13(11), 2498-504.

Shibue, T. and Weinberg, R. A. (2009) 'Integrin beta1-focal adhesion kinase signaling directs the proliferation of metastatic cancer cells disseminated in the lungs', *Proc Natl Acad Sci U S A,* 106(25), 10290-5.

Shihab, H. A., Gough, J., Cooper, D. N., Stenson, P. D., Barker, G. L., Edwards, K. J., Day, I. N. and Gaunt, T. R. (2013) 'Predicting the functional, molecular, and phenotypic consequences of amino acid substitutions using hidden Markov models', *Hum Mutat,* 34(1), 57-65.

Shimizu, K., Nakata, M., Hirami, Y., Yukawa, T., Maeda, A. and Tanemoto, K. (2010) 'Tumor-Infiltrating Foxp3+ Regulatory T Cells are Correlated with Cyclooxygenase-2 Expression and are Associated with Recurrence in Resected Non-small Cell Lung Cancer', *Journal of Thoracic Oncology,* 5(5), 585-590.

Sim, N. L., Kumar, P., Hu, J., Henikoff, S., Schneider, G. and Ng, P. C. (2012) 'SIFT web server: predicting effects of amino acid substitutions on proteins', *Nucleic Acids Res,* 40(Web Server issue), W452-7.

Simoes-Pereira, J., Moura, M. M., Marques, I. J., Rito, M., Cabrera, R. A., Leite, V. and Cavaco, B. M. (2019) 'The role of EIF1AX in thyroid cancer tumourigenesis and progression', *J Endocrinol Invest,* 42(3), 313-318.

Sintchak, M. D., Fleming, M. A., Futer, O., Raybuck, S. A., Chambers, S. P., Caron, P. R., Murcko, M. A. and Wilson, K. P. (1996) 'Structure and mechanism of inosine monophosphate dehydrogenase in complex with the immunosuppressant mycophenolic acid', *Cell,* 85(6), 921-30.

Sipos, J. A. and Mazzaferri, E. L. (2010) 'Thyroid cancer epidemiology and prognostic variables', *Clin Oncol (R Coll Radiol),* 22(6), 395-404.

Smallridge, R. C., Marlow, L. A. and Copland, J. A. (2009) 'Anaplastic thyroid cancer: molecular pathogenesis and emerging therapies', *Endocr Relat Cancer,* 16(1), 17-44.

Smith, V. E., Franklyn, J. and J., M. C. (2011) 'Expression and function of the novel proto-oncogene PBF in thyroid cancer: a new target for augmenting radioiodine uptake', *Journal of Endocrinology,* 210(2), 157-163.

Sobin, L. G., M; Wittekind, C; (2011) *TNM Classification of Malignant Tumours, 7th Edition,* [online], available: https://www.wiley.com/en-gb/TNM+Classification+of+Malignant+Tumours%2C+7th+Edition-p-9781444358964 [accessed

Solarski, M., Rotondo, F., Foulkes, W. D., Priest, J. R., Syro, L. V., Butz, H., Cusimano, M. D. and Kovacs, K. (2018) 'DICER1 gene mutations in endocrine tumors', *Endocr Relat Cancer,* 25(3), R197-r208.

Sponziello, M., Rosignolo, F., Celano, M., Maggisano, V., Pecce, V., De Rose, R. F., Lombardo, G. E., Durante, C., Filetti, S., Damante, G., Russo, D. and Bulotta, S. (2016) 'Fibronectin-1 expression is increased in aggressive thyroid cancer and favors the migration and invasion of cancer cells', *Mol Cell Endocrinol,* 431, 123-32.

Steward, D. L., Carty, S. E., Sippel, R. S., Yang, S. P., Sosa, J. A., Sipos, J. A., Figge, J. J., Mandel, S., Haugen, B. R., Burman, K. D., Baloch, Z. W., Lloyd, R. V., Seethala, R. R., Gooding, W. E., Chiosea, S. I., Gomes-Lima, C., Ferris, R. L., Folek, J. M., Khawaja, R. A., Kundra, P., Loh, K. S., Marshall, C. B., Mayson, S., McCoy, K. L., Nga, M. E., Ngiam, K. Y., Nikiforova, M. N., Poehls, J. L., Ringel, M. D., Yang, H., Yip, L. and Nikiforov, Y. E. (2019) 'Performance of a Multigene Genomic Classifier in Thyroid Nodules With Indeterminate Cytology: A Prospective Blinded Multicenter Study', *JAMA Oncol,* 5(2), 204-212.

Stokowy, T., Wojtaś, B., Krajewska, J., Stobiecka, E., Dralle, H., Musholt, T., Hauptmann, S., Lange, D., Hegedüs, L., Jarząb, B., Krohn, K., Paschke, R. and Eszlinger, M. (2015) 'A two miRNA classifier differentiates follicular thyroid carcinomas from follicular thyroid adenomas', *Molecular and Cellular Endocrinology,* 399, 43-49.

Sun, C. M., Xiong, D. B., Yan, Y., Geng, J., Liu, M. and Yao, X. D. (2016) 'Genetic alteration in phosphofructokinase family promotes growth of muscle-invasive bladder cancer', *Int J Biol Markers,* 31(3), e286-93.

Sun, Y., Yu, S., Liu, Y., Wang, F., Liu, Y. and Xiao, H. (2013) 'Expression of miRNAs in Papillary Thyroid Carcinomas Is Associated with BRAF Mutation and Clinicopathological Features in Chinese Patients', *Int J Endocrinol,* 2013, 128735.

Svoronos, A. A., Engelman, D. M. and Slack, F. J. (2016) 'OncomiR or Tumor Suppressor? The Duplicity of MicroRNAs in Cancer', *Cancer Research,* 76(13), 3666.

Takano, T., Matsuzuka, F., Miyauchi, A., Yokozawa, T., Liu, G., Morita, S., Kuma, K. and Amino, N. (1998a) 'Restricted expression of oncofetal fibronectin mRNA in thyroid papillary and anaplastic carcinoma: an in situ hybridization study', *British Journal of Cancer,* 78(2), 221-224.

Takano, T., Miyauchi, A., Yokozawa, T., Matsuzuka, F., Liu, G., Higashiyama, T., Morita, S., Kuma, K. and Amino, N. (1998b) 'Accurate and objective preoperative diagnosis of thyroid papillary carcinomas by reverse transcription-PCR detection of oncofetal fibronectin messenger RNA in fine-needle aspiration biopsies', *Cancer Res,* 58(21), 4913-7.

Tallini, G., de Biase, D., Repaci, A. and Visani, M. (2019) 'What's New in Thyroid Tumor Classification, the 2017 World Health Organization Classification of Tumours of Endocrine Organs' in Kakudo, K., ed. *Thyroid FNA Cytology: Differential Diagnoses and Pitfalls*, Singapore: Springer Singapore, 37-47.

Tate, J. G., Bamford, S., Jubb, H. C., Sondka, Z., Beare, D. M., Bindal, N., Boutselakis, H., Cole, C. G., Creatore, C., Dawson, E., Fish, P., Harsha, B., Hathaway, C., Jupe, S. C., Kok, C. Y., Noble, K., Ponting, L., Ramshaw, C. C., Rye, C. E., Speedy, H. E., Stefancsik, R., Thompson, S. L., Wang, S., Ward, S., Campbell, P. J. and Forbes, S. A. (2018) 'COSMIC: the Catalogue Of Somatic Mutations In Cancer', *Nucleic Acids Res,* 47(D1), D941-D947.

The Royal College of Pathologists (2016) 'Guidance on the reporting of thyroid cytology specimens', [online], available: https://www.rcpath.org/uploads/assets/7d693ce4-0091-4621-97f79e2a0d1034d6/g089_guidancereportingthyroidcytology_jan16.pdf [Accessed 13th September 2019].

ThermoFisher Scientific, A. B. (2016) 'A technical guide to identifying miRNA normalizers using TaqMan Advanced miRNA Assays', [online], available: https://assets.thermofisher.com/TFS-Assets/GSD/Reference-Materials/identifying-mirna-normalizers-white-paper.pdf].

Trovato, M., Campennì, A., Giovinazzo, S., Siracusa, M. and Ruggeri, R. M. (2017) 'Hepatocyte Growth Factor/C-Met Axis in Thyroid Cancer: From Diagnostic Biomarker to Therapeutic Target', *Biomarker insights,* 12, 1177271917701126-1177271917701126.

Trusolino, L., Bertotti, A. and Comoglio, P. M. (2010) 'MET signalling: principles and functions in development, organ regeneration and cancer', *Nat Rev Mol Cell Biol,* 11(12), 834-48.

Ueno, K., Hirata, H., Hinoda, Y. and Dahiya, R. (2013) 'Frizzled homolog proteins, microRNAs and Wnt signaling in cancer', *International journal of cancer,* 132(8), 1731-1740.

Uhlen, M., Fagerberg, L., Hallstrom, B. M., Lindskog, C., Oksvold, P., Mardinoglu, A., Sivertsson, A., Kampf, C., Sjostedt, E., Asplund, A., Olsson, I., Edlund, K., Lundberg, E., Navani, S., Szigyarto, C. A., Odeberg, J., Djureinovic, D., Takanen, J. O., Hober, S., Alm, T., Edqvist, P. H., Berling, H., Tegel, H., Mulder, J., Rockberg, J., Nilsson, P., Schwenk, J. M., Hamsten, M., von Feilitzen, K., Forsberg, M., Persson, L., Johansson, F., Zwahlen, M., von Heijne, G., Nielsen, J. and Ponten, F. (2015) 'Proteomics. Tissue-based map of the human proteome', *Science,* 347(6220), 1260419.

Valderrabano, P., Hallanger-Johnson, J. E., Thapa, R., Wang, X. and McIver, B. (2019) 'Comparison of Postmarketing Findings vs the Initial Clinical Validation Findings of a Thyroid Nodule Gene Expression Classifier: A Systematic Review and Meta-analysis', *JAMA Otolaryngology–Head & Neck Surgery,* 145(9), 783-792.

Vander Heiden, M. G., Cantley, L. C. and Thompson, C. B. (2009) 'Understanding the Warburg effect: the metabolic requirements of cell proliferation', *Science,* 324(5930), 1029-33.

Vasko, V., Espinosa, A. V., Scouten, W., He, H., Auer, H., Liyanarachchi, S., Larin, A., Savchenko, V., Francis, G. L., de la Chapelle, A., Saji, M. and Ringel, M. D. (2007) 'Gene expression and functional evidence of epithelial-to-mesenchymal transition in papillary thyroid carcinoma invasion', *Proc Natl Acad Sci U S A,* 104(8), 2803-2808.

Venter, J. C., Adams, M. D., Myers, E. W., Li, P. W., Mural, R. J., Sutton, G. G., Smith, H. O., Yandell, M., Evans, C. A., Holt, R. A., Gocayne, J. D., Amanatides, P., Ballew, R. M., Huson, D. H., Wortman, J. R., Zhang, Q., Kodira, C. D., Zheng, X. H., Chen, L., Skupski, M., Subramanian, G., Thomas, P. D., Zhang, J., Gabor Miklos, G. L., Nelson, C., Broder, S., Clark, A. G., Nadeau, J., McKusick, V. A., Zinder, N., Levine, A. J., Roberts, R. J., Simon, M., Slayman, C., Hunkapiller, M., Bolanos, R., Delcher, A., Dew, I., Fasulo, D., Flanigan, M., Florea, L., Halpern, A., Hannenhalli, S., Kravitz, S., Levy, S., Mobarry, C., Reinert, K., Remington, K., Abu-Threideh, J., Beasley, E., Biddick, K., Bonazzi, V., Brandon, R., Cargill, M., Chandramouliswaran, I., Charlab, R., Chaturvedi, K., Deng, Z., Di Francesco, V., Dunn, P., Eilbeck, K., Evangelista, C., Gabrielian, A. E., Gan, W., Ge, W., Gong, F., Gu, Z., Guan, P., Heiman, T. J., Higgins, M. E., Ji, R. R., Ke, Z., Ketchum, K. A., Lai, Z., Lei, Y., Li, Z., Li, J., Liang, Y., Lin, X., Lu, F., Merkulov, G. V., Milshina, N., Moore, H. M., Naik, A. K., Narayan, V. A., Neelam, B., Nusskern, D., Rusch, D. B., Salzberg, S., Shao, W., Shue, B., Sun, J., Wang, Z., Wang, A., Wang, X., Wang, J., Wei, M., Wides, R., Xiao, C., Yan, C., et al. (2001) 'The sequence of the human genome', *Science,* 291(5507), 1304-51.

Verburg, F. A., Lips, C. J., Lentjes, E. G. and de Klerk, J. M. (2004) 'Detection of circulating Tg-mRNA in the follow-up of papillary and follicular thyroid cancer: how useful is it?', *Br J Cancer,* 91(2), 200-4.

Vlachos, I. S., Zagganas, K., Paraskevopoulou, M. D., Georgakilas, G., Karagkouni, D., Vergoulis, T., Dalamagas, T. and Hatzigeorgiou, A. G. (2015) 'DIANA-miRPath v3.0: deciphering microRNA function with experimental support', *Nucleic Acids Res,* 43(W1), W460-W466.

Volante, M., Collini, P., Nikiforov, Y. E., Sakamoto, A., Kakudo, K., Katoh, R., Lloyd, R. V., LiVolsi, V. A., Papotti, M., Sobrinho-Simoes, M., Bussolati, G. and Rosai, J. (2007) 'Poorly differentiated thyroid carcinoma: the Turin proposal for the use of uniform

diagnostic criteria and an algorithmic diagnostic approach', *Am J Surg Pathol,* 31(8), 1256-64.

Wang, H., Fu, W., Im, J. H., Zhou, Z., Santoro, S. A., Iyer, V., DiPersio, C. M., Yu, Q.-C., Quaranta, V., Al-Mehdi, A. and Muschel, R. J. (2004) 'Tumor cell alpha3beta1 integrin and vascular laminin-5 mediate pulmonary arrest and metastasis', *The Journal of Cell Biology,* 164(6), 935-941.

Wang, K., Li, M. and Hakonarson, H. (2010) 'ANNOVAR: functional annotation of genetic variants from high-throughput sequencing data', *Nucleic Acids Res,* 38(16), e164.

Wang, Y., Chen, J., Yang, W., Mo, F., Senz, J., Yap, D., Anglesio, M. S., Gilks, B., Morin, G. B. and Huntsman, D. G. (2015) 'The Oncogenic Roles of DICER1 RNase IIIb Domain Mutations in Ovarian Sertoli-Leydig Cell Tumors', *Neoplasia,* 17(8), 650-660.

Wang, Y. and Zhou, B. P. (2013) 'Epithelial-mesenchymal Transition---A Hallmark of Breast Cancer Metastasis', *Cancer Hallm,* 1(1), 38-49.

Watanabe, R., Hayashi, Y., Sassa, M., Kikumori, T., Imai, T., Kiuchi, T. and Murata, Y. (2009) 'Possible Involvement of BRAFV600E in Altered Gene Expression in Papillary Thyroid Cancer', *Endocrine Journal,* 56(3), 407-414.

Watkins, R. J., Imruetaicharoenchoke, W., Read, M. L., Sharma, N., Poole, V. L., Gentilin, E., Bansal, S., Bosseboeuf, E., Fletcher, R., Nieto, H. R., Mallick, U., Hackshaw, A., Mehanna, H., Boelaert, K., Smith, V. E. and McCabe, C. J. (2016) 'Pro-invasive Effect of Proto-oncogene PBF Is Modulated by an Interaction with Cortactin', *The Journal of Clinical Endocrinology & Metabolism,* 101(12), 4551-4563.

Wei, Z. L., Gao, A. B., Wang, Q., Lou, X. E., Zhao, J. and Lu, Q. J. (2019) 'MicroRNA-221 promotes papillary thyroid carcinoma cell migration and invasion via targeting RECK and regulating epithelial-mesenchymal transition', *OncoTargets and therapy,* 12, 2323-2333.

Wells, S. A., Jr., Asa, S. L., Dralle, H., Elisei, R., Evans, D. B., Gagel, R. F., Lee, N., Machens, A., Moley, J. F., Pacini, F., Raue, F., Frank-Raue, K., Robinson, B., Rosenthal, M. S., Santoro, M., Schlumberger, M., Shah, M., Waguespack, S. G. and American Thyroid Association Guidelines Task Force on Medullary Thyroid, C. (2015) 'Revised American Thyroid Association guidelines for the management of medullary thyroid carcinoma', *Thyroid,* 25(6), 567-610.

Wen, D. Y., Pan, D. H., Lin, P., Mo, Q. Y., Wei, Y. P., Luo, Y. H., Chen, G., He, Y., Chen, J. Q. and Yang, H. (2018) 'Downregulation of miR4865p in papillary thyroid carcinoma tissue: A study based on microarray and miRNA sequencing', *Mol Med Rep,* 18(3), 2631-2642.

Wieder, T., Braumuller, H., Kneilling, M., Pichler, B. and Rocken, M. (2008) 'T cell-mediated help against tumors', *Cell Cycle,* 7(19), 2974-7.

Wikman, H., Vessella, R. and Pantel, K. (2008) 'Cancer micrometastasis and tumour dormancy', *Apmis,* 116(7-8), 754-70.

Willis, A., Jung, E. J., Wakefield, T. and Chen, X. (2004) 'Mutant p53 exerts a dominant negative effect by preventing wild-type p53 from binding to the promoter of its target genes', *Oncogene,* 23(13), 2330-8.

Wojcicka, A., Kolanowska, M. and Jazdzewski, K. (2016) 'MECHANISMS IN ENDOCRINOLOGY: MicroRNA in diagnostics and therapy of thyroid cancer', *Eur J Endocrinol,* 174(3), R89-98.

Wu, C., Chung, A. E. and McDonald, J. A. (1995) 'A novel role for alpha 3 beta 1 integrins in extracellular matrix assembly', *J Cell Sci,* 108 (Pt 6), 2511-23.

Wu, G. and Haw, R. (2017) 'Functional Interaction Network Construction and Analysis for Disease Discovery', *Methods Mol Biol,* 1558, 235-253.

Xia, S., Wang, C., Postma, E. L., Yang, Y., Ni, X. and Zhan, W. (2017) 'Fibronectin 1 promotes migration and invasion of papillary thyroid cancer and predicts papillary thyroid cancer lymph node metastasis', *OncoTargets and therapy,* 10, 1743-1755.

Xiao, W., Ma, W., Wei, S., Li, Q., Liu, R., Carney, R. P., Yang, K., Lee, J., Nyugen, A., Yoneda, K. Y., Lam, K. S. and Li, T. (2019) 'High-affinity peptide ligand LXY30 for targeting α3β1 integrin in non-small cell lung cancer', *Journal of Hematology & Oncology,* 12(1), 56.

Xing, M. (2007) 'BRAF Mutation in Papillary Thyroid Cancer: Pathogenic Role, Molecular Bases, and Clinical Implications', *Endocrine Reviews,* 28(7), 742-762.

Xing, M. (2010) 'Genetic alterations in the phosphatidylinositol-3 kinase/Akt pathway in thyroid cancer', *Thyroid,* 20(7), 697-706.

Xing, M. (2016) 'Clinical utility of RAS mutations in thyroid cancer: a blurred picture now emerging clearer', *BMC medicine,* 14, 12-12.

Yadav, R. K., Chae, S.-W., Kim, H.-R. and Chae, H. J. (2014) 'Endoplasmic reticulum stress and cancer', *Journal of cancer prevention,* 19(2), 75-88.

Yang, X., Li, J., Li, X., Liang, Z., Gao, W., Liang, J., Cheng, S. and Lin, Y. (2017) 'TERT Promoter Mutation Predicts Radioiodine-Refractory Character in Distant Metastatic Differentiated Thyroid Cancer', *J Nucl Med,* 58(2), 258-265.

Yang, Y., Ding, L., Li, Y. and Xuan, C. (2019) 'Hsa_circ_0039411 promotes tumorigenesis and progression of papillary thyroid cancer by miR-1179/ABCA9 and miR-1205/MTA1 signaling pathways', *J Cell Physiol*.

Yang, Y. J., Na, H. J., Suh, M. J., Ban, M. J., Byeon, H. K., Kim, W. S., Kim, J. W., Choi, E. C., Kwon, H. J., Chang, J. W. and Koh, Y. W. (2015) 'Hypoxia Induces Epithelial-Mesenchymal Transition in Follicular Thyroid Cancer: Involvement of Regulation of Twist by Hypoxia Inducible Factor-1α', *Yonsei medical journal,* 56(6), 1503-1514.

Young, S., Harari, A., Smooke-Praw, S., Ituarte, P. H. G. and Yeh, M. W. (2013) 'Effect of reoperation on outcomes in papillary thyroid cancer', *Surgery,* 154(6), 1354-1362.

Yun, S. J., Jo, S. W., Ha, Y. S., Lee, O. J., Kim, W. T., Kim, Y. J., Lee, S. C. and Kim, W. J. (2012) 'PFKFB4 as a prognostic marker in non-muscle-invasive bladder cancer', *Urol Oncol,* 30(6), 893-9.

Zhai, T., Muhanhali, D., Jia, X., Wu, Z., Cai, Z. and Ling, Y. (2019) 'Identification of gene co-expression modules and hub genes associated with lymph node metastasis of papillary thyroid cancer', *Endocrine*.

Zhang, H., Lu, C., Fang, M., Yan, W., Chen, M., Ji, Y., He, S., Liu, T., Chen, T. and Xiao, J. (2016) 'HIF-1alpha activates hypoxia-induced PFKFB4 expression in human bladder cancer cells', *Biochem Biophys Res Commun,* 476(3), 146-52.

Zhang, Y., Xu, D., Pan, J., Yang, Z., Chen, M., Han, J., Zhang, S., Sun, L. and Qiao, H. (2017) 'Dynamic monitoring of circulating microRNAs as a predictive biomarker for the diagnosis and recurrence of papillary thyroid carcinoma', *Oncology letters,* 13(6), 4252-4266.

Zhang, Z., Chhieng, D., Harshan, M., Zheng, X. and Zakowski, M. (2019) 'Cytological features of noninvasive follicular thyroid neoplasm with papillary-like nuclear features (NIFTP)', *J Am Soc Cytopathol,* 8(1), 5-10.

Zhao, S., Guo, Y., Sheng, Q. and Shyr, Y. (2014) 'Heatmap3: an improved heatmap package with more powerful and convenient features', *BMC Bioinformatics,* 15(Suppl 10), P16-P16.

Zhou, L., Xia, D., Zhu, J., Chen, Y., Chen, G., Mo, R., Zeng, Y., Dai, Q., He, H., Liang, Y., Jiang, F. and Zhong, W. (2014) 'Enhanced expression of IMPDH2 promotes metastasis and advanced tumor progression in patients with prostate cancer', *Clin Transl Oncol,* 16(10), 906-13.

Zimmermann, A. G., Spychala, J. and Mitchell, B. S. (1995) 'Characterization of the human inosine-5'-monophosphate dehydrogenase type II gene', *J Biol Chem,* 270(12), 6808-14.

Chapter 10 Appendix 1

10 Appendix 1

Patient ID	Sex	Age	Tumour Stage			Neoplasm Histologic Type Name	Laterality	Vital Status
TCGA-BJ-A0Z2	Male	57	T2	N0	M1	Thyroid Papillary Carcinoma - Follicular (>= 99% follicular patterned)	Left lobe	Alive
TCGA-BJ-A28X	Female	32	T3	N1a	M0	Thyroid Papillary Carcinoma - Tall Cell (>= 50% tall cell features)	Left lobe	Alive
TCGA-BJ-A290	Male	70	T3	N1a	M0	Thyroid Papillary Carcinoma - Tall Cell (>= 50% tall cell features)	Left lobe	Alive
TCGA-BJ-A2N9	Female	42	T2	N0	M0	Thyroid Papillary Carcinoma - Classical/usual	Right lobe	Alive
TCGA-BJ-A2NA	Male	77	T3	N0	M0	Thyroid Papillary Carcinoma - Classical/usual	Bilateral	Alive
TCGA-BJ-A3PU	Male	52	T3	N1a	M0	Thyroid Papillary Carcinoma - Classical/usual	Left lobe	Alive
TCGA-BJ-A45I	Female	51	T3	N0	M0	Thyroid Papillary Carcinoma - Tall Cell (>= 50% tall cell features)	Bilateral	Alive
TCGA-DE-A0Y3	Female	60	T4a	N1b	M1	Thyroid Papillary Carcinoma - Classical/usual	Bilateral	Alive
TCGA-DE-A4MC	Female	43	T3	N1b	M0	Thyroid Papillary Carcinoma - Classical/usual	Right lobe	Alive
TCGA-DE-A4MD	Male	71	T3	N1b	M0	Thyroid Papillary Carcinoma - Classical/usual	Right lobe	Alive
TCGA-DE-A69K	Female	58	T3	N0	M0	Thyroid Papillary Carcinoma - Classical/usual	Right lobe	Alive
TCGA-DJ-A1QO	Male	69	T3	N0	M0	Thyroid Papillary Carcinoma - Tall Cell (>= 50% tall cell features)	Bilateral	Alive
TCGA-DJ-A2Q3	Female	61	T3	N1a	M0	Thyroid Papillary Carcinoma - Tall Cell (>= 50% tall cell features)	Left lobe	Alive
TCGA-DJ-A3UO	Male	63	T3	N1b	M0	Thyroid Papillary Carcinoma - Classical/usual	Bilateral	Alive
TCGA-DJ-A3VL	Male	38	T1a	N0	M0	Thyroid Papillary Carcinoma - Follicular (>= 99% follicular patterned)	Right lobe	Alive
TCGA-DJ-A4UR	Female	36	T3	N1b	M1	Thyroid Papillary Carcinoma - Follicular (>= 99% follicular patterned)	Right lobe	Alive
TCGA-DO-A1K0	Female	30	T3	N1b	MX	Thyroid Papillary Carcinoma - Classical/usual	Bilateral	Alive
TCGA-E3-A3E3	Female	49	T2	N0	M0	Thyroid Papillary Carcinoma - Classical/usual	Right lobe	Alive
TCGA-E8-A432	Female	57	T2	N0	M0	Thyroid Papillary Carcinoma - Classical/usual	Left lobe	Alive
TCGA-EL-A3CZ	Female	37	T1	N1a	M0	Thyroid Papillary Carcinoma - Classical/usual	Left lobe	Alive
TCGA-EL-A3GO	Female	31	T2	N0	M0	Thyroid Papillary Carcinoma - Classical/usual	Right lobe	Alive
TCGA-EL-A3GU	Female	72	T3	N1	M0	Thyroid Papillary Carcinoma - Classical/usual	Left lobe	Alive
TCGA-EL-A3GX	Female	41	T2	N1	M0	Thyroid Papillary Carcinoma - Classical/usual	Right lobe	Alive
TCGA-EL-A3MX	Female	66	T4	N1	M1	Thyroid Papillary Carcinoma - Classical/usual	Left lobe	Dead

TCGA-EL-A3T2	Female	55	T2	N1	M0	Thyroid Papillary Carcinoma - Classical/usual	Right lobe	Alive
TCGA-EL-A4K6	Male	75	T4	N1	MX	Thyroid Papillary Carcinoma - Classical/usual	Right lobe	Alive
TCGA-EL-A4KI	Male	63	T3	N0	MX	Thyroid Papillary Carcinoma - Classical/usual	Bilateral	Alive
TCGA-EM-A2P1	Male	33	T2	N1b	MX	Thyroid Papillary Carcinoma - Classical/usual	Left lobe	Alive
TCGA-EM-A3FM	Male	57	T2	N1b	MX	Thyroid Papillary Carcinoma - Classical/usual	Right lobe	Alive
TCGA-EM-A3ST	Female	62	T3	N0	MX	Thyroid Papillary Carcinoma - Follicular (>= 99% follicular patterned)	Right lobe	Alive
TCGA-EM-A4FF	Female	40	T1b	N1	MX	Thyroid Papillary Carcinoma - Classical/usual	Left lobe	Alive
TCGA-EM-A4FU	Male	35	T3	NX	MX	Thyroid Papillary Carcinoma - Follicular (>= 99% follicular patterned)	Left lobe	Alive
TCGA-ET-A39K	Female	48	T3	N1a	MX	Thyroid Papillary Carcinoma - Classical/usual	Left lobe	Alive
TCGA-ET-A3BT	Female	60	T2	N1b	MX	Thyroid Papillary Carcinoma - Tall Cell (>= 50% tall cell features)	Isthmus	Alive
TCGA-ET-A3BV	Female	47	T2	N1a	MX	Thyroid Papillary Carcinoma - Classical/usual	Left lobe	Alive
TCGA-ET-A3DO	Female	33	T2	NX	MX	Thyroid Papillary Carcinoma - Classical/usual	Right lobe	Alive
TCGA-ET-A40Q	Male	38	T3	N1b	MX	Thyroid Papillary Carcinoma - Tall Cell (>= 50% tall cell features)	Right lobe	Alive
TCGA-FE-A22Z	Female	61	T4a	N1	MX	Thyroid Papillary Carcinoma - Follicular (>= 99% follicular patterned)	Left lobe	Alive
TCGA-FE-A230	Female	30	T3	N1a	MX	Thyroid Papillary Carcinoma - Classical/usual	Left lobe	Alive
TCGA-FE-A233	Female	18	T2	NX	MX	Thyroid Papillary Carcinoma - Classical/usual	Right lobe	Alive
TCGA-FE-A234	Female	26	T2	N1	MX	Thyroid Papillary Carcinoma - Classical/usual	Right lobe	Alive
TCGA-FE-A237	Female	19	T3	N1	MX	Thyroid Papillary Carcinoma - Classical/usual	Bilateral	Alive
TCGA-H2-A3RI	Female	29	T3	N0	MX	Thyroid Papillary Carcinoma - Classical/usual	Left lobe	Alive

Table 10.1: Clinical parameters for recurrent thyroid cancer patients included in somatic mutation analysis

Chr	Position	Reference	Alt	Filter	Gene	SS	VC	VT	SIFT	Polyphen2
11	129034262	AT	A	PASS	ARHGAP32	Somatic	Frame_Shift_Del	DEL	.	.
7	140477826	CTGCTGAGGTGTAGGT	C	PASS	BRAF	Somatic	In_Frame_Del	DEL	.	.
7	21468303	AAGG	A	PASS	SP4	Somatic	In_Frame_Del	DEL	.	.
15	93552546	T	TG	PASS	CHD2	Somatic	Frame_Shift_Ins	INS	.	.
16	58560012	G	A	PASS	CNOT1	Somatic	Missense_Mutation	SNP	0.01	1
16	58560012	G	A	PASS	CNOT1	Somatic	Missense_Mutation	SNP	0.01	1
6	33141287	C	G	PASS	COL11A2	Somatic	Missense_Mutation	SNP	0	1
19	12297911	C	T	PASS	ZNF136	Somatic	Nonsense_Mutation	SNP	.	.
20	44520006	C	CT	PASS	CTSA	Somatic	Frame_Shift_Ins	INS	.	.
20	60511927	T	C	PASS	CDH4	Somatic	Missense_Mutation	SNP	.	.
14	95557639	C	G	PASS	DICER1	Somatic	Missense_Mutation	SNP	0	1
3	52433173	C	A	PASS	DNAH1	Somatic	Missense_Mutation	SNP	0	1
6	38697694	A	AT	PASS	DNAH8	Somatic	Frame_Shift_Ins	INS	.	.
11	103029463	TG	T	PASS	DYNC2H1	Somatic	Frame_Shift_Del	DEL	.	.
1	28087060	TCA	T	PASS	FAM76A	Somatic	Frame_Shift_Del	DEL	.	.
9	34649475	C	T	PASS	GALT	Somatic	Missense_Mutation	SNP	0	1
14	65008100	C	A	PASS	HSPA2	Somatic	Missense_Mutation	SNP	0	1
3	49062646	G	A	PASS	IMPDH2	Somatic	Missense_Mutation	SNP	.	1
3	49064023	G	C	PASS	IMPDH2	Somatic	Missense_Mutation	SNP	0	0.999
10	64967937	TG	T	PASS	JMJD1C	Somatic	Frame_Shift_Del	DEL	.	.
2	150017335	AT	A	PASS	LYPD6B	Somatic	Frame_Shift_Del	DEL	.	.
10	99220480	TG	T	PASS	MMS19	Somatic	Frame_Shift_Del	DEL	.	.
10	111986019	GT	G	PASS	MXI1	Somatic	Intron	DEL	.	.
8	24774944	GA	G	PASS	NEFM	Somatic	Frame_Shift_Del	DEL	.	.
3	48561154	T	C	PASS	PFKFB4	Somatic	Missense_Mutation	SNP	0	1
20	62198498	AC	A	PASS	PRIC285	Somatic	Frame_Shift_Del	DEL	.	.
10	119798739	TC	T	PASS	RAB11FIP2	Somatic	Frame_Shift_Del	DEL	.	.
X	106016280	A	AT	PASS	RNF128	Somatic	Frame_Shift_Ins	INS	.	.
3	38889182	G	A	PASS	SCN11A	Somatic	Missense_Mutation	SNP	0	0.996
19	52033046	CCTT	C	PASS	SIGLEC6	Somatic	In_Frame_Del	DEL	.	.
19	39370316	CA	C	PASS	SIRT2	Somatic	Frame_Shift_Del	DEL	.	.
8	134050953	TTC	T	PASS	SLA	Somatic	Frame_Shift_Del	DEL	.	.
5	1232375	G	A	PASS	SLC6A18	Somatic	Missense_Mutation	SNP	0	1
5	53814142	GC	G	PASS	SNX18	Somatic	Frame_Shift_Del	DEL	.	.
12	56397582	TG	T	PASS	SUOX	Somatic	Frame_Shift_Del	DEL	.	.
7	97858473	CA	C	PASS	TECPR1	Somatic	Frame_Shift_Del	DEL	.	.
2	85552042	TG	NA	PASS	TGOLN2	Somatic	Frame_Shift_Del	DEL	.	.
5	94858951	C	A	PASS	TTC37	Somatic	Missense_Mutation	SNP	0.01	1
5	94858951	C	A	PASS	TTC37	Somatic	Missense_Mutation	SNP	0.01	1
1	7837370	A	T	PASS	VAMP3	Somatic	Missense_Mutation	SNP	0	1
1	247420154	G	C	PASS	VN1R5	Somatic	Missense_Mutation	SNP	.	.
2	175446092	C	A	PASS	WIPF1	Somatic	Missense_Mutation	SNP	0	1
2	219503377	G	C	PASS	ZNF142	Somatic	Missense_Mutation	SNP	0	0.952
11	124121061	C	A	PASS	OR8G1	Somatic	Silent	SNP	.	.

12	104100607	G	T	PASS	STAB2	Somatic	Missense_Mutation	SNP	0	0.999
11	124121061	C	A	PASS	OR8G1	Somatic	Silent	SNP	.	.
12	104100607	G	T	PASS	STAB2	Somatic	Missense_Mutation	SNP	0	0.999

Table 10.2: List of the 47 variants from TCGA Mutect vcf file analysis

Genes	Median Diff	W	p value
FN1	353701.486	7201	0.00376792
TG	218135.677	12504	0.00311069
SLC34A2	61440.0868	7603	0.01416126
FTH1	13899.7015	8009	0.04497247
S100A6	11731.9057	7798	0.0252301
HSP90B1	6575.5353	12560	0.00254107
HSPA5	6524.3576	13254	0.00015395
ITGA3	5908.8077	7406	0.00757069
CALR	5735.3045	12000	0.01638821
ACTG1	5248.7467	7145	0.00308849
MET	4412.7637	7696	0.01874962
PROS1	3831.5854	7787	0.02444859
ZFP36L1	3809.4879	7313	0.00554885
TIMP3	3125.9834	12580	0.00236195
PDIA3	3095.5959	12587	0.00230204
SQSTM1	2997.4883	7167	0.00334083
EGR1	2931.5528	12203	0.00868348
PLVAP	2798.8076	12784	0.0010919
PPL	2674.0898	8035	0.04813132
VEGFA	2563.5843	12142	0.0105602
PPIB	2447.4012	11757	0.03301714
MYH14	2351.8587	7269	0.00477414
APP	2327.8479	11603	0.04977939
RGS5	2324.4882	12538	0.00275238
SPARCL1	2292.7339	13598	3.12E-05
CPE	2269.2728	12499	0.00316683
A2M	2237.6495	12502	0.00313304
S100A1	2137.4636	7696	0.01874962
TPO	2082.4104	12509	0.00305546
IGFBP7	2051.9799	13042	0.00038443
PABPC1	2045.0202	7217	0.00398558
KCNJ16	2033.7837	12570	0.00245001
TM7SF4	1988.2786	7711	0.0195997
FCGBP	1958.4645	12307	0.00616096
PDK4	1948.5597	11629	0.04652934
DPP4	1875.6236	7350	0.00628623
MUC1	1760.1563	7739	0.0212789
VAT1	1682.1978	6767	0.00073518
EPAS1	1633.0726	13264	0.00014726
AHNAK2	1608.0723	7571	0.01282921

Table 10.3: Median differential RNA expression recurrent patients versus non-recurrent patients (primary tumour sample) top 40 significant genes.

miRNA_ID	W	p-value
hsa-mir-1179	13170	0.00036003
hsa-mir-1233-1	9681	0.00108624
hsa-mir-3649	9681	0.00108624
hsa-mir-554	9681	0.00108624
hsa-mir-648	9681	0.00108624
hsa-mir-145	12652	0.00270044
hsa-mir-3658	9493.5	0.00293778
hsa-mir-139	12619	0.00303868
hsa-mir-455	12617	0.00306038
hsa-let-7b	12598	0.0032736
hsa-mir-363	12557	0.00378054
hsa-mir-556	7413.5	0.00494259
hsa-mir-600	11481	0.00500639
hsa-mir-126	12410	0.00623858
hsa-mir-3074	12384	0.00679957
hsa-mir-100	12328	0.00816446
hsa-mir-1277	7529	0.00910783
hsa-mir-636	7619	0.0097946
hsa-mir-935	12256.5	0.01026014
hsa-mir-221	7585	0.01087612
hsa-mir-548f-4	9516	0.011758
hsa-mir-20b	12132	0.01507391
hsa-mir-513a-2	8303	0.01732066
hsa-mir-3190	7994.5	0.01878554
hsa-mir-3622a	12053	0.01879619
hsa-mir-4284	8397	0.01907757
hsa-mir-190	12052	0.01912891
hsa-mir-3189	7928.5	0.01966642
hsa-mir-3926-1	12016	0.02124198
hsa-mir-3922	7849	0.02342212
hsa-mir-486	11937	0.02661626
hsa-mir-346	11935	0.02676493
hsa-mir-3126	11445	0.02683648
hsa-mir-30c-2	11931	0.02706835
hsa-mir-1294	11885	0.02720769
hsa-mir-200c	7909	0.02838542
hsa-mir-193a	11910	0.02870323
hsa-mir-7-2	11895.5	0.02987934

hsa-mir-586	9539.5	0.0303763
hsa-mir-133a-1	11886	0.03067512
hsa-mir-195	11851	0.03375874
hsa-mir-491	11844	0.0344063
hsa-mir-1825	9402	0.03483756
hsa-mir-3167	9702	0.03560623
hsa-mir-3646	9702	0.03560623
hsa-mir-3665	9702	0.03560623
hsa-mir-4263	9702	0.03560623
hsa-mir-548i-2	9702	0.03560623
hsa-mir-1185-2	8723	0.035647
hsa-mir-1184-1	9703	0.03649748
hsa-mir-130a	11806	0.03810971
hsa-mir-450a-2	11794.5	0.03929523
hsa-mir-3688	8356	0.04317771
hsa-mir-939	11747.5	0.04444387
hsa-mir-1278	8765	0.04503439
hsa-mir-514-1	8098	0.04714562
hsa-mir-19b-1	8113	0.04900298
hsa-mir-222	8116	0.0493817
hsa-mir-153-2	11705	0.04963555
hsa-mir-23c	11704	0.04974332
hsa-mir-146a	8120	0.04989049
hsa-mir-30b	11703	0.04989049

Table 10.4: Median differential microRNA expression recurrent patients versus non-recurrent patients (primary tumour sample) all significant miRs (total n=62).

Chapter 11 Bibliography

Bibliography

10.1 Publications relating to thesis

Nieto H, Boelaert K. Thyroid-stimulating hormone in thyroid cancer: does it matter? Endocrine Related Cancer 2016: T109-T121. PMID: 27633516

Watkins R, Imruetaicharoenchoke W, Read M, Sharma N, Poole V, Gentilin E, Bansal S, Bosseboeuf E, Fletcher A, **Nieto HR**, Mallick U, Hackshaw A, Mehanna H, Boelaert K, Smith V, McCabe C. Pro-invasive Effect of Proto-oncogene PBF Is Modulated by an Interaction with Cortactin. The Journal of Clinical Endocrinology & Metabolism, 2016, 101(12):4551–4563. PMID: 27603901

Read ML, Fong JC, Modasia B, Fletcher A, Imruetaicharoenchoke W, Thompson RJ, **Nieto H**, Reynolds JJ, Bacon A, Mallick U, Hackshaw A, Watkinson JC, Boelaert K, Turnell AS, Smith VE, McCabe CJ. Elevated PTTG and PBF predicts poor patient outcome and modulates DNA damage response genes in thyroid cancer. Oncogene. 2017; 36(37):5296-5308. PMID: 28504713

Imruetaicharoenchoke W, Fletcher A, Lu W, Watkins RJ, Modasia B, Poole VL, **Nieto HR**, Thompson RJ, Boelaert K, Read ML, Smith VE, McCabe CJ. Functional consequences of the first reported mutations of the proto-oncogene PTTG1IP/PBF. Endocr Relat Cancer. 2017; 24(9):459-474. PMID: 28676500

Read ML, Modasia B, Fletcher A, Thompson RJ, Brookes K, Rae PC, **Nieto HR**, Poole VL, Roberts S, Campbell MJ, Boelaert K, Turnell AS, Smith VE, Mehanna H, McCabe

CJ. PTTG and PBF Functionally Interact with p53 and Predict Overall Survival in Head and Neck Cancer. Cancer Research. 2018; 78(20):5863-5876. PMID: 30154144

Thompson RJ, Fletcher A, Brookes K, **Nieto H**, Alshahrani MM, Mueller JW, Fine NH, Hodson DJ, Boelaert K, Read ML, Smith VE, McCabe CJ. Dimerization of the sodium/iodide symporter (NIS). Thyroid. 2019; 29(10):1485-1498. PMID: 31310151

Fletcher A, Read ML, Thornton CEM, Larner DP, Poole VL, Brookes K, **Nieto HR**, Alshahrani M, Thompson RJ, Lavery G, Landa I, Fagin JA, Campbell MJ, Boelaert K, Turnell AS, Smith VE, McCabe CJ. Targeting Novel Sodium Iodide Symporter Interactors ADP-Ribosylation Factor 4 and Valosin-Containing Protein Enhances Radioiodine Uptake. Cancer Research. 2019 Oct epub. PMID: 31672844

10.2 Presentations

Oral presentation at Society for Endocrinology BES - November 2019, Brighton

Oral presentation at European Society of Endocrinology - May 2019, Lyon

Oral presentation at British Thyroid Association meeting - May 2019, London

Oral presentation at Society for Endocrinology Thyroid Neoplasia meeting – March 2019, Cambridge

Poster presentation at Society for Endocrinology BES - November 2017, Harrogate